UNIVERSITY OF CAPE TOWN
IYUNIVESITHI YASEKAPA • UNIVERSITEIT VAN KAAPSTAD

Hydraulic Characteristics and Nutrient Degradation Kinetics of a Horizontally Orientated Subsurface Flow Biofilter

Kalpana Maraj

In fulfilment of the requirements for the degree of Master of Science in Engineering

Supervisor:
Professor Susan Harrison

Co-Supervisor:
Dr. Kevin Winter

FEBRUARY 2022

PLAGIARISM DECLARATION

1. I know the meaning of plagiarism and declare that all the work in the document, save for that which is properly acknowledged, is my own. This dissertation has been submitted to the Turnitin module (or equivalent similarity and originality checking software) and I confirm that my supervisor has seen my report and any concerns revealed by such have been resolved with my supervisor.
2. I have used the Harvard system for citation and referencing. Each significant contribution to, and quotation in, this report from the work, or works, of other people has been attributed, and has been cited and referenced.
3. This report is my own unaided work, except for assistance received from the teaching staff.
4. I have not allowed and will not allow anyone to copy my work with the intention of passing it off as his or her own work.

Signed by candidate

Signature

ABSTRACT

Polluted runoff from densely populated and poorly serviced informal settlements is a growing issue in South Africa that leads to various health risks and environmental degradation. Surface waters affected by informal settlements are known to display high nutrient (NH_3, NO_2^-, NO_3^- and PO_4^{3-}) concentrations. These nutrient concentrations are highly variable due to the fluctuations in the type and frequency of human activities occurring in the informal settlements.

A decentralised, non-invasive and easy to maintain surface water rehabilitation system that is capable of handling variable inlet nutrient concentrations is therefore necessary in these areas. Engineered nature-based solutions such as horizontally orientated subsurface flow biofilters are a potential suitable remediation measure, as they are cost-effective, scalable and easy to maintain. However, the variable nutrient levels in surface waters affected by informal settlements pose a challenge to achieving consistent nutrient reduction in a system.

The nutrient degradation potential of a microbially colonised horizontally orientated subsurface flow pilot-scale biofilter (length: 2 m; width: 0.44 m; depth: 0.7 m) that was packed with stones of 8-11 mm in diameter was assessed in this study. The purpose of performing controlled experiments on the pilot-scale biofilter was to enable data collection for the design of optimum full scale biofilters. Pulse tracer studies at varying flow rates (0.5 -3 L/min) determined that the flow behaviour in the pilot-scale biofilter approximated plug flow; with the extent of plug flow behaviour and degree of mixing in the radial direction increasing with a decrease in flow rate

Surface runoff from the Stiebeuel River, contaminated by an upstream informal settlement called Langrug, was used as the polluted water source for the pilot-scale biofilter. Six nutrient degradation studies were carried out on the microbially colonised pilot biofilter with each study occurring over a 10-day period (228 hours). Three of the nutrient degradation studies were carried out at a flow rate of 0.5 L/min and three were carried out at a flow rate of 1.5 L/min. Water from the Stiebeuel River (200 L) was circulated through the system during the batch nutrient degradation studies with samples being taken every six hours.

The inlet concentration varied in each study with an inlet concentration range of 8.41 - 24.2 mg/L NH_3, 1.06 - 2.30 mg/L NO_3^- and 1.45 - 6.82 mg/L PO_4^{3-} being observed. An NH_3 reduction of up to 91.8%, total nitrogen reduction of up to 82.4% and a PO_4^{3-} reduction of up to 88.3% was observed. The main biological processes occurring within the pilot biofilter were nitrification and denitrification. An extent of nitrification of up to 91.7% and an extent of denitrification of up to 95.6% were observed in the nutrient degradation studies. Ammonia degradation and orthophosphate removal in

the system was described using the double first-order in parallel reaction kinetic model which expresses the reaction kinetics as the sum of first two order reactions.

The results of the nutrient degradation studies show that the microbial community in the pilot-scale biofilter system is able to metabolise moderate pulses of nutrients when fresh contaminated water is introduced to the system at varying inlet concentrations. The microbial community is able to survive under nutrient limited conditions. These findings indicate the effectiveness of stone biofilters at degrading nutrients in polluted runoff from informal settlements in a controlled batch experiment.

ACKNOWLEDGEMENTS

I would like to thank my supervisor, Professor Sue Harrison for her guidance, encouragement and patience throughout this process. I am deeply grateful to my co-supervisor Dr. Kevin Winter for his enthusiasm, encouragement and willingness to dedicate his time to assist with the logistics surrounding the project. I am thankful to both my supervisors for providing their expertise and knowledge in shaping this project.

I would like to thank the administrative staff at CeBER, Sue Jobson and Ruegshana Ederies, for their support and assistance in all matters, big and small. Thanks to the CeBER lab manager, Tich Samkange, for his assistance in the labs and for providing me with extra encouragement whenever I needed it. Thanks to the CeBER Bioenvironmental Discussion Group and Future Water Stormwater Research Group for their advice and support during meetings.

I extend my heartfelt gratitude to Sayed Hess, the Technical Assistant in the Environmental and Geographical Sciences Department, for his assistance in the construction of the pilot biofilter. I would also like to thank the CoMSIRU lab manager, Noor Hassen for providing a lab space for the pilot biofilter and going above and beyond to offer me assistance at every turn. Thanks to Miranda Waldron from UCT's Electron Microscope Unit for her technical assistance in capturing SEM images. I would like to thank Miss Adeebah Rakiep for her assistance in developing the biofilm detachment method and her assistance in SEM analysis. Thank you to Emily Nicklin for assistance with the sampling for the tracer studies and for being a great sounding board for my ideas.

Financial support from the NRF South African Research Chair Initiative in Bioprocess Engineering is acknowledged and greatly appreciated.

To my amazing parents and my Dadima: I am immensely grateful for your unwavering love and support throughout this process. Thanks to my siblings, Sapna and Ashutosh, for always being there to encourage me and for cheering me up when things were tough. A huge thank you to my friends who walked this path with me and supported me along the way. A special thank you to Divine Ssebunnya, for giving me no option but to keep making progress and without whom this dissertation would not exist.

“Matru Devo Bhava, Pitru Devo Bhava” - Taittiriya Upanishad

*To **Mom and Pithaji**, who taught me that I could do anything I put my mind to.*

Scan the above code from your Spotify application or follow the link below for a listening experience to accompany this dissertation.

https://open.spotify.com/playlist/1jcEgta2uJmCJV9grIGsyk?si=420e858b830343ce

CONTENTS

LIST OF FIGURES

LIST OF TABLES

GLOSSARY OF TERMS

Adsorption	The adhesion of atoms, ions or molecules from a gas, liquid or solid to a surface.
Advection	The transport of a substance or quantity by bulk motion of a fluid.
Biofilter	Microbially colonised filter which removes contaminants and suspended solids from water through biological degradation and filtration.
Denitrification	Microbially facilitated process where nitrate is reduced to produce molecular nitrogen
Mixed Flow	Fluid flow behaviour that displays mixing in both the axial and radial directions.
Nitrification	Microbially facilitated oxidation of ammonia to nitrite followed by the oxidation of the nitrite to nitrate
Plug Flow	Fluid flow behaviour where there is perfect mixing in the radial direction and no mixing in the axial direction.
Tracer	A non-reactive and non-adsorptive substance that is added to a reactor inlet to determine the residence time distribution of the reactor

ACCRONYMS AND ABBREVIATIONS

COD	Chemical oxygen demand
CSTR	Continuous stirred tank reactor
EPS	Extracellular polymeric substances
GAC	Granular activated carbon
PFR	Plug flow reactor
RTD	Residence time distribution

SEM	Scanning electron microscope
DFOP	Double first-order in parallel kinetic model

NOMENCLATURE

ST1	Outlet of Settling Tank 1
ST2	Outlet of Settling Tank 2
LSO	Outlet of Large Stones Biofilter
SSO	Outlet of Small Stones Biofilter
$\boldsymbol{\tau}$	Theoretical Residence Time
$\boldsymbol{\bar{t}_m}$	Mean Residence Time Distribution
$\boldsymbol{e}$	Bed Voidage
$\boldsymbol{\Lambda}$	Hydraulic Efficiency
$\boldsymbol{Pe}$	Peclet Number
$\boldsymbol{N}$	Number of Tanks in Series
$\boldsymbol{k}$	Kinetic Rate Constant

1. INTRODUCTION

1.1. Background to the Study

Surface water runoff from densely populated and poorly serviced informal settlements present a growing problem in South Africa, resulting in health risks, environmental degradation, and inefficient water usage (SERI, 2018). In developed areas, runoff is channelled into sewer systems and is treated via a city or municipality's stormwater management plan. This is not the case for informal settlements where the polluted runoff is discharged into rivers and other nearby water bodies without being treated. As such, the rivers near informal settlements often contain high nutrient concentrations and are polluted with chemically hazardous substances as well as unknown pathogens (Jones, 2017).

Of particular concern are high nutrient concentrations in surface waters affected by informal settlements. Nutrient pollution is the process whereby an excess of nutrients such as nitrogen and phosphorus are added to bodies of water and have the potential to act as fertiliser. This causes eutrophication and algal blooms within the water body, thereby disrupting the ecology of the river or water system (Nyenje *et al.*, 2010). Nutrient concentrations in surface waters affected by informal settlements are highly variable, being affected by time of day, day of week and seasonality, amongst others. This poses multiple challenges to the treatment of these surface waters.

River rehabilitation and surface water remediation efforts in waters affected by informal settlements need to be small-scale and cost-effective (Morgan, 2019). Engineered nature-based solutions are a popular option for surface water remediation as they are energy-efficient and easy to maintain. Biological water treatment systems are an engineered nature-based solution that involve a combination of physical, biological and chemical treatment processes and utilise the potential of microorganisms to remove contaminants from wastewater (Zhang *et al.*, 2015). Biofiltration is a low cost and effective biological method of treating contaminated that can be implemented to treat surface waters affected by informal settlements (Ramírez-Agudelo *et al.*, 2020). Biofiltration will be explored as a treatment method for the remediation of surface waters affected by informal settlements in this study.

1.2. The Focus of the Study

The main aim of this study was to assess the nutrient uptake ability of an engineered non-vegetated stone biofilter system, where the nutrient concentrations in the contaminated water source are highly variable (i.e., surface runoff from informal settlements). A pilot-scale biofilter was designed and constructed for this purpose. The suitability of the design was assessed using residence time distribution studies. The

residence time distribution studies were used to determine the hydraulic characteristics of the pilot biofilter, with these characteristics being used to assess the applicability of the biofilter design. The extent of non-ideal fluid flow behaviour was quantified in the residence time studies.

The Franschhoek Water Hub, a water research facility and living lab, was used as a reference site for this study. Surface water runoff contaminated by an informal settlement was collected from the Water Hub and used as the contaminated water source for the pilot-scale biofilter.

The Water Hub is situated in Franschhoek, which is located in the Stellenbosch Municipality of the Western Cape (Figure 1.1). The land use in the area is mostly agricultural land as shown in the map. The Water Hub is located along the Stiebeuel River downstream from an informal settlement, Langrug, and as such is affected by polluted runoff from an informal settlement. The human activities (e.g., cooking, cleaning of dishes and vehicles, washing of clothing, open defecation etc.) at Langrug contribute to nutrient pollution in the Stiebeuel River, making nutrient levels in the river highly elevated and variable. Polluted runoff collected from the Stiebeuel River was used as the contaminated water source in this study. Details regarding the Water Hub, Langrug informal settlement and the Stiebeuel River are further explored in Section 4.1.1.

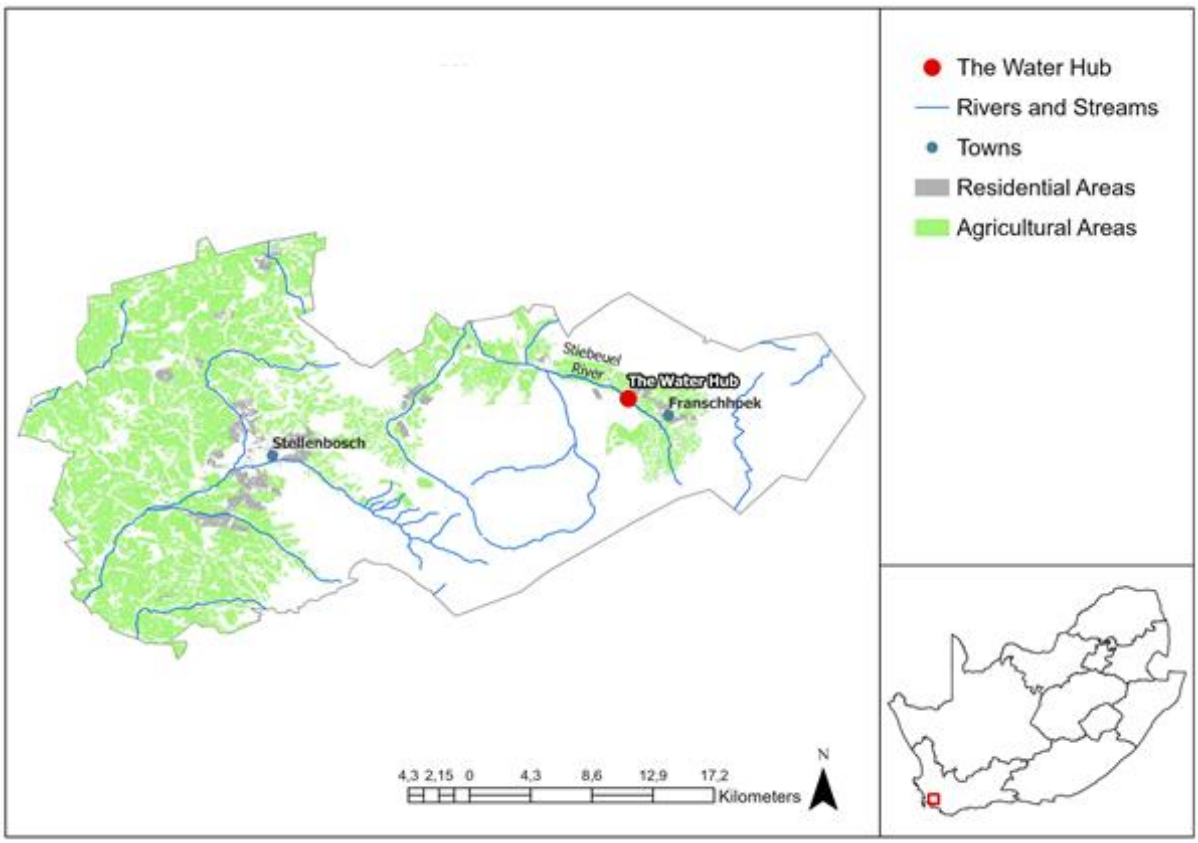

Figure 1.1: Water Hub location in relation to Stellenbosch Municipality

The Water Hub houses six large-scale biofiltration cells that are used to treat runoff from an informal settlement. These biofilters are defined as large-scale due to their dimensions (16 m long, 3.5 m wide and 0.7 m deep) and nominal capacity to treat up to 5000 L of contaminated water each; van Niekerk and Rudert (1999) define this as full-scale field operation for biofiltration treatment systems. Three of these large-scale biofiltration cells are vegetated while the other three are non-vegetated. Stones of various sizes and peach pips are used as filtration media in these biofilters. This study builds on the proof of concept of the six large-scale Water Hub biofilters in achieving significant nutrient reductions through determining key physical and biological sub-processes that occur in biofilter systems.

While nutrient concentration data from the Water Hub biofilters are available, accompanying information regarding inflows and outflows are not available. This results in an incomplete narrative on the performance of each of the biofiltration cells at the Water Hub, despite the proof of concept of their value being achieved. Detailed data from which to derive kinetic insight as well as to assess the flow patterns and potential zoning of the biofilters is difficult to obtain from the Water Hub itself due to logistical difficulties and the inability to operate the Water Hub Biofilters on a continuous flow regime. Through the pilot biofilter, the study sets out to explore fluid flow patterns in the biofilter and associated residence times. Bringing these together with nutrient degradation studies opens potential to explore degradation kinetics and establish key factors to inform biofilter design and operation.

The aims of this study were therefore as follows:

1. To ascertain the fluid flow patterns within a non-vegetated stone pilot biofilter and to assess the requirements for avoiding zoning and short circuiting.
2. To assess the nutrient uptake ability of an engineered non-vegetated stone biofilter system where the nutrient concentrations are low and variable
3. To investigate key physical and biological processes that govern biofilter operation.

1.3. Objectives of the Study

The aim of this study was to assess the extent of nutrient degradation that can be achieved in a pilot biofilter system and provide insights into biofilter design. To initiate the study, the pilot biofilter design was based on the design of the biofiltration cells at the Water Hub. To provide improved insight into the extent of nutrient degradation achievable, the hydraulic characteristics of the pilot-scale biofilter system were first determined. This indicates the appropriateness of the pilot-scale biofilter design and allows improvements in operation where necessary. Developing an understanding of fluid flow behaviour within the biofilter enabled the hydraulic characterisation of the

biofilter. Hydraulic characteristics such as fluid mixing, flow distribution and effective volume utilisation are important as they describe deviation from ideal behaviour. It is then possible to adjust the expected treatment performance to allow for the non-ideal behaviour of the biofilter.

Nutrient degradation studies determine the extent to which the pilot-scale biofilter can reduce the nutrient load from the contaminated water source through adsorption by the filtration media or biofilm activity. It also informs the system's tolerance of low nutrient phases. The nutrient degradation kinetics of the system have been quantified in these nutrient degradation studies. Nutrient degradation kinetics are defined as the rate at which nutrients, specifically nitrogen and phosphorus, are consumed by a system due to processes such as biodegradation and adsorption.

The specific objectives of this study are as follows:

1. To characterise the biofilter influent water quality (which is sourced from the Stiebeuel River).
2. To design and construct a biofilter based on the design of the biofiltration cells at the Water Hub.
3. To determine the hydraulic characteristics of the pilot biofilter using a residence time distribution model obtained through pulse tracer studies at a variety of flow rates.
4. To determine the nutrient degradation kinetics in the pilot biofilter through nutrient degradation studies conducted at a variety of flow rates.
5. To integrate these findings to determine potential for fit-for-purpose water exiting the biofilter.

1.4. Scope and Limitations of Study

By using a pilot-scale non-vegetated horizontally orientated subsurface flow stone biofilter, controlled operation is facilitated and data collection is made easier. This enables a more rigorous exploration of the biofilter-mediated water treatment process. The design of this pilot-scale biofilter is based on the design of the biofilters at the Water Hub. The construction of the pilot biofilter allows investigation of biofilter performance under a controlled laboratory environment; through this the impact of key variables were addressed.

The focus of the study is on the hydraulic characteristics and fluid flow dynamics of the system as well as the nutrient degradation kinetics within the pilot biofilter system. Investigating these aspects of the system provides an insight into whether physical or biological processes are more prominent as nutrient uptake mechanisms. This will provide guidance in developing a standard operating procedure to optimise nutrient

reduction in surface waters affected by informal settlements. This study also provides a basis for developing a standard operating procedure for the Water Hub biofilters to optimise their operation.

The main lab studies carried out on the pilot biofilter were tracer studies to determine the hydraulic characteristics of the pilot biofilter system and kinetic studies of nutrient degradation using contaminated runoff from the Stiebeuel River. The tracer studies were carried out under a continuous flow regime and steady state conditions. Due to constraints on the transport and storage of water from the Water Hub, nutrient degradation studies were carried out as a batch process with recycled flow of effluent to ensure continuous stable flow conditions in the biofilter.

The nutrient degradation studies focused on the degradation rates of ammonia, nitrate, nitrite and orthophosphate. The hydraulic and nutrient degradation studies are limited to the pilot biofilter. Further studies verifying the findings from pilot biofilter laboratory studies on the Water Hub biofilters form part of the recommended future work, due to limited field work potential. The nutrient degradation studies have been limited to the low-rainfall period, characterised by higher nutrient concentrations in the Stiebeuel River. The conditions in which the nutrient degradation studies occur are largely aerobic.

The water quality of the Stiebeuel River was characterised over a twelve-month field work period. Ammonia, nitrate, nitrite and orthophosphate concentrations were considered when characterising the water quality of the Stiebeuel River. Samples were collected at least twice a month. More frequent sampling was not possible due to logistical constraints.

1.5. Dissertation Structure

Chapter Two provides an in-depth review of the relevant literature and culminates with identifying the limitations in the literature to inform key research questions. The relevant literature includes insight into water quality in informal settlements as well as nature-based solutions to treat contaminated water with a focus on biofilters. The relevant literature on biofilters encompasses environmental biofilms, modelling fluid dynamics in a packed bed system as well as the pollutant removal mechanisms in constructed wetland systems. In Chapter Three, the research approach for this project is presented and the main experimental activities and their purpose are detailed. Chapter Four introduces the Franschhoek Water Hub and presents environmental data collected from the site. This chapter also discusses the implications of the environmental data on the lab studies. Chapter Five details the hydraulic characteristics of the pilot biofilter. Chapter Six focuses on the inoculation of the pilot biofilter, while Chapter Seven describes the nutrient degradation kinetics associated

with the pilot biofilter. The findings presented in Chapter Seven are the most pertinent when applied to the context of understanding the physical and biological processes that govern biofilter systems. Conclusions of the findings from this study as well as recommendations on further research are presented in Chapter Eight.

2. LITERATURE REVIEW

2.1. Introduction

Engineered nature-based solutions (NBS) to treat polluted runoff are a cost-effective and easy to maintain treatment option. NBS play an important role in improving biodiversity and facilitating the delivery of services while also providing numerous social, economic and environmental benefits (Oral *et al.*, 2020). Constructed wetlands, also known as biofilters, have proven to be a reliable engineered nature-based solution due to the ability to support physical, biological and chemical processes which reduce the pollutant load in contaminated surface waters (Ilyas and Masih, 2017).

Extensive research has been carried out in developed countries regarding the use of constructed wetlands and biofilters in the remediation of industrial effluent (Wu *et al.*, 2015), stormwater (Lucas *et al.*, 2015) and agricultural effluent (Vymazal and Březinová, 2015; Wang *et al.*, 2018; Li *et al.*, 2021). Some studies have targeted heavy metals as the target pollutants when using constructed wetlands to treat industrial effluent (Wu *et al.*, 2015) while nutrients (nitrogen and phosphorus) and pesticides are the target pollutants when using constructed wetlands to treat agricultural effluent (Vymazal and Březinová, 2015). Nutrients are also the target pollutant when using these systems to treat stormwater (Lucas *et al.*, 2015). Research regarding the use of constructed wetlands to treat polluted runoff from informal settlements is severely limited.

This chapter focuses on the relevant literature surrounding bioremediation of surface waters using biofilters, residence time distributions and the nutrient uptake processes that typically occur in biofilter systems. These are the key concepts that must be understood to design a biofilter system for the purpose of remediating surface waters affected by informal settlements and to develop an operating regime for the system. It is also important to understand water quality in surface waters affected in informal settlements, therefore this will also be discussed. The literature review will culminate in the objectives and key research questions associated with this project.

2.2. Water Quality in Surface Waters Affected by Informal Settlements

Informal settlements are usually located on the periphery of urban or peri-urban areas and are characterised by a high population density, inadequate access to clean water, drainage and sanitation (Housing Development Agency, 2012). Surface runoff from an informal settlement is a mixture of stormwater, greywater and sewage. This contaminated runoff drains into local rivers and can cause both health and environmental issues (Sampath *et al.*, 2010).

Informal settlements are often established adjacent to perennial rivers and streams as they provide a constant water source for domestic activities. Domestic water usages include but are not limited to drinking water, washing clothes, water for cooking and water for washing vehicles. In some cases, the contaminated river water is also used as an irrigation source for subsistence farming (Sampath *et al.*, 2010). The water quality in river systems that are in close proximity to informal settlements is therefore expected to continue to deteriorate due to the projected growth of these settlements. Consequently, water in these river systems will be unsuitable for domestic and agricultural use.

The water quality requirements for domestic use in South Africa as well as limits for disposal into rivers is shown in Table 2.1 (Department of Water Affairs and Forestry, 1996). Nitrate, nitrite, ammonium and orthophosphate are commonly focused on in water quality research because nutrient pollution is the leading source of water pollution in peri-urban areas (Ramírez-Agudelo *et al.*, 2020). The water quality requirements in Table 2.1 stipulate the nutrient concentration limits for domestic usage. Domestic usage entails water for drinking, cooking and sanitation.

Table 2.1: Water quality requirements for domestic use and disposal into rivers (Department of Water Affairs and Forestry, 1996)

Nutrient	Water Quality Requirements for Safe Domestic Use (mg/L)	Limit for Disposal into Rivers and Other Water Bodies (mg/L)
Nitrate (NO_3^-) & Nitrite (NO_2^-)	< 6	< 15
Ammonia (NH_3)	< 2	< 6
Orthophosphate (PO_4^{3-})	< 2.5	< 10

Table 2.2 shows selected water quality data from rivers downstream of informal settlements in South Africa. The Umlaas River catchment is located in the eThekwini Municipality in Kwa-Zulu Natal and discharges into the Indian Ocean. The river is located in an industrial urban area where pollutant loads from sewage treatment works and industrial effluent are discharged into the river. The Umlazi informal settlement, situated along the Umlaas River is a major non-point source of pollution in the river. Samples were taken 500 m downstream of the Umlazi informal settlement (Gangoo, 2003). The Fontein Spruit River is located in Bloemfontein, a city in the Free State province of South Africa. There are industrial activities occurring within the catchment from the Hamilton industrial area with the rest of the catchment land use being

primarily residential. There are several informal settlements contained within the catchment area with samples taken downstream of these settlements as well as downstream of the industrial area (Pretorius and de Villiers, 2002). The Plankenbrug River, a tributary of the Eerste River, is located in the Stellenbosch Municipality in the Western Cape. The land use in this area is predominantly peri urban. The Kayamandi informal settlement is situated within the catchment and is a major non-point source (due to runoff from precipitation carrying the pollutants into waterways) of pollution in the river. Samples were taken downstream of Kayamandi (Barnes, 2003).

Table 2.2: Water quality data for rivers downstream of informal settlements in South Africa

River	Province	NO_3^- [mg/L]	PO_4^{3-} [mg/l]	COD [mg/L]	Reference
Umlaas River	Kwa-Zulu Natal	9.5-16	156-192	187-197	(Gangoo, 2003)
Fontein Spruit	Free State	11.6-16.2	-	28-67	(Pretorius and de Villiers, 2002)
Plankenbrug River	Western Cape	137-472	16-38	-	(Barnes, 2003)

NO_3^- concentrations exceeded the limits for domestic use in all three rivers. The limit for discharge into rivers for NO_3^- was exceeded in the Plankenbrug River. The PO_4^{3-} concentrations exceeded the limits for discharge in the Umlaas, Fontein Spruit and Plankenbrug rivers. Chemical oxygen demand (COD) is an indicator of the amount of oxygen required to oxidise the organic matter in a sample. The COD range of 187-197 mg/L in the Umlaas River implied that the organic matter load in the Umlaas River was much higher than that of the Plankenbrug River. This comparison between rivers affected by informal settlements shows that the pollutant concentrations in these systems are highly variable and that each informal settlement and river system is unique.

It is projected that 2 billion people will be living in informal settlements worldwide by 2030 (United Nations Human Settlement Programme, 2003). Approximately 5.1 million people live in informal settlements in South Africa with local governments having the sole mandate to provide water and sanitation services to those living in informal settlements within their municipal areas. The Western Cape government provides full flush communal toilets to informal settlements with these toilets being drained by simplified sewers (rely on gravity to transport sewage), settled sewers

(small diameter sewers designed to prevent solids from entering the sewer network) or vacuum sewers (use differential air pressure to propel sewage) (Taing *et al.*, 2013). However, these sanitation services are often inadequate, overloaded or poorly maintained leading to an estimated 10.5% of informal households practicing open defecation (Housing Development Agency, 2012).

The rapid rate of urbanisation and thus the growth of informal settlements will inevitably lead to an increase in surface water pollution and so suitable treatment methods must be implemented to treat surface water runoff in informal settlements. Such suitable treatment options include nature-based solutions which are processes that involve the sustainable management and use of nature for tackling environmental challenges and more specifically in this case, water management challenges (Ramírez-Agudelo *et al.*, 2020).

Nature-based solution options in peri-urban areas are limited to permeable pavements, bioswales and constructed wetlands/biofilters. While permeable pavements and bioswales are efficient treatment options; they are severely limited in the volume of contaminated water that they are able to process, making them more suitable for stormwater management than river rehabilitation (Ramírez-Agudelo *et al.*, 2020). Biofilters and constructed wetlands are passive treatment systems that can significantly reduce nutrient concentrations in surface water runoff from informal settlements if designed correctly (Sletto, Tabory and Strickler, 2019). Biofilters will be discussed in more detail in this literature review as they are the focus of this study.

2.3. Biofilters as a Water Treatment Method

Biological wastewater treatment systems utilise the potential of microorganisms to remove contaminants from wastewater (Nemani *et al.*, 2018) and involve a combination of physical, biological and chemical treatment processes. These processes include sedimentation of suspended solids, adsorption of pollutants, precipitation of nutrients, redox reactions and microbial respiration (Bratieres *et al.*, 2008).

Biofiltration is a process that removes biodegradable compounds from wastewater through biodegradation, filtering suspended solids and adsorption of micropollutants (Jing *et al.*, 2015). Fixed film biofiltration systems are biological treatment processes that utilise natural or synthetic solid media such as rock, ceramic or wood that will support the formation of a biofilm within its porous structure (Cohen, 2001). The biofilm is a wet layer surrounding the filter media which houses a diverse microbial community. The biofilm is made up of extracellular polymeric substances (EPS) as well as microorganisms (Cheng *et al.*, 2017). This microbial community is responsible for the removal of nutrients, primarily nitrites, nitrates and ammonia, from the polluted

water (Li *et al.*, 2017). Biofilters can be vegetated or non-vegetated. Non-vegetated biofilters rely solely on physical filtration and microbial activity to reduce the pollutant load. The majority of the activity within vegetated biofilters can be attributed to the vegetation itself. The vegetation acts as a physical filter, a substrate for microorganisms and contributes to the creation of anaerobic zones which is key for certain biological processes (Nivala et al., 2017). The major disadvantage of vegetated biofilters is that the vegetation results in non-ideal fluid flow patterns and inefficient volume utilisation which is why non-vegetated biofilters will be the focus of this study (Zhang *et al.*, 2016). Non-vegetated biofilters are classified into one of two groups according to the hydraulic regime under which they are operated: surface flow or subsurface flow (Fu *et al.*, 2017). Subsurface flow systems are relevant to this study and will be discussed further below.

2.3.1. Types of biofilters

Subsurface flow biofilters consist of a deep basin containing porous, granular media such as gravel, peach pips, rocks or biochar (Samsó *et al.*, 2016). This filter media supports the growth of emerging vegetation if the biofilter is vegetated. The fluid flow in the system occurs below the surface of the filtration media with the flow being either in the vertical or horizontal direction (Fu *et al.*, 2017). Anaerobic processes are dominant in subsurface flow systems due to the volume beneath the surface of the filter media being saturated with water. Aerobic zones are usually present towards the surface allowing aerobic pollutant removal processes to occur within the system (Robertson *et al.*, 2018).

Subsurface flow systems have several advantages over surface flow systems and are thus more suitable as a treatment method. Some of these advantages include a low likelihood of insects breeding within the system and a lack of a foul odour due to the fluid flow occurring below the surface of the filter media (Nivala *et al.*, 2017). The main advantage is the greater surface area provided for treatment by the filter media as compared to surface flow systems. This means that smaller subsurface flow systems result in greater pollutant removal than their larger surface flow counterparts (Fu *et al.*, 2017).

Subsurface flow biofilters are further classified into horizontal flow systems or vertical flow systems. In vertical subsurface flow biofilters, fluid is introduced to an inlet at the top of the biofilter and flows downwards through the filter media. Vertical flow systems are limited to batch operation with contaminated water being intermittently loaded into the system (Robertson *et al.*, 2018). Vertical flow systems are largely aerobic in nature due to air entering the system between loading cycles. This limits the anaerobic pollutant removal processes in the system. These systems are highly efficient at

removing suspended solids due to the rapid gravity assisted flow causing suspended solids to be trapped by the filter media (McKie *et al.*, 2019). An example of a vertical flow system is seen in Figure 2.1.

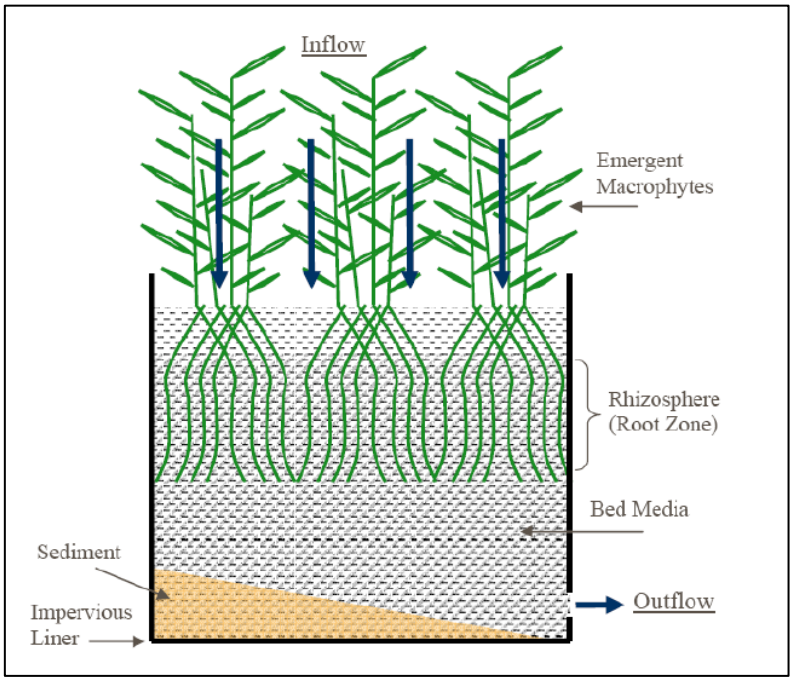

Figure 2.1: A vertical subsurface flow biofilter (Russo, 2008)

An advantage of vertical flow systems is that they are more efficient than horizontal flow systems with a smaller surface area being required to achieve the same pollutant removal as a horizontal flow system (Fu *et al.*, 2017). A drawback of the vertical flow system is the limited phosphorus removal capability due to the flow direction regularly dislodging adsorbed substrates. A further disadvantage of vertical flow systems is frequent clogging of the pores of the biofilter due to the high rate of sedimentation achieved in vertical flow system (Robertson *et al.*, 2018). The operation of subsurface flow vertically orientated biofilters requires greater technical expertise and more frequent maintenance than horizontally orientated biofilters (McKie *et al.*, 2019).

At the laboratory scale, bioretention columns are an effective vertical flow system that allows for up-flow, down-flow and mixed flow. Bioretention columns are effective at nutrient and heavy metal reduction but scalability and feeding methods must be considered before attempting these systems at the field scale. Column systems are often difficult to scale-up but a cascaded system can be used to increase treatment capacity (Takaijudin *et al.*, 2021). A barrier to implementation of the up-flow and mixed flow bioretention systems presented in Zhang et al. (2019) is the non-passive treatment nature of the system which requires an energy input to generate fluid flow patterns in the system. A constant energy supply would be challenging in resource-

scarce areas and the skilled personnel for maintenance of such a system may not be available.

Fluid flows horizontally through the filter media below the surface in horizontal flow systems. Anaerobic conditions are dominant in horizontal flow systems due to the area beneath the surface being water saturated. This generally makes anaerobic pollutant removal processes more efficient than aerobic pollutant removal processes in horizontal flow systems (Fu *et al.*, 2017). Smaller aerobic zones are usually present towards the surface of the biofilter as well as around the roots of vegetation with aerobic pollutant removal processes occurring in these zones (Robertson *et al.*, 2018). An example of a horizontal subsurface flow biofilter can be seen in Figure 2.2.

A disadvantage of the horizontal flow systems is the larger surface area required to achieve the same extent of pollutant removal as a smaller vertical flow system. The main advantage of horizontal flow systems is that they can be operated continuously or cyclically (batch process). These systems are easier to maintain with filter clogging occurring less frequently than in other types of biofilters (McKie *et al.*, 2019).

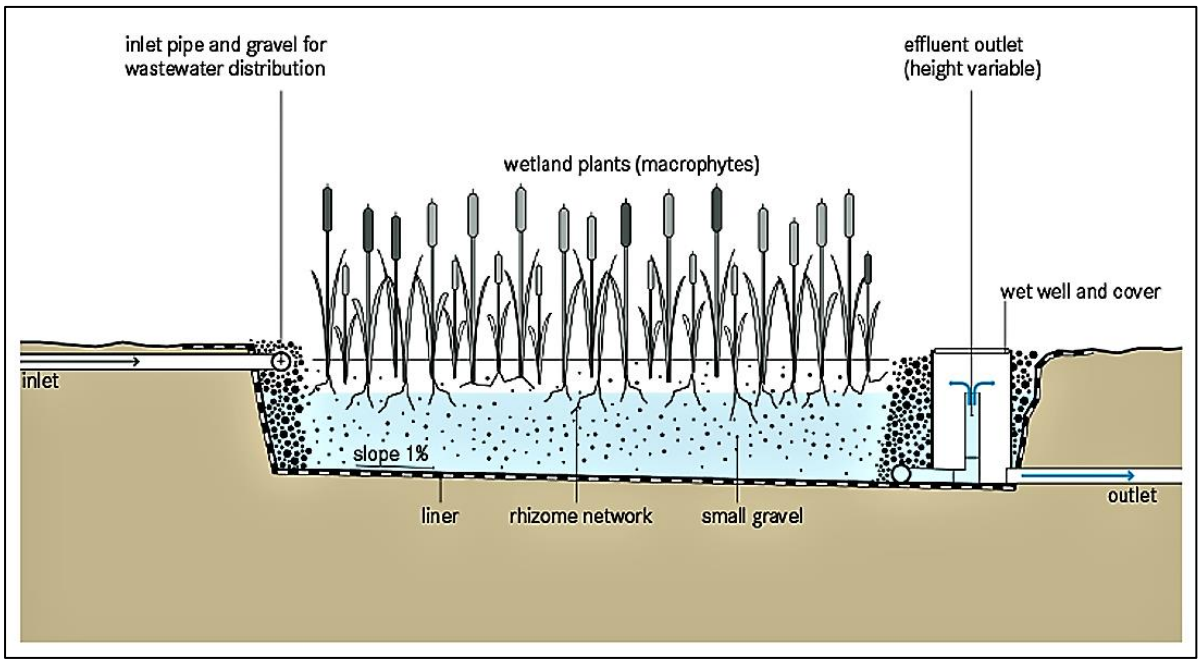

Figure 2.2: A horizontal subsurface flow biofilter (Image Taken from Tilley et al., 2014)

2.3.2. Filter media

Filter media in horizontal subsurface flow biofilters are granular in nature and serve multiple purposes, namely screening suspended solids and providing a structure for the growth of biomass (Fu *et al.*, 2017). Materials such as stone, quartz sand, gravel and ceramic have commonly been used as packing material for biofilters (Robertson *et al.*, 2018). These materials are commonly used due to their cost-effective nature.

More expensive substances such as granular activated carbon have also been known to be used as packing material for biofilters (McKie *et al.*, 2019). Granular anthracite, which is a hard, compact variety of coal, has been used as a cheaper alternative to granular activated carbon (Velten *et al.*, 2011).

The filter media should have an exposed surface area that is large enough for biofilm development. The texture of the media surface is also of importance as high surface texture will protect the biofilm from shear stress (Robertson *et al.*, 2018). Biofilm is a thin slimy layer surrounding the filter media which consists of water, extracellular polymeric substances and a diverse microbial community (McKie *et al.*, 2019).

Biofilm formation occurs in a three-step process. The first step occurs when microorganisms attach themselves to the filter media. The second step is the growth and expansion of microbial colonies on the surface of the filter media. The microbial growth consumes organic matter and eventually decays and detaches from the filter media (Velten *et al.*, 2011). Biological acclimation is the process whereby the biofilm becomes fully developed. Biological acclimation generally takes 30 to 40 days, but this acclimation time is highly variable and is dependent on the filter operating conditions (Nemani *et al.*, 2018).

A study by Cheng *et al.* (2017) found that typical biofilms contain approximately 90% extracellular polymeric substances (EPS) with less than 10% of the dry weight being microorganisms. The extracellular matrix is produced by the microorganisms situated in the biofilm and contains lipids, proteins, polysaccharides and nucleic acid. The main purpose of the extracellular matrix is to allow for adhesion of the biofilm onto the filter media. The extracellular matrix also acts as a source of nutrients for the microbial community and ensures aggregation of microorganisms. To a lesser extent, the matrix also facilitates the adsorption of nutrients and contaminants to the biofilm (di Tommaso *et al.*, 2019).

The filter media must also have a porosity high enough to ensure maximum adsorptive potential for the removal of pollutant (Robertson *et al.*, 2018). Granular media less than 2 mm in diameter, such as sand, are disadvantageous due to the media regularly clogging with biomass and adsorbed pollutants (Zhang *et al.*, 2015).

Granular activated carbon (GAC) has proven to be the most effective filter medium as it results in the highest total pollutant removal. GAC can house more biomass due to its high porosity, large surface area and irregular shape (Atabaki, Siong and Idris, 2013). It has been known to accommodate five times as much biomass as anthracite which can be attributed to the larger available surface area for biomass growth (Yapsakli and Çeçen, 2010). GAC also has high pollutant removal efficiencies at

temperatures below 20°C as well as having high adsorptive capabilities which is instrumental to phosphorus removal from wastewater (Ross *et al.*, 2019).

The main drawbacks associated with GAC are the high expenses of the filter medium itself and the costs associated with regularly replacing the granular activated carbon media as it becomes saturated and loses its adsorptive capacity (Sbardella *et al.*, 2018). It is recommended that a smaller granular activated carbon biofilter is used as a secondary treatment or polishing step due to the high costs associated with this filter medium (Lin *et al.*, 2019).

Anthracite is a fuel material and the exploration of its suitability as a substrate in water treatment is a recent development. It is often used in lieu of granular activated carbon as they are both carbon-based substrates with anthracite being significantly cheaper. Quartz sand is a readily available and cost-effective environmental filter medium. It is a stable silicate that possesses excellent adsorptive capabilities and is widely used as a filter medium (Jiang *et al.*, 2014). Stone and gravel are the most readily available and inexpensive filter media which makes them an appropriate choice for a low-cost filtration system. River stones are a popular choice as the filter media for biofilters and constructed wetlands as they are cost-effective and mimic the natural environment (Nivala *et al.*, 2017).

Table 2.3: Performance of different types of filter media

Filter Media	COD Reduction	Total Nitrogen Reduction	Total Phosphorus Reduction	Reference
Small River Stones	85.6%	85%	88%	(Rasool *et al.*, 2018)
Quartz Sand	82.1%	73.8%	63.1%	(Lin *et al.*, 2019)
Anthracite	89%	78.1%	90.4%	(Moges *et al.*, 2017)
GAC	92%	89%	91.5%	(Jiang *et al.*, 2014)

Table 2.3 compares the performance of four different types of filter media. The treatment performance with respect to chemical oxygen demand (COD), total nitrogen and total phosphorus reduction are compared in the table. All studies referenced in

Table 2.3 were conducted at the pilot-scale on horizontal subsurface flow biofilters. A biological acclimation period of at least 30 days was observed to allow microbial colonisation of the biofilter systems and the biofilters were operated cyclically with a treatment period of 4 – 7 days being observed. Artificial wastewater was used as the contaminated water source in the studies.

It can be seen from Table 2.3 that granular activated carbon is the filter media with the highest COD, total nitrogen and total phosphorus reduction. Quartz sand performed the poorest with the lowest COD, total nitrogen and total phosphorus reduction. The performance of anthracite as a filter media is comparable to granular activated carbon for COD and total phosphorus removal. However, the performance of anthracite with respect to total nitrogen removal is significantly lower than that of granular activated carbon with anthracite achieving a 78.1% reduction in total nitrogen as compared to the 89% achieved by granular activated carbon. River stone proved to be a reliable filter media with high COD, total nitrogen and total phosphorus reductions.

Filter clogging becomes a concern as the age of the filter media increases. Clogging is a phenomenon that occurs when there is too much microbial growth or a high accumulation of organic matter and pollutants in the filter which impedes fluid flow within the biofilter (Samsó *et al.*, 2016). Clogging can be resolved by replacing the filter media, which is often expensive, or by employing the backwashing procedure. Backwashing refers to pumping water backwards through the filter media. This will dislodge the accumulated matter and will purge the system of excess biomass. Factors that must be considered are the backwashing rate, duration as well as the handling of wastewater generated from backwashing (Tilley *et al.*, 2014). Another method that is used to minimise filter clogging is the addition of a sedimentation pre-treatment step to reduce the quantity of suspended solids entering the biofilter system (Greenstein *et al.*, 2018).

2.3.3. Continuous vs. cyclical operation

A study by Oh, Hammes and Liu (2018) found that horizontal subsurface flow biofilters display a greater total nitrogen and organic carbon reduction when operated cyclically. The microbial population is highly dependent on the way the filter is operated and cyclical operation preferentially selects for healthy microorganisms which increases the biodegradation rate (Nemani *et al.*, 2018). This is known as the fasting and feasting phenomenon where the microorganisms are deprives of nutrients for a certain period which results in competition for nutrients between the microbial species with the strongest species surviving.

Continuous flow systems are known to be predominantly anaerobic in nature due to the filter media being constantly saturated with water. Cyclically operated systems

contain both aerobic and anaerobic zones due to the introduction of air to the system in the non-operational periods between wastewater loading (di Tommaso *et al.*, 2019). This makes cyclically operated systems well suited to biodegradation processes that require aerobic or anaerobic conditions (McKie *et al.*, 2019). While cyclical operation provides greater total nitrogen and organic carbon reduction; this method of operation is limited to smaller volumes of contaminated water as compared to continuous flow operation.

2.3.4. Operating temperature

Temperature has a significant effect on biofilter performance with biofilter performance deteriorating at temperatures below 10°C (Tilley *et al.*, 2014). This holds particularly true for total nitrogen reduction as microbial activity within the biofilter is mostly responsible for nitrogen removal. Temperature has a profound impact of the activity and growth rate of nitrifying and denitrifying microorganisms in the biofilm (Lauderdale, 2011). Studies have found that that the maximum growth rate of nitrifying bacteria occurs between 15°C and 30°C. The growth of nitrifying bacteria sharply declines below 15°C and reaches a minimum at 10°C (Liu *et al.*, 2021; Manirakiza and Sirotkin, 2021).

In general, lower temperatures correlate to lower pollutant removal efficiencies. This is due to a decrease in microbial activity and a change in the composition of the microbial community which occurs at lower temperatures. The effect of low seasonal temperatures can be mitigated by increasing the hydraulic retention time to achieve the desired water quality (Moges *et al.*, 2017). Higher HRT indicates greater exposure to lower functioning microbes due to reduction in metabolic activity

It has been found that the major energy inputs to the system occurs in the form of influent water to the system and heat transfer from the ground. Heat transfer from the ground can be circumvented through the insulation of the biofilter with a concrete or plastic lining. This lining also prevents leakages and infiltration of contaminated water into groundwater if the system is an outdoor one. The implication is that the temperature of the influent contaminated water has a greater influence on the temperature throughout the biofilter than the ambient temperature (Nivala *et al.*, 2017). This inlet temperature is maintained throughout the biofilter with a slight increase in temperature experienced during periods of microbial respiration.

2.3.5. Hydraulic retention time in cyclically operated systems

Hydraulic retention time has a significant impact on nutrient and organic carbon reduction in biofilters that are operated cyclically. A hydraulic retention time of 3-5 days is considered sufficient for total phosphorus and organic carbon removal (Tilley *et al.*,

2014). The performance of a cyclically operated pilot-scale horizontal subsurface flow constructed wetland was monitored over numerous hydraulic retention times with the results being reported in Table 2.4 (Merino-Solís *et al.*, 2015).

Table 2.4: Constructed wetland performance over different hydraulic retention times (Merino-Solís *et al.*, 2015)

Hydraulic Retention Time	COD Reduction (%)	Total Nitrogen Reduction (%)	Total Phosphorus Reduction (%)
2 Days	84.2 ± 4.0	32.5 ± 13.2	43.8 ± 12.3
3 Days	83.2 ± 3.1%	32.9 ± 17.7	55.4 ± 16.0
4 Days	85.7 ± 3.90	34.1 ±16.0	71.2 ± 8.7

The dimensions of the pilot constructed wetland used in this study are: 0.65 m deep, 2.3 m wide and 4 m long. The constructed wetland was filled with stones that are 25 mm in diameter. The results of this study are presented in Table 2.4. It can be seen that majority of the COD reduction occurs within 2 days while it takes up to 4 days for a 71.2% reduction in total phosphorus.

2.4. Residence Time Distributions in Horizontal Subsurface Flow Biofilters

Hydraulic residence time has been identified as a key factor that affects the performance of horizontally orientated subsurface flow biofilters (Singh Chaudhary *et al.*, 2003). However, the actual hydraulic residence time of the system tends to differ from the theoretic hydraulic residence time in continuous flow systems. This is due to the type of mixing patterns and non-ideal fluid flow behaviour in the system (Benjamin and Lawler, 2013). The theoretical residence time of a system, τ, is calculated using equation 2.1 (Fogler, 2011).

$$\tau = \frac{V}{Q} \qquad \text{Equation 2.1}$$

Where V is the theoretical available volume of the system (L);

Q is the volumetric flow rate (L/min)

In an ideal system, all fluid molecules spend the same amount of time in the system. However, most systems have a residence time distribution meaning that all molecules do not spend the same amount of time in the system. This is an indicator of non-ideal fluid flow behaviour. A residence time distribution is essentially an exit age distribution which determines fraction of the fluid that has remained in the reactor between t1 and t2 (Benjamin and Lawler, 2013).

Determining the residence time distribution of the biofilter system is key to gaining a better understanding of the flow characteristics of the system. It is a tool used in reactor theory to enable the determination of the available volume of and degree of mixing in the system. The residence time distribution of a reactor has a large impact on reactor performance. Operating decisions such as feed flow rate are often made with the assumption that there is ideal fluid flow behaviour in the system. It is therefore necessary to quantify the residence time distribution at the proposed system operating conditions in order to diagnose and adjust for non-ideal fluid flow (Fogler, 2011).

2.4.1. Using tracer studies to determine the system's residence time distribution

A tracer study is a method of determining the hydraulic behaviour within a reactor. Tracer studies are a valuable tool to help understand the residence time distribution of a reactor as well as to diagnose non-ideal fluid behaviour (Fogler, 2011). A tracer is a non-reactive and non-adsorptive substance that is added to a reactor inlet to determine the residence time distribution of the reactor (Bonner, Aylward, Harley, *et al.*, 2017). The tracer is introduced to the reactor feed and its concentration is measured at the reactor outlet. Chemical dyes are the most popular tracers as they are inexpensive (Benjamin and Lawler, 2013).

Tracer studies must be carried out under steady state flow conditions. It is prudent to conduct tracer studies at multiple flow rates to determine whether the hydraulic characteristics are substantially affected by flow rate. There are two types of tracer studies: the pulse input and the step input (Fogler, 2011). In a pulse tracer study, a volume of tracer is injected to the system inlet at time 0. In a step input tracer study, a constant concentration is continually introduced to the system inlet until the concentration of tracer at the outlet is indistinguishable from the feed. The tracer concentration at the outlet is continuously monitored in both these types of studies. The input and concentration response curve for a pulse tracer study is shown in Figure 2.3.

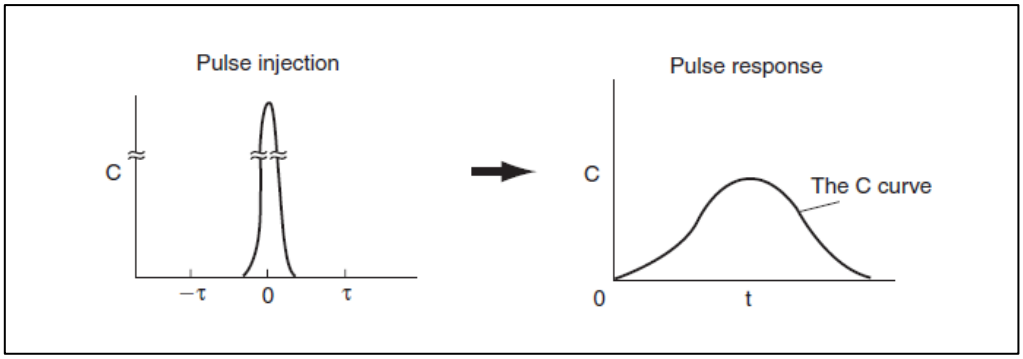

Figure 2.3: A pulse tracer injection and the corresponding concentration response curve (Fogler, 2011)

The residence time distribution function obtained from the concentration-time data of a pulse tracer is shown in Equation 2.2.

$$E(t) = \frac{C(t)}{\int_0^\infty C(t)\,dt} \qquad \text{Equation 2.2}$$

It is important to note that $\int_0^\infty E(t)\,dt = 1$ as the fraction of the fluid residing in the system between t = 0 and t = ∞ is 1. The advantage of a pulse tracer study is that a much smaller amount of dye is required as compared to a step tracer study. Less equipment is required for a pulse tracer study than a step tracer study. The drawbacks of a pulse tracer study include that fact that it is possible to miss the tracer concentration peak at the system outlet (Benjamin and Lawler, 2013). This negatively affects the reproducibility of the tracer study results. The input and concentration response curve for a step tracer study, taken from (Fogler, 2011) is shown in Figure 2.4.

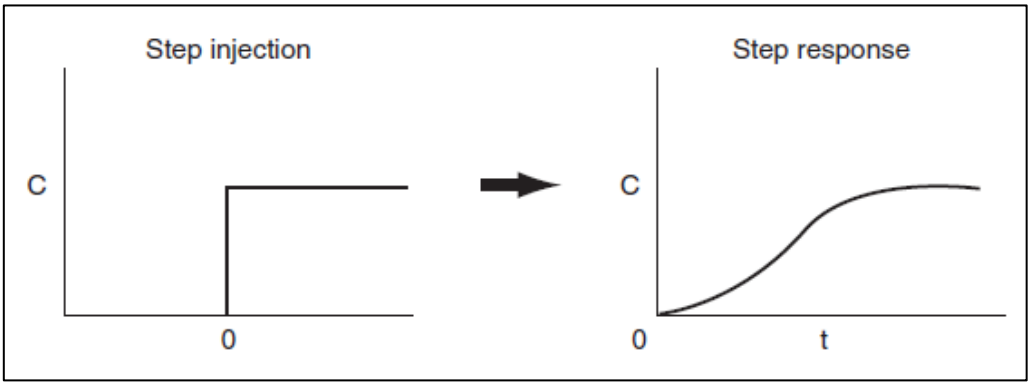

Figure 2.4: A step tracer injection and the corresponding concentration response curve (Fogler, 2011)

In a step tracer study, the concentration-time data is related to a cumulative distribution function, F(t), shown in Equation 2.3.

$$F(t) = \frac{C(t)}{C_0}$$ Equation 2.3

Where C(t) is the concentration measured at the outlet at the given point in time while C_0 is the initial inlet concentration.

The residence time distribution of a step tracer study is determined by the following equation:

$$E(t) = \frac{dF(t)}{dt}$$ Equation 2.4

The advantages of a step tracer study include the fact that it is not necessary to keep track of the amount of tracer that is introduced to the reactor inlet. The drawbacks of a step tracer study include the fact that much larger quantities of tracer as well as more equipment are required than in a pulse tracer study. It is also difficult to maintain a consistent tracer inlet concentration which leads to discrepancies in the results obtained from the step tracer study (Benjamin and Lawler, 2013).

2.4.2. Ideal fluid behaviour

The fluid flow in biofilters is usually modelled after the behaviour of ideal continuous stirred tank reactors (CSTRs) or ideal plug flow reactors (PFRs). Each of these exhibit vastly different mixing patterns and behaviours. CSTRs are operated at steady state with ideal CSTRs being perfectly mixed. This means that the temperature, concentration and reaction rate of a molecule are independent of time and position. Molecules are indistinguishable from each other in CSTRs with every variable being the same at every point in the system. It can then be assumed that the concentration at the reactor outlet is identical to the fluid inside the reactor (Fogler, 2011). CSTRs are known to be less efficient than PFRs due to a larger reactor volume being required to achieve the same reaction rate as a PFR. However, CSTRs are preferable for systems with microbial activity as immediate mixing allows for microbial activity to commence with inhibitory concentration levels are avoided (Benjamin and Lawler, 2013).

Ideal plug flow in packed bed reactors occurs when there are no radial gradients in concentration, temperature and reaction rate. The concentration of fluid moving through the reactor is dependent on the fluid molecule's position in the reactor. There is no mixing in the axial direction but perfect mixing in the radial direction. This means that the velocity and concentration are uniform across any cross-sectional 'slice' of the reactor (Fogler, 2011). The uniform velocity across cross-sectional "slices" of the reactor results in greater hydraulic efficiency than is typically displayed in CSTRS. This

means that effective volume utilisation is greater in PFRs than in CSTRs (less dead space). For equally sized reactors, plug flow reactors are also known to exhibit superior performance over CSTRs for reactions where reaction rate is dependent on reactant concentration (first, second or third order reactions) (Benjamin and Lawler, 2013).

2.4.3. Non-ideal fluid behaviour

Non-ideal fluid flow behaviour in a reactor includes dead zones/ dead spaces and fluid channelling. Dead space is a phenomenon the occurs when a portion of the available volume of the reactor is not utilised, generally due to the design of the reactor (Fogler, 2011). Dead zones are usually associated with corners of the reactor but can also arise when the influent has a different density to the fluid already in the reactor (Benjamin and Lawler, 2013).

Short-circuiting is a term that is used to describe the phenomenon that occurs when some of the fluid follows a shorter path through the reactor than the intended path. The fluid therefore bypasses a certain volume of the reactor and exits after a shorter than intended residence time. Packed bed reactors are prone to short circuiting (Benjamin and Lawler, 2013).

There are numerous causes of non-ideal behaviour in horizontal subsurface flow biofilters. The first of these is filter media that is non-uniform in both size and shape. The position of inlets and outlets can also lead to fluid channelling if poorly positioned. For example, a biofilter with the inlet and outlet at the same height will cause short-circuiting at the height of the inlet and outlet as well as a large dead zone below the height of the inlet and outlet. The third and most prominent cause of dead space in biofilters is filter clogging that occurs due to biofilm growth on the filter media as well as due to adsorption of pollutants onto the filter media (Bonner, Aylward, Kappelmeyer, *et al.*, 2017).

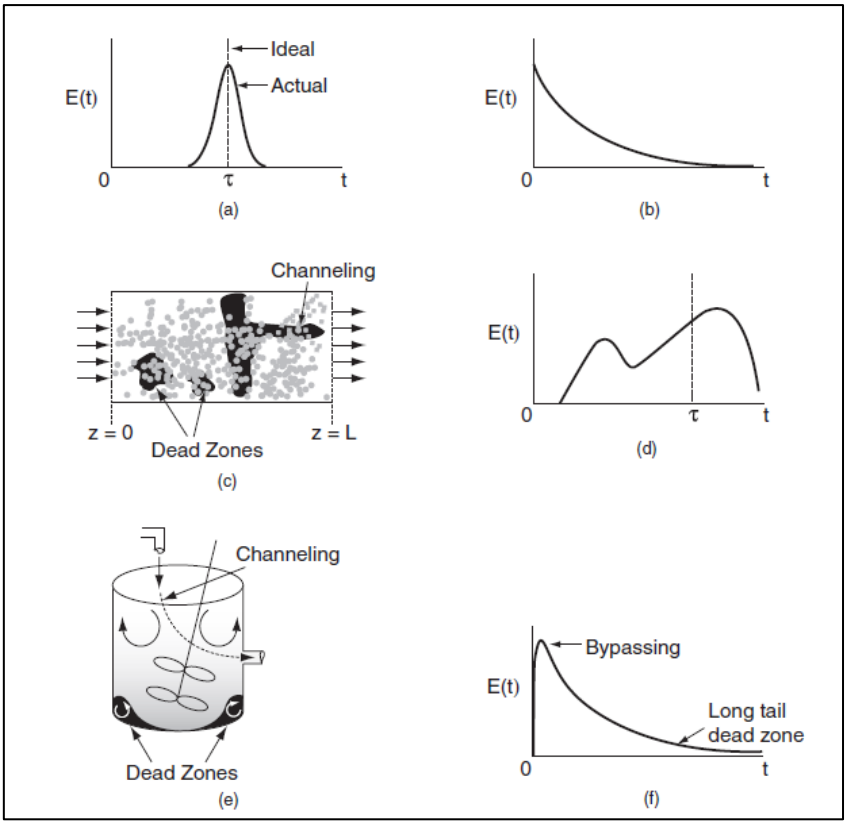

Figure 2.5: Ideal and non-ideal residence time distributions taken from Fogler, 2011

Figure 2.5 shows the common characteristics of residence time distributions under ideal and non-ideal conditions. (a) shows the RTD of an ideal plug flow reactor while (b) shows the RTD of an ideal continuous stirred tank reactor. (d) is the RTD associated with the packed bed reactor (c) that has dead zones and channelling. (f) is the RTD associated with the tank reactor (e) that has both dead zones and channelling.

2.4.4. Expected fluid behaviour in horizontal subsurface flow biofilters

The hydraulic characteristics of horizontal subsurface flow biofilters often approximate plug flow behaviour. Subsequently, there is minimal mixing in these systems while pollutant concentrations vary along the length of the biofilter (concentration gradient in axial direction). Empirical data from analysis of horizontally orientated subsurface flow fixed film biofiltration systems show that fluid flow in the axial direction is dominant and axial dispersion is minimal. These systems favour pollutant degradation where reaction rate is dependent on reactant concentration due to the low degree of mixing in the system. Therefore, adequately designed horizontal subsurface flow biofilters should display the characteristics of plug flow dispersion reactors (Narayanan and Narayan, 2019).

2.5. Pollutant Removal Mechanisms in Horizontal Subsurface Flow Biofilters

Nutrient pollutants such as inorganic nitrogen (NH_3, NO_3^-, NO_2^-) and inorganic phosphorus are usually found in high concentrations (exceeding 30 mg/L) in waters affected by informal settlements (Jones, 2017). It is therefore important to understand the physical, chemical and biological processes that govern the removal of these pollutants in non-vegetated biofilters. It is widely accepted that phosphorus is mostly removed through adsorption onto the filter media while inorganic nitrogen is mostly removed through biological processes occurring in the biofilm (Greenstein *et al.*, 2018).

2.5.1. Mechanisms of phosphorus removal

Phosphorus is theorised to be the most limiting nutrient in most aquatic environments which means that the quantity of phosphorus available in an aquatic ecosystem determines the rate at which vegetation and algae are produced. Phosphorus is a growth limiting nutrient because it occurs in naturally low concentrations in the environment. The most bioavailable form of phosphorus is orthophosphate (PO_4^{-3}) which is present in water systems in a dissolved state (Hauer and Lamberti, 2017). Phosphorus is a major contributor to eutrophication in water bodies which makes its removal from polluted water imperative (Nyenje *et al.*, 2010).

Figure 2.6 shows that the phosphorus found in catchment areas is introduced through surface runoff. This is mostly a result of the runoff from agricultural lands where fertilisers are used extensively. Phosphate in the soil is also leached into aquatic systems such as rivers, streams and lakes (Hauer and Lamberti, 2017). The majority of the orthophosphate present in the influent waters of constructed wetland systems are removed through adsorption and chemical precipitation. Microbial activity accounts for just 4% of orthophosphate removal in constructed wetlands (Ilyas and Masih, 2017).

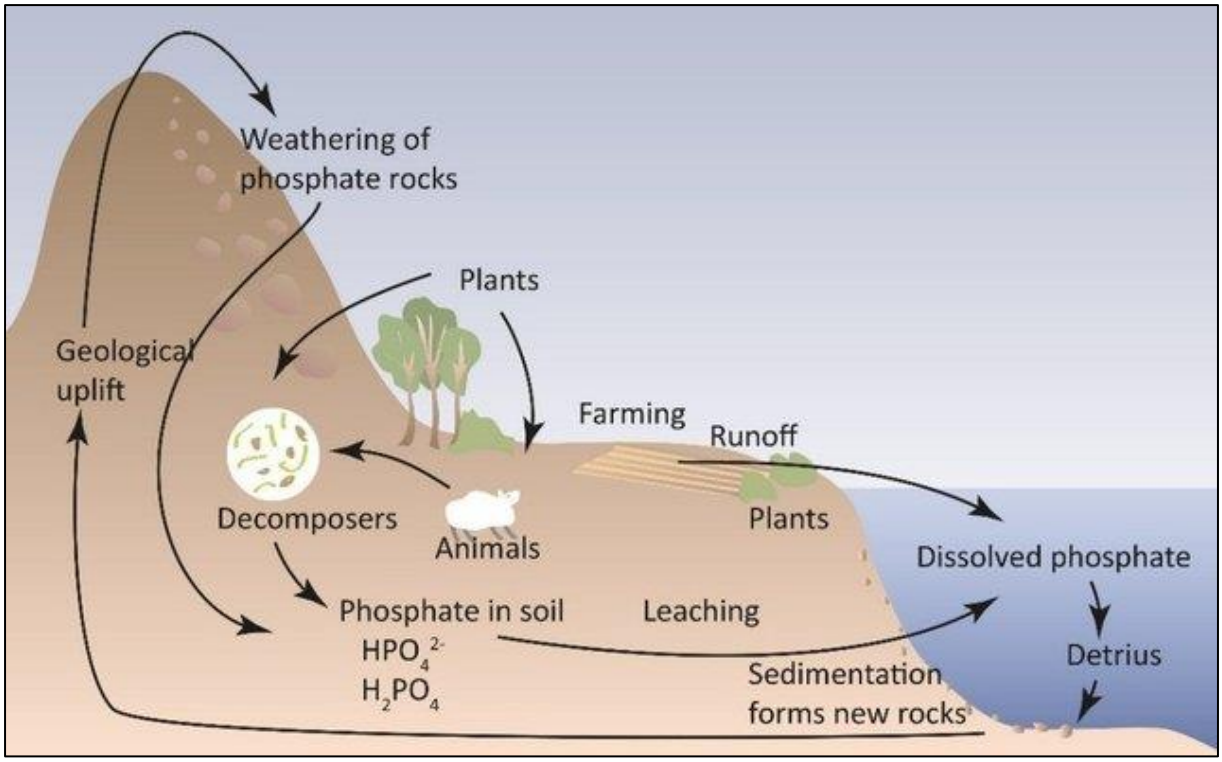

Figure 2.6: The phosphorus cycle taken from Lappalainen et al., 2016.

Orthophosphate can also be removed from contaminated water through chemical precipitation. This occurs through precipitation reactions with minerals containing aluminium, magnesium, calcium or iron. Filter media containing magnesium, calcium or iron therefore promotes orthophosphate removal. These precipitation reactions occur in low pH environments with insoluble phosphate salts forming as a product of the precipitation reactions (Hauer and Lamberti, 2017).

2.5.2. Mechanisms of nitrogen removal

Inorganic nitrogen pollutants found in water systems include ammonia, nitrate, nitrite and atmospheric nitrogen (N_2 gas). An excess of inorganic nitrogen in aquatic ecosystems can be harmful to aquatic life (Lappalainen *et al.*, 2016). Figure 2.7 depicts the nitrogen cycle and shows the various nitrogen transformation processes.

From Figure 2.7, it can be seen that ammonia is transformed and removed through the nitrification process. The nitrification process is followed by the denitrification process. These two biological processes are responsible for the removal of majority of inorganic nitrogen in biofilter systems.

Nitrification is defined as the biological oxidation of ammonium to nitrate with nitrite being an intermediary in the process. Nitrification occurs in aerobic environments. The overall nitrification reaction is shown in Equation 2.5 (Hauer and Lamberti, 2017).

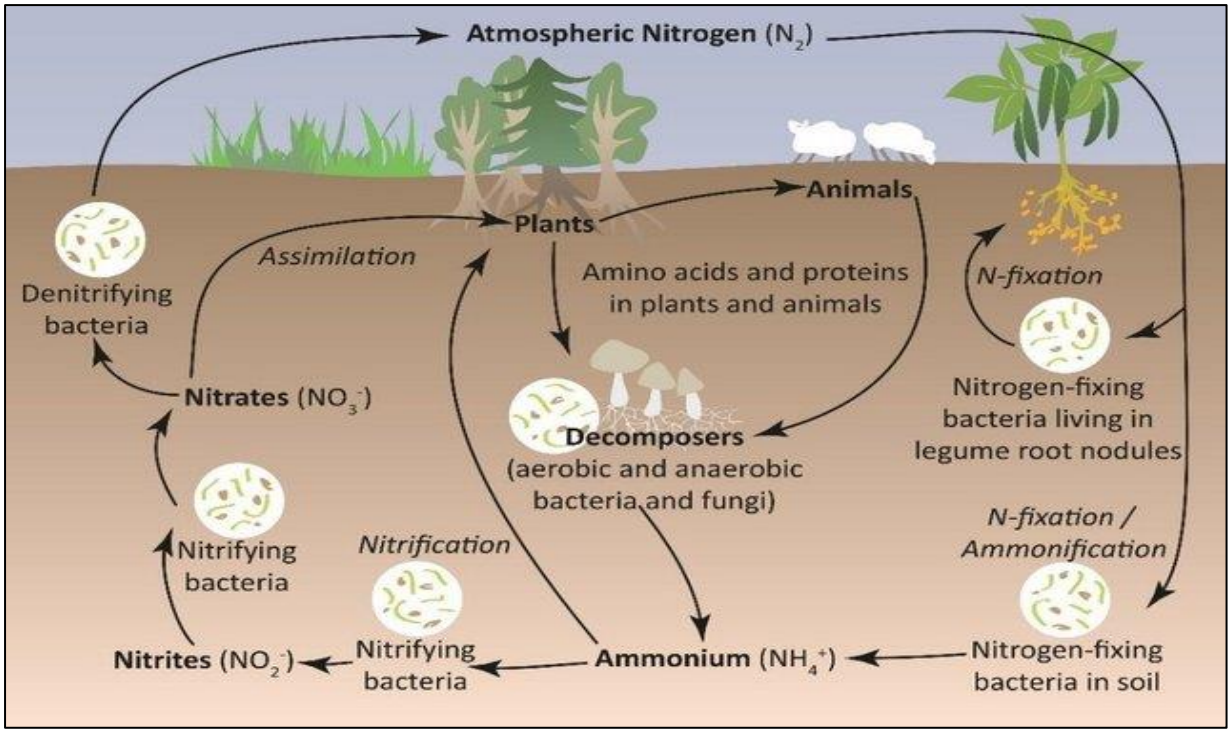

Figure 2.7: The nitrogen cycle taken from Lappalainen et al., 2016.

$$NH_3 + 2O_2 \rightarrow NO_3^- + H_2O + H^+$$ Equation 2.5

The reaction depicted in equation 2.5 occurs in two steps which can be seen in Equation 2.6 and Equation 2.7 (Lappalainen *et al.*, 2016).

$$NH_4^+ + \frac{3}{2}O_2 \rightarrow NO_2^- + H_2O + 2H^+$$ Equation 2.6

$$NO_2^- + \frac{1}{2}O_2 \rightarrow NO_3^-$$ Equation 2.7

The reaction depicted in equation 2.6 is the first part of the nitrification process and is mainly carried out by the genus of gram-negative bacteria known as *Nitrosomonas.* The reaction depicted in equation 2.7 is mainly carried out by the genus of gram-negative bacteria known as *Nitrobacter* (Ilyas and Masih, 2017).

Denitrification is the process whereby nitrate is reduced to form atmospheric nitrogen. Denitrification occurs in anaerobic environments and requires a source of organic carbon. Equation 2.8 shows the overall denitrification reaction (Hauer and Lamberti, 2017).

$$4NO_3^- + 5C + 2H_2O \rightarrow 2N_2 + 4HCO_3^- + CO_2$$ Equation 2.8

The extent of nitrification and denitrification in a biofilter depends on oxygen availability as nitrification requires an oxygen-rich environment while denitrification requires an oxygen-scarce environment (Ilyas and Masih, 2017).

Hydraulic retention time has a profound effect on the nitrification and denitrification processes. A study by Li *et al.* (2013) compared the nitrification activity in a fixed film treatment system at a range of hydraulic retention times varying from 30 hours to 5 hours. The results of this study showed that a higher hydraulic retention time results in an increase in the population of ammonia oxidising bacteria meaning that ammonia degradation was greatest at the highest hydraulic retention time of 30 hours while it was lowest at a hydraulic retention time of 5 hours (Li *et al.*, 2013).

2.6. Limitations of the Literature

There is extensive research on biofilter performance using artificial wastewater and surface water runoff. However, research on the use of surface water runoff contaminated by informal settlements as the influent to biofilter systems is severely limited. There is extensive literature on the physical, chemical and biological process that are known to occur within biofilter and constructed wetland systems but case studies that quantify these processes are not readily available.

2.7. Key Research Questions

The need for key information is targeted from the literature review and informs key research questions for this study. These are presented below, grouped under the relevant research objectives (research objectives presented in Section 1.3).

Key Questions Associated with Research Objective 1:

a) What nutrient concentrations are observed in the Stiebeuel River and is there a trend observed in the nutrient concentrations over the twelve-month sampling period?

Key Questions Associated with Research Objective 3:

b) What mixing pattern best describes the fluid flow behaviour in the pilot biofilter?
c) Does flow rate influence the hydraulic characteristics of the pilot biofilter?
d) What is the extent of non-ideal fluid flow behaviour in the pilot biofilter?

Key Questions Associated with Research Objective 4:

e) What implications do the nutrient concentrations observed in the Stiebeuel River have on the pilot biofilter performance?
f) What biological and physical processes are occurring within the pilot biofilter?

Key Questions Associated with Research Objective 5:

g) Can the nutrient degradation in the pilot biofilter be described by a reaction kinetic model (such as zero order, first order, second order or complex kinetic model)?

3. RESEARCH APPROACH

Biofilters are usually operated as passive treatment processes with the main design and operating decisions being the type of filter media and loading rate, respectively. A shift to engineered biofilter design and operation requires insight into the factors affecting biofilter performance.

In this project, the potential for treatment of run-off water from informal settlements is considered in context of the run-off from the Langrug informal settlement that flows past the Water Hub in Franschhoek. The project is focused on improving the understanding of and thereby, performance of the biofilters at the Franschhoek Water Hub. To this end, the project involves both lab work and field work, with the field work being carried out at the Franschhoek Water Hub. In order to obtain a deeper understanding of the physical and biological processes that govern biofilters, a pilot-scale biofilter was designed and constructed to carry out pilot-scale studies. The design of the pilot biofilter was based on the design of the biofilters at the Water Hub in order to build improved understanding of their operation and inform optimisation of this field facility. The focus of this project is on biofilters characterised by horizontal subsurface flow systems.

The main factors affecting the performance of horizontal subsurface flow biofilters are the type of filter media, method of operation (continuous or batch), operating temperature, extent of microbial colonisation, as well as the hydraulic retention time and fluid flow dynamics of the system (Velten *et al.*, 2011). The fluid flow dynamics of the system inform the residence time distribution of the system and vice versa.

Stone biofilters have been the focus of this study. On the pilot-scale, operating temperatures were largely constant at the ambient temperature of the laboratory. A detailed investigation into the fluid flow dynamics and residence time distribution was carried out in order to understand the fluid flow rate at which the biofilter can be expected to achieve optimum nutrient removal performance. The pilot biofilter was inoculated and colonised with the same microbial community that is present in the Water Hub biofilters, with the extent of colonisation being monitored over time.

There are four major experimental studies associated with this project:

1. Characterisation of the water quality in the Stiebeuel River, running from the Langrug informal settlement past the Franschhoek Water Hub, over a twelve-month period.
2. Steady state tracer studies to determine the hydraulic characteristics of the pilot biofilter.

3. Inoculation of the pilot biofilter with inoculum harvested from the Water Hub biofilters. This is followed by a biological acclimation period to allow for the microbial colonisation of the filter media.
4. Nutrient degradation studies using contaminated water from the Stiebeuel River as feed to the pilot biofilter.

The purpose of the twelve-month field work component was to determine the typical nutrient concentrations in the river and their fluctuations throughout the year. Seasonal trends in nutrient concentrations were identified. This informs when to carry out the nutrient degradation studies as higher nutrient concentrations are desired for the nutrient degradation studies. This component of the project also provided information regarding the level of variability in water quality throughout the year. Nutrient concentrations in the Water Hub biofilters were also monitored over the twelve-month period to determine how the biofilters process highly variable influent water quality.

The steady state tracer studies were carried out at a range of flow rates of 0.5 L/min – 3 L/min. The minimum and maximum flow capacity needed to maintain a constant hydrostatic pressure in the pilot biofilter system was considered when choosing these flow rates. The resulting residence time distributions enable the determination of the hydraulic characteristics of the pilot biofilter system. From analysis of these, one can diagnose non-ideal fluid flow behaviour within the pilot biofilter and also inform the optimal flow rates at which to carry out the nutrient degradation studies.

The inoculation of the pilot biofilter and subsequent biological acclimation period is necessary as it allows for the nutrient degradation studies to be carried out on a microbially active system. The pilot biofilter was inoculated with inoculum harvested from the Water Hub biofilters to ensure the formation of a microbial colony similar in composition to that of the Water Hub biofilters. This manner of inoculation allows for the findings from this study to be used to provide context to the performance of the Water Hub biofilters. The nutrient degradation studies were carried out at multiple flow rates using water from the Stiebeuel River as the contaminated water source. These studies were used to determine the extent of nutrient removal in the pilot biofilter system and also to assist in determining the type of physical and biological processes occurring within the system and the factors affecting these processes. An understanding of fluid hydrodynamics further informed this analysis

The findings from the nutrient degradation studies are of the utmost importance as these findings provide insight as to whether nutrient degradation in non-vegetated stone biofilters can be modelled using reaction kinetic principles. This provides a basis for biofilter design, determining operating conditions and for developing operating regimes to optimise biofilter performance.

4. THE FRANSCHHOEK WATER HUB

4.1. Introduction

The Water Hub is situated in Franschhoek's peri-urban catchment area along the Stiebeuel River. The Stiebeuel River is a perennial river that has its source in the mountains of the Haweqwa Nature Reserve. The catchment contains an informal settlement (Langrug), a low-income built-up area (Groendal) as well as agricultural land. The Water Hub is situated further downstream, just before the confluence of the Stiebeuel River with the Franschhoek River. Figure 4.1 shows the location of the Water Hub in relation to Langrug informal settlement, Groendal and Franschhoek.

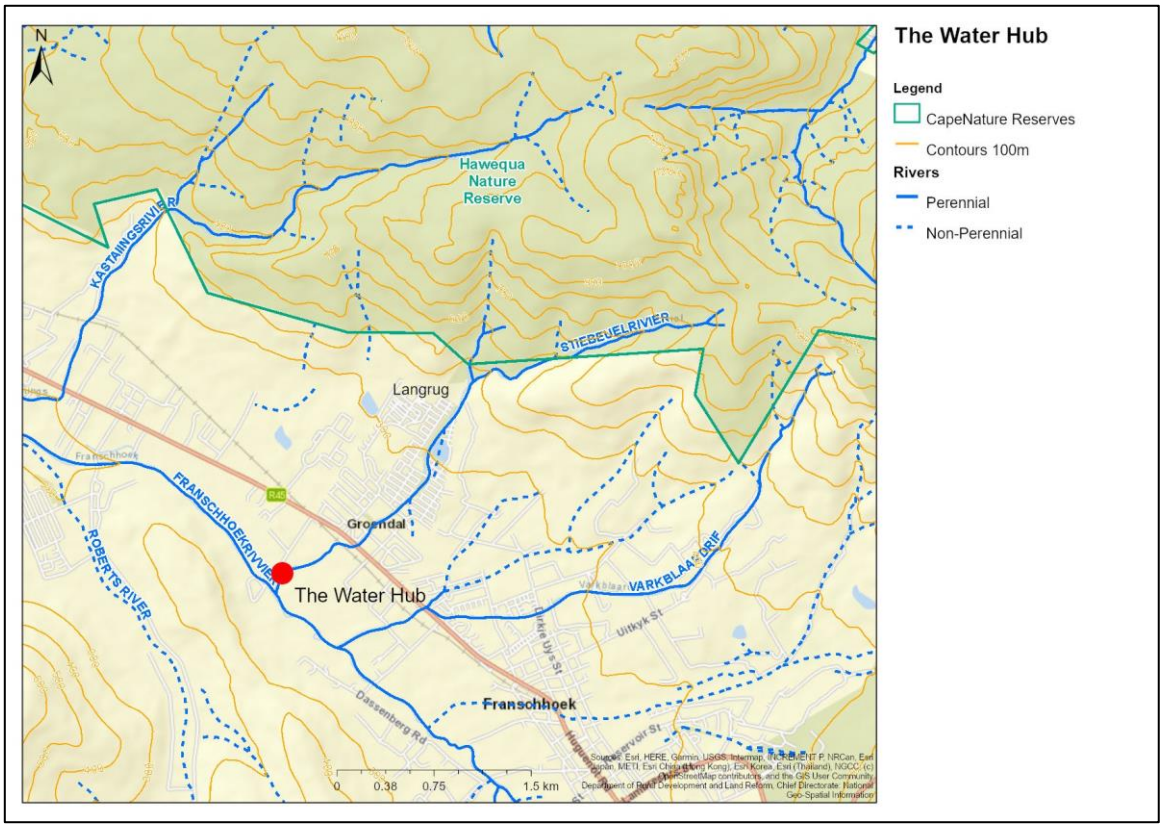

Figure 4.1: Detailed map of location of the Water Hub

4.1.1. Langrug Informal Settlement

The Water Hub is situated downstream from Langrug which was established in 1992 and is now home to 2500 shacks and more than 7000 people. The residents of this informal settlement are seasonal workers on the farms, wineries and restaurants in the area with approximately 72% of the population being migrant workers from the Eastern Cape (Community Organisation Resource Centre, 2011)

As is characteristic of a cramped informal settlement, Langrug is plagued by poor drainage, lack of access to basic sanitation and widespread flooding. The settlement

has one working tap for every 72 residents and one toilet for every 49 people (Community Organisation Resource Centre, 2011). The residents rely on the Stiebeuel River as a primary water source for domestic use. Figure 4.2 depicts the densely populated informal settlement.

Figure 4.2: Langrug Informal Settlement (Community Organisation Resource Centre, 2011)

The water quality of the Stiebeuel River varies throughout the year due to natural factors such as seasonal variations in runoff volume and weather conditions as well as human influences (Nivala *et al.*, 2017). The major human influences affecting water quality in the Stiebeuel River are the domestic activities in Langrug informal settlement and to a lesser extent, agricultural activities.

4.1.2. Introduction to biofilters at the Water Hub

Six biofilters are used to remediate contaminated surface runoff from the Stiebeuel River. Since an informal settlement is located upstream of the Water Hub; the water quality of the Stiebeuel River here is poor and nutrient levels in the river are highly variable. The cells are 3.5 m wide, 16 m long and 0.7 m deep. Each Water Hub biofilter cell is filled with either peach pips, small stones or large stones as filtration media. The large stones are 17-19 mm in diameter while the small stones are 7-9 mm in diameter. The non-vegetated large stone biofilters have a bed voidage of 0.54 while the non-

vegetated small stones biofilters have a bed voidage of 0.46 Three of the cells are vegetated while the others remain unvegetated. Figure 4.3 is a simple diagram showing the configuration of the biofilters at the Water Hub.

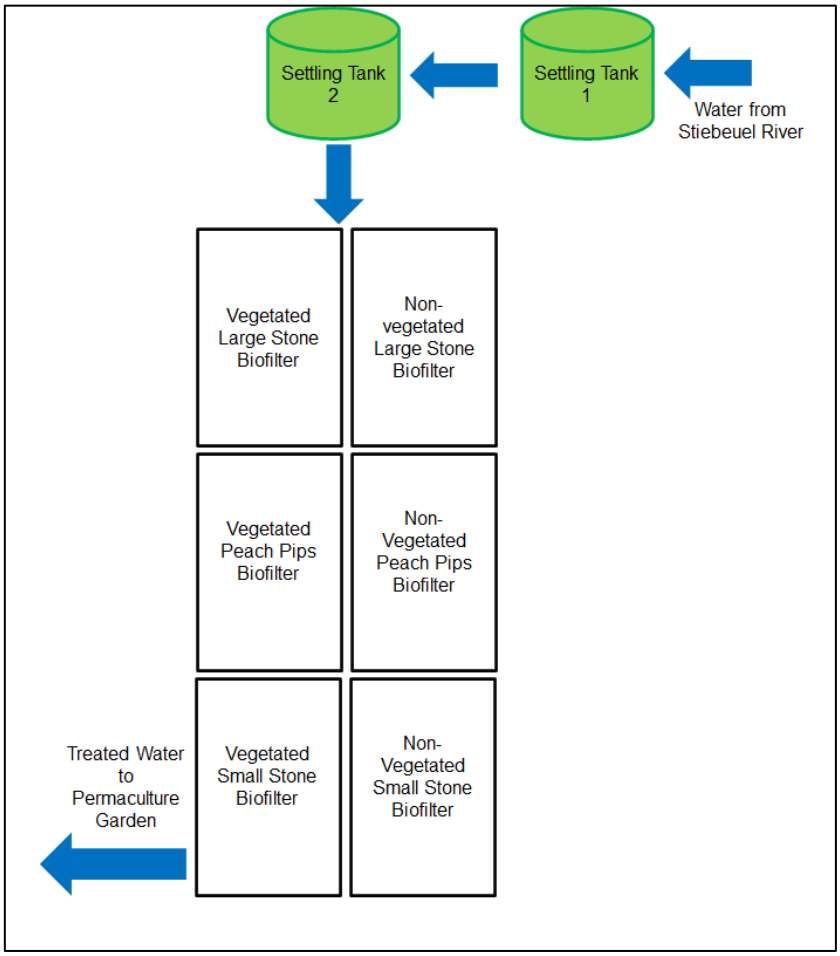

Figure 4.3: Configuration of six biofiltration cells at the Water Hub

The operation of the system is as follows: contaminated runoff is pumped from the river into a 10 000 L settling tank (Settling Tank 1) before being transferred into a second 10 000 L settling tank (Settling Tank 2) after which the water is fed into biofilters. The settling tanks serve two main functions: storage of influent water as well as the removal of suspended solids from the river water. Each cell is filled separately, and a residence time of 3-5 days is observed before the treated water is sent to the irrigation tank. This water is then used to irrigate the permaculture garden that is also housed at the Water Hub.

The biofilters are designed such that a perforated inlet pipe runs along the width of each cell. This allows water from settling tank 2 to enter the biofiltration cell in question in an evenly distributed manner. The design of the inlets and outlets of the Water Hub biofilters can be seen in Figure 4.4. Figure 4.5 shows the longitudinal view of the biofilters and details the placement of inspection holes that are sealed with a cap.

These inspection holes are able to provide a visual indication of volume of water present in each biofiltration cell and also serve as possible sampling points in each of the filters.

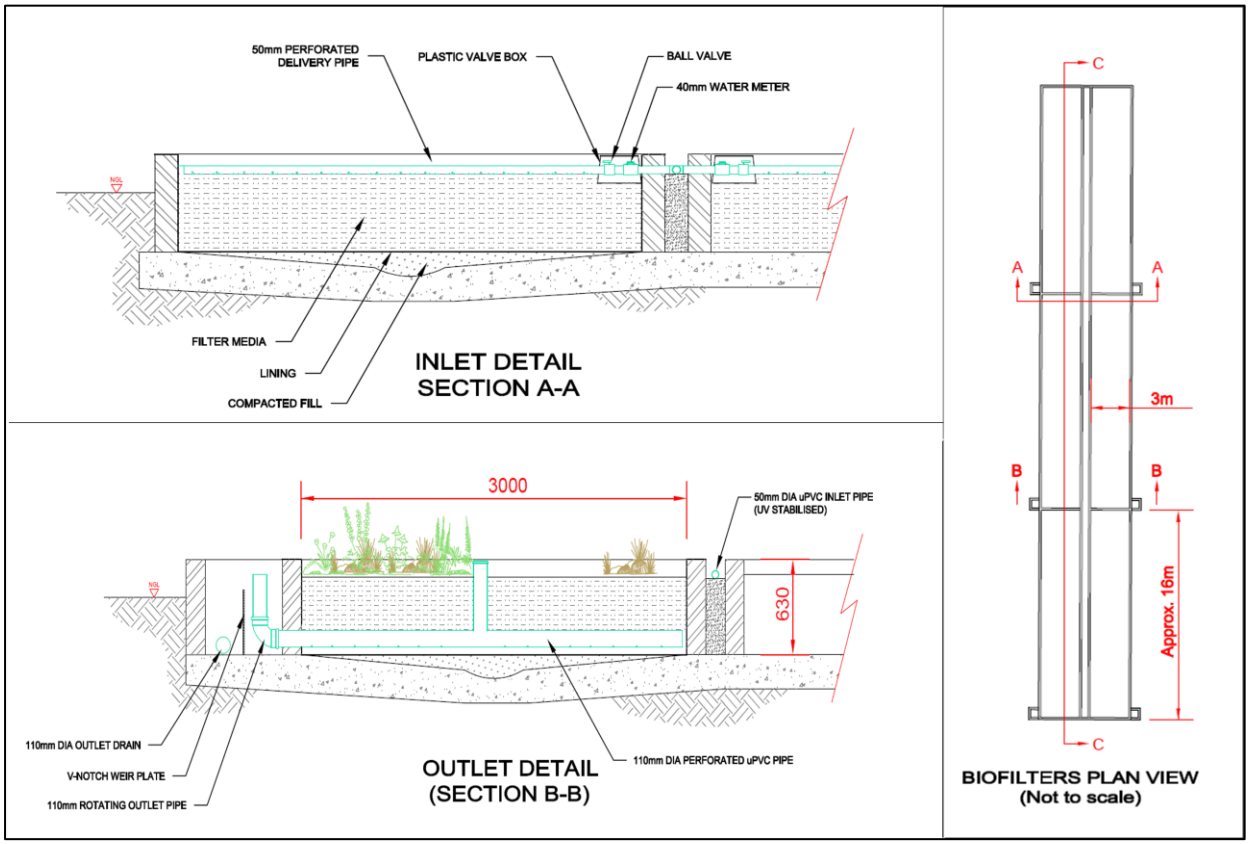

Figure 4.4: Cross sectional view showing inlet and outlet designs of Water Hub biofilters

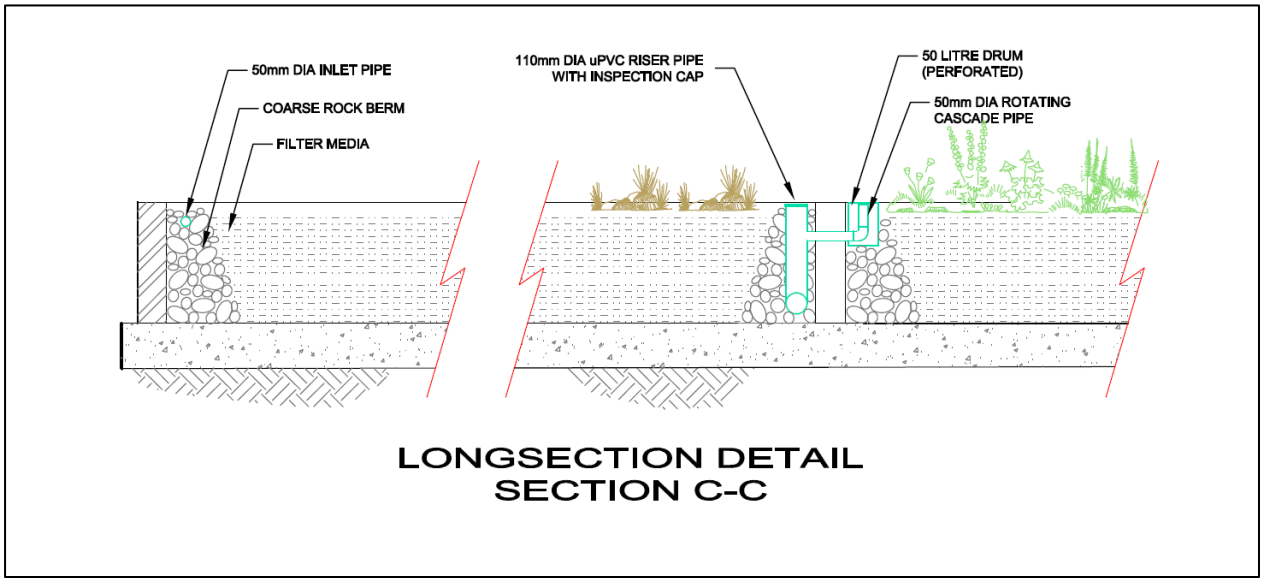

Figure 4.5: Longitudinal view of biofiltration cells

Figure 4.6 shows the large stone and peach pip biofilters at the Water Hub. It can be seen that the vegetated and non-vegetated cells of the same filtration media type are

adjacent. The large size and lack of sufficient sampling points can be seen in Figure 4.6.

Figure 4.6: Peach pip and small stone biofilters at the Water Hub

4.1.3. Aim of this chapter

The aim of this chapter is to illustrate the dynamic nutrient levels in the Stiebeuel River as well as in a handful of selected sampling sites within the Water Hub biofiltration system. This will identify the influent concentration range for the Water Hub biofilters and determine the extent to which the biofilters need to perform in order to produce water that is fit for irrigation purposes. The documentation of nutrient levels in the Stiebeuel River has implications for the lab studies as the contaminated runoff from the Stiebeuel River will be used as the influent for the nutrient degradation studies. It is important to understand the water quality of the contaminated water source for these studies as influent nutrient concentrations, specifically NH_3, NO_2^- and NO_3^-, will have an effect on the extent of nitrification and denitrification achieved in the pilot biofilter system.

4.2. Materials and Methods

Samples were collected from five sampling sites at the Water Hub over a twelve-month period beginning in March 2019 and ending in February 2020. Samples were collected three times a month where possible but where this was not possible, at least two samples a month were collected.

The aforementioned sampling sites are as follows:

1. Outlet of Settling Tank 1 (ST1)
2. Outlet of Settling Tank 2 (ST2)
3. Outlet of the Non-Vegetated Large Stones Biofilter (LSO)
4. Outlet of the Non-Vegetated Small Stone Biofilter (SSO)
5. The Stiebeuel River – sampling site is adjacent to the biofiltration system (River)

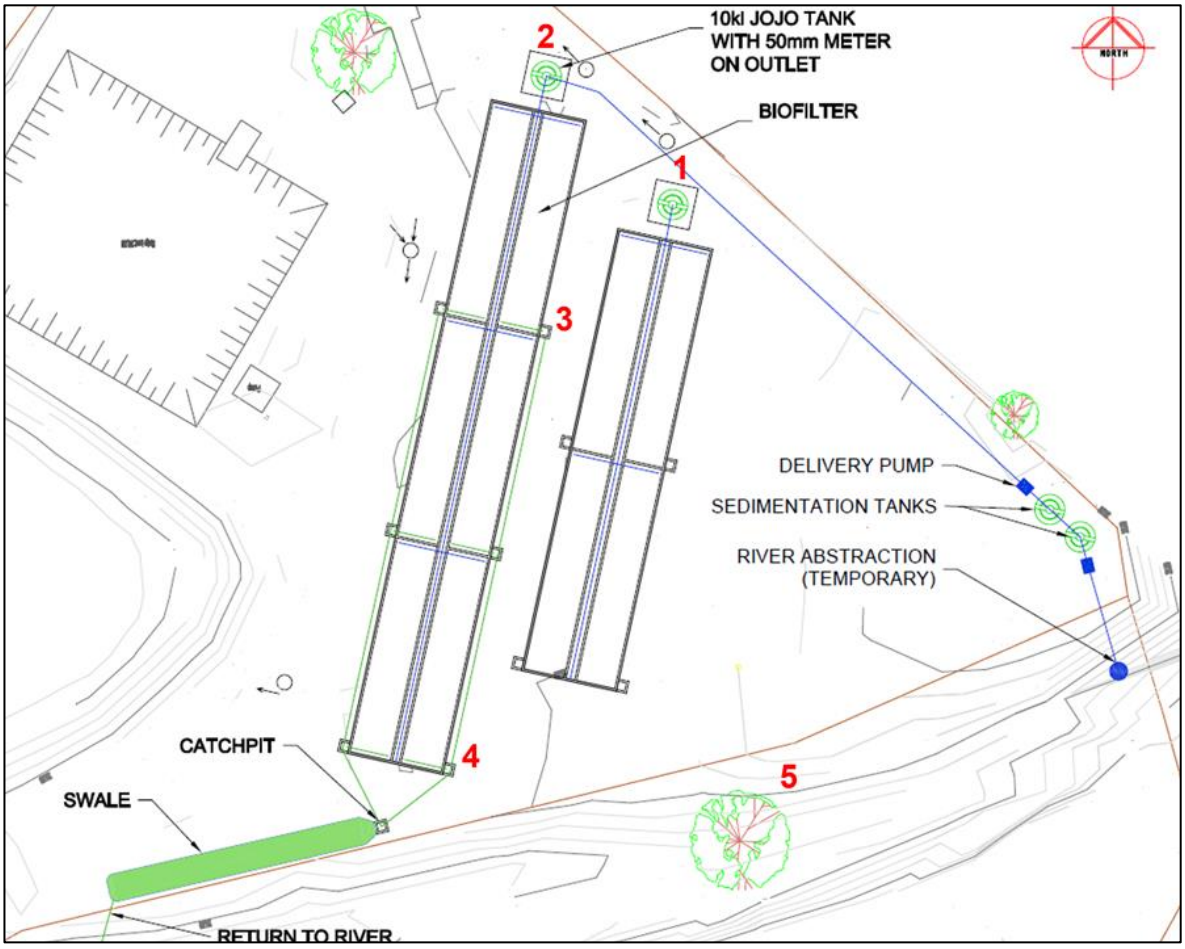

Figure 4.7: Layout of the biofilters at the Water Hub

Figure 4.7 shows the layout of the biofilters at the Water Hub with the sampling sites all being situated around the biofiltration system and indicated on Figure 4.7. These biofilters are described in detail in Section 4.1.2.

The following sampling procedure was followed:

- A lab coat and latex gloves were worn when collecting and handling samples.
- Samples were collected in 250 ml autoclaved glass jars.
- The water was allowed to run for 120 seconds before collecting samples when sampling from ST1, ST2, LSO and SSO to ensure that the pipes had been flushed of solids and other contaminants.
- All samples were stored in a sealed crate while being transported to prevent contamination.
- The samples were stored in the refrigerator.

The HACH benchtop spectrophotometer and reagent set was used to determine the NH_3, NO_3^-, NO_2^- and PO_4^{3-} concentrations in the samples. The following methods were used to determine NH_3, NO_3^-, NO_2^- and PO_4^{3-} concentrations (HACH Company, 2008):

- The Ascorbic Acid Method was used to determine PO_4^{3-} concentrations (Murphy and Riley, 1962).
- The Diazotization Method was used to determine NO_2^- concentrations (Fishman, Skougstad and Scarbro, 1964).
- The Cadmium Reduction Method was used to determine NO_3^- concentrations (Jones, 1984).
- The Salicylate Method was used to determine NH_3 concentrations (Verdouw, van Echteld and Dekkers, 1978).

The detailed method for using the HACH equipment for each nutrient is presented in Appendix A. Appendix A also details the reproducibility of the results and limits of detection for each nutrient.

4.3. Results and Discussion

4.3.1. The Stiebeuel River

The nutrient concentrations in the Stiebeuel River were monitored periodically over a year, from March 2019 to February 2020. Figure 4.8 depicts the median monthly total nitrogen concentration in the Stiebeuel River over twelve months. The median concentrations have been used instead of mean concentrations due to the high variability of concentrations observed. The median monthly concentration provides a less distorted representative concentration as it is not as affected by outliers as the mean.

The total nitrogen depicted in Figure 4.8 is comprised of ammonia, nitrate and nitrite. Figure 4.8 also includes the total monthly rainfall experienced at the Water Hub

(detailed rainfall data can be found at https://figshare.com/s/f64b77047dacf7064b01). The highest median total nitrogen concentration of 38.0 mg/L was seen in March 2019 with the total rainfall in this month being 21 mm. The total monthly rainfall experienced at the Water Hub increased steadily from March 2019 to June 2019 with a large increase in total rainfall in July 2019. The rainfall of 267 mm in July 2019 was the highest amount of rainfall experienced at the Water Hub in the twelve-month sampling period. The median total nitrogen concentration decreased 3.5-fold from 29.1 mg/L in March 2019 to 8.60 mg/L in July 2019, with increasing rainfall and associated dilution.

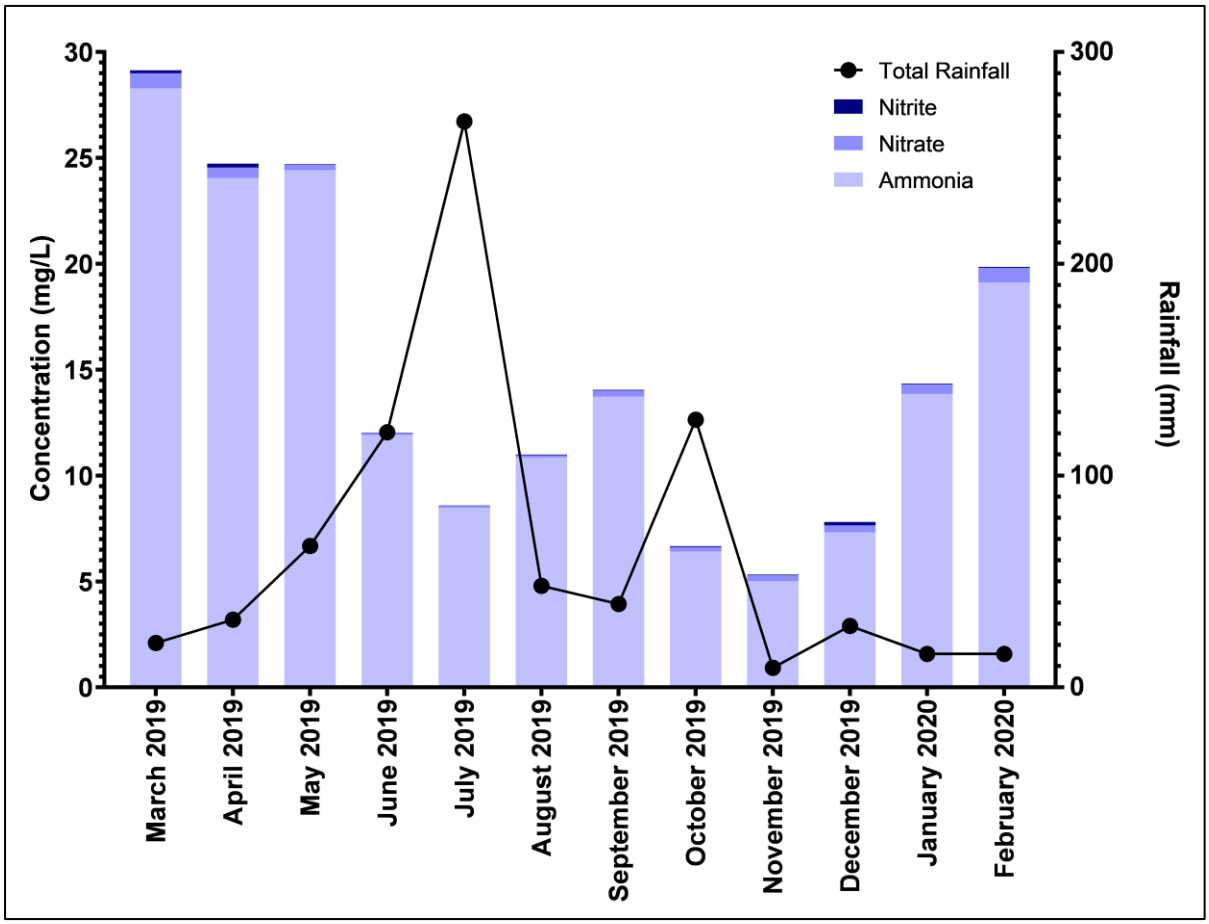

Figure 4.8: Median monthly total nitrogen concentrations and component species correlated with total monthly rainfall data for the Stiebeuel River

It can be seen from Figure 4.8 that the total nitrogen concentrations are generally higher in periods of low rainfall with the concentrations dropping during periods of high rainfall, which supports the theory that the lower concentrations observed in low rainfall months are due to dilution. However, this is not the case for every month. An example of this is the lowest median total nitrogen concentration of 5.33 mgl/L being seen in November 2019 with the total rainfall being 9.2 mm in this month.

Ammonia accounts for majority of the total nitrogen concentration in the river with each sample containing upward of 93.8% ammonia (Figure 4.8). The maximum ammonia

content was seen in June 2019 at a median composition of 99.5% ammonia in the river. The mean ammonia contribution to total nitrogen in the Stiebeuel River is 96.9%.

Nitrate is second largest contributor to total nitrogen and has been observed to contribute up to 5.1% of the total nitrogen concentration in the river. The nitrate content in the river is seen to decrease from June 2019 to September 2019 which coincides with the high rainfall period. Nitrate contributes 0.75 – 2.01% of total nitrogen in this period as compared to the mean nitrate contribution of 2.47%. Nitrite is the lowest contributor to total nitrogen with the mean nitrite contribution to total nitrogen being 0.48%. The maximum nitrite content was seen in December 2019 and made up 2.05% of total nitrogen (Figure 4.8).

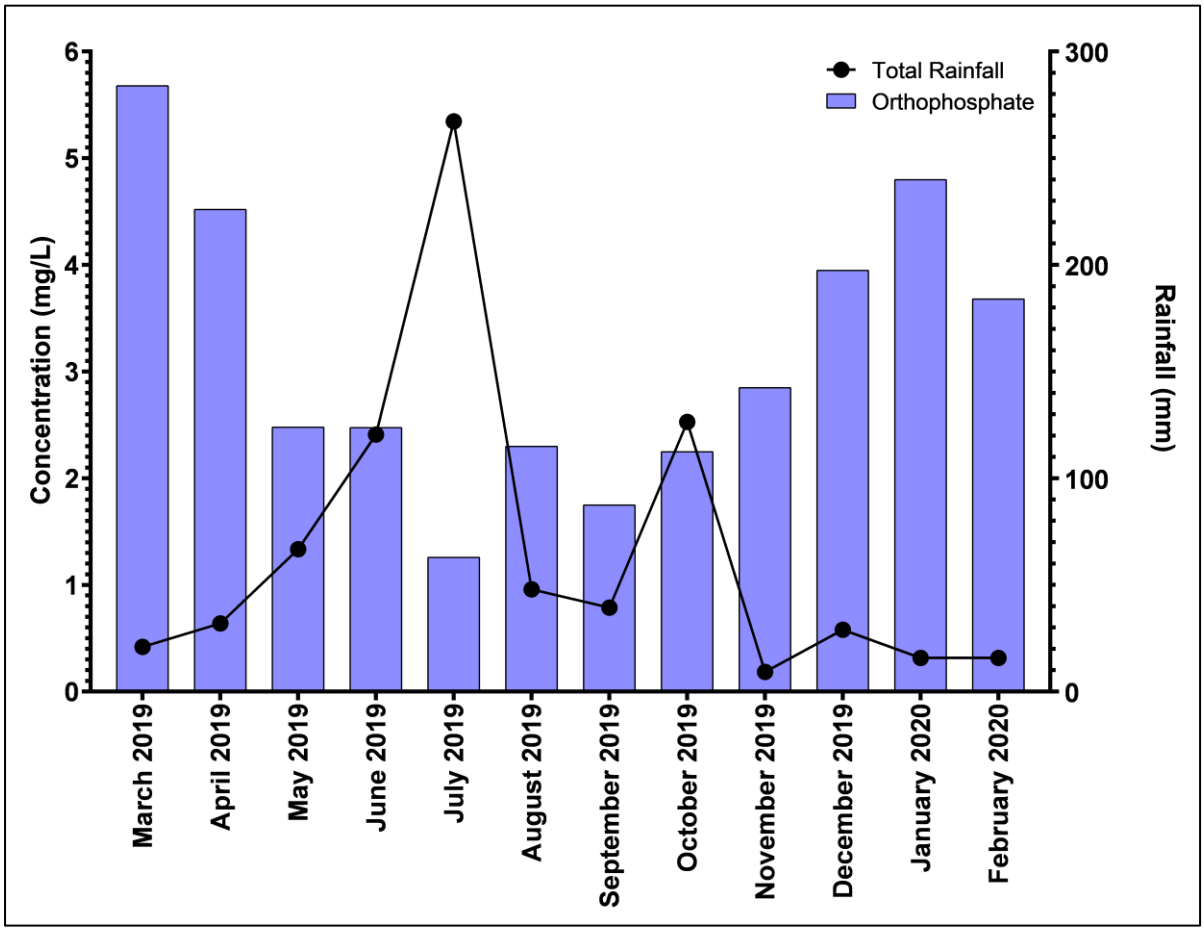

Figure 4.9: Median monthly orthophosphate concentrations and total monthly rainfall data for the Stiebeuel River

Figure 4.9 depicts the median monthly orthophosphate concentration and rainfall data in the Stiebeuel River over twelve months. The median orthophosphate concentration is higher in periods of low rainfall with a decrease in orthophosphate concentrations seen in high rainfall periods. The highest median orthophosphate concentration is seen in March 2019 at a concentration of 5.68 mg/L. The lowest median orthophosphate concentration of 1.26 mg/L is observed in July 2019 which is also the

month with the highest total rainfall i.e., 4.5-fold decrease in orthophosphate concentration and some 10-fold increase in rain received.

It can be noted that orthophosphate concentrations follow a more consistent trend with the higher concentrations occurring in dry periods. This is not the case for total nitrogen as was seen in Figure 4.8. Previous research on this catchment has attributed the varying and often elevated total nitrogen concentrations to fertiliser use in adjacent agricultural land as well as to NH_3 enriched runoff from the informal settlement ((Fell, 2017). Elevated nutrient concentrations in the summer months can also be attributed to the human activities of the additional 1000 seasonal migrant workers living in Langrug during the summer fruit picking season (Community Organisation Resource Centre, 2011).

4.3.2. Nutrient concentrations in the biofiltration system

As discussed in Section 4.1.2, the biofiltration system is comprised of the two settling tanks which serve as holding tanks for contaminated runoff from the Stiebeuel River and the six biofiltration cells. During the operation of these biofilters, nutrient concentrations were determined at each of the sampling points across a time period of 29 March 2019 to 26 February 2020 (26 samples per sampling point in total). Raw data can be viewed on https://figshare.com/s/f64b77047dacf7064b01.

Box and whisker analyses were carried out to determine the spread of the data in the five sampling sites within the biofiltration system. The box and whisker plots (Figure 4.10, Figure 4.11, Figure 4.12) show the spread of data. The median (second quartile) is indicated on each box with a line that splits the box into two parts. The lowest point on the box is the first quartile while the highest point on the box represents the third quartile. The whiskers show the minimum and maximum data points.

Figure 4.10 shows the box and whisker plots for ammonia, nitrate, nitrite, and orthophosphate at the river, ST1, ST2, LSO and SSO over the twelve-month sampling period. Statistical analysis is expanded in Figures 4.13 to 4.17. Detailed inferential statistical tests in the form of Wilcoxon Signed-Rank Tests can be seen in Appendix B. Figure 4.10 shows that the data for both the large stones outlet and small stones outlet is less dispersed than the river and settling tanks. The ammonia box and whisker plots show the large spread of the data in the Stiebeuel River. The minimum ammonia concentration at this sampling site is 3.20 mg/L and the maximum concentration is 34.4 mg/L. The median ammonia concentration in the river is 14.0 mg/L. It can be seen that the median ammonia concentrations in settling tank 1 and settling tank 2 are 16.0 mg/L and 16.5 mg/L, respectively. The median ammonia concentration for the large stone outlet is 1.23 mg/L while the median ammonia concentration for the small

stones outlet is 1.49 mg/L. This implies that there is a large reduction in ammonia from the biofilter inlet (settling tank 2) to the outlet of the small stone and large stone filters.

The box and whisker plot for nitrite shows that the minimum nitrite concentration in the river is 0.030 mg/L while the maximum nitrite concentration is 0.880 mg/L. The median nitrite concentration in the river is 0.105 mg/L. The median nitrite concentration for the large stones outlet and small stones outlet are 0.096 mg/L and 0.093 mg/L, respectively.

A large reduction in nitrate concentration can be seen from the biofilter inlet to the large and small stones outlets with the greater nitrate reduction occurring in the small stones biofilter. The median nitrate concentration in the river is 1.20 mg/L while the median nitrate concentrations in settling tank 1 and settling tank 2 are 1.17 mg/L and 1.19 mg/L, respectively. The median nitrate concentrations in the large stones outlet and small stones outlet are smaller in comparison at 0.630 mg/L and 0.350 mg/L, respectively.

The range of orthophosphate concentrations seen in the river, settling tank 1 and settling tank 2 were similar with the median orthophosphate concentrations at these locations being 2.60 mg/L, 2.65 mg/L and 2.70 mg/L, respectively. A large reduction in orthophosphate concentrations can be seen from settling tank 2 to the large stones outlet and small stones outlet. The median orthophosphate concentration in the large stones outlet is 0.602 mg/L while the median orthophosphate concentration in the small stones outlet is 0.285 mg/L.

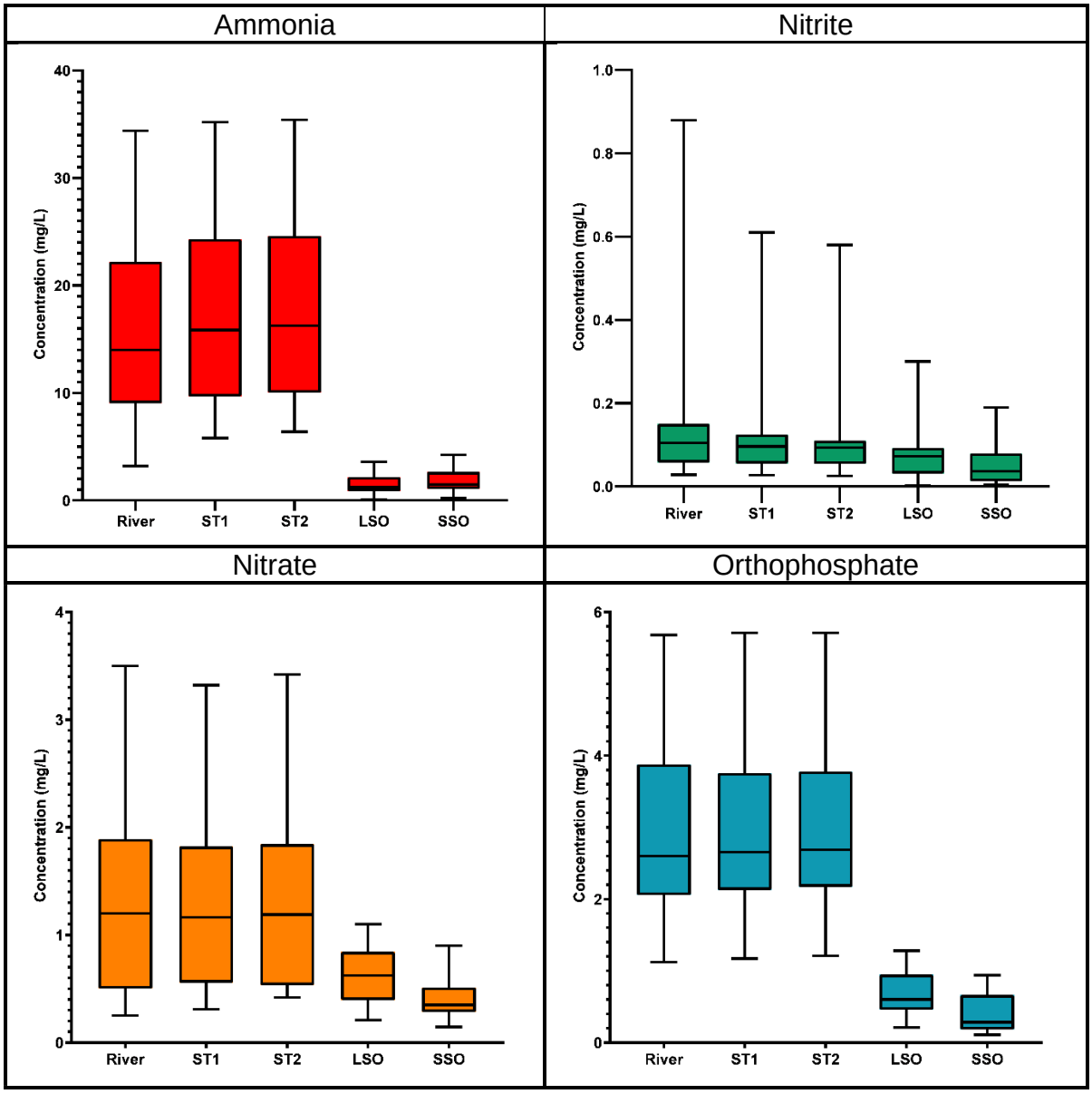

Figure 4.10: Box & whisker plots of nutrient concentrations at various sampling sites over a 12 month period. Sampling sites: River, Outlet of Settling Tank 1 (ST1), Outlet of Settling Tank 2 (ST2), Outlet of Non-Vegetated Large Stones Biofilter (LSO), Outlet of Non-Vegetated Small Stones Biofilter (SSO)

The spread of data in the Stiebeuel River and both settling tanks over the 12-month sampling period is quite large. Seasonal difference in the spread of data may be prominent and so separate box and whisker plots for the summer (dry months) and winter (wet months) were produced. The winter sampling period was May 2019 to August 2019 while the summer sampling period was November 2019 to February 2020.

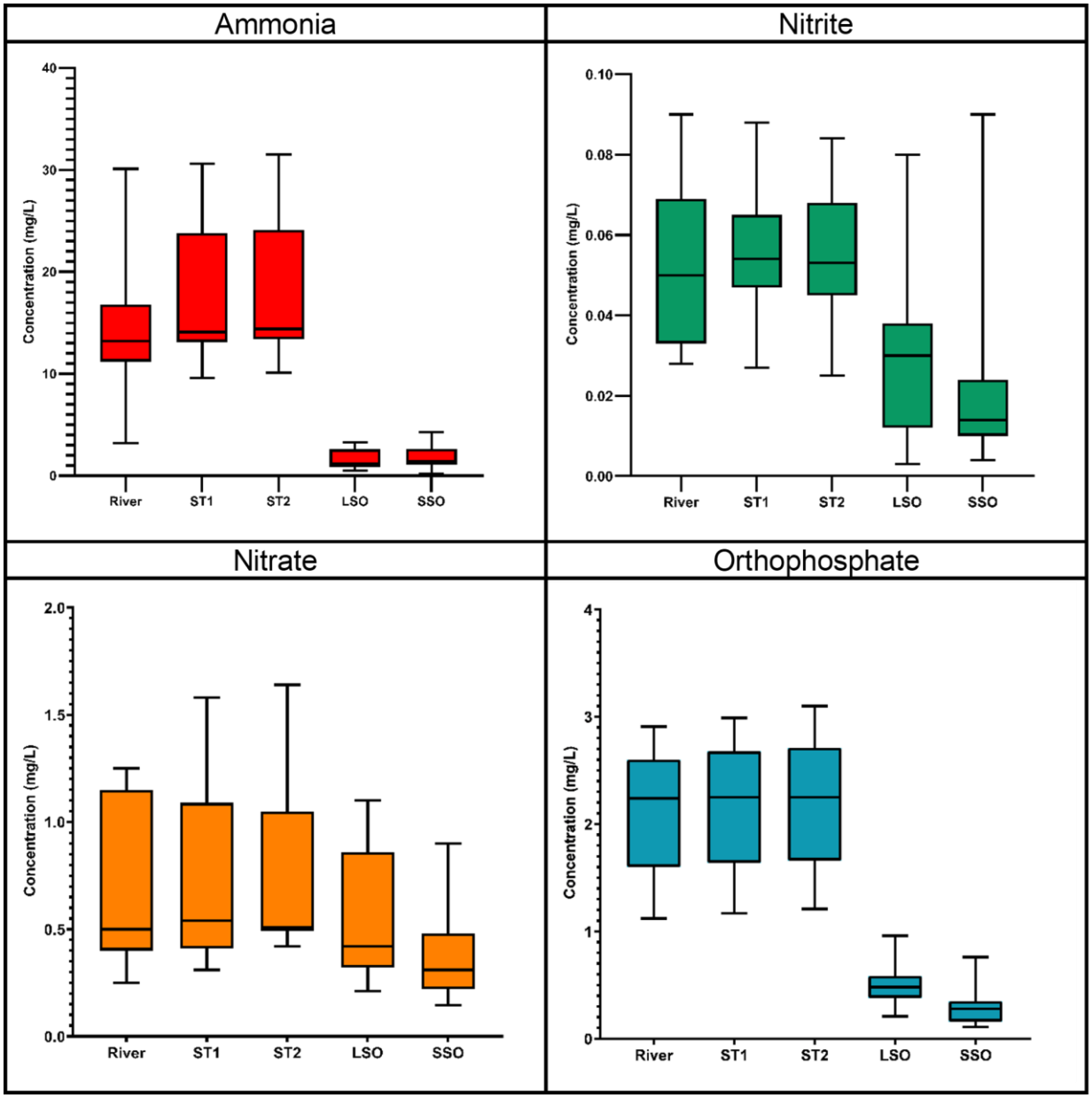

Figure 4.11: Box & whisker plots of nutrient concentrations at various sampling sites over winter period. Sampling sites: River, Outlet of Settling Tank 1 (ST1), Outlet of Settling Tank 2 (ST2), Outlet of Non-Vegetated Large Stones Biofilter (LSO), Outlet of Non-Vegetated Small Stones Biofilter (SSO)

Figure 4.11 shows the box and whisker plots for ammonia, nitrate, nitrite, and orthophosphate at the river, ST1, ST2, LSO and SSO over the winter months. The box and whiskers include all samples that were taken from May 2019 to August 2019. The box and whisker for ammonia shows that spread of data in the river is more dispersed than the spread of data in the settling tanks. The minimum ammonia concentration in Stiebeuel River in winter is 3.26 mg/L while the maximum ammonia concentration during this period is 30.1 mg/L. The median ammonia concentration in the river during the winter period is 13.2 mg/L. The median ammonia concentrations in ST1 and ST2

are higher than in the river at 14.1 mg/L and 14.4 mg/L, respectively. The median ammonia concentration at the LSO is 1.31 mg/L while the median ammonia concentration at the SSO is 1.48 mg/L.

The box and whisker for nitrite in Figure 4.11 shows that the data is greatly dispersed in both the large stones outlet and small stones outlet. The median nitrite concentration in the river is 0.050 mg/L while the median nitrite concentration in settling tank 1 and settling tank 2 is 0.054 mg/L and 0.053 mg/L, respectively. The median nitrite concentration in the large stones outlet and small stone outlet is 0.030 mg/L and 0.010 mg/L, respectively.

The box and whisker plot for nitrate shows that the median nitrate concentration in the river during the winter period is 0.500 mg/L. The median nitrate concentration in settling tank 1 and settling tank 2 are 0.540 mg/L and 0.510 mg/L, respectively. The median nitrate concentration in the large stones outlet is 0.420 mg/L while the median nitrate concentration in the small stones outlet is 0.310 mg/L.

The box and whisker plots for orthophosphate clearly show a reduction in orthophosphate concentration in the large stone and small stone biofilters. The spread of data is also smallest in the large and small stone biofilters. The median orthophosphate concentration in the river is 2.24 mg/L while the median orthophosphate concentration in settling tank 1 and settling tank 2 are the same at 2.25 mg/L. The median orthophosphate concentration in the large stones outlet of 0.480 mg/L is greater than that of the median orthophosphate concentration in the small stones outlet of 0.280 mg/L.

Figure 4.12 shows the box and whisker plots for ammonia, nitrate, nitrite, and orthophosphate at the river, ST1, ST2, LSO and SSO over the summer months. The box and whiskers include all samples that were taken from November 2019 to February 2020.

The median ammonia concentration in the river during the summer period is 12.7 mg/L while the median ammonia concentration in settling tank 1 and settling tank 2 are 13.4 mg/L and 13.8 mg/L, respectively. The median ammonia concentration in the large stones outlet is 1.13 mg/L while the median ammonia concentration at the small stones outlet is 1.34 mg/L. When comparing Figure 4.11 and Figure 4.12, it is evident that ammonia concentrations in the Stiebeuel River are greater in the summer months.

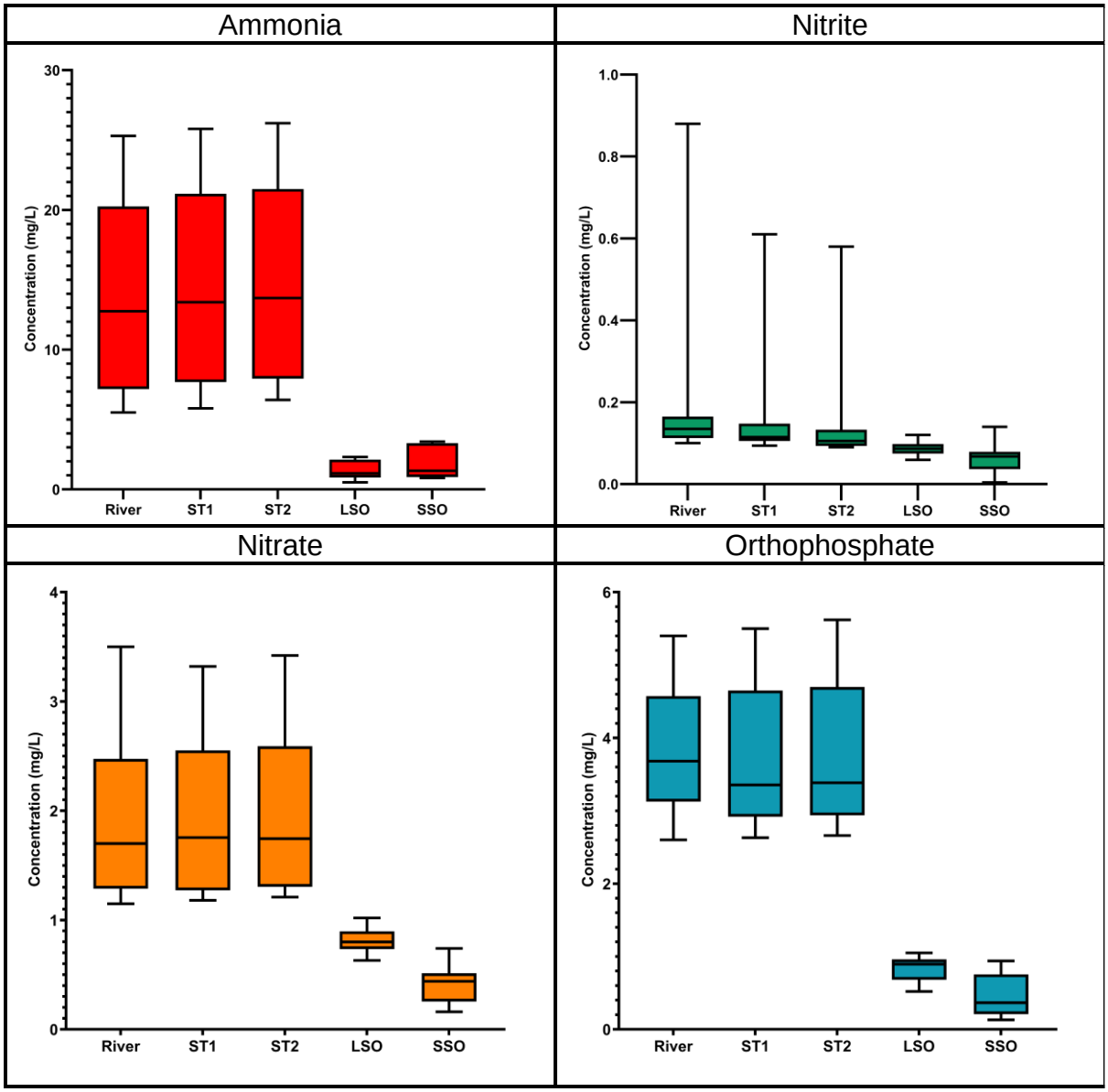

Figure 4.12: Box & whisker plots of nutrient concentrations at various sampling sites over summer period. Sampling sites: River, Outlet of Settling Tank 1 (ST1), Outlet of Settling Tank 2 (ST2), Outlet of Non-Vegetated Large Stones Biofilter (LSO), Outlet of Non-Vegetated Small Stones Biofilter (SSO)

The box and whisker plots for nitrite during the summer period show that the data is more dispersed in the river and settling tanks than in the large and small stone biofilters. The minimum nitrite concentration in the river during summer is 0.100 mg/L while the maximum nitrite concentration in the river during summer is 0.880 mg/L. The median nitrite concentration in the river is 0.130 mg/L while the median nitrite concentrations in settling tank 1 and settling tank 2 are 0.110 mg/L and 0.100 mg/L, respectively. The mean nitrite concentration in the large stones biofilter is 0.080 mg/L while the mean nitrite concentration in the small stones biofilter is 0.070 mg/L. When

comparing Figure 4.11 and Figure 4.12, it is evident that nitrite concentrations in the Stiebeuel River are greater in the summer months.

The box and whisker plots for nitrate in Figure 4.12 show that the median nitrate concentration in the river is 1.70 mg/L while the median nitrate concentration in settling tank 1 and settling tank 2 are 1.76 and 1.74 mg/L, respectively. The median nitrate concentration at the small stones outlet of 0.430 mg/L is smaller than the median nitrate concentration at the large stones outlet of 0.790 mg/L. A comparison between Figure 4.11 and Figure 4.12 shows that nitrite concentrations are higher in the summer months.

The box and whisker plots for orthophosphate in the summer period show that the median orthophosphate concentration in the river is 3.67 mg/L. The median orthophosphate concentration in settling tank 1 and settling tank 2 are 3.36 mg/L and 3.38 mg/L, respectively. The median orthophosphate concentration in the large stone outlet is 0.890 mg/L while the median orthophosphate concentration in the small stones outlet is 0.360 mg/L. By comparing Figure 4.11 and Figure 4.12, it is observed that orthophosphate concentrations are greater in the summer months than in the winter months.

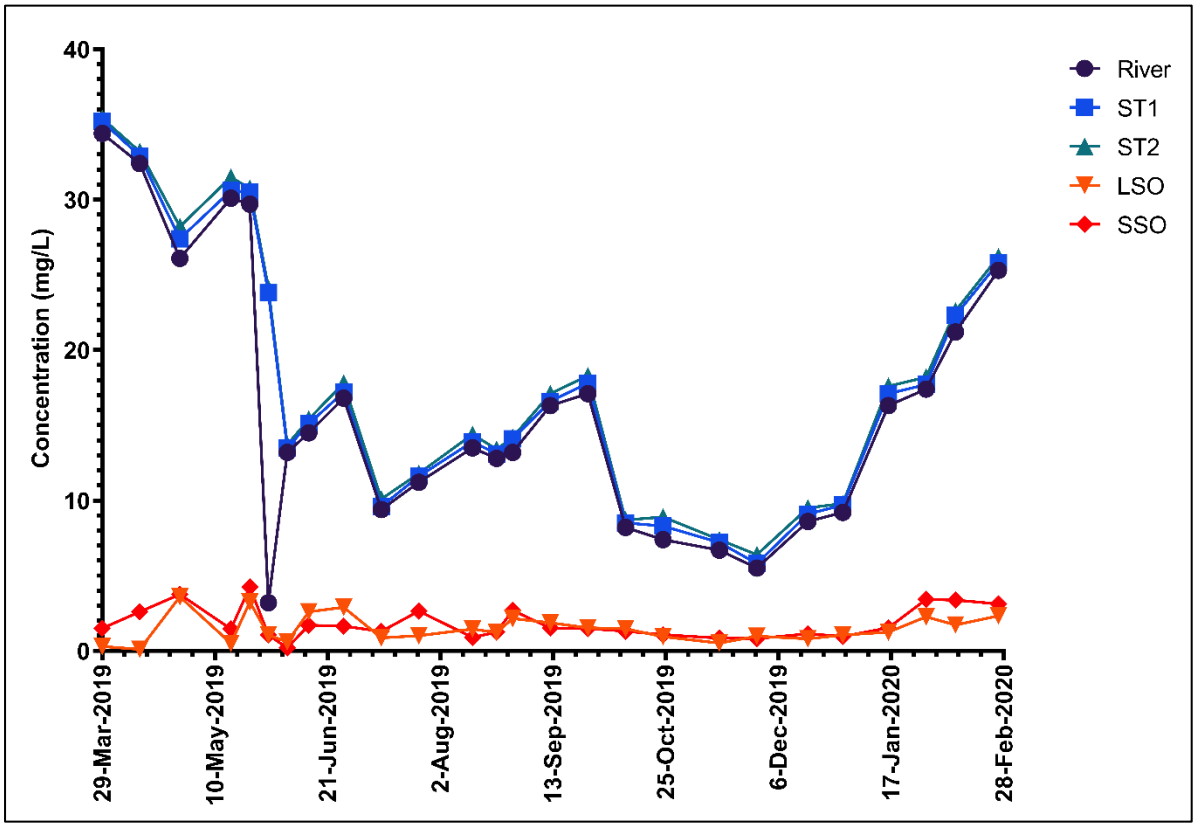

Figure 4.13: Ammonia concentrations at various sampling sites over a 12-month period (n=26 for each sampling site, std dev < 0.42 mg/L)

Figure 4.13 shows ammonia concentrations from duplicate analysis at the five sampling sites in the Water Hub biofiltration system over the twelve-month sampling period. The ammonia concentrations in the river, settling tank 1 and settling tank 2 vary greatly longitudinally. The ammonia concentrations at these sampling sites are greatest on 29 March 2019 after which ammonia concentrations fluctuate in response to, among others, rainfall and human activities. The ammonia concentrations in the large stones outlet and small stones outlet remain lower than 4.25 mg/L implying that the biofilters are able to perform robustly across the varying ammonium load to maintain residual ammonia below this concentration. A Wilcoxon Signed-Ranked Test showed that the difference between the ammonia concentrations observed in the large stones outlet and small stones outlet is not statistically significant (see Appendix B for detailed statistical test).

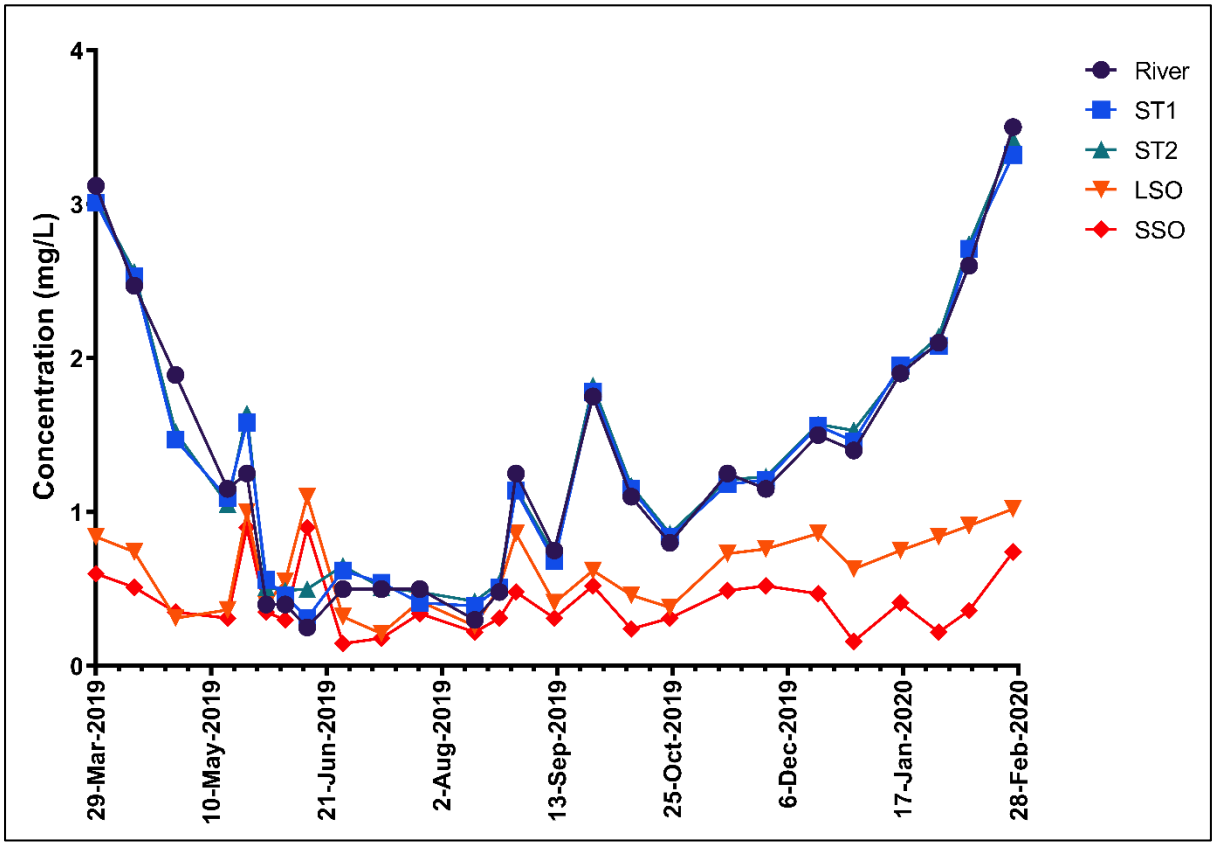

Figure 4.14: Nitrate concentrations at various sampling sites over a 12-month period (n = 26 for each sampling site, std dev < 0.14 mg/L)

Figure 4.14 shows nitrate concentrations in the five sampling sites over a twelve-month period. Nitrate concentrations in the river, settling tank 1 and settling tank 2 decrease from March 2019 to June 2019 after which the concentrations remain at approximately 0.500 mg/L until August 2019. The nitrate concentrations in the river and settling tanks steadily increase after this point. The nitrate levels in the small stones biofilter are consistently lower than in the large stones biofilter and both below

1.0 mg/L; this difference is statistically significant (see Appendix B). This implies that the small stones biofilter is more efficient at nitrate removal than the large stones biofilter.

Figure 4.15 shows nitrite concentrations at the five samplings sites over a twelve-month period. Nitrite concentrations in the river and settling tanks remain between 0.400 mg/L and 0.650 mg/L from 29 March 2019 until 27 April 2019. After this, the nitrite concentrations at these sampling sites plummet to 0.068 mg/L and remain below this concentration until 14 August 2019. The nitrite levels in the river and settling tanks begin to rise after 14 August 2019. Nitrite concentrations at the large stones outlet and small stones outlet remain below 0.3 mg/L. The difference between the nitrite concentrations observed in the large stones outlet and the small stones outlet statistically significant (see Appendix B). Nitrite concentrations are generally greater in the small stones outlet as compared to the large stones outlet. Nitrite concentrations remain well below 1 mg/L which could be due to the fact that nitrite is an intermediary in the nitrification process with ammonia being oxidised to form nitrite; and nitrite in turn being oxidised to form nitrate.

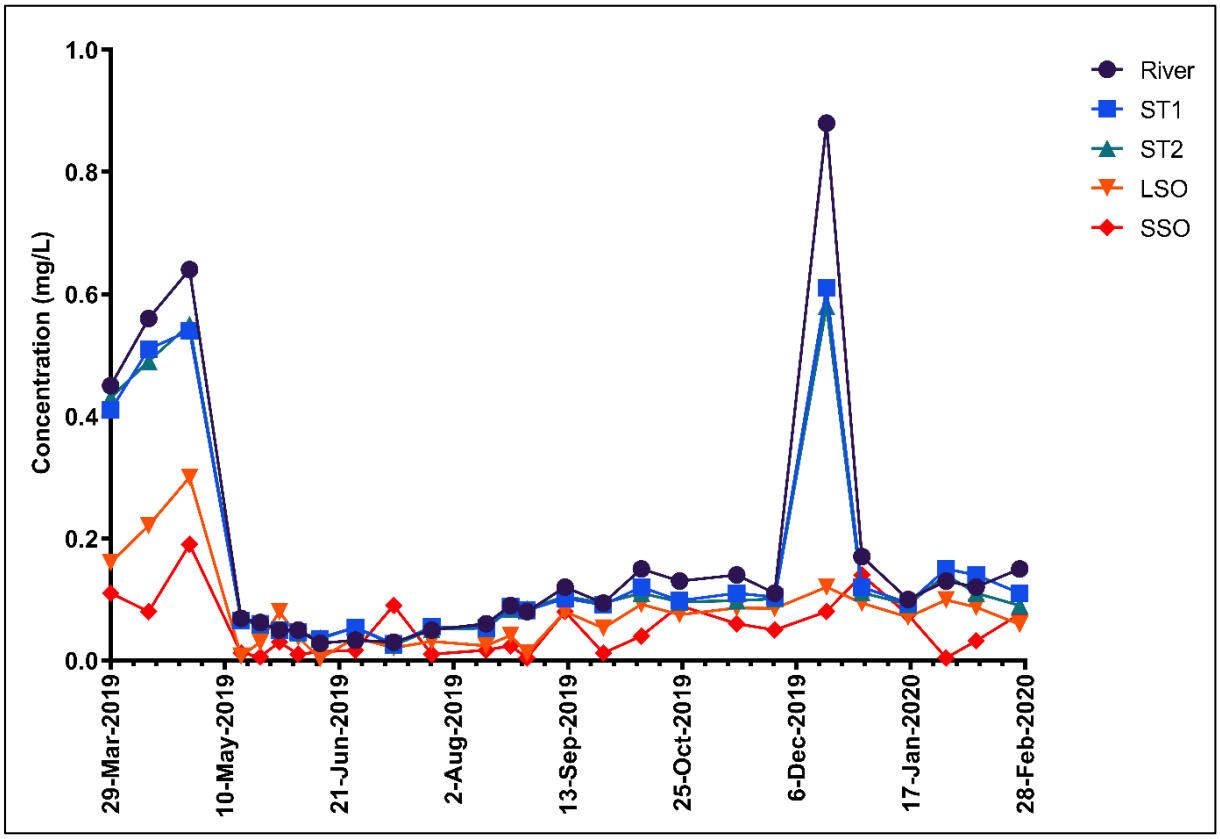

Figure 4.15: Nitrite concentrations at various sampling sites over a 12-month period (n = 26 for each sampling site, std dev < 0.028 mg/L)

Figure 4.16 shows the total nitrogen concentrations at the five sampling sites over the twelve-month sampling period. There is a large decrease in total nitrogen from the

biofilter inlet (ST2) to the large stones and small stones outlets. The total nitrogen concentrations in the large and small stones outlets remains below 0.223 mmol/L indicating the efficiency of the large and small stone biofilters in total nitrogen removal from an inlet concentration of 0.400 – 2.14 mmol/L through nitrification and denitrification. The Wilcoxon Signed-Ranked Test showed that the difference between the total nitrogen concentrations observed in the large stones outlet and small stones outlet is not statistically significant (see Appendix B).

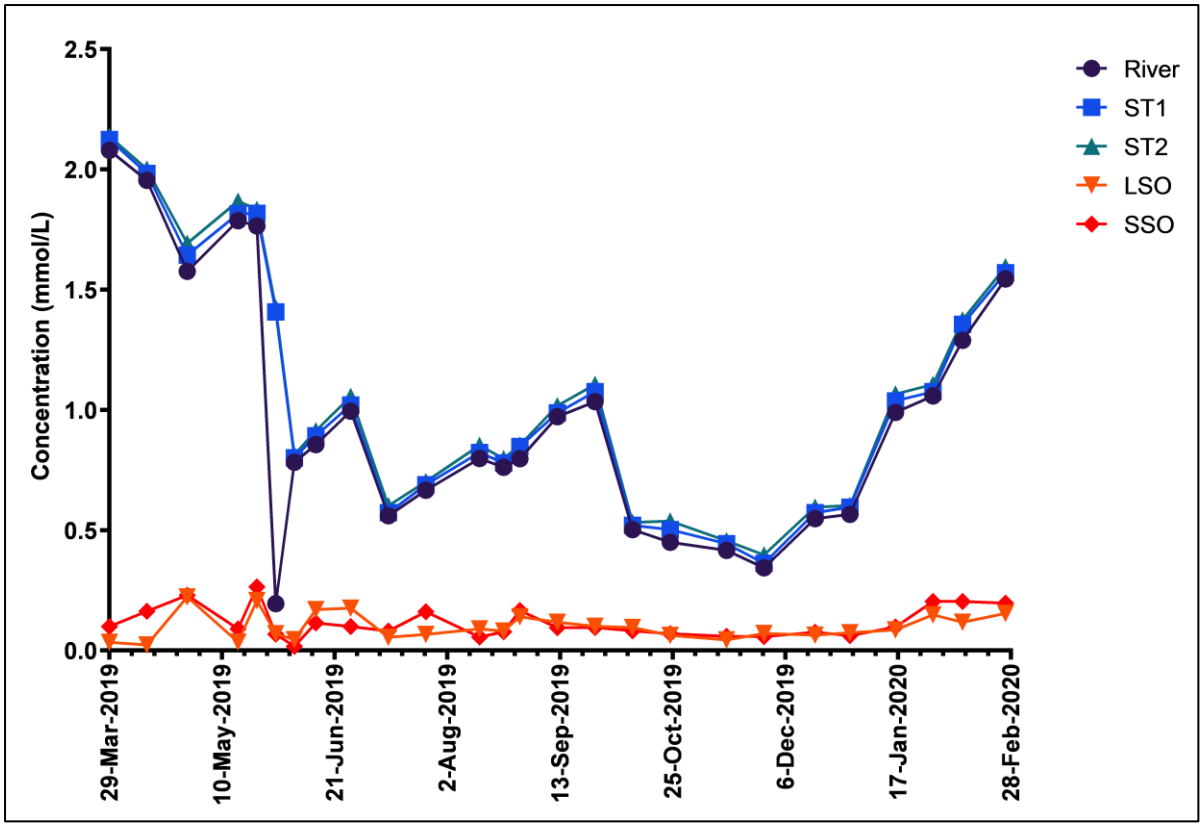

Figure 4.16: Total nitrogen concentrations at various sampling sites over a 12-month period

Figure 4.17 shows orthophosphate concentrations at the five sampling sites. The outlet of the large stones biofilter sees concentrations of less than 1.28 mg/L while the orthophosphate concentrations in the small stones outlet remain below 0.940 mg/L. The difference between the orthophosphate concentrations observed in the large stones outlet and the small stones outlet is statistically significant (see Appendix B) with the small stones biofilter being more effective in orthophosphate removal than the large stones biofilter.

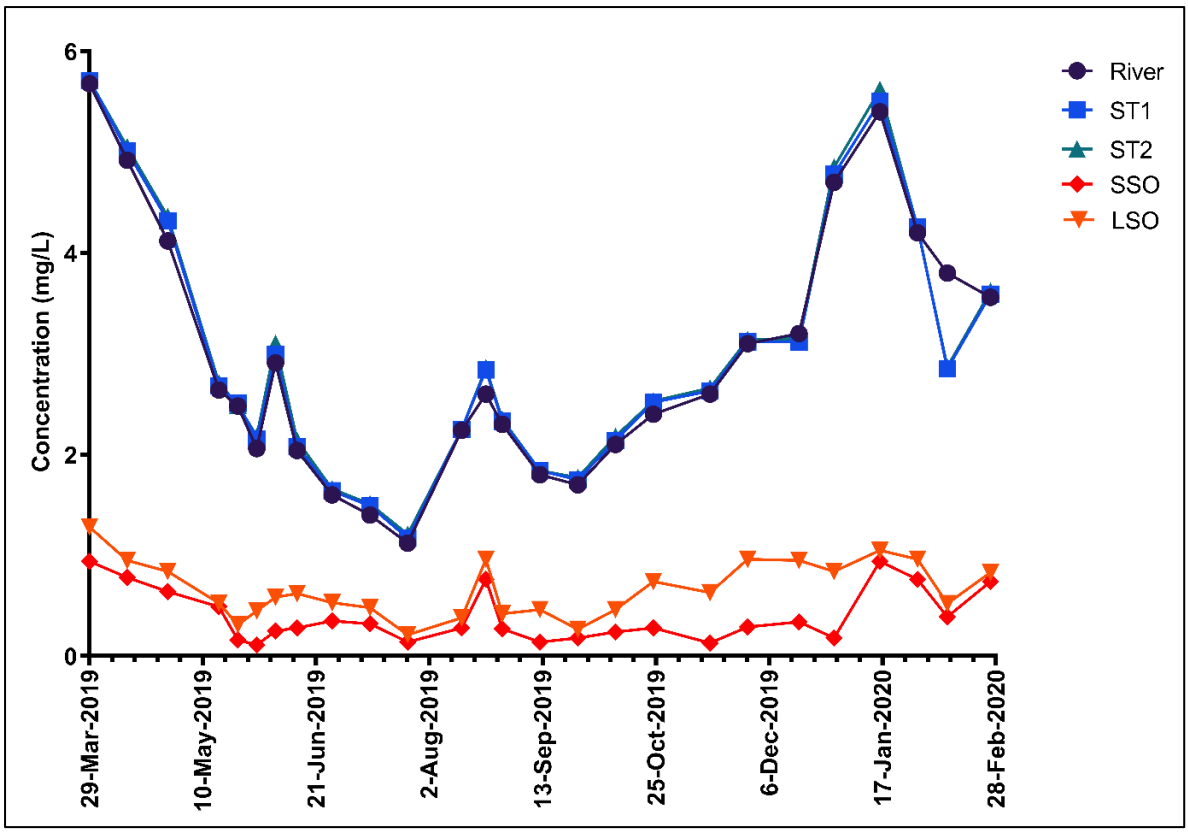

Figure 4.17: Orthophosphate concentrations at various sampling sites over a 12-month period (n = 26 for each sampling site, std dev < 0.042 mg/L)

Table 4.1 shows the mean and median residual ammonia, nitrate and orthophosphate concentrations in both the large and small stone biofilters along with those observed in Settling Tank 2 over the 12-month sampling period. The median concentrations are presented below the mean concentrations. Settling Tank 2 is used to feed the biofilters, representing the biofilter inlet concentration range.

The mean residual ammonia concentration in the large and small stone biofilters is below 2 mg/L. This is acceptable for domestic use as per the South African Domestic Water Use Guidelines; however, there is a possibility of poor taste and odour if used for drinking purposes. The mean residual nitrate and nitrite concentrations in the stone biofilters are well below 6 mg/L making the treated water safe for domestic use (Department of Water Affairs and Forestry, 1996). The stone biofilters are able to reduce orthophosphate concentrations to an average of 0.660 mg/L for the large stones biofilter and 0.400 mg/L for the small stones biofilter. This is below the water quality requirement of less than 2.5 mg/L for domestic use (Department of Water Affairs and Forestry, 1996). When compared to the water quality guidelines in Table 2.1, it is apparent that the treated water is safe for discharge into rivers and meets the water quality requirements for domestic use.

Table 4.1: Mean and median residual nutrient concentrations in large & small stones biofilters

	Concentrations in Settling Tank 2 (Biofilter Inlet) (mg/L)	Mean & Median Residual Concentration in Large Stones Biofilter (mg/L)	Mean & Median Residual Concentration in Small Stones Biofilter (mg/L)
Ammonia	6.40 - 35.4	1.47 ± 0.915 1.23	1.83 ± 1.05 1.49
Nitrate	0.415 – 3.42	0.630 ± 0.259 0.625	0.410 ± 0.203 0.350
Orthophosphate	0.510 – 5.71	0.660 ± 0.276 0.603	0.400 ± 0.264 0.285

*** Median concentrations are presented below mean concentrations**

Concentration data is easily obtainable from the Water Hub biofilters, however a lack of supporting data such as the volume of water being pumped into each biofilter as well as the hydraulic residence time for each treatment batch precludes rigorous analysis of the performance of the biofilters in terms of nutrient reduction. To explore the factors impacting biofilter performance, a controlled lab study on biofilter performance using the pilot biofilter has been conducted. The impact of inlet nutrient concentrations on performance are presented in Chapter 7, along with analysis to provide a greater understanding of nutrient degradation kinetics in non-vegetated stone biofilters.

4.4. Conclusions

The nutrient concentrations in the Stiebeuel River vary seasonally with concentrations being higher in the summer months characterised by low rainfall and a higher occupancy at Langrug. Ammonia concentrations in the river are 5.50 - 25.3 mg/L during the summer period and 3.20 – 30.1 mg/L in the winter months. Nitrate concentrations in the Stiebeuel River range between 1.15 – 3.50 mg/L in the summer months and 0.300 – 1.25 mg/L in the winter months. The range of orthophosphate concentrations in the river is 2.60 – 5.40 mg/L during the summer months and 1.12 – 2.91 mg/L in the winter months.

The biofilters are able to achieve significant nutrient reductions with average residual ammonia concentrations of 1.47 mg/L in the large stones biofilter and 1.83 mg/L in the small stones biofilter. The average residual orthophosphate concentrations are 0.660 mg/L in the large stones biofilter and 0.400 mg/L in the small stones biofilter.

The findings from this twelve-month data gathering task shows that the nutrient concentrations in the Stiebeuel River are highly variable. It would be appropriate to carry out the nutrient degradation studies in the summer months as the nutrient concentrations are generally higher in summer. The approximate expected inlet nutrient concentration ranges for the nutrient degradation studies, which will be carried out in the summer period, are therefore: 5.5 – 25 mg/L ammonia; 1.4 – 3.5 mg/L nitrate and 2.6 – 4.7 mg/L orthophosphate.

5. HYDRAULIC CHARACTERISTICS OF THE PILOT BIOFILTER

5.1. Introduction

The pilot biofilter was designed to represent the Water Hub biofilters. The results from the pilot biofilter studies provide context against which to consider the performance of the Water Hub biofilters.

Following pilot biofilter design, the hydraulic characterisation of the pilot biofilter at various flow rates using residence time distribution modelling was carried out and mixing patterns within the biofilter explored. The hydraulic characterisation was also used to diagnose non-ideal flow within the biofilter through multiple tracer studies.

5.2. Materials and Methods

5.2.1. Pilot biofilter design

The pilot biofilter was designed to mimic the Water Hub biofilters so that the experiments performed on the pilot system provide insight into the design and operation of the Water Hub biofilters. The length and width of the pilot biofilter were scaled down from the length and width of the Water Hub biofilters by a factor of 8. The depth, equivalent to bed height, was kept the same as the Water Hub biofilters to create aerobic and anaerobic zones in the pilot biofilter that imitate the aerobic and anaerobic zones in the Water Hub biofilters.

The pilot biofilter is representative of a “slice” of the Water Hub biofilters with 64 identical pilot biofilters being able to fit into a single Water Hub biofilter. The structure of the pilot biofilter was constructed out of plywood. The exterior edges and corners were waterproofed using silicon sealant. The interior edges and corners of the biofilter were waterproofed with a fibreglass layer. A layer of plastic sheeting was placed over the fibreglass as a further waterproofing measure. Figure 5.1, Figure 5.2 and Figure 5.3 are labelled scale diagrams of the aerial and end views of the pilot biofilter.

Table 5.1 shows the design specifications of the pilot biofilter compared to that of the small stones biofilter at the Water Hub. The length and width of the pilot biofilter were scaled down from the length and width of the Water Hub biofilters by a factor of 8. The depth, equivalent to bed height, was kept the same as the Water Hub biofilters to create aerobic and anaerobic zones in the pilot biofilter that imitate the aerobic and anaerobic zones in the Water Hub biofilters.

The pilot biofilter is representative of a “slice” of the Water Hub biofilters with 64 identical pilot biofilters being able to fit into a single Water Hub biofilter. The structure

of the pilot biofilter was constructed out of plywood. The exterior edges and corners were waterproofed using silicon sealant. The interior edges and corners of the biofilter were waterproofed with a fibreglass layer. A layer of plastic sheeting was placed over the fibreglass as a further waterproofing measure. Figure 5.1, Figure 5.2 and Figure 5.3 are labelled scale diagrams of the aerial and end views of the pilot biofilter.

Table 5.1: Pilot biofilter equipment specification sheet

EQUIPMENT SPECIFICATION SHEET: PILOT BIOFILTER			
Specification	**Unit**	**Value**	
		Small Stones Biofilter at Water Hub	**Pilot Biofilter**
Maximum Volumetric Flow Rate	L/min	-	9
Empty Volume	m^3	39.2	0.616
Packing Material		Small Stones	Small Stones
Size Distribution of Packing Material	mm	7-9	8-11
Bed Voidage		0.46	0.42
Volume Available to Contain Liquid	m^3	18.0	0.225
Filter Shape	-	Rectangular Prism	Rectangular Prism
Aspect Ratio	-	4.6	4.5

Bed Length	m	16	2
Bed Width	m	3.5	0.44
Bed Height	m	0.7	0.7
Wall thickness	mm	-	20
Inlet Pipe Diameter	mm	50	25
Width of Inlet Distributor	cm	350	42
Number of Inlet Points on Inlet Distributor		4	4
Diameter of Inlet Points	mm	15	5
Outlet Diameter	mm	50	25
Number of Outlets		1	3
Orientation	-	Horizontal	Horizontal
Material of Construction	-	Concrete Exterior Plastic Interior	Wood Exterior Fibreglass and Plastic Interior
Operating Pressure	atm	1.00	1.00

Aerial View of Pilot Biofilter (Without Packing)	**Scale:** 1 drawing unit = 1 cm

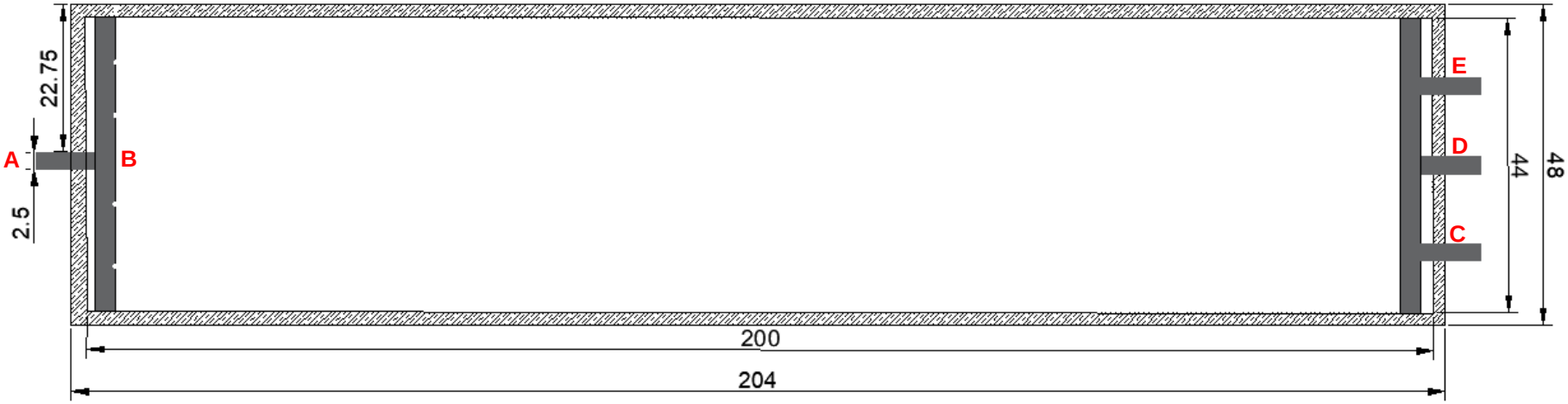

A - 25 mm inlet pipe

B - Inlet distributor with 4 inlet points

C - Outlet A

D - Outlet B

E - Outlet C

Figure 5.1: Aerial schematic of pilot biofilter

End View of Pilot Biofilter (Facing Inlet)	**Scale:** 1 drawing unit = 1 cm

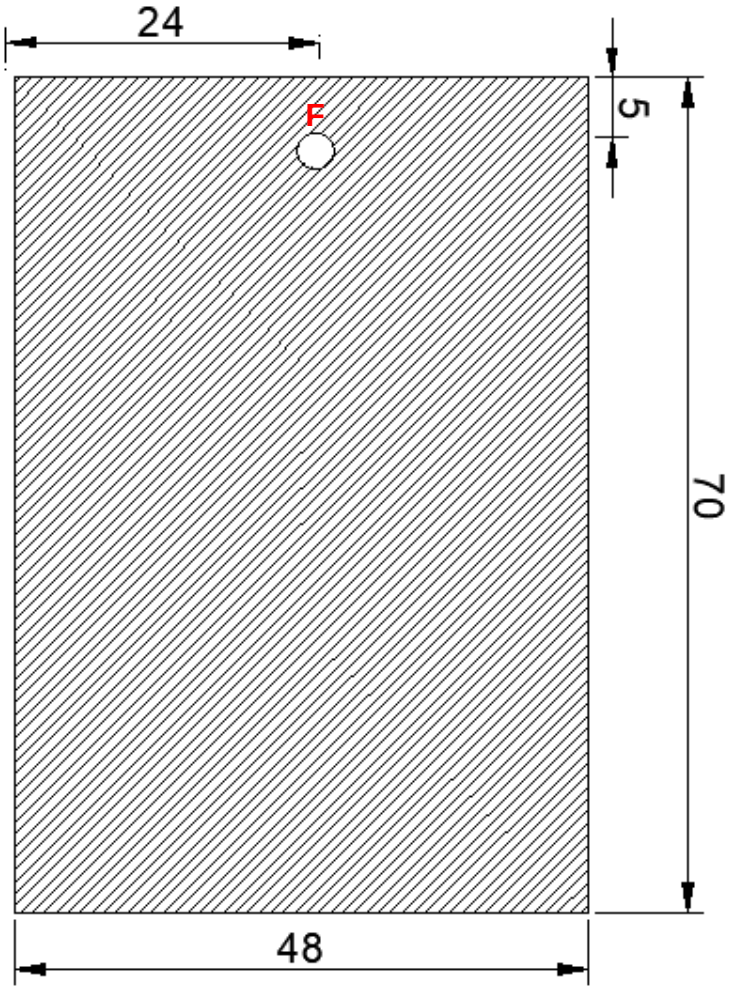

F - 25 mm inlet pipe

Figure 5.2: End view of pilot biofilter (facing inlet)

End View of Pilot Biofilter (Facing Outlet)	**Scale:** 1 drawing unit = 1 cm

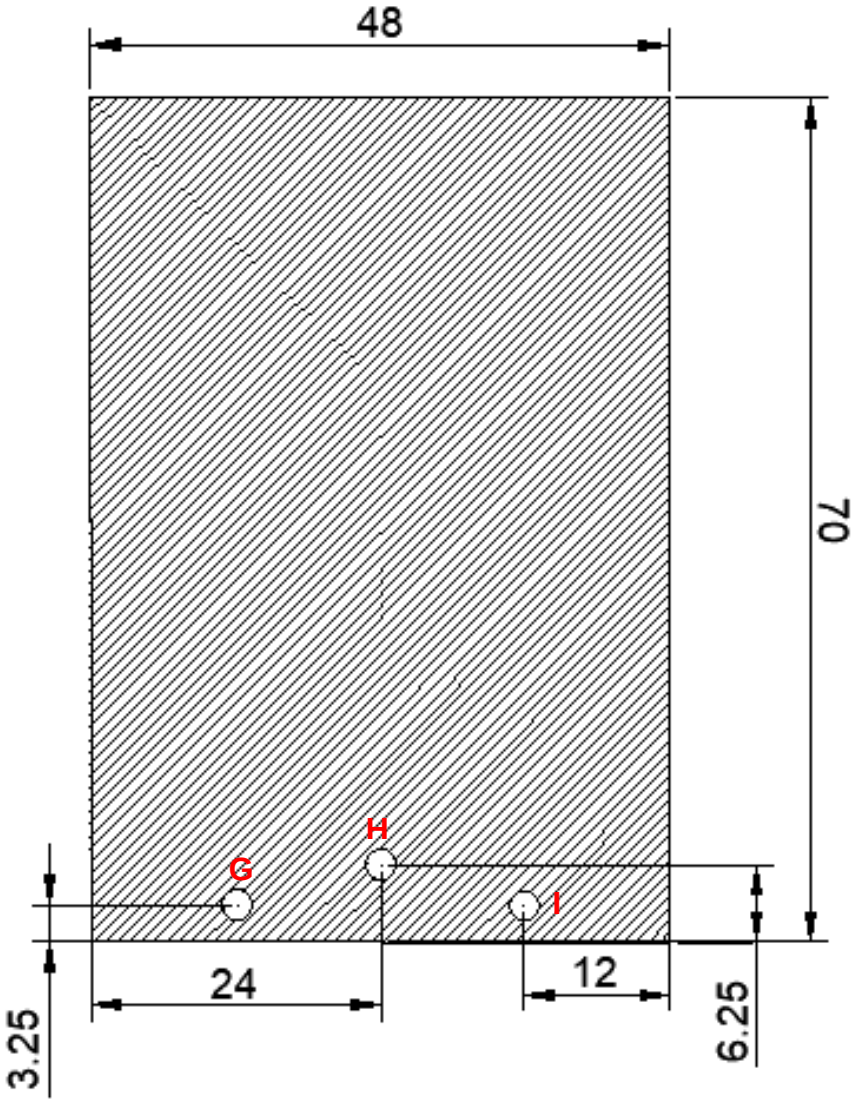

G - Outlet A

H - Outlet B

I - Outlet C

Figure 5.3: End view of pilot biofilter (facing outlets)

River stones with a density of 1470 kg/m^3 were used as the filter media. The stones were crushed to a size range of 8–11 mm using a jaw crusher with the undersize stones being discarded. The undersize stones were discarded instead of being used as packing material to prevent silting at the bottom of the pilot biofilter. The 8-11 mm small stones were then used as the filter media. 600 L of stones in total were used to pack the pilot biofilter. Table 5.2 shows the size distribution of the crushed stones as recorded during the sieving process. The mean particle diameter of the stones after crushing is 9 mm.

Table 5.2: Size distribution of stones following removal of fines to prevent silting of filter

Sieve Diameter	Volume (litres)	% Retained	Cumulative % Passing
11 mm	0	0	100%
9 mm	465	77.5%	22.5%
8 mm	135	22.5%	0

Ten sampling ports constructed as stainless-steel mesh wire cylinders with a diameter of 20 mm were placed in the pilot biofilter to enable sampling at different depths. Samples can be taken by inserting flexible silicon tubing into the sampling port and drawing the liquid out using an appropriately sized syringe. The silicon tubing allowed for sampling at different depths within the sampling ports. This was particularly useful in the tracer studies where tracer concentrations were taken from 5 cm below the surface as well as 35 cm below the surface. Figure 5.4 is an aerial view of the pilot biofilter with the sampling ports (1 to 10) and outlets (A, B and C) labelled in red. The distances of the sampling ports to the filter walls can be noted from Figure 5.4.

Figure 5.5 shows the pilot biofilter with the three outlets, sampling ports and stone filter media clearly visible in the image. The two side outlets (outlet A and outlet C) are positioned 2 cm above the bottom of the pilot biofilter. These outlets may experience obstructed flow in the event of a sediment build-up at the bottom of the biofilter. The middle outlet (outlet B) is therefore positioned 3 cm above outlets A and C. This is to ensure that effluent can always exit the pilot biofilter unimpeded.

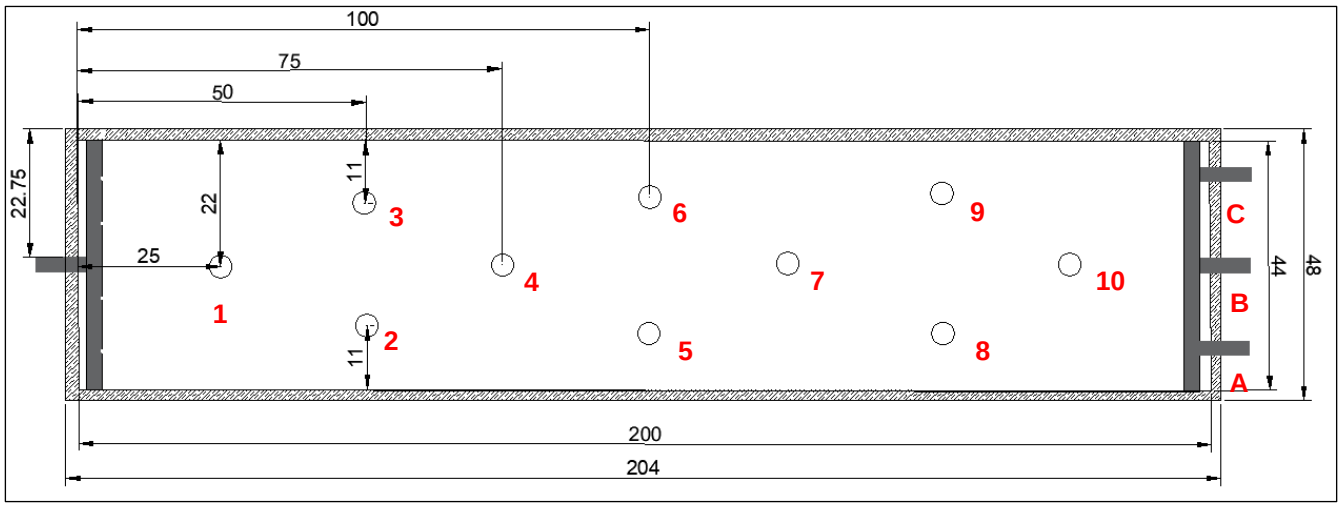

Figure 5.4: Aerial view of pilot biofilter with position of sampling ports 1- 10 and outlets (A, B and C) labelled in red (dimensions in cm)

Figure 5.5: Complete pilot biofilter

Figure 5.6: Pilot biofilter inlet (photographed during construction)

Figure 5.6 shows the inlet distributor which spanned the width of the pilot biofilter. This inlet distributor was 25 mm in diameter and contained four 5 mm holes that were spaced 10cm apart to allow an even flow distribution at the inlet of the pilot biofilter.

5.2.2. Pulse tracer studies

Pulse tracer studies at multiple flow rates were conducted to generate concentration-time data to determine the residence time distributions of the pilot biofilter at the respective flow rates. In a pulse tracer study, a fixed volume of tracer of known concentration is injected into the system inlet as a single pulse and the concentration of the tracer being monitored at the outlet.

Allura Red AC ($C_{18}H_{14}N_2Na_2O_8S$) dye was chosen as the tracer for the pulse tracer studies as it contains two sulfonic acid groups which minimise adsorption onto the filtration media thus reducing tracer loss due to adsorption.

Laminar flow is required for tracer studies since laminar flow is reversible. The resulting residence time distributions can be normalised with time, thereby allowing comparisons between residence time distributions of different flow rates. The Reynolds number (equation 5.1) for laminar flow in a packed bed reactor is less than 10 and is greater than 2000 for turbulent flow.

$$Re = \frac{D_p u_s \rho}{(1-\varepsilon)\mu} \qquad \text{Equation 5.1}$$

where D_p is particle diameter (m);

u_s is superficial velocity (m/s);

ρ is density of fluid (kg/m^3);

μ is the dynamic viscosity of the fluid (Pa.s)

A flow rate of less than 10.5 L/min resulted in laminar flow in the pilot biofilter while a flow rate of greater than 2150 L/min resulted in turbulent flow. Empirically, the maximum flow capacity in the pilot biofilter was 9 L/min (avoiding splashing and spillage) while the minimum flow capacity was 0.5 L/min. The flow rates selected for the nutrient degradation kinetics studies were considered when choosing the flow rates to conduct the pulse tracer studies. The flow rate range of 0.5 L/min - 3 L/min was selected for the nutrient degradation kinetic studies to provide a sufficiently long residence time to yield substantial nutrient degradation. The pulse tracer studies were therefore conducted at 3 L/min, 2 L/min, 1.5 L/min, 1 L/min, 0.75 L/min and 0.5 L/min.

The following procedure was conducted during the pulse tracer studies:

1. The pilot biofilter inlet was connected to a tap supplying municipal water using a 20 mm hosepipe.
2. The tap was adjusted to ensure a constant inlet flow rate at the desired flow rate and the liquid level in the pilot biofilter was monitored until liquid could be seen below the surface of the stones. Flow rates were monitored using a digital flow meter.
3. The middle outlet valve of the pilot biofilter (outlet B) was adjusted such that the outlet flow rate was the same as the inlet flow rate (steady state).
4. 50 ml of Allura Red dye at a concentration of 5 g/L was injected into the tracer inlet of the pilot biofilter (seen in Figure 5.7).
5. Samples were taken from outlet B and the sampling ports according to the sampling regime for each flow rate (example seen in Table 5.3) for the duration of the experiment.
6. The pulse tracer study was conducted three times for each flow rate to ensure the reproducibility of the results obtained.

Figure 5.7 shows the inlet for tracer injection. The inlet was sealed after tracer injection to prevent leakages. Table 5.3 is an example of the sampling regime followed for the pulse tracer study at 3 L/min. Samples were taken using flexible silicon tubing and a 10 ml syringe at two different depths: 5 cm below the surface and 35 cm below the surface. The sampling regime for the tracer studies at 2 L/min, 1.5 L/min, 1L/min, 0.75 L/min and 0.5 L/min can be found in Appendix C. Samples were taken from outlet B every 5 minutes for the pulse tracer study at 3 L/min. The absorbance at a wavelength

of 504 nm was measured for each sample within 24 hours. The concentrations were then calculated using the calibration curve for Allura Red Dye (see Appendix D).

Figure 5.7: Inlet for tracer injection (inlet opened in left image and closed in right image).

Table 5.3: Sampling regime for pulse tracer study at 3 L/min

Time (min)	SP 1	SP 2 & 3	SP 4	SP 5 & 6	SP 7	SP 8 & 9	SP 10
0	X						
5	X						
10	X	X					
15	X	X					
20	X	X	X				
25	X	X	X				
30	X	X	X				
35		X	X	X			
40		X	X	X			
45			X	X	X		
50				X	X		
55				X	X		
60					X	X	X
65					X	X	X
70						X	X
75						X	X
80						X	X
85							X
90							X

5.2.3. Modelling hydraulic performance using residence time distribution

Hydraulic performance has been modelled according to Fogler (2011). The theoretical residence time, τ, of the pilot biofilter system was calculated using Equation 5.2. The theoretical residence time describes the hydraulic residence time that would be observed if the pilot biofilter operated in an ideal manner (i.e., no dead zones or channelling).

$$\tau = \frac{V}{Q} \qquad \text{Equation 5.2}$$

where V is the available volume of the pilot biofilter (L);
Q is the experimental flow rate (L/min)

The residence time distribution function, E(t), is derived from the concentration-time data observed in the pulse tracer studies using Equation 5.3.

$$E(t) = \frac{C(t)}{\int_0^\infty C(t)\,dt} \qquad \text{Equation 5.3}$$

The mean residence time distribution is calculated using Equation 5.4. This is a representation of the actual hydraulic residence time in the system.

$$\bar{t}_m = \int_0^\infty t\,E(t)\,dt \qquad \text{Equation 5.4}$$

The variance is the centred second moment of the residence time distribution. It is used to describe the spread of the data and is calculated using Equation 5.5.

$$\sigma^2 = \int_0^\infty t^{\,2} E(t)\,dt - \bar{t}_m{}^2 \qquad \text{Equation 5.5}$$

The reversible flow properties of laminar flow allow for the residence time distributions to be normalised with respect to time. This is valuable as it enables comparisons between hydraulic data generated at different flow rates. Equation 5.6 and Equation 5.7 show the normalisation of the hydraulic data into dimensionless variables.

$$\theta = \frac{t}{\bar{t}_m} \qquad \text{Equation 5.6}$$

$$E(\theta) = \bar{t}_m E(t)$$ Equation 5.7

where θ represents the number of reactor volumes that have flown through the system.

The effective volume utilisation, e, describes the portion of the reactor volume that is being utilised. The unutilised portion of the reactor is assumed to be dead space. The effective volume utilisation can be calculated using Equation 5.8.

$$e = \frac{\bar{t}_m}{\tau}$$ Equation 5.8

The tanks in series model is used to determine the number of equally sized, ideal continuous stirred tank reactors (CSTRs) in series that approximate the hydraulic performance of the system. The number of tanks in series is determined using Equation 5.9.

$$N = \frac{\bar{t}_m{}^2}{\sigma^2}$$ Equation 5.9

The fluid dynamics of the system approach mixed flow behaviour when N → 1 while the fluid dynamics approach ideal plug flow behaviour when N → ∞.

The hydraulic efficiency is used to determine the hydraulic performance of non-ideal reactors with ideal plug flow systems being 100% efficient. Hydraulic efficiency can be calculated using Equation 5.10.

$$\Lambda = e\left(1 - \frac{1}{N}\right)$$ Equation 5.10

The Peclet number (Pe) can be used to determine whether advective flow or dispersive mass transfer is dominant in the system. Pe is calculated using the relationship described in Equation 5.11.

$$\frac{\sigma^2}{\bar{t}_m{}^2} = \frac{2}{Pe} - \frac{2}{Pe^2}\left(1 - e^{-Pe}\right)$$ Equation 5.11

Advective flow is dominant and dispersive mass transfer is negligible if Pe >> 1. The system approaches ideal plug flow behaviour as Pe increases with mixing occurring in the radial direction.

Tracer recovery (%) is calculated using Equation 5.12.

$$recovery = \frac{Q \int_0^\infty C(t)\, dt}{M_0}$$ Equation 5.12

where M_0 is the mass of tracer injected into the system at time 0.

5.3. Results

5.3.1. Pulse tracer study at 3 L/min

This concentration vs. time data for all sampling points and outlet B as well as residence time distribution (as measured at outlet B) for the pulse tracer study at 3 L/min is presented in detail in this section. The concentration vs time data and residence time distributions as measured at outlet B for all six experimental flow rates is presented in Section 5.3.2. The concentration profiles as measured 5 cm below the surface and 35 cm below the surface is also presented in Section 5.3.2.

Figure 5.8 and Figure 5.9 show the concentration vs. time data and residence time distribution, respectively, for the pulse tracer study at 3 L/min as measured at outlet B. The long tail seen from 80 minutes to 100 minutes is indicative of a dead zone or fluid hold-up in tortuous pathways. The large error bars are likely due to the sensitivity of the tracer concentration to slight variations in sampling times at this higher flow rate.

Figure 5.10 shows the concentration profiles along the length of the pilot biofilter at 5 cm below the surface and 35 cm below the surface. Figure 5.10 shows that there was an even flow distribution across the width of the pilot biofilter at 5 cm below the surface, with sampling points on left and right at the same distance along the biofilter giving the same profiles. The peak concentration at each sampling port was approximately 6 mg/L. Figure 5.10 also shows a slight increase in concentration along the length of the pilot biofilter as measured 35 cm below the surface. This can be attributed to the dye infiltrating deeper into the bed of the pilot biofilter, while also evenly distributed radially.

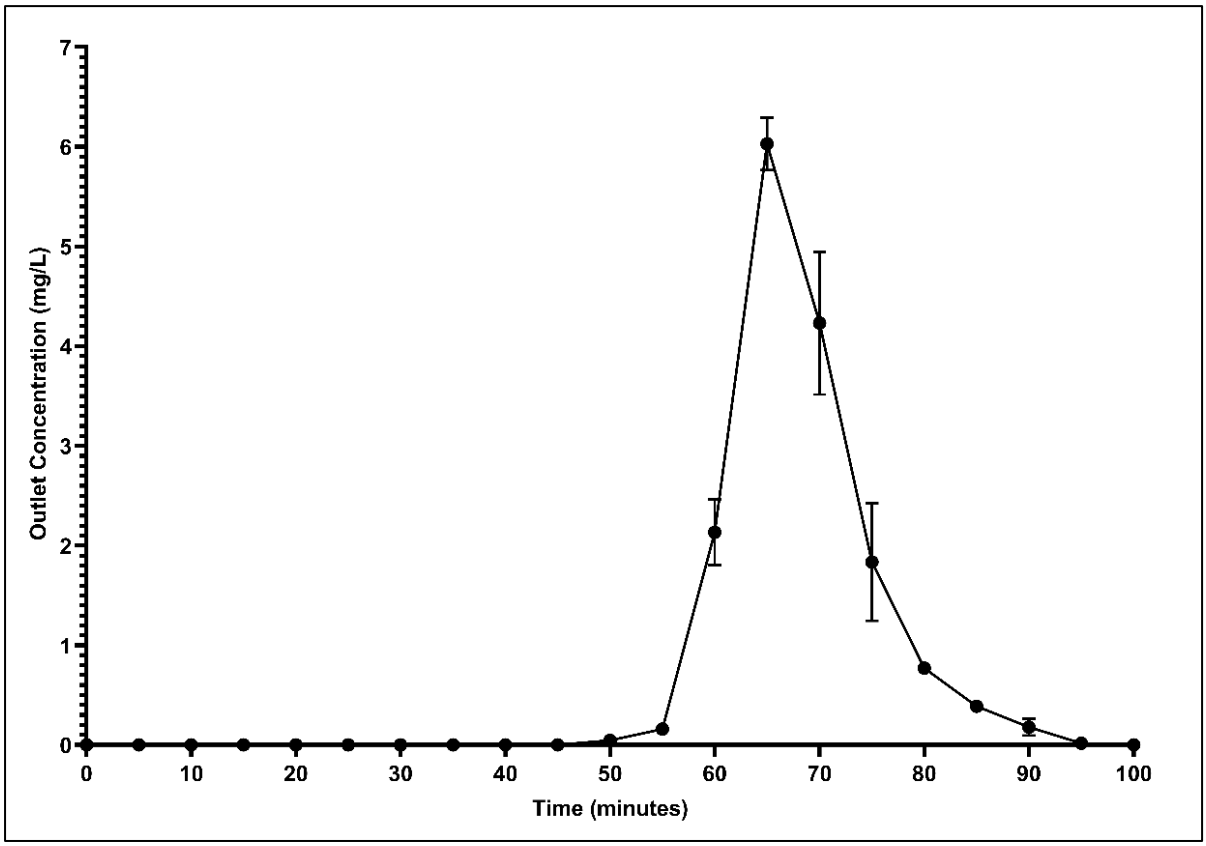

Figure 5.8: Concentration vs. time for tracer study at 3 L/min as measured at Outlet B

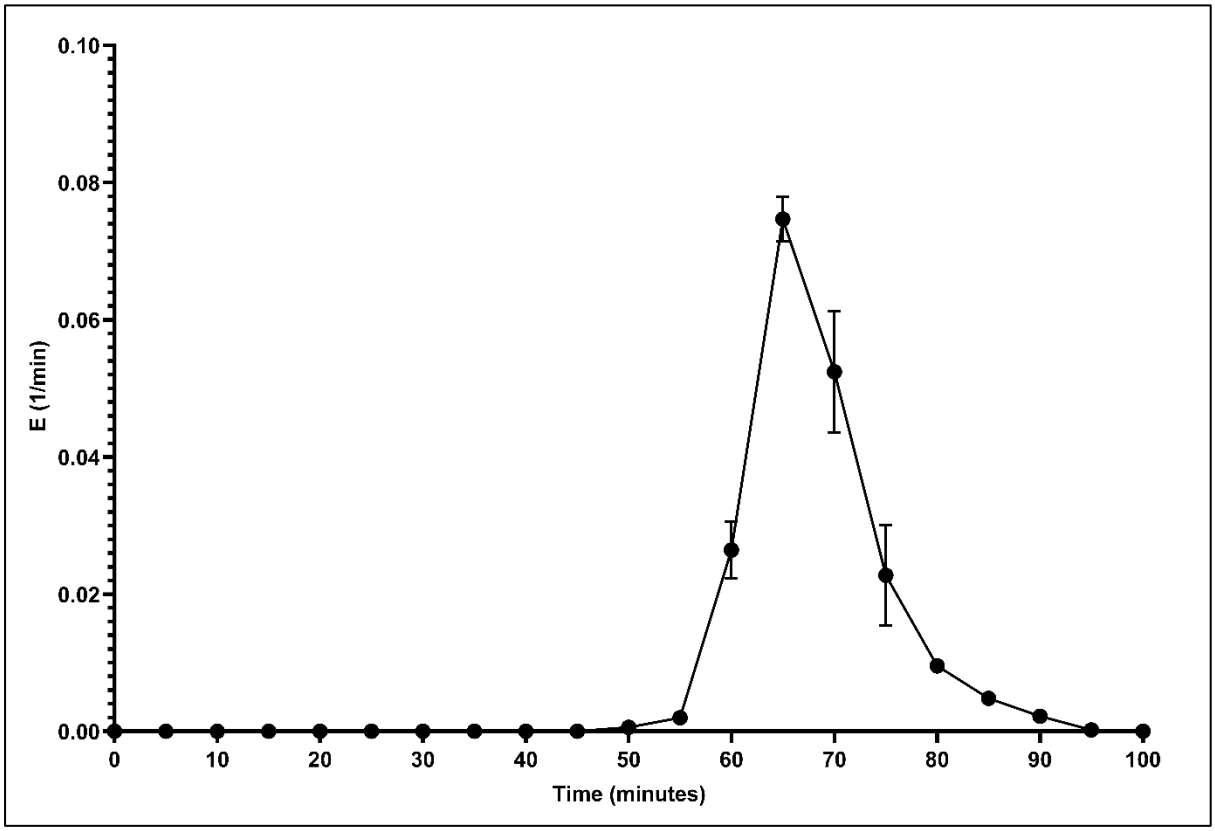

Figure 5.9: Residence time distribution for tracer study at 3 L/min as measured at Outlet B

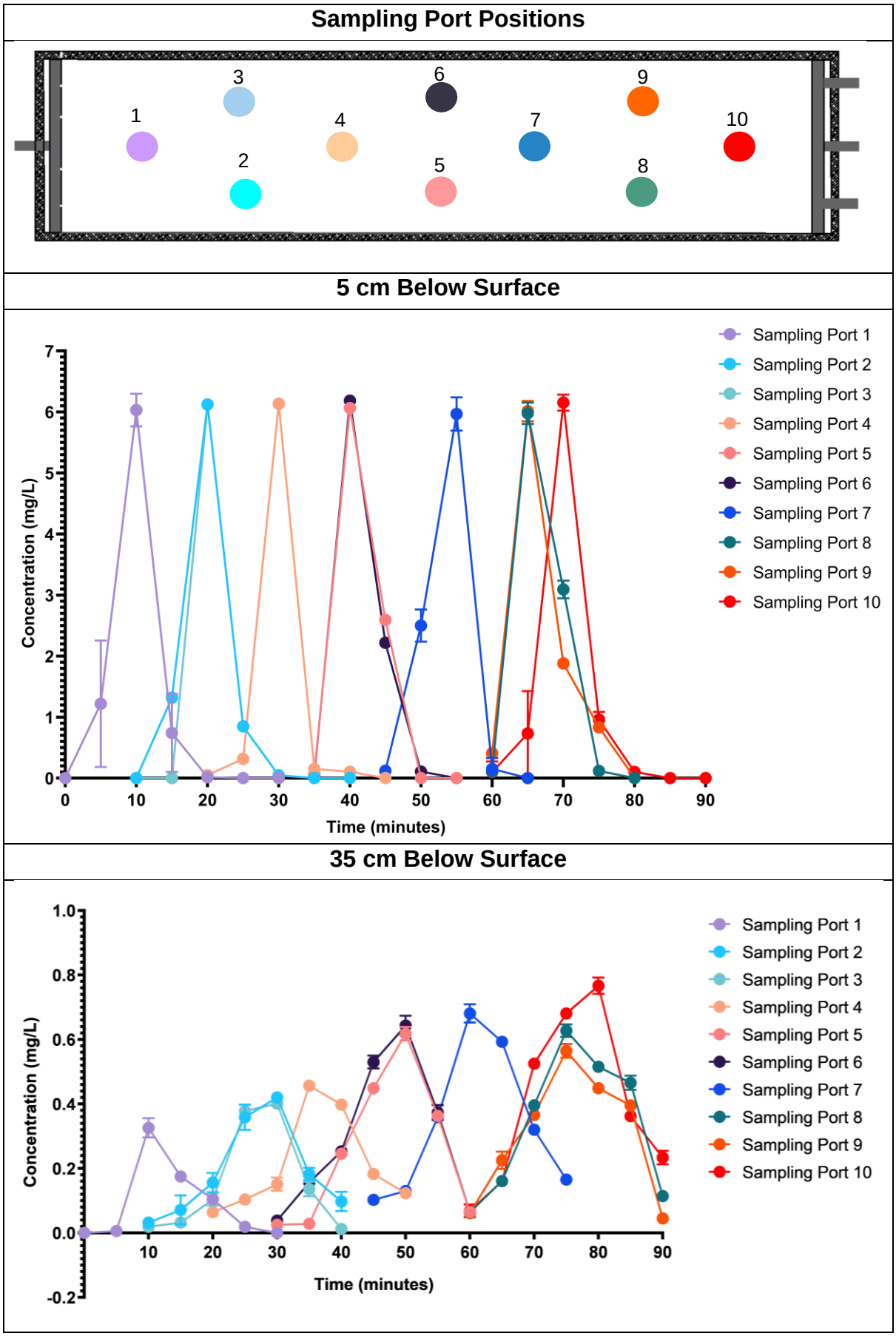

Figure 5.10: Concentration profiles across pilot biofilter for pulse tracer study at 3 L/min

5.3.2. RTD and concentration data at all experimental flowrates

Figure 5.11 shows concentration data measured at outlet B for all tracer studies.

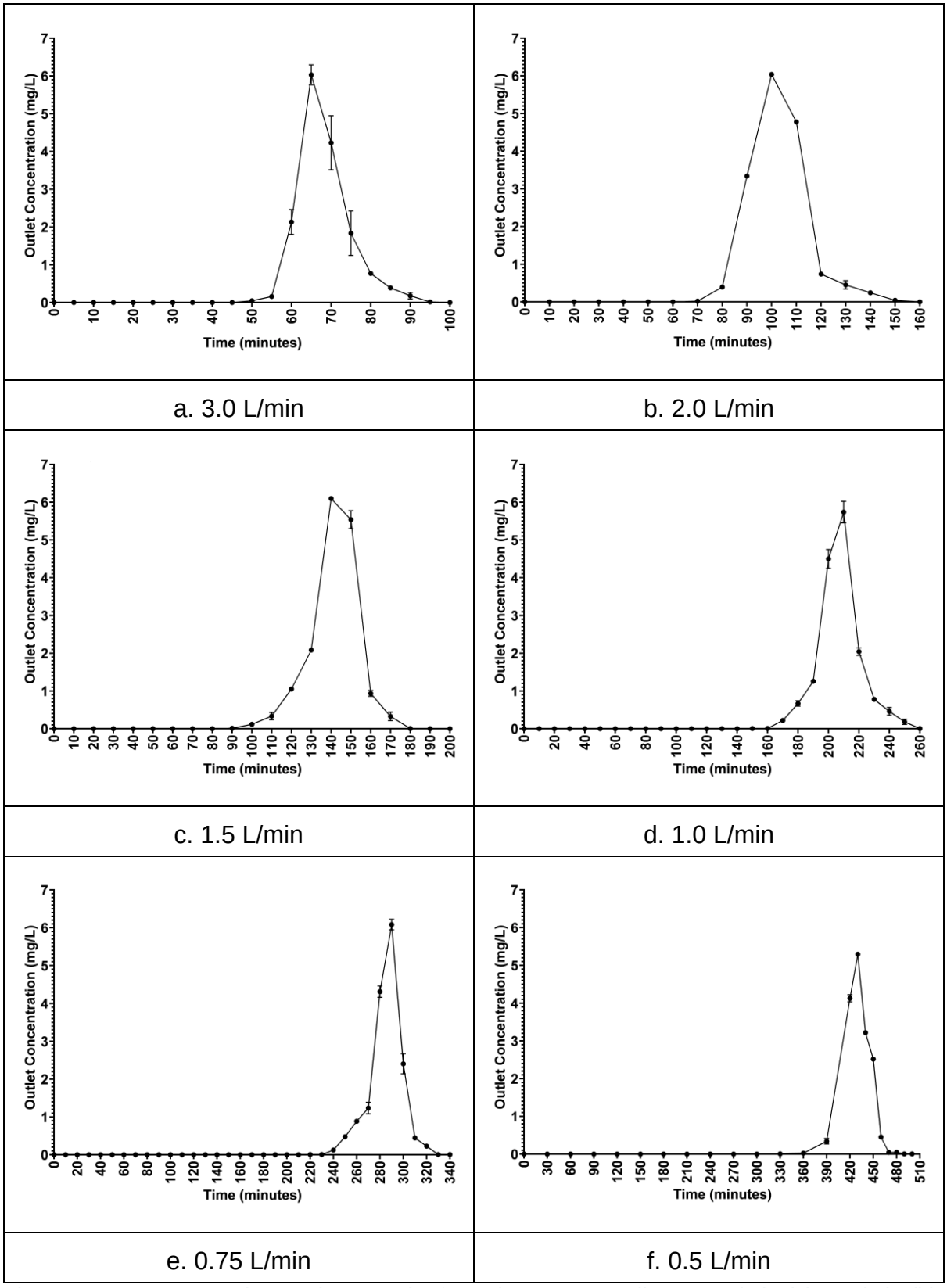

Figure 5.11: Concentration vs time graphs for pulse tracer studies at 3 L/min (a), 2 L/min (b), 1.5 L/min (c), 1 L/min (d), 0.75 L/min (e) and 0.5 L/min (f)

Figure 5.12 shows the residence time distribution at outlet B for the pulse tracer studies at all six experimental flow rates.

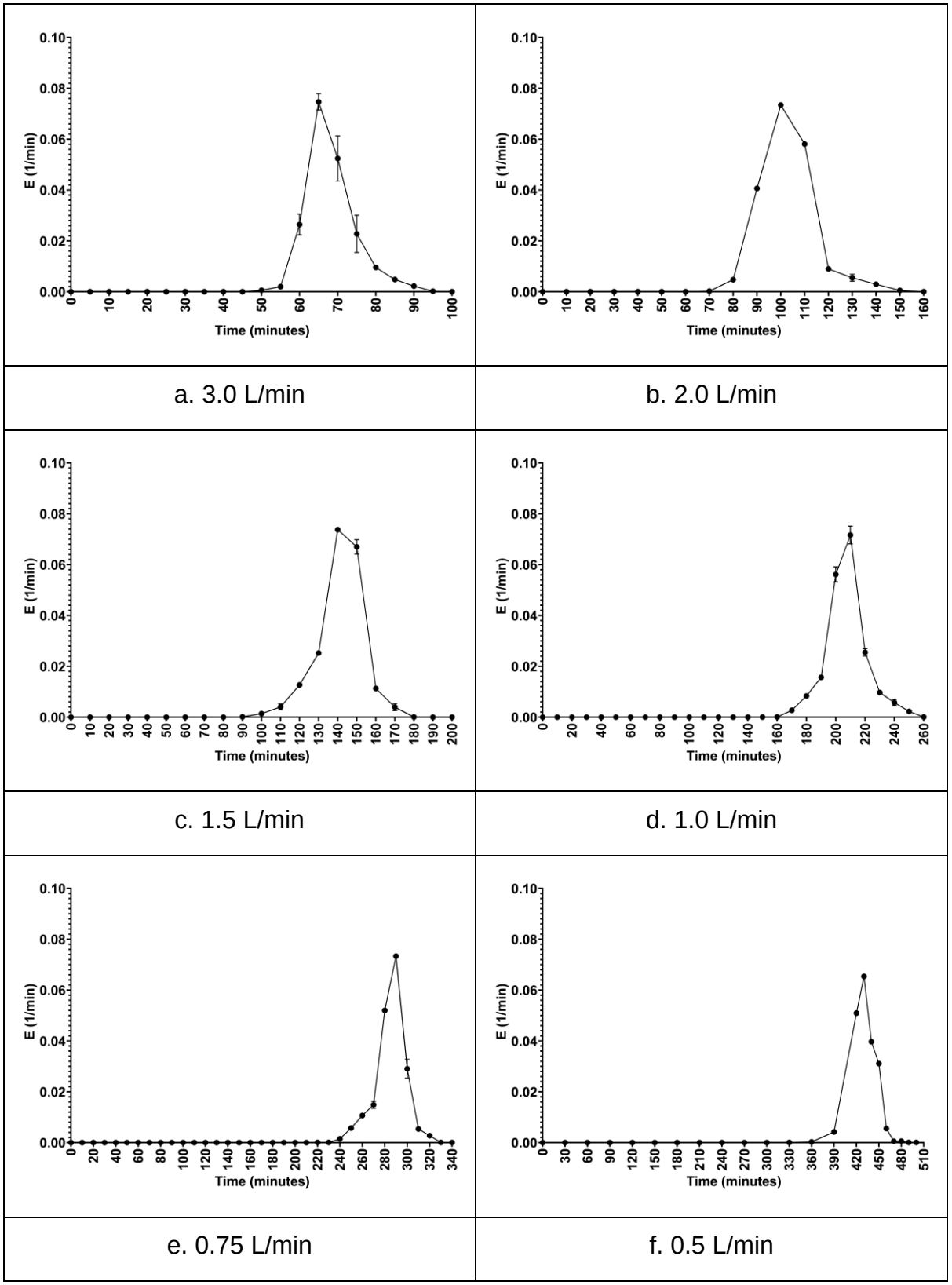

Figure 5.12: Residence time distributions for pulse tracer studies at 3 L/min (a), 2 L/min (b), 1.5 L/min (c), 1 L/min (d), 0.75 L/min (e) and 0.5 L/min (f)

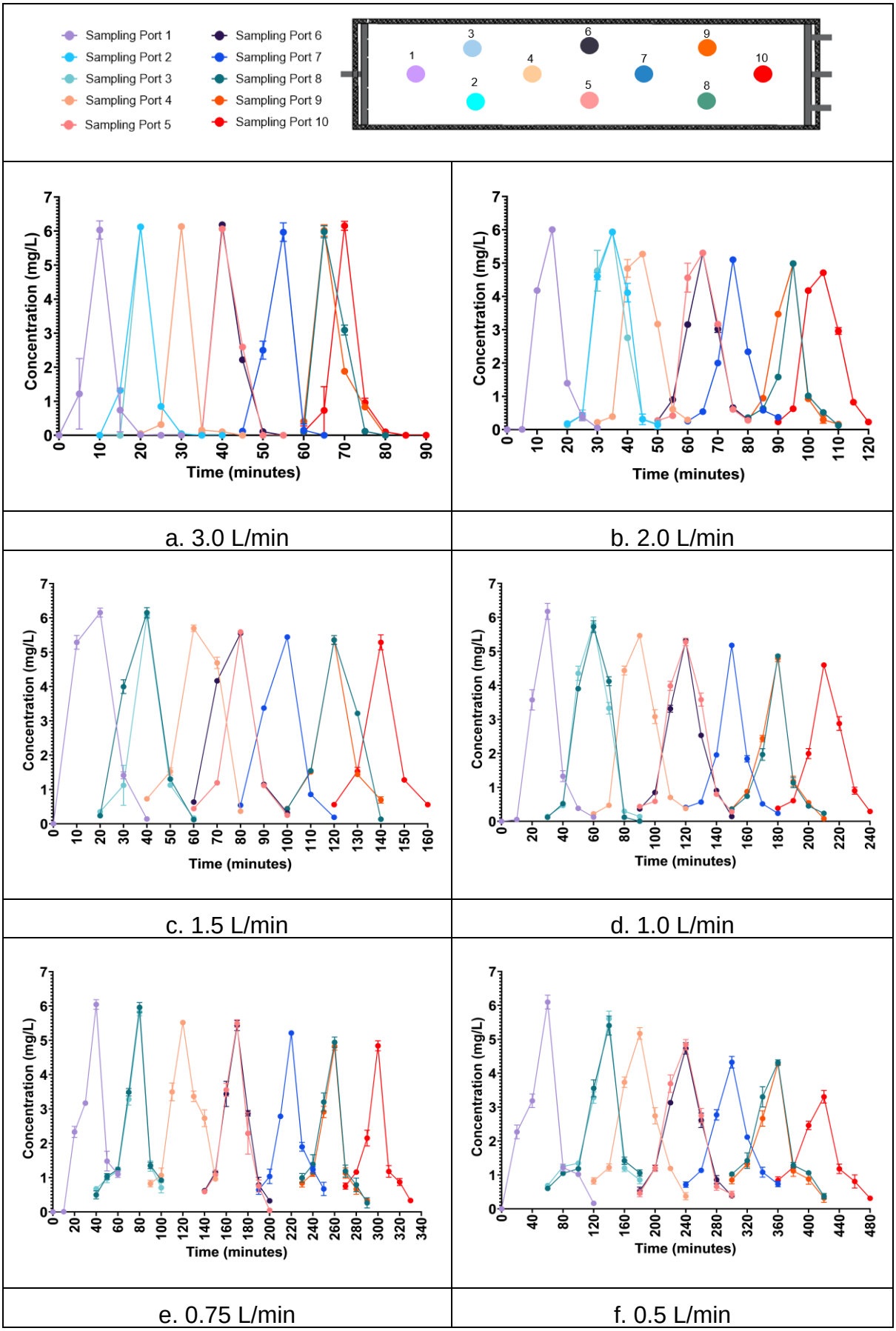

Figure 5.13: Concentration profiles 5 cm below surface for pulse tracer studies 3 L/min (a), 2 L/min (b), 1.5 L/min (c), 1 L/min (d), 0.75 L/min (e) and 0.5 L/min (f)

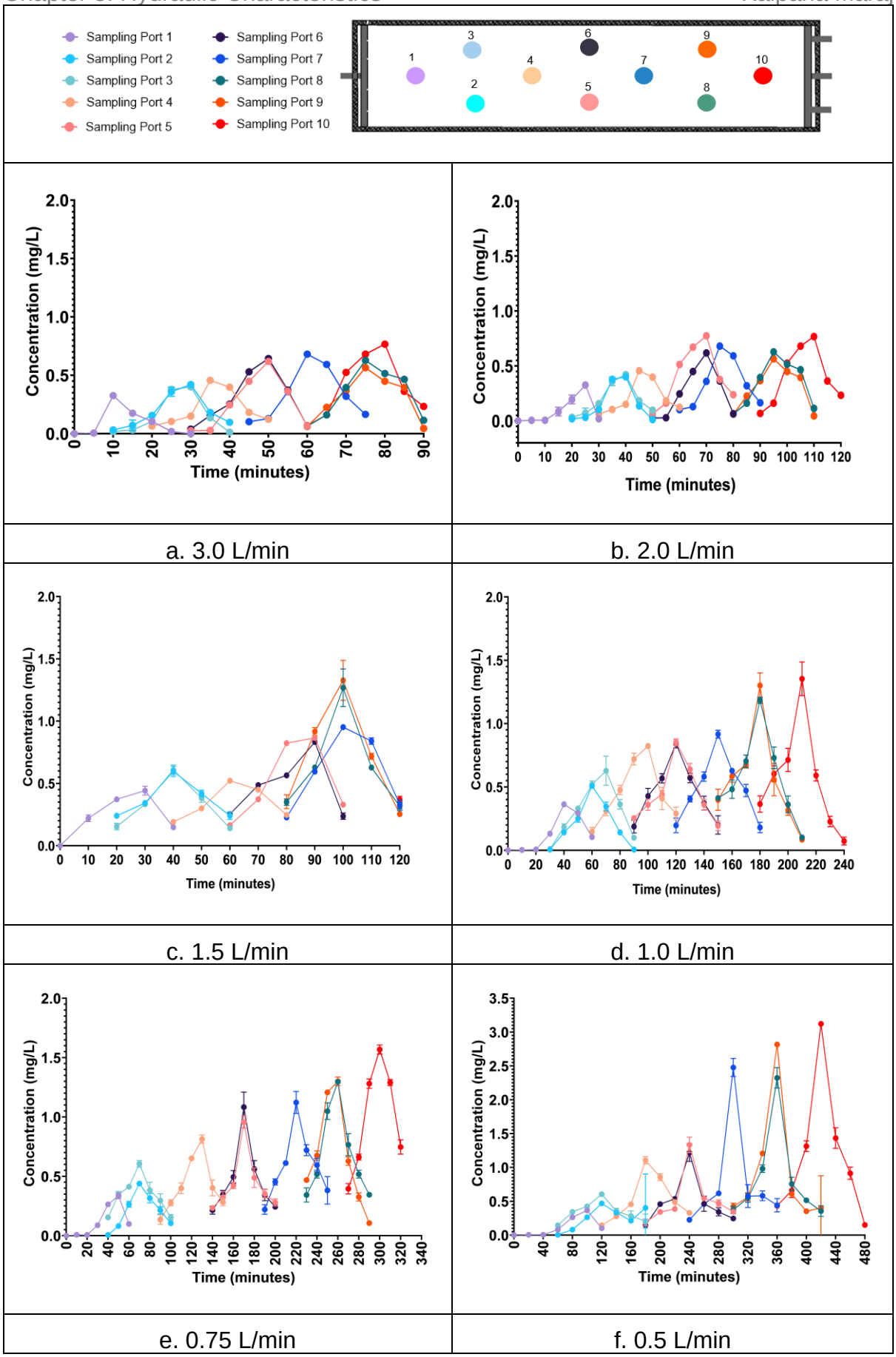

Figure 5.14: Concentration profiles 35 cm below surface for pulse tracer studies 3 L/min (a), 2 L/min (b), 1.5 L/min (c), 1 L/min (d), 0.75 L/min (e) and 0.5 L/min (f)

Figure 5.11 shows the concentration as measured at outlet B for pulse tracer studies carried out at all six experimental flow rates. The maximum concentration observed across all pulse tracer studies is approximately 6 mg/L. The lowest peak concentration observed is seen at a flow rate of 0.5 L/min (Figure 5.11f) where the maximum concentration observed is 5.30 mg/L.

The longer tail on Figure 5.12b (RTD at experiment flow rate of 2 L/min), similar to the long tail seen on Figure 5.12 (discussed in Section 5.3.1), from 120 minutes to 150 is indicative of a dead zone or fluid hold-up in tortuous pathways. A dead-zone is more likely as the stone packing is assumed to be non-porous due to their large size (meaning that tortuous flow should be minimal in this system where the packing size is larger and fines are limited).

Figure 5.13b (experimental flow rate of 2 L/min) shows that there is a decrease in tracer concentration of 1 mg/L from sampling port 1 to sampling port 10 at 5 cm below the surface. The concentration profile in Figure 5.13b shows that fluid flow is approximately evenly distributed along the width of the pilot biofilter. Figure 5.14b shows an increase in concentration along the length of the pilot biofilter at a depth of 35 cm with the maximum concentration at sampling port 1 being 0.3 mg/L and that of sampling port 10 being 0.8 mg/L. There is a correlation between the decrease in concentration seen along the length of the biofilter at a depth of 5 cm in Figure 5.13b and the increase in dye concentration at a depth of 35 cm seen in Figure 5.14b which is attributed to the infiltration of the dye below the surface.

Figure 5.13c shows that there is an even flow distribution across the width of the pilot biofilter at a flow rate of 1.5 L/min. Figure 5.14c depicts an increase in concentration along the length of the pilot biofilter 35 cm below the surface which is attributed to infiltration of the tracer.

Figure 5.13d shows a decrease in the maximum concentration observed in sampling port 1 as compared to sampling port 10 with a 1.3 mg/L difference in tracer concentration observed. There is an increase in tracer concentration along the length of the pilot biofilter 35 cm below the surface as seen in Figure 5.14d which is attributed to infiltration.

Figure 5.13e shows that the fluid flow is distributed evenly across the width of the pilot biofilter. There is a significant increase in tracer concentration along the length of the pilot biofilter 35 cm below the surface as seen in Figure 5.14e, corresponding to the decreasing concentration closer to the surface at a depth of 5 cm.

Figure 5.13f shows that the flow is evenly distributed across the width of the pilot biofilter at a flow rate of 0.5 L/min. There is a significant reduction in tracer

concentration observed along the length of the pilot biofilter at 5 cm below the surface. The maximum tracer concentration observed in sampling port 1 is 6.1 mg/L while that of sampling point 10 is 3.3 mg/L. Figure 5.14f shows an increase in tracer concentration along the length of the pilot biofilter at 35 cm below the surface. The maximum tracer concentration observed in sampling port 1 is 0.37 mg/L while that of sampling point 10 is 3.2 mg/L. This increase in tracer concentration along the length of the pilot biofilter 35 cm below the surface at an experimental flow rate of 0.5 L/min is greater than those observed at higher flow rates. This implies that the depth of infiltration achieved by the tracer increases as the flow rate decreases.

5.4. Analysis and Discussion

Figure 5.15 shows the normalised residence time distribution of the pulse tracer studies. Θ represents the number of reactor volumes of fluid, based on entrance conditons, that have passed through the system, in time,*t*.

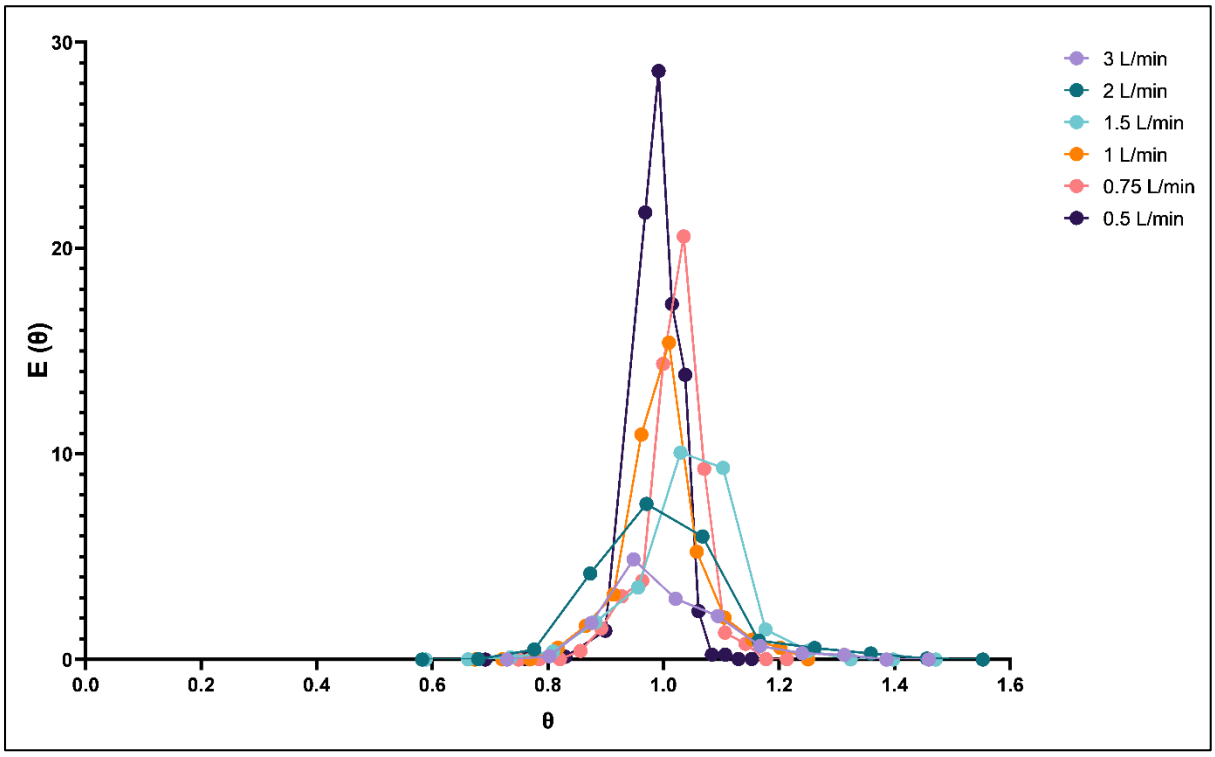

Figure 5.15: Normalised residence time distribution at all experimental flowrates

Figure 5.15 shows that different flow and mixing behaviours occur at different flow rates. This implies that the flow rate, and hence the superficial velocity of the fluid has an effect on the mixing characteristics in the pilot biofilter system. The normalised residence time distribution at 0.5 L/min approximates the mixing characteristics of plug flow more so than the residence time distributions at the higher flow rates. The sharp,

tall peak at θ = 1 and lack of a long tail is evidence of plug flow with minimal short circuiting or dead zones.

As the flow rate increases, the peaks of the residence time distributions are shorter and broader, meaning that there is a greater degree of mixing in the axial direction at higher flow rates. The normalised residence time distributions at the higher flow rates (1.5 L/min, 2 L/min and 3 L/min) have long tails which are indicative of non-ideal fluid behaviour such as dead zones, hold-up and channelling. The peaks at 1.5 L/min, 2 L/min and 3 L/min are not as well defined as their counterparts at the lower flow rates. The peaks at these flow rates also do not occur at θ = 1 which is a deviation from ideal plug flow behaviour and is characteristic of non-ideal fluid flow behaviour.

Table 5.4: Hydraulic characteristics of the pilot biofilter at various flowrates

	3 L/min	**2 L/min**	**1.5 L/min**	**1 L/min**	**0.75 L/min**	**0.5 L/min**
Tracer Recovery	95.1%	98.7%	98.9%	96.3%	96.9%	96.4%
τ (minutes)	75	112.5	150	225	300	450
$\bar{t}_m$ (minutes)	68.1	103	136	208	280	434
σ^2 (minutes^2)	39.4	133	174	188	201	175
e	90.8%	91.6%	90.7%	92.5%	93.4%	96.4%
Λ	90.1%	90.5%	89.8%	92.1%	93.2%	96.3%
N	118	93	106	230	391	1070
Pe	215	143	205	401	584	1410

Table 5.4 shows the hydraulic characteristics of the pilot biofilter system, defined in Section 5.2.3, at the six experimental flow rates. The mean tracer recovery across all

the pulse tracer studies that were conducted is 97.1% which is acceptable. The mean tracer loss of 2.9% can be attributed to adsorption onto the surface of the stones.

In each instance, the mean residence time in the system, $\bar{t}_m$, is lower than the theoretical residence time, τ. This is proof of non-ideal flow behaviour in the pilot biofilter system as $\bar{t}_m = \tau$ for ideal flow behaviour. In general, the effective volume utilisation, e, and hydraulic efficiency, Λ, are greater at the lower flow rates. The greatest effective volume utilisation of 96.4% and greatest hydraulic efficiency of 96.3% are seen at 0.5 L/min.

The number of tanks in series, N, is greatest at a flow rate of 0.5 L/min with the number of tanks in series being 1070. This implies that the extent of plug flow behaviour and degree of mixing in the radial direction increases with a decrease in flow rate. This is supported by the fact that the number of tanks in series is lower at the higher flow rates.

The Peclet number, Pe, is an indicator of whether flow is governed by radial advection or dispersion in the axial direction. The large Pe indicates that there is majority advection occurring in the system. Pe is greatest at a flow rate of 0.5 L/min and significantly lower at the higher flow rates, implying that Pe → ∞ as flow rate decreases. This shows that the extent of dispersive mass transfer decreases as the flow rates decreases even though flow is governed by advection at all the flow rates.

It has been shown that the pilot biofilter system approximates plug flow behaviour with the extent of plug flow behaviour increasing as the system flow rate decreases. A maximum dead space of 9.3% is seen at a flow rate of 1.5 L/min while a minimum dead space of 3.6% is seen at a flow rate of 0.5 L/min. The plug flow behaviour of the system is in contrast to the findings in a study by Bonner, Aylward and Kappelmeyer (2017) where a pilot-scale constructed wetland filled with gravel displayed mixed flow characteristics. However, this was attributed to the poor inlet and outlet design of the system which created a hulls shaped flow profile. A study on a pilot-scale horizontal subsurface flow constructed wetland filled with coarse gravel by Dittrich et al., 2021) found that the flow pattern in the system was dispersed plug flow. This aligns with the results from this study where the system displays plug flow behaviour.

5.5. Conclusions and Implications on Nutrient Degradation Studies

The pilot biofilter displays the characteristics of a plug flow dispersion reactor at all six experimental flow rates where plug flow behaviour is dominant and mixing is negligible. The pilot biofilter was adequately designed as the fluid behaviour is in accordance with the fluid flow characteristics described in Section 2.4.4 (Narayanan and Narayan, 2019) for a packed bed subsurface flow biofiltration system. The

effective volume utilisation of above 90.8% at all six experimental flow rates can be attributed to the plug flow behaviour where fluid velocity profiles are constant across each differential “slice” of the pilot biofilter, thus minimising dead zones.

The findings from the pulse tracer studies are valuable when applied in context of the nutrient degradation studies. The plug flow characteristics displayed at all six experimental flow rates mean that the pilot biofilter lends itself to a greater extent of nutrient degradation provided that the degradation kinetics are first or second order (Benjamin and Lawler, 2013). However, the concentration profile data at depths of 5 cm below the surface and 35 cm below the surface show that the fluid flow pathways penetrate deeper into the filter bed at lower flow rates with a flow rate of 0.5 L/min showing the greatest extent of tracer infiltration at 35 cm below the surface. Lower flow rates are therefore favoured for the nutrient degradation studies in order to maximise the depth, and therefore volume, at which nutrients are readily dispersed and hence at which microbial and adsorptive activity occur in the system.

Hydraulic retention time has a profound impact on microbial population dynamics, particularly planktonic microbial species which are washed out of the system when the hydraulic residence time is less than their doubling rate, and therefore on biological activities within the system with ammonia degradation being favoured at higher hydraulic retention times (as discussed in Section 2.5.2).

It is important to carry out the nutrient degradation studies at both a high flow rate (low hydraulic retention time) and low flow rate (high hydraulic retention time). A low hydraulic retention time allows for a greater throughput and therefore, higher treatment capacity. However, a higher hydraulic retention time allows for a greater extent of nitrification and dentifrication as well as for the microbes in the system to proliferate.

The hydraulic retention time plays a significant role in how fast the microorganisms in the system are able to metabolise large pulses of nutrients and so it is necessary to carry out the nutrient degradation studies at a higher and lower hydraulic retention time. The chosen higher flow rate must also display sufficient fluid flow activity throughout the depth of the pilot biofilter in order to ensure sufficient microbial and adsorptive activity in the bottom of the pilot biofilter. Flowrates of 1.5 L/min and 0.5 L/min were considered for the nutrient degradation studies. While 1.5 L/min is the flow rate with the lower hydraulic retention time, similar dispersion of tracer to 35 cm below the surface was seen for the pulse tracer studies at 1.5 L/min and 1 L/min making 1.5 L/min a suitable option for the higher flow rate.

6. INOCULATION AND ESTABLISHMENT OF BIOMASS IN THE PILOT BIOFILTER

6.1. Introduction

The pilot biofilter was inoculated with an active mixed microbial consortium, recovered from the large and small stone biofilters at the Franschhoek Water Hub and re-suspended as a cell suspension in order to accelerate the microbial colonisation of the system. This microbial consortium was used to facilitate nutrient degradation studies. Following inoculation by the culture from the Water Hub, a biological acclimation period allowed the microbial communities to multiply and colonise the system. For this, the pilot biofilter was operated in recirculation mode. The aim of this chapter is to detail the inoculation procedure and track the activity within the biofilter during the biological acclimation period.

6.2. Materials and Methods

6.2.1. Modification of the lab system for fluid recirculation

Additions were made to the pilot biofilter system to allow a closed circulatory flow within the system. Figure 6.1 is a process flow diagram showing this setup.

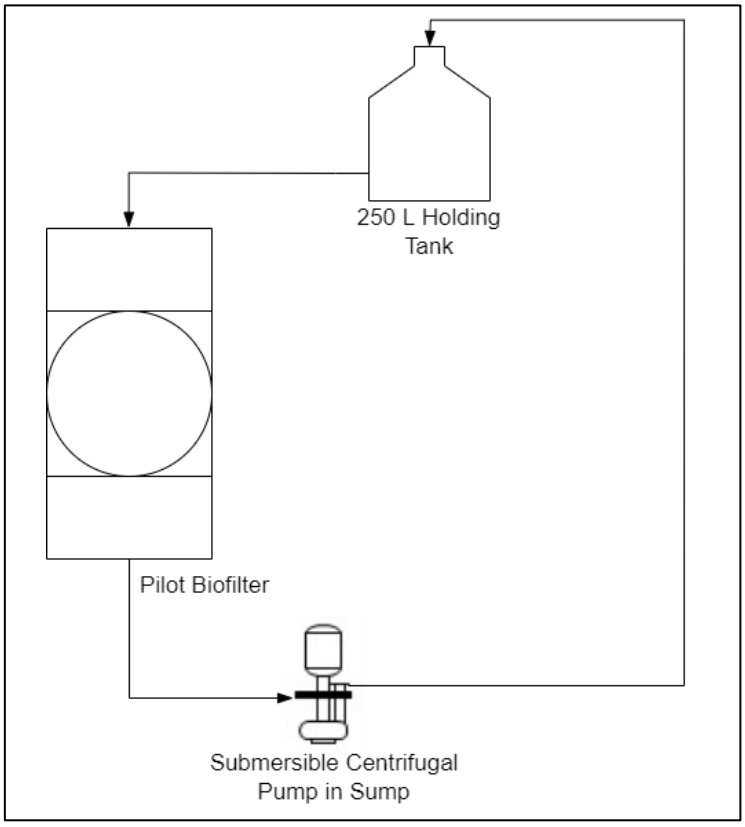

Figure 6.1: Pilot biofilter with sump & Eco Tank holding tank (liquid volume in Eco Tank = 60 L and of the sump = 25 L)

An effluent sump (total volume of 50 L; operating volume of 25 L) containing a submersible pump was attached to the outlet of the pilot biofilter. The pump was attached to a 20 mm hosepipe which connected to the inlet of a 250 L Eco Tank which serves as a holding tank for 60 L effluent before it re-entered the pilot biofilter. An aerator pump was placed inside the Eco Tank maintaining a DO concentration of 7 mg/L within the Eco Tank. The purpose of aeration was to ensure that no anaerobic reactions occur in the Eco Tank as anaerobic reactions usually result in partially degraded organic matter, typically causing foul odours. The aeration within the Eco Tank therefore prevented foul odours within the laboratory. However, the high dissolved oxygen concentrations in the Eco Tank promote aerobic reactions. The working volume of the holding tank remained constant at 60 L. The volume of water in the biofilter remained constant at 140 L.

The methods used for biofilm detachment, total cell counts, inoculation and SEM analysis are outlined below.

6.2.2. Cell suspension preparation

In an exploratory SEM analysis (method detailed in Section 6.2.5), most of the microorganisms could be found in the small granules of sediment (a fine sand-like substance) at the bottom of the biofilters at the Water Hub rather than on the surface of the stone media. In Figure 6.2, a sample of SEM micrographs of the stone media surface indicate the presence of a small number of individual microbes on the stone media surface while dense microbial colonies in the form of biofilm was found on the sediment surface (as seen in Figure 6.2 and Figure 6.3). Extended SEM data is available at https://figshare.com/s/f64b77047dacf7064b01.

Sediment samples were collected from the bottom of the large and small stone biofilters in 50 ml Falcon tubes. It must be noted that most of the sediment was found at the very bottom of the large and small stones biofilter and was attached to the surface of the stone media. Therefore, the only way to collect the sediment samples was to collect the stones that had sediment attached to them from the very bottom of both the large and small stones biofilters.

An aliquot of 150 ml of stone and sediment was collected from each of the large stone and small stone biofilters (300 ml total). Two separate cell suspensions were prepared (one from the large stones biofilter and another from the small stones biofilter) through the following process: Each sample of stone and sediment was washed with 75 ml quarter strength sterile phosphate buffer solution (12.5 mM) [full strength phosphate buffer (50 mM) contained 5.62g K_2HPO_4 and 2.13g KH_2PO_4, distilled water to 1 L, pH adjusted to 7.0, autoclaved] followed by agitation for 10 minutes at 60 rpm on a shaking

platform. This resulted in 70 ml of runoff being collected from each sample of stones and sediment with the sediment being suspended in the runoff.

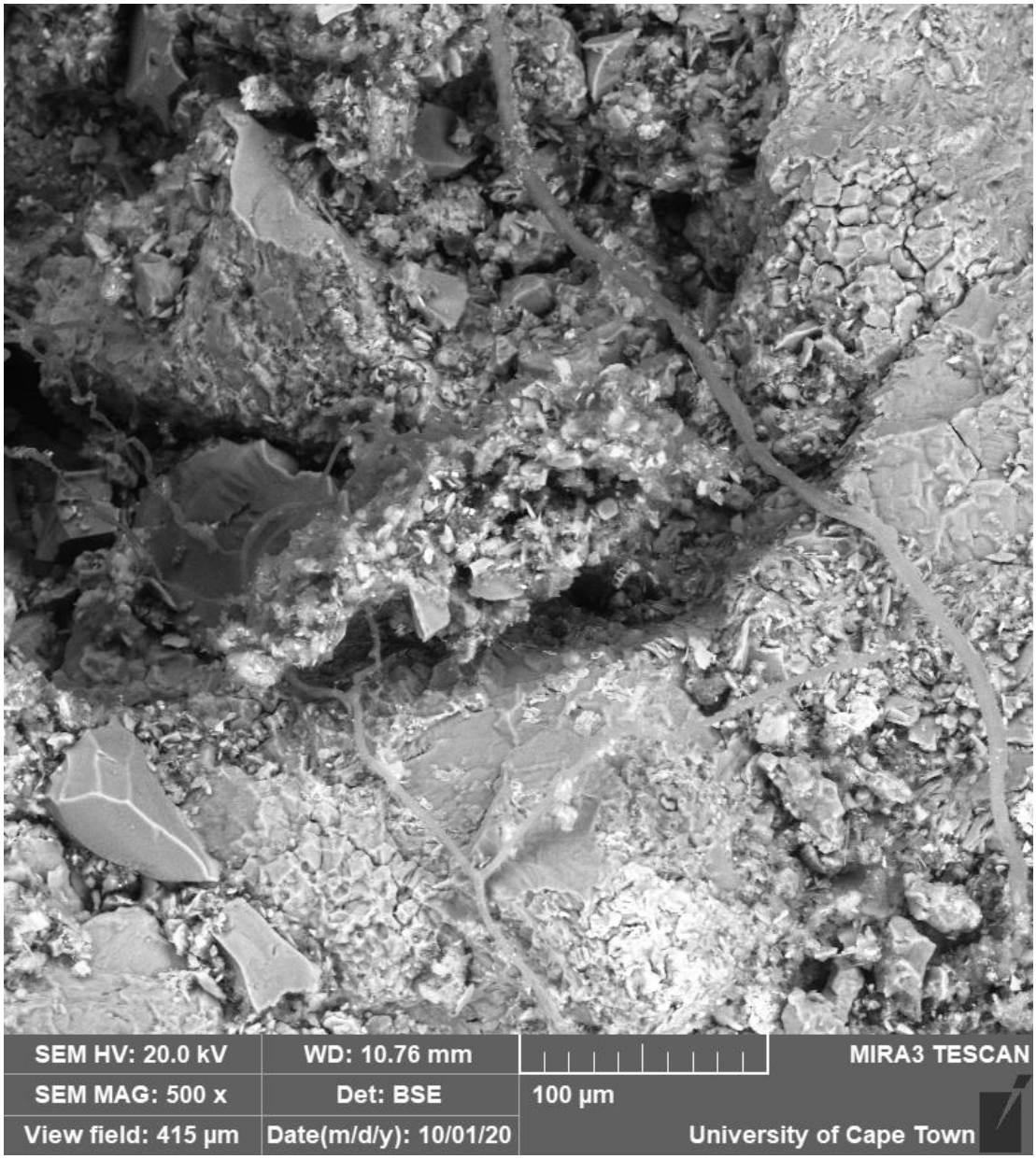

Figure 6.2: SEM micrograph at 500 x magnification showing stone media surface from the large stones biofilters with filamentous cell (likely fungi) on surface.

The runoff from the washing and agitation process (70 ml runoff from each sample of stone and sediment) was then collected in two sterile glass beakers while the stones were set aside (refrigerated at 4°C for possible future analysis of microbial communities). The purpose of washing the stones with phosphate buffer solution followed by the short agitation period is to detach the sediment granules (fine sand) from the surface of the stones. This runoff contained the sediment in the form of fine sand which is known to have biofilm attached to its surface.

The sterile glass beakers, each containing 70 ml of runoff (sediment suspended in the phosphate buffer solution), were covered with foil and were then agitated for 12 hours at 60 rpm on a shaking platform. This gentle agitation resulted in the cells detaching from the surface of the sediment. The liquid was then collected in 50 ml Falcon Tubes (2 falcon tubes per beaker, 35 ml in each falcon tube). This liquid contained suspended cells that had detached from the surface of the sediment during the washing and subsequent agitation.

The four Falcon tubes were centrifuged for 5 minutes at 1400g (4000 rpm) to allow the debris to sink to the bottom. This process yielded 65 ml of supernatant from the large stone sediment and 65 ml of supernatant from the small stones sediment. This supernatant was the cell suspension that would then be used as inoculum for the pilot biofilter. A 5 ml aliquot of each of the large stones and small stones cell suspension was set aside for SEM analysis. Another 5 ml of both cell suspensions were set aside for cell counts. A further 5 ml of each cell suspension was frozen for use in possible future analysis of the microbial communities. The remaining 50 ml of the large stones cell suspension and 50 ml of the small stones cell suspension was used to inoculate the pilot biofilter.

6.2.3. Cell counts by microscopy

Total microbial cell counts were conducted using a Hawksley Thoma counting chamber in conjunction with an Olympus BX40 microscope. The magnification on the microscope during counting is 1500 (15× magnification eyepiece, 100× magnification objective, immersion oil). The volume of one large square in a Hawksley Thoma counting chamber is 8×10^{-4} mm^3. The total cell count is therefore obtained from the following equation:

$$Cell\ concentration\ \left(\frac{cells}{ml}\right) = \frac{1000\ \times\ cell\ count}{(8 \times 10^{-4})(N_S)} \qquad \text{Equation 6.1}$$

where N_S is number of large squares counted.

6.2.4. Inoculation procedure

The following process was followed to inoculate the pilot biofilter:

1. Stone and sediment samples were collected from the bottom of both the large stone and small stone biofilters at the Water Hub.

2. The biofilm and loose cells were detached from the stones and sediment, as described in Section 6.2.2. This cell suspension was used as the inoculum for the pilot biofilter.
3. Following re-suspension and minimising of microbial clumps, the total microbial cell count was undertaken microscopically (see Section 6.2.3) to determine the concentration of cells in the inoculum.
4. The inoculum was added to the pilot biofilter by diluting the cell suspension into 200 L of contaminated runoff from the Stiebeuel River and introducing this mixture from the Eco Tank into the pilot biofilter.
5. The contaminated water was re-circulated in the system 24/7 at a flow rate of 0.5 L/min. Nutrient levels were replenished periodically by the addition of concentrated nutrient solution to the Eco Tank, thus returning nutrient concentrations in the Eco Tank to the initial concentrations. This continued for 35 days which is known as the biological acclimation period.

6.2.5. SEM analysis

The Scanning Electron Microscope (SEM) was used for the visual analysis the surface of stones from the Water Hub biofilters, biofilm attachment on the sediment samples as well as for visual analysis of the cell suspension that was used as inoculum. The SEM is a valuable tool to visualise the variety of microorganisms present in the inoculum as well as the abundance of cells. To prepare samples for SEM visualisation, sediment samples were fixed in 2.5% (v/v) glutaraldehyde for 24 hours and then rinsed with sterile water before being dehydrated.

The dehydration was carried out using 30%, 50%, 75%, 90% and 100% ethanol with a contact time of 10 minutes. The dehydrated sediment samples were kept in 100% alcohol for no longer than 4 hours before being analysed. The cell suspension samples were prepared by filtering the cells onto filter paper discs prior to fixing through the same procedure. Samples were mounted onto stubs and dried further using hexamethyldisilane (HMDS) before being sputter coated with carbon. The prepared samples were then visualised at various magnifications using the Nova NanoSEM and Tescan MIRA3 RISE Scanning Electron Microscopes.

6.3. Results and Discussion

6.3.1. Inoculation

Figure 6.3 shows biofilm coating the surface of the individual sediment granules. The SEM shows multiple sediment granules from the large stone biofilter at 1000 x magnification. Figure 6.4 shows one of the sediment granules at a higher magnification

(2000 x magnification). The darker smooth grey layer coating the sediment granule can be identified as the exopolysaccharide material within the biofilm. The sediment granule itself had a rough ridged surface with crevices that are ideal for biofilm growth.

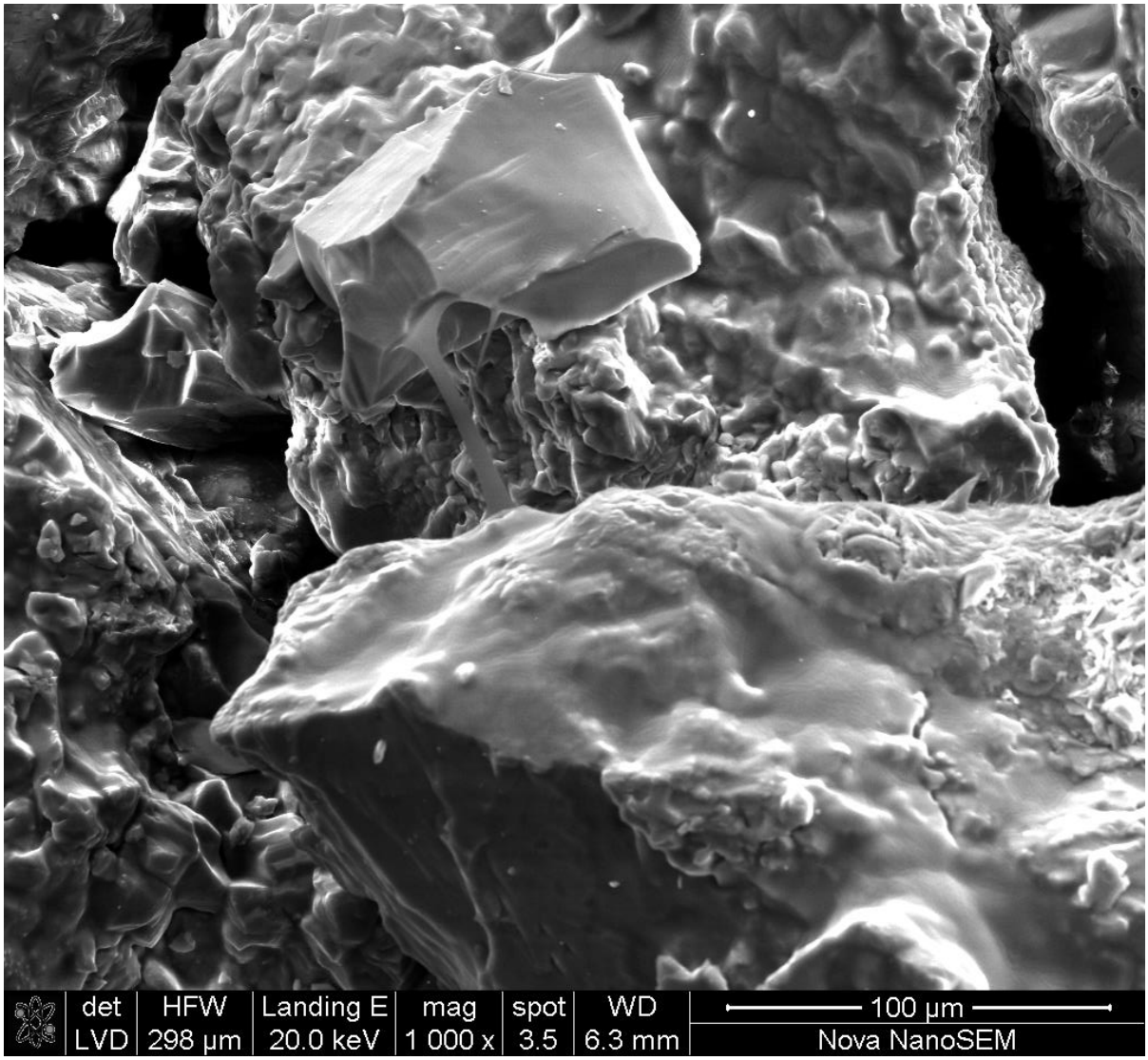

Figure 6.3: SEM micrograph at 1000 x magnification showing sediment granules from the large stones biofilters with biofilm coating the surface of the granules.

Figure 6.3 and Figure 6.4 show the biofilm that is firmly attached to the sediment. This biofilm contained cells and microbial colonies that were detached from the sediment surface through the cell suspension preparation procedure described in the Materials and Methods section of this chapter (Section 6.2.2). The resulting cell suspensions can be seen in Figure 6.5, Figure 6.6 and Figure 6.7 which show the SEM micrographs of the cells recovered from the suspensions originating on detachment from the large and small stone biofilters. Figure 6.5, Figure 6.6, and Figure 6.7 are a visual depiction of the cell suspensions used to inoculate the pilot biofilter.

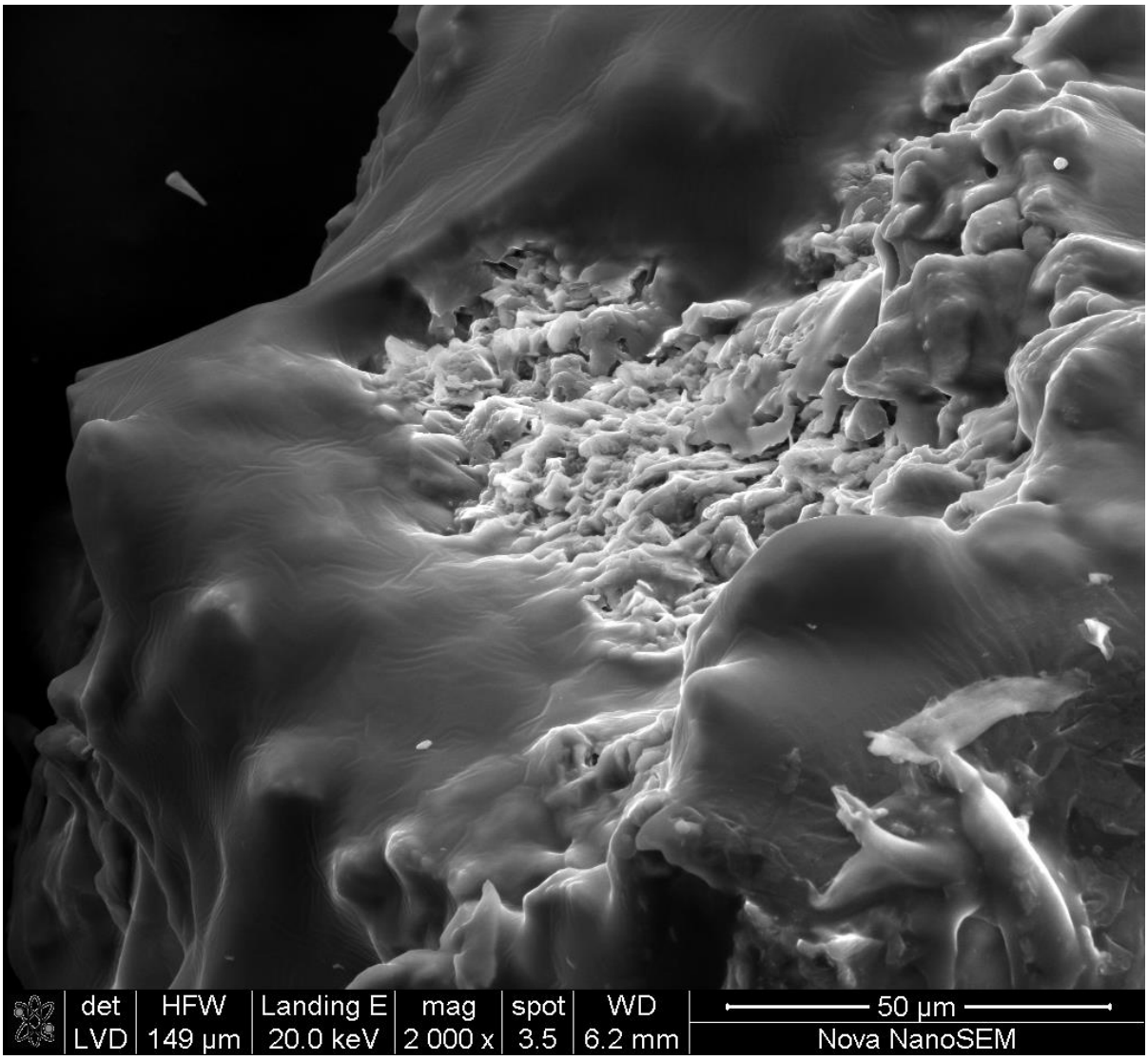

Figure 6.4: SEM micrograph at 2000 x magnification showing a biofilm layer covering the rough surface of a sediment granule from the large stones biofilter.

Figure 6.5 shows the SEM micrograph of a cell suspension prepared from biofilm extracted from sediment collected from the large stones biofilter. A variety of microorganisms can be seen in the micrograph with the following being examples:

A - cocci (spherical cell; most likely yeast)

B - vibrio (curved-rod shaped cells; potentially algal cell)

C - filamentous cells (most likely fungus due to size)

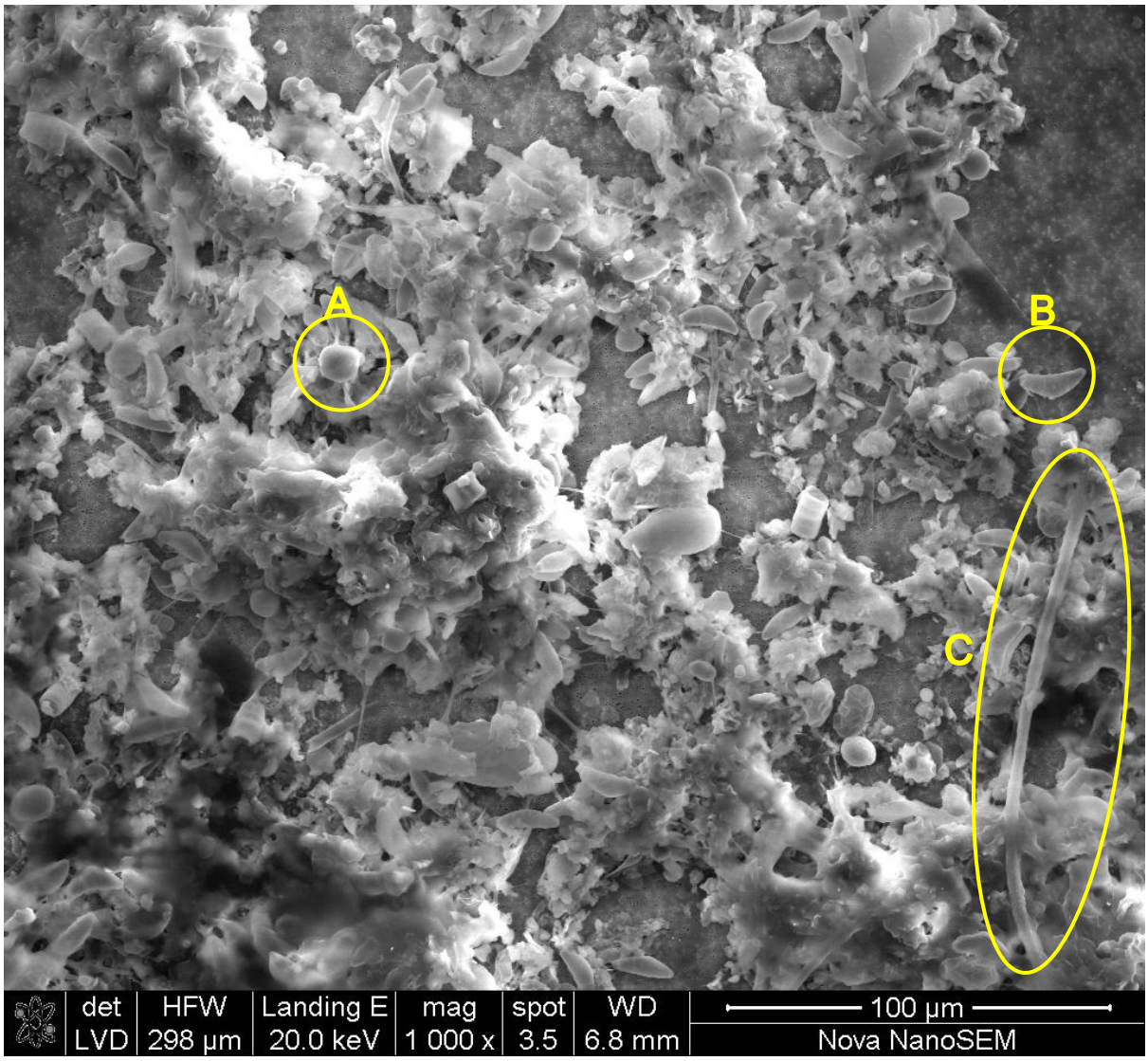

Figure 6.5: SEM micrograph at 1000 x magnification showing a cell suspension prepared from the large stones biofilter.

Figure 6.6 shows the same cell suspension depicted in Figure 6.5 but at a greater magnification of 2500 x. The different types of microorganisms (A, B, C) can be seen at a higher magnification in Figure 6.6. The greater magnification also allows bacteria to be seen in the micrograph. An example of bacteria is labelled D in Figure 6.6 (the bacteria are the very small circular shapes and are ~0.7 µm in size). Another example of larger bacteria is outlined by green circles in Figure 6.6.

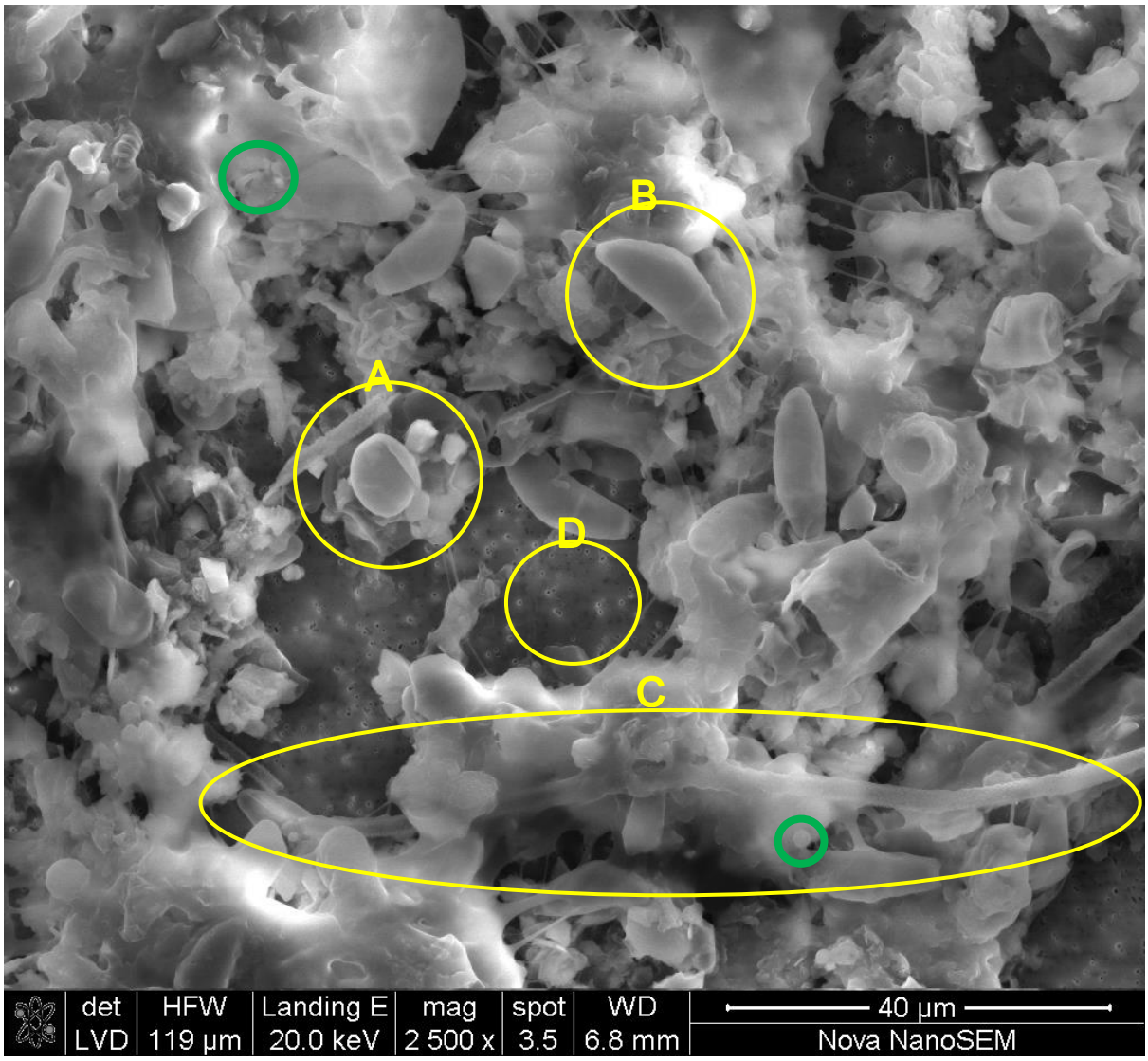

Figure 6.6: SEM micrograph at 2500 x magnification showing a cell suspension prepared from the large stones biofilter.

Figure 6.7 shows the cell suspension prepared using sediment from the small stones biofilter. It can clearly be seen that the cell suspension from the small stone biofilter has a microbial community that is distinct from that of the large stones biofilter. The cells outlined by green circles on Figure 6.7 are examples of bacteria. The following are examples of the abundant types of microorganisms seen in the cell suspension prepared from the large stones biofilter:

E – filamentous fungi

F – elliptical cell (identified as diatom due to size and shape)

G – spherical cell (most likely yeast)

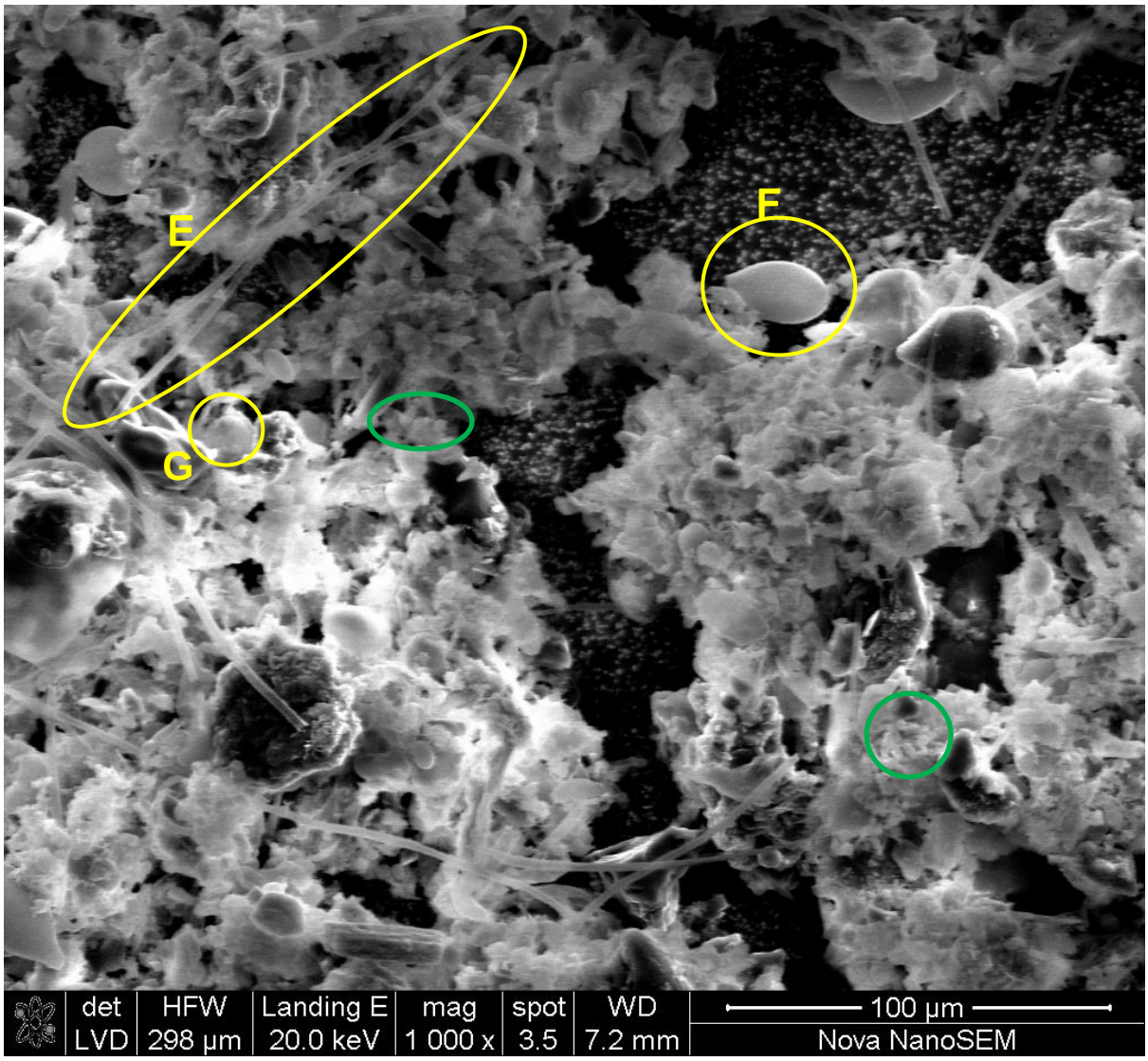

Figure 6.7: SEM micrograph at 1000 x magnification showing a cell suspension prepared from the small stones biofilter.

Table 6.1 summarises the cell concentrations and volume of inoculum used in the pilot biofilter. An inoculum suspension of 100 ml (see Table 6.1) was introduced to the pilot biofilter resulting in a cell to filtration media ratio of 2 million cells/kg stones. The inoculation was immediately followed by a 35-day biological acclimation period whereby contaminated water was circulated through the system at 0.5 L/min. The cell count in the water circulating the pilot biofilter system was monitored during this period to assess the extent of proliferation of cells in the pilot biofilter.

Table 6.1: Source & total cell count of inoculum

Inoculum Source	Inoculum Cell Count	Inoculum Volume
Small Stones Biofilter	27 million cells/ml	50 ml
Large Stones Biofilter	5.5 million cells/ml	50 ml

6.3.2. Biological activity and acclimation indicators

Figure 6.8 shows the planktonic cell counts in the liquid stream recirculated through the pilot biofilter over the 35-day acclimation period. The total cell count in the system was 400 000 cells/ml after 5 days and proceeded to increase exponentially until the cell count at 35 days was 21.7 million cells/ml. The exponential trend line can be seen on Figure 6.8 along with the equation representing the growth of the system. This is indicative of a strong microbial presence in the pilot biofilter system and is expected to be reflective of an increasing attached or sessile microbial community within the biofilter bed.

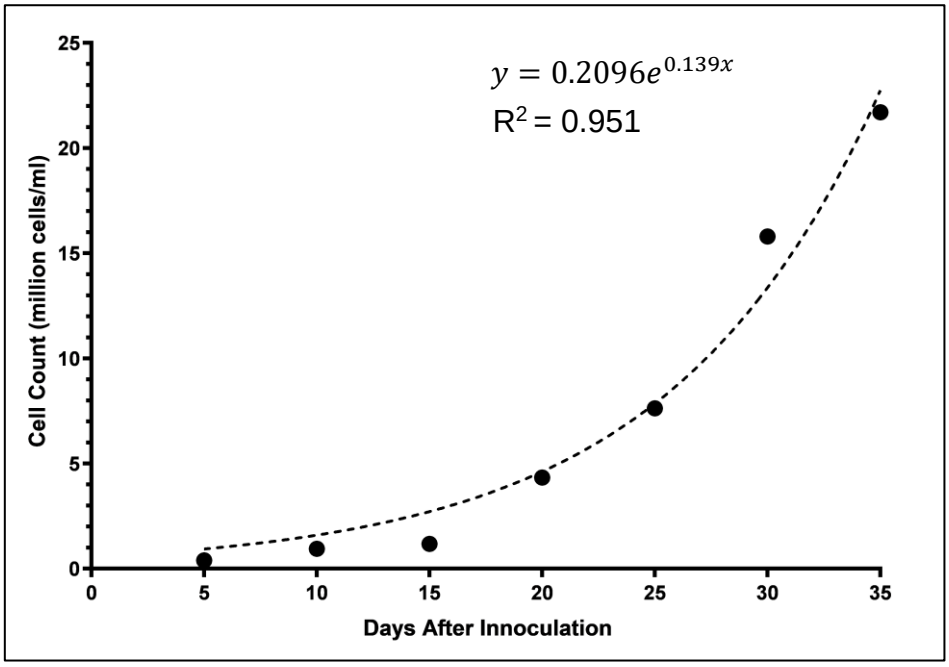

Figure 6.8: Planktonic Cell Counts in Liquid Stream Recirculated Through System During Acclimation Period

The nutrient levels in the system were also monitored periodically as decrease in nutrient concentration within the system is an indicator of microbial activity. The 200 L of contaminated water from the Stiebeuel River circulating in the system during the acclimation period had an initial concentration of 15 mg/L ammonia, 3.8 mg/L nitrate

and 5 mg/L orthophosphate. The nutrient levels were replenished to these concentrations periodically using concentrated nutrient solutions to prevent substrate depletion which would adversely affect the colonisation of the filtration media.

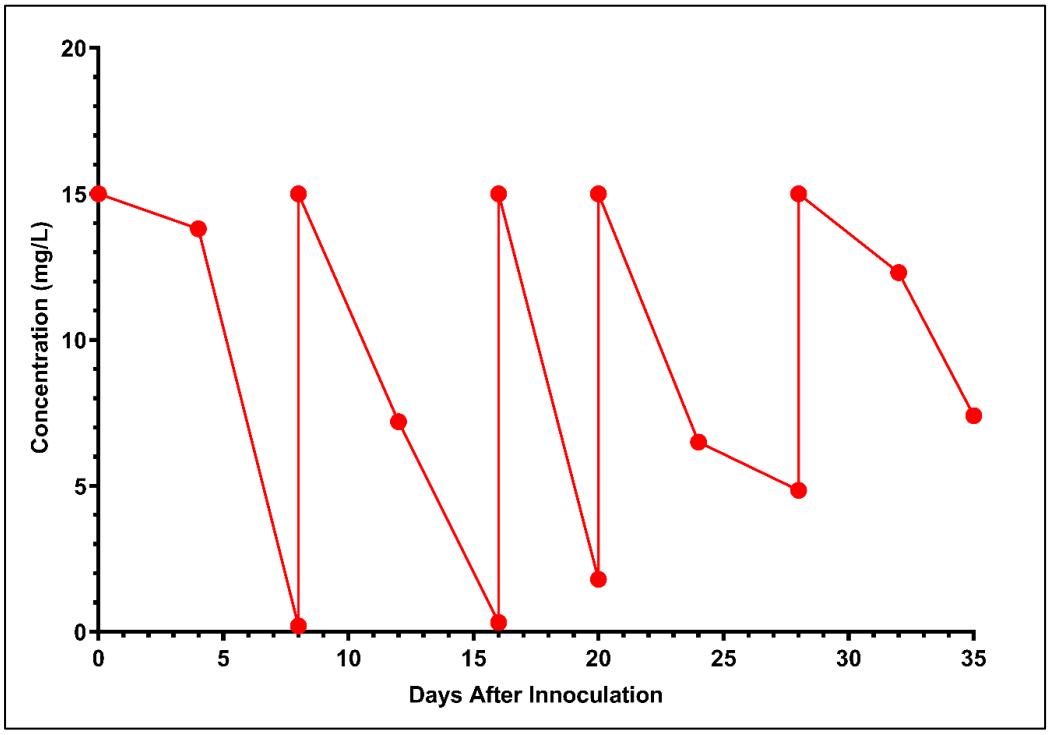

Figure 6.9: Ammonia concentration in pilot biofilter system during acclimation period

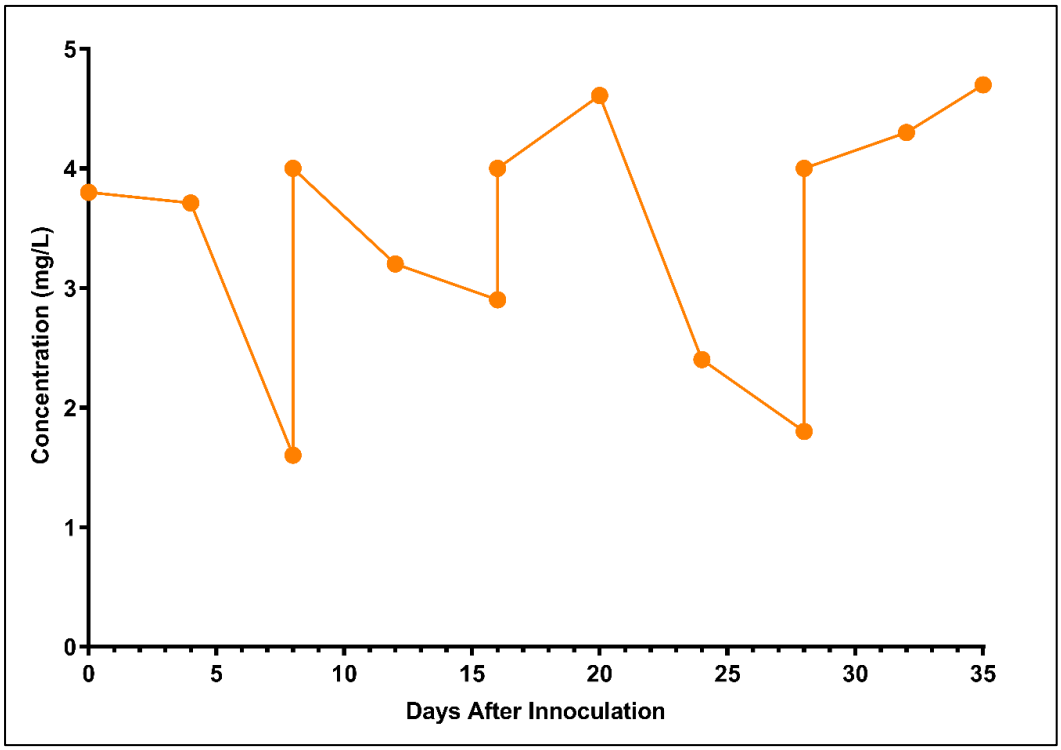

Figure 6.10: Nitrate concentration in pilot biofilter system during acclimation period

Figure 6.9 shows the ammonia concentrations in the pilot biofilter during the 35-day biological acclimation period. The depletion of the ammonia is indicative of microbial activity within the system. Figure 6.10 shows nitrate levels in the system during the acclimation period. The changing nitrate concentrations imply nitrification is occurring in the system (per Equation 2.6 and Equation 2.7 as discussed in Section 2.5.2) as the nitrate concentration increases from day 16 to day 20 as well as from day 28 to day 35.

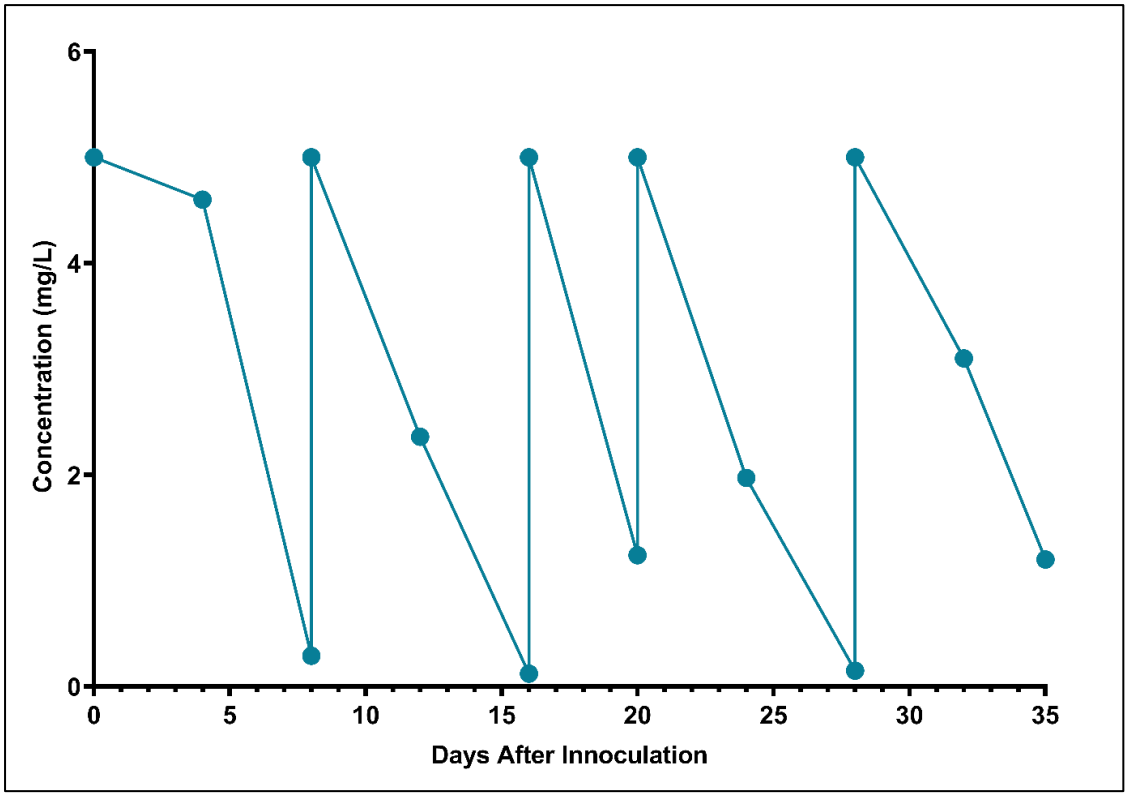

Figure 6.11: Orthophosphate concentration in pilot biofilter system during acclimation period

Figure 6.11 shows the orthophosphate concentrations in the pilot biofilter system during the biological acclimation period. It is noted that the orthophosphate concentration in the liquid phase of the system is decreasing, but it is uncertain whether this is due to microbial activity or adsorption onto the filtration media. This is explored further in the nutrient degradation study.

6.4. Conclusions and Implications on Nutrient Degradation Studies

The results from the biological acclimation period indicate that the pilot biofilter is biologically active as it is able to consistently metabolise the nutrients being introduced to the system. This supports the literature which states that the biological acclimation period of a lab-scale or pilot-scale system is 30-40 days (Nemani *et al.,* 2018). A study by Lin *et al*. (2019) found that the biological acclimation period of a pilot-scale single

stage denitrifying biofilter was 30 days. Furthermore, this is an indicator that the system has been sufficiently prepared for the nutrient degradation studies.

7. NUTRIENT DEGRADATION KINETICS

7.1. Introduction

The microbial activity and nutrient degradation observed during the biological acclimation period signifies that nutrient degradation studies are now possible in the pilot biofilter system. The purpose of the nutrient degradation studies is to assess the potential for nutrient reduction in the pilot biofilter and to determine the nutrient degradation kinetics and its order of reaction in the pilot biofilter.

The nutrient degradation studies were carried out at two flow rates: 0.5 L/min and 1.5 L/min (0.5 L/min was identified as the lowest flow rate at which it is possible to operate the system while conducting the tracer studies). Water from the Stiebeuel River was used as the nutrient source for this study. The nutrient degradation studies were carried out on a closed (i.e., batch) system. It must be noted that the nutrient degradation studies were carried out in the summer months as the nutrient concentrations in the Stiebeuel River were higher than in the winter months, providing maximum challenge to the filter.

Using water from the Stiebeuel River as the contaminated water source for the nutrient degradation studies is significant because it assesses the ability of the pilot biofilter to treat polluted runoff from an informal settlement. The water quality of this polluted runoff is highly variable. The nutrient degradation studies, therefore, determine whether non-vegetated stone biofilters are suitable for use in the treatment of runoff from this informal settlement.

7.2. Materials and Methods

The setup of the biofilter with recycle, shown in Figure 6.1, was maintained for the nutrient degradation kinetic studies. The following procedure was followed for the nutrient degradation kinetic studies:

1. 200 L of water from the Stiebeuel River was added to the pilot biofilter system and the submersible pump was switched on to enable constant circulatory flow within the system. The aerator pump in the Eco Tank remained switched on providing a dissolved oxygen concentration of 7mg/L at the inlet.
2. The valve on the Eco Tank (connected to the biofilter inlet) was adjusted to obtain the desired inlet flow rate.
3. The middle outlet valve was adjusted so that the outlet flow rate matched the inlet flow rate.

4. Samples were taken every 6 hours with a 12 h spacing at night once the flow in the system stabilised. Sampling occurred at 6am, 12pm and 6pm.
5. The system was operated for 10 days (228 hours) with the final sample being taken at 6pm on the tenth day. A volume of 140 L was maintained in the pilot biofilter while a volume of 10-15 L was maintained in the sump tank and a volume of 45-50 L is maintained in the Eco Tank.

Six nutrient degradation studies were carried out in total with three being done at 1.5 L/min and three at 0.5 L/min. It must be noted that the three runs are not replicates of each other due to the variability of the nutrient concentrations in the contaminated water from the Stiebeuel River. Each experiment began within 12 hours of the contaminated water arriving in the laboratory to prevent algal growth in the transportation containers. The chronology of the nutrient degradation studies was as follows: Run A at 0.5 L/min, Run B at 0.5 L/min, Run A at 1.5 L/min, Run B at 1.5 L/min, Run C at 1.5 L/min and finally, Run C at 0.5 L/min. Each nutrient degradation study was run on a fresh batch of contaminated runoff. Each nutrient degradation study was carried out on a closed (i.e., batch) system.

The HACH benchtop spectrophotometer and reagent set was used to determine the NH_3, NO_3^-, NO_2^- and PO_4^{3-} concentrations in the samples. The method for using the HACH test kits outlined in Appendix A was used. Appendix A also outlines the principle of the analysis, reproducibility of results and limits of detection of nutrients. Samples were analysed within three hours of being taken to ensure the accuracy of the readings. PO_4^{3-} concentrations were monitored for 108 hours as the PO_4^{3-} concentrations plateaued from 96 to 108 hours.

Equation 7.1 was used to calculate formation rate of ammonia, nitrate, nitrite and total nitrogen (a positive rate means nutrient formation while a negative rate means nutrient degradation):

$$Rate\ (mmol.L^{-1}.h^{-1}) = \frac{C_{t2} - C_{t1}}{t2 - t1} \quad \text{Equation 7.1}$$

where C_{t1} is concentration at time 1 in mmol/L and C_{t2} is concentration at time 2 in mmol/l.

Equation 7.2 was used to calculate the orthophosphate removal rate.

$$Rate\ (mmol.L^{-1}.h^{-1}) = \frac{C_{t1} - C_{t2}}{t1 - t2} \quad \text{Equation 7.2}$$

The order of reaction was determined experimentally to model degradation kinetics. It is used to predict the relationship between the rate of formation or degradation and the concentration of the species being formed or degraded.

Figure 7.1 describes the integrated rate laws for zero, first and second order reactions; plots of the natural logarithm of substrate concentration (first order) or inverse of concentration (second order) over time are produced to determine the rate constant (*k*). These plots were produced from the experimental data to determine whether the reactions with respect to the species being analysed are zero, first or second order. In some cases, the reaction order is of a higher order or complex order and cannot be described by any of the integrated rate laws described in Figure 7.1.

	Zero Order	**First Order**	**Second Order**
Differential Rate Law	$Rate = \frac{-\Delta[C]}{\Delta t} = k$	$Rate = \frac{-\Delta[C]}{\Delta t} = k[C]$	$Rate = \frac{-\Delta[C]}{\Delta t} = k[C]^2$
Concentration vs. Time	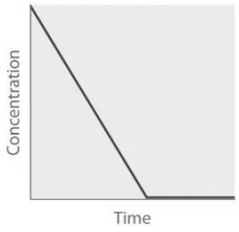	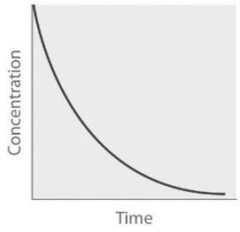	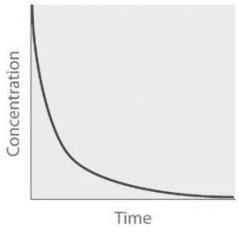
Integrated Rate Law	$[C] = [C]_0 - kt$	$[C] = [C]_0 e^{-kt}$	$\frac{1}{[C]} = \frac{1}{[C]_0} + kt$
Straight Line Plot to Determine Rate Constant	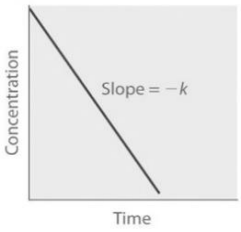	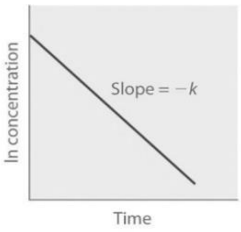	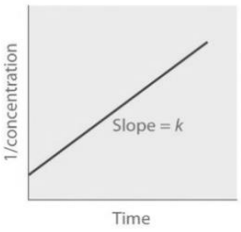
Relative Rate vs Concentration	$[C](M)$ Rate(M/s) 1 1 2 1 3 1	$[C](M)$ Rate(M/s) 1 1 2 2 3 3	$[C](M)$ Rate(M/s) 1 1 2 4 3 9
Units of *k*, rate constant	M/s	1/s	$M^{-1}. s^{-1}$

Figure 7.1: Determining order of reaction & rate laws [adapted from Levenspiel (1999)]

A study done by Wang et al. (2017) investigating ammonia degradation kinetics in a stone constructed wetland 1.6 m long, 0.6 m wide and 0.6 m deep showed that ammonia degradation in stone constructed wetland can be described as first order

(Wang *et al.*, 2017). Studies done by Gajewska et al. (2020) yielded similar results and concluded that the order of ammonia degradation in horizontally orientated constructed wetlands can generally be described by first order kinetic models (Gajewska *et al.*, 2020).

In instances where simple zero, first or second order cannot be used to describe the reaction kinetics occurring within a system; more complex models can be used. Complex first order models such as the Double First-order in Parallel (DFOP) kinetic model can be used to represent reaction rates for environmental degradation processes accurately when the simple first order model does not yield accurate results (White *et al.*, 2021). The DFOP model uses the sum of two first order equations, resulting in a more accurate estimation of experimental data. Equation 7.3 is used to describe the DFOP kinetic model.

$$C_t = C_o g e^{-k_1 t} + C_o (1 - g) e^{-k_2 t} \quad \text{Equation 7.3}$$

where C_t is the concentration at time, t (mmol/L);
C_0 is the initial concentration (mmol/L);
g is the fraction of degradation occurring under rate constant k_1;
k_1 and k_2 are the first order rate constants (h^{-1})

Due to the two exponentials in Equation 7.3, an iterative procedure must be used to solve for the rate constants. This can be done using programming environments such as MATLAB or software such as CAKE (Computer Assisted Kinetic Evaluation). The CAKE software has been used to solve for k_1 and k_2 for the DFOP model in this investigation.

7.3. Results and Discussion

Concentration profiles and rates of reaction for all experimental runs is discussed in Section 7.3 while further analysis on system performance based on nutrient removal is explored in Section 7.4. Kinetic models for ammonia degradation and orthophosphate removal are explored in Section 7.5.

7.3.1. Run A at 0.5 L/min

Figure 7.2 to Figure 7.8 depict the outcomes of Run A at 0.5 L/min of the nutrient degradation kinetic studies. The results for this initial run are explained in detail; for subsequent runs, results are summarised with further detailed data being found in Appendix G and Appendix H. Figure 7.2 shows the mass-based concentrations of ammonia, nitrate and nitrite over the experimental period. The same data is presented in molar concentration in Figure 7.3.

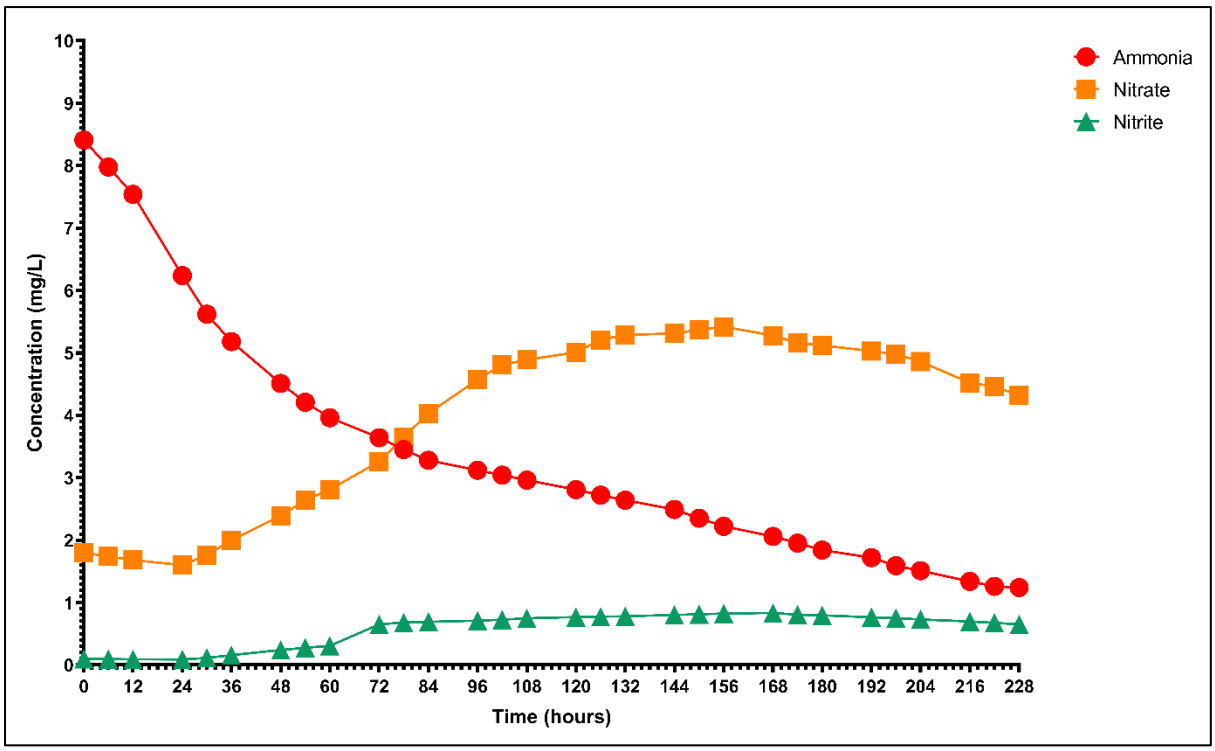

Figure 7.2: Ammonia, nitrate and nitrite concentrations (mg/L) for Run A at 0.5 L/min

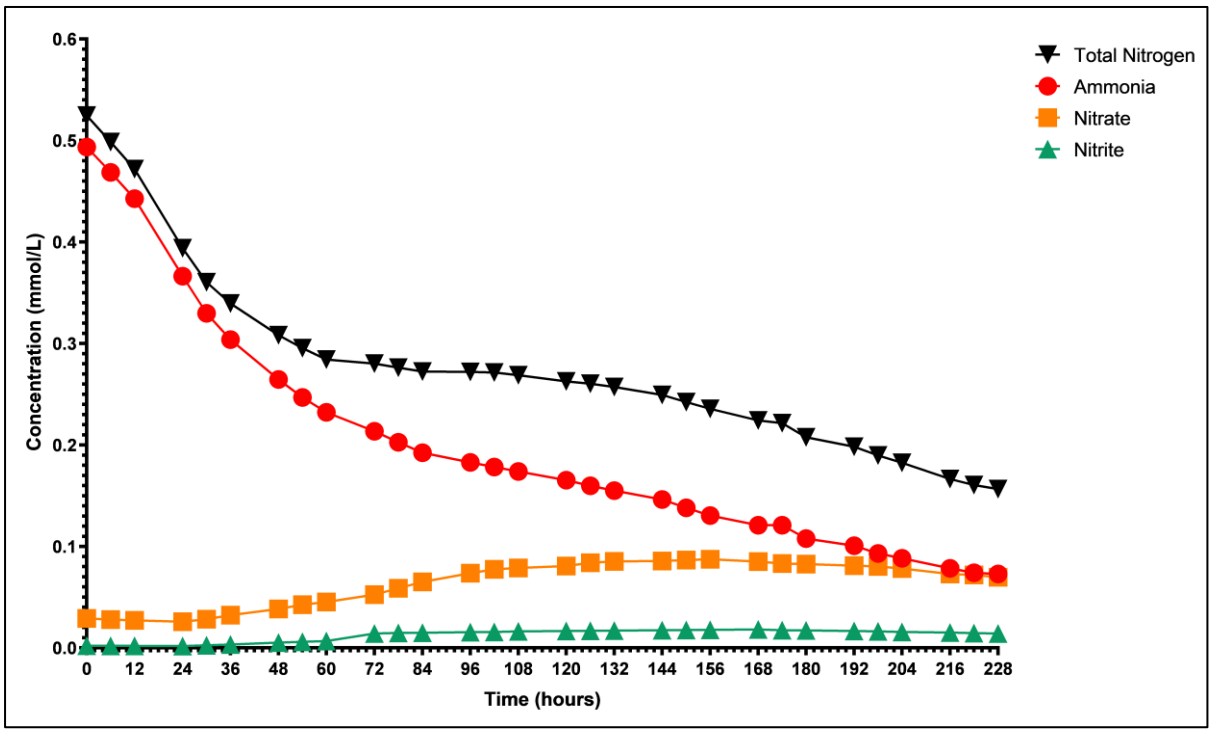

Figure 7.3: Ammonia, nitrate, nitrite and total nitrogen concentrations (mmol/L) for Run A at 0.5 L/min

The measured reduction in ammonia concentration and subsequent increase in nitrate concentration indicates that the nitrification is occurring in the system. The lowering of nitrate concentration compared to the rate of decrease in ammonia concentration on

a molar basis and the overall decrease in nitrate concentration from 156 hours onwards is an indication that denitrification is occurring in the system. The nitrite concentration does not increase beyond 0.83 mg/L because nitrite is an intermediary in the nitrification process with ammonia being oxidised to form nitrite and nitrite subsequently being oxidised to form nitrate.

Referring back to the two steps of the nitrification process, shown in Equation 2.6 and Equation 2.7 as well as the denitrification reaction as per Equation 2.8; the molar concentrations of ammonia, nitrate, nitrite and total nitrogen (seen in Figure 7.3) can be used to determine the extent of nitrification and denitrification in the system for Run A at 0.5 L/min

$$NH_4^+ + \frac{3}{2}O_2 \rightarrow NO_2^- + H_2O + 2H^+$$ Equation 2.6

$$NO_2^- + \frac{1}{2}O_2 \rightarrow NO_3^-$$ Equation 2.7

$$4NO_3^- + 5C + 2H_2O \rightarrow 2N_2 + 4HCO_3^- + CO_2$$ Equation 2.8

Table 7.1 shows the change in concentration observed for ammonia, nitrate, nitrite and total nitrogen for Run A at 0.5 L/min. It is possible to use the reaction stoichiometry from Equations 2.6, 2.7 and 2.8 along with the observed change in concentrations shown in Table 7.1 to determine the extent of nitrification and denitrification.

Table 7.1: Change in ammonia, nitrate, nitrite and total nitrogen concentrations over the course of Run A at 0.5 L/min

Compound	Initial Concentration (mmol/L)	Net Change in Concentration (mmol/L)	Final Concentration (mmol/L)
Ammonia	0.494	-0.421	0.073
Nitrate	0.029	+0.041	0.070
Nitrite	0.002	+0.012	0.014
Total Nitrogen	0.525	-0.368	0.157

The extent of ammonia degradation is 85.2% according to the change in ammonia concentration that is seen in Table 7.1. This should result in the formation of 0.421 mmol/L of nitrite as per the reaction stoichiometry seen in Equation 2.6, however there is a net formation of nitrite amounting to 0.012 mmol/L. This is due to the fact that

nitrite is an intermediary in the nitrification process with nitrite being oxidised to form nitrate as per Equation 2.7. This implies that the conversion of the nitrite that was formed in the system in Equation 2.6 to nitrate is 97.1%, leaving the 0.012 mmol/L of the nitrite formed from ammonia oxidation unreacted.

The formation of 0.409 mmol/L nitrate was expected as per the reaction stoichiometry of Equation 2.7; however, there was a net nitrate formation amounting to 0.041 mmol/L. This was due to denitrification also occurring in the system as per Equation 2.8, transforming the nitrate into atmospheric nitrogen. The extent of nitrification in the system was determined to be 82.8% using the fact that 0.494 mmol/L ammonia was initially available. The extent of denitrification as per Equation 2.8, based on the amount of nitrate available for reaction, was determined to be 90.6%. The total nitrogen removal in the system for run A at 0.5 L/min amounted to 70.1%. The method of calculation for the extent of nitrification and denitrification in the pilot biofilter for Run A at 0.5 L/min can be seen in Appendix H.

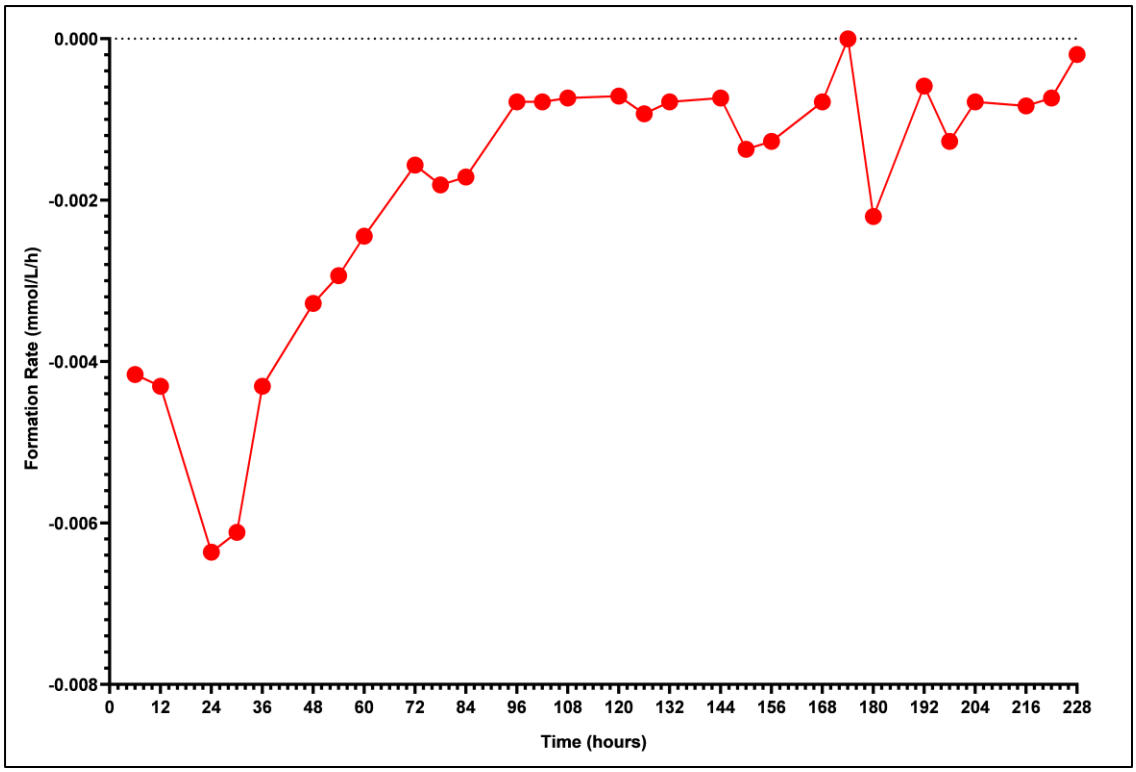

Figure 7.4: Ammonia formation rate vs. time for run A at 0.5 L/min

The formation rate of ammonia, nitrate, nitrite and total nitrogen was calculated using Equation 7.1 while the orthophosphate removal rate was calculated using Equation 7.2. The ammonia degradation rate as seen in Figure 7.4 initially increases to a maximum of 0.006 mmol/L/h. This is followed by a sharp decline in degradation rate that can be seen from 30 hours to 96 hours. The degradation rate then remains constant at approximately 0.0007 mmol/L/h from 96 hours to 144 hours. This is

followed by a period of fluctuations in the degradation rate until 228 hours. These fluctuations could be due to the microbes in the system scavenging for nutrients in a substrate depleted system as seen in a study done by (Zheng et al., (2020).

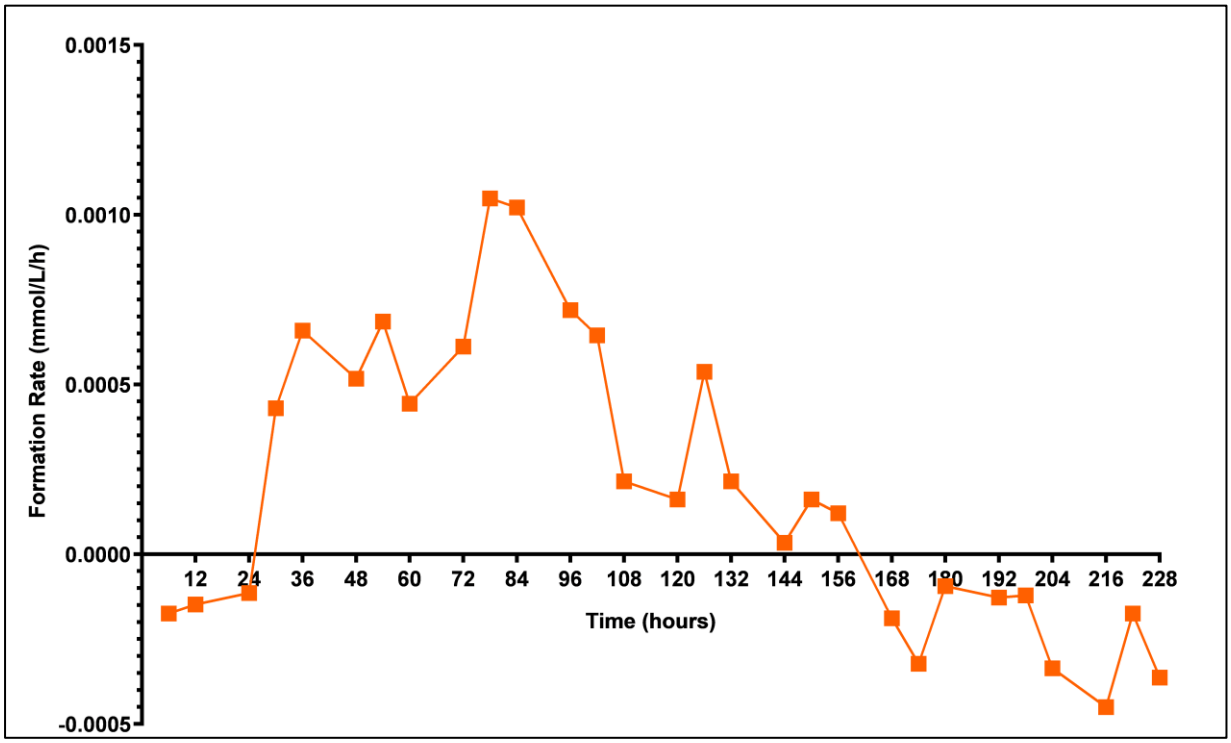

Figure 7.5: Nitrate formation rate for Run A at 0.5 L/min

Figure 7.5 shows the rate of net nitrate formation over the 228-hour experimental period. Initially, the net reaction shows nitrate as being degraded from 0 hours to 24 hours. Following this, the nitrate formation rate (due to nitrification) exceeds the degradation rate (due to denitrification), resulting in a net production of nitrate from 30 hours to 162 hours. This is followed by a net degradation period from 168 hours to 228 hours.

The nitrate formation rate peaks at 78 hours at a net formation rate of 0.0010 mmol/L/h (0.065 mg/L/h). This is followed by a rapid decline in the rate of nitrate formation from 78 hours to 120 hours during which time the nitrification rate stabilises at a low value. The formation rate once again increases from 120 hours to 126 hours followed by a sharp decline in formation rate from 126 hours to 144 hours. The net nitrate degradation rate was at a maximum of 0.00045 mmol/L/h (0.028 mg/L/h) at 216 hours.

Figure 7.6 shows the rate of net nitrite formation and degradation over the 228-hour experimental period. There is a period of net nitrite degradation from 0 hours to 24 hours. This is followed by a net nitrite formation period from 24 hours to 168 hours. The net nitrite formation rate reaches a peak of 0.00062 mmol/L/h (0.029 mg/L/h) between 60 and 80 hours; however, this high formation rate is short-lived with the

typical formation rate between 30 and 80 hours in the range 0.00014 mmol/L/h to 0.00016 mmol/L/h. This suggests that confirmation of the maximum rate of 0.00062 mmol/L/h is required. The net nitrite degradation rate reaches a peak of 0.00011 mmol/L/h (0.005 mg/L/h) at 174 hours.

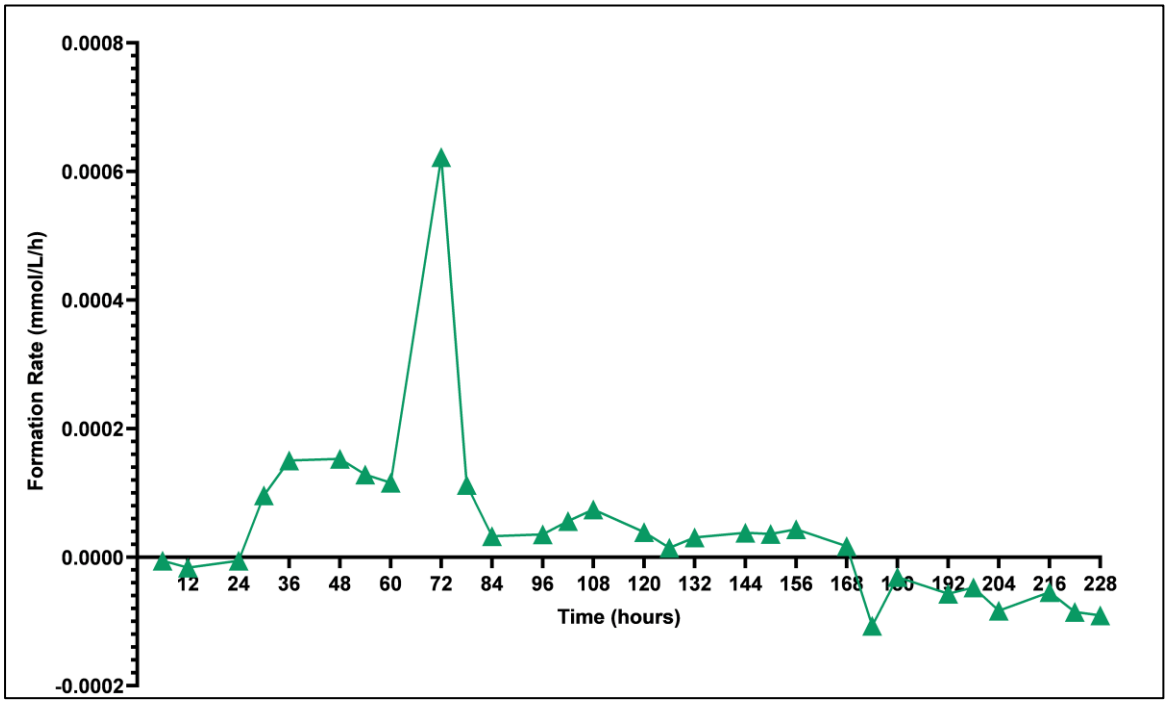

Figure 7.6: Nitrite formation rate for Run A at 0.5 L/min

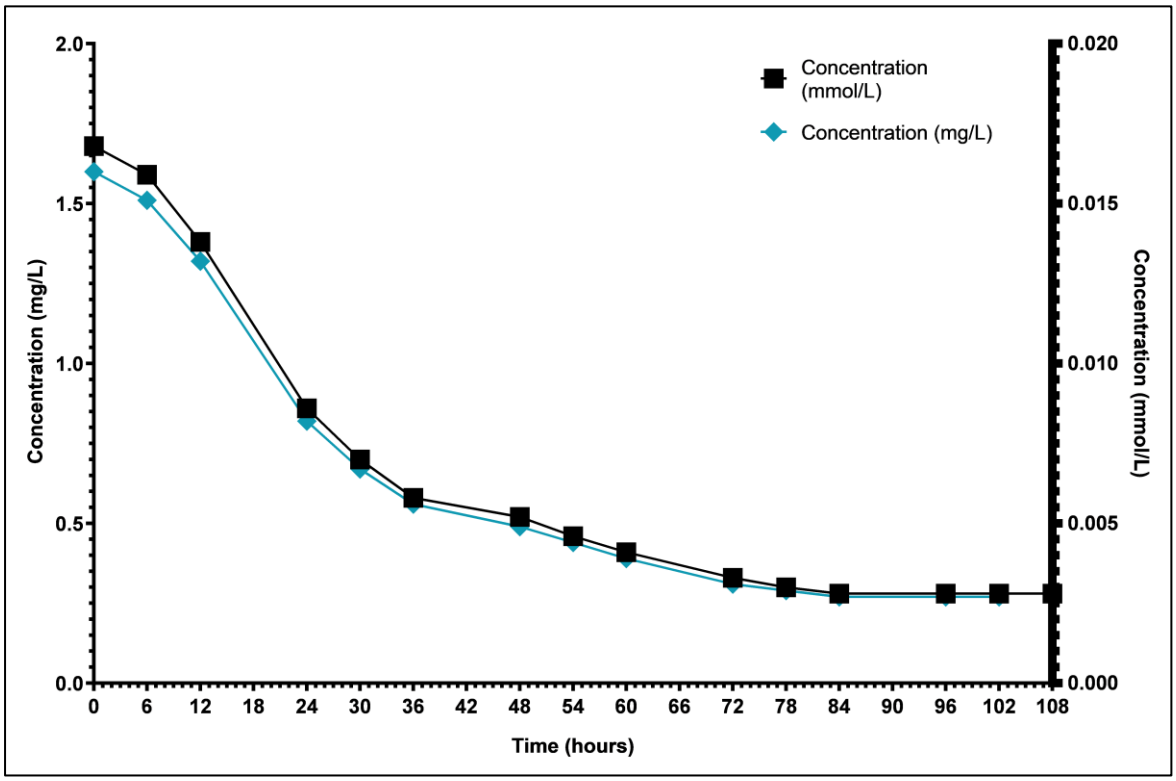

Figure 7.7: Orthophosphate concentration for Run A at 0.5 L/min

Figure 7.7 shows the orthophosphate concentration for Run A at 0.5 L/min. The orthophosphate concentration decreases from an initial concentration of 1.6 mg/L to 0.27 mg/L at 84 hours, whereafter no further decrease is seen until the end of the orthophosphate monitoring period of 108 hours. This plateauing of the orthophosphate concentration curve was unexpected as orthophosphate is believed to be primarily removed through adsorption onto the filtration media (Greenstein *et al.*, 2018). A beaker study on uncolonised stones showed that the rate of orthophosphate removal through adsorption onto the stone surface is zero order (Appendix E).

Figure 7.8 shows the orthophosphate removal rate for Run A at 0.5 L/min as calculated per Equation 7.2. The rate of orthophosphate removal increases from 6 hours to where it reaches its maximum at 24 hours of 0.00044 mmol/L/h. There is a sharp decline in the removal rate from 24 hours to 48 hours. The removal rate drops to 0 mmol/L/h after 84 hours and remains at this rate until 108 hours.

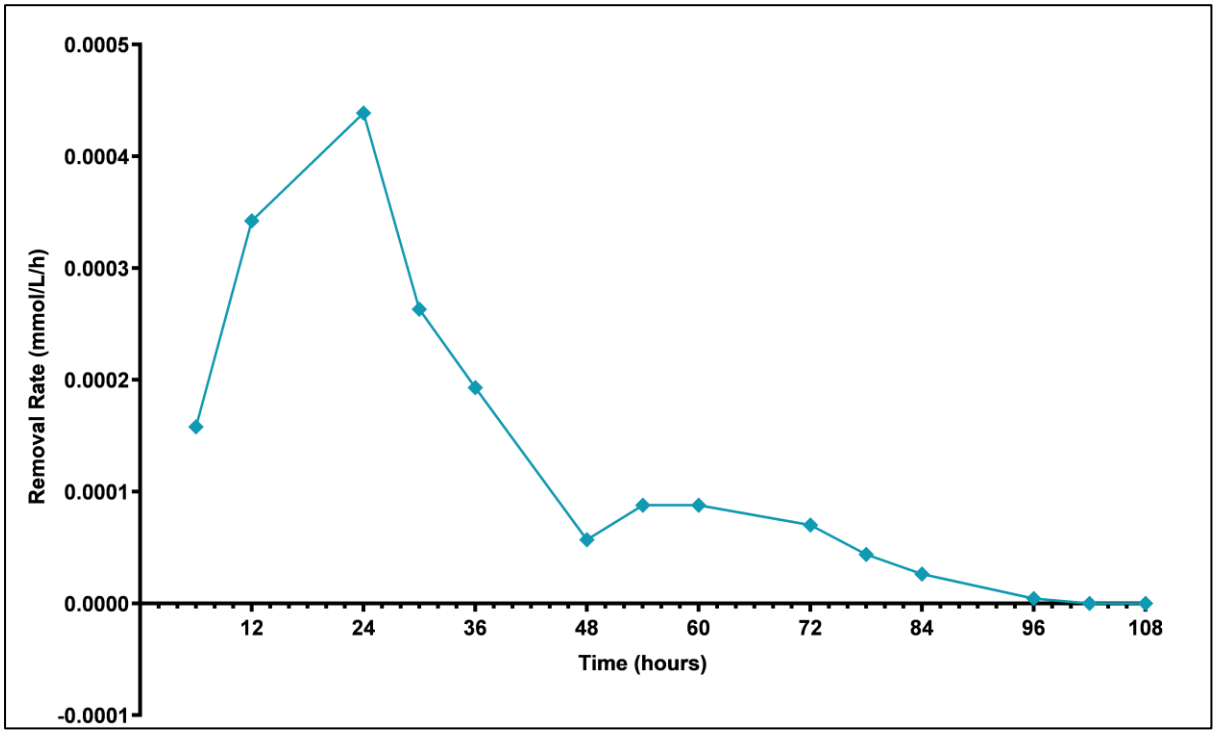

Figure 7.8: Orthophosphate removal rate vs. time for Run A at 0.5 L/min

7.3.2. Run B at 0.5 L/min

For the remaining five conditions of operation, the results are summarised into a set of four graphs presented as a composite figure. The results for Run B are presented in Figure 7.9. The top left graph shows that the ammonia concentration declines from an initial concentration of 21.5 mg/L to a final concentration of 6.32 mg/L at 228 hours. The initial nitrate concentration of 1.22 mg/L increases until it reaches a concentration of 9.84 mg/L at 174 hours. This is followed by a nett decrease in concentration to 8.04 mg/L at 228 hours. There is a direct relationship between net ammonia degradation

and net nitrate formation between 0 hours and 150 hours with 4.50 mg/L of ammonia being degraded in this time period and 4.50 mg/L of nitrate forming in this period.

The initial nitrite concentration is 0.224 mg/L. The nitrite concentration increases until it reaches a peak concentration of 0.682 mg/L at 72 hours. The concentration then decreases until reaching 0.122 mg/L at 228 hours. The orthophosphate concentration steadily declines from an initial concentration of 6.82 mg/L to 1.03 mg/L at 96 hours, where it plateaus from 96 hours to 108 hours.

The molar concentrations of ammonia, nitrate, nitrite and total nitrogen (top right graph in Figure 7.9) were used to determine the extent of nitrification and denitrification in the system for Run B at 0.5 L/min. The extent of nitrification (based on amount of ammonia available) for Run B at 0.5 L/min is 70.8% while the extent of denitrification (based on the amount of nitrate available for reaction) is 88.0%. The total nitrogen removal for Run B at 0.5 L/min is 60.9%. There was an orthophosphate removal of 85.2% in the system.

The initial ammonia degradation rate is 0.0158 mmol/L/h as seen in the bottom left graph in Figure 7.9. The ammonia degradation rate rapidly declines from 0.0158 mmol/L/h at 6 hours to 0.027 mg/L/h at 48 hours. The ammonia degradation rate proceeds to fluctuate from 48 hours to 228 hours. A 12-hour cycle is observed where the degradation rate is lowest at the beginning of the cycle and at its highest after 12 hours.

The net nitrate formation rate increases from an initial rate of 0.00055 mmol/L/h (0.033 mg/L/h) to 0.0023 mmol/L/h (0.12 mg/L/h) at 36 hours. This is followed by a sharp decline in the net formation rate to 0.00052 mmol/L/h (0.033 mg/L/h) at 54 hours. The net nitrate formation rate reaches a minimum at 72 hours. This is followed by a period of fluctuations in the formation rate until 174 hours. The 12-hour cycle is also observed for nitrate formation where the formation rate is lowest at the beginning of the cycle and highest at the end of the 12 hours. There is a net degradation of nitrate between 180 hours to 228 hours. A maximum net degradation rate of 0.001 mmol/L/h (0.063 mg/L/h) is observed at 180 hours. A potential cause of the 12-hour cycle is temperature fluctuation within the lab or the biofilter itself. This is investigated in the next run with the temperature being monitored over the 228-hour experimental period for Run C at 0.5 L/min.

The initial orthophosphate removal rate is 0.000895 mmol/L/h (0.085 mg/L/h). The removal rate reaches a maximum of 0.0013 mmol/L/h (0.12 mg/L/h) at 30 hours.

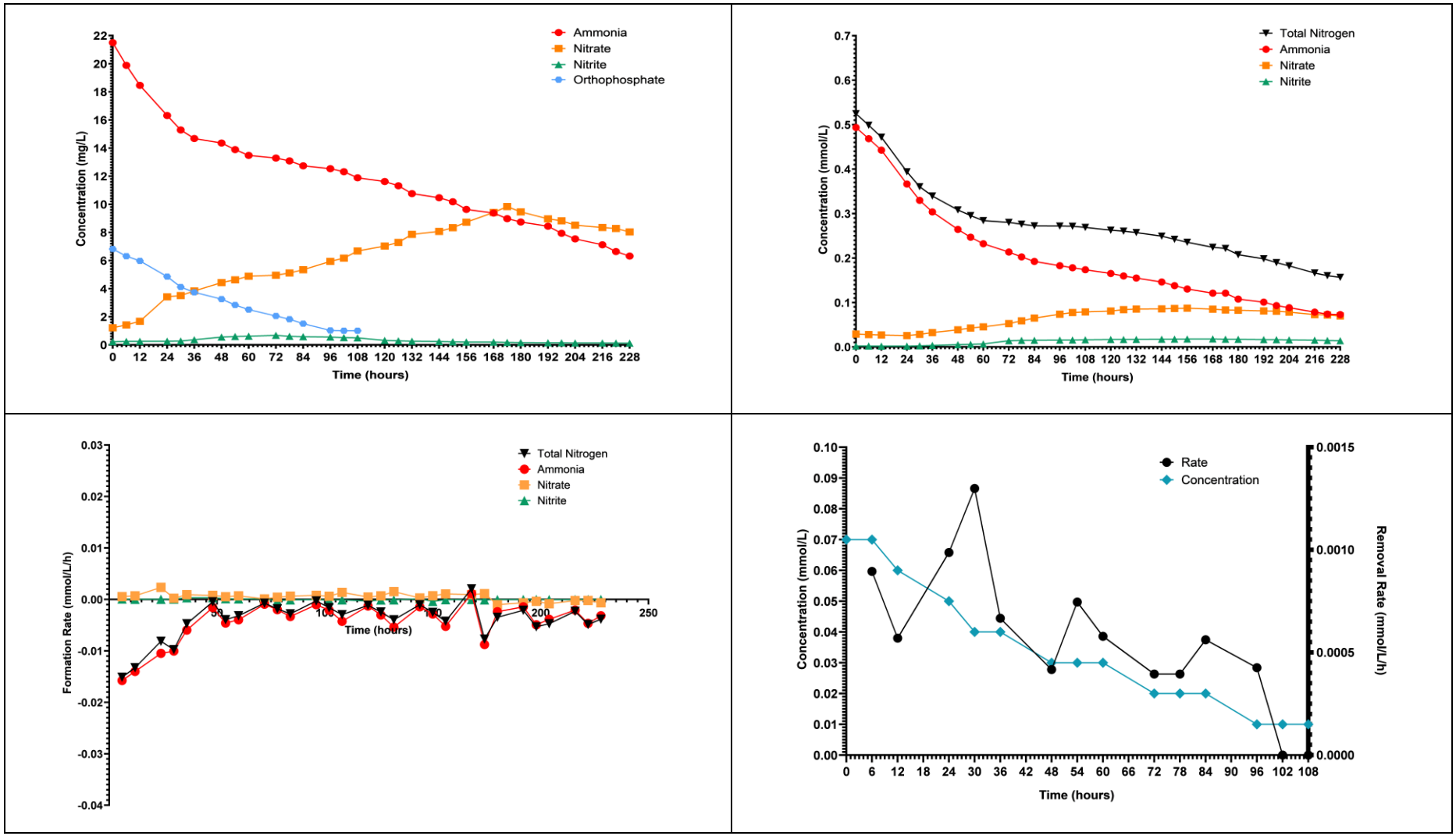

Figure 7.9: Ammonia, nitrate, nitrite and orthophosphate concentration over time in mg/L (top left); ammonia, nitrate, nitrite and total nitrogen concentration over time in mmol/L (top right); ammonia, nitrate, nitrite and total nitrogen formation rates over time (bottom left); orthophosphate concentration and removal rate over time (bottom right) for Run B at 0.5 L/min

7.3.3. Run C at 0.5 L/min

The initial ammonia concentration of 12.85 mg/L seen in the top left graph of Figure 7.10 decreases to 1.08 mg/l at 228 hours. The initial nitrate concentration is 2.3 mg/L and increases until a peak concentration of 6.12 mg/L is reached at 180 hours. Thereafter, the nitrate concentration decreases to 4.32 mg/L at 228 hours. The nitrite concentration increases from an initial concentration of 0.135 mg/L to 0.456 mg/L at 108 hours. The nitrite concentration then declines to 0.122 mg/L at 228 hours. The orthophosphate concentration decreases from 4.5 mg/L at 0 hours to 1.14 mg/L at 108 hours.

The molar concentrations of ammonia, nitrate, nitrite and total nitrogen were used to determine the extent of nitrification and denitrification in the system for Run C at 0.5 L/min. The extent of nitrification for Run C at 0.5 L/min is 91.7% while the extent of denitrification is 95.6%. The total nitrogen removal for Run C at 0.5 L/min is 82.3%. There was an orthophosphate removal of 72.4% from the system.

The bottom left graph in Figure 7.10 shows an initial ammonia degradation rate of 0.018 mmol/L/h. The ammonia degradation rate sharply declines from this initial rate to 0.002 mmol/L/h at 54 hours. The degradation rate then increases to 0.0026 mmol/L/h at 84 hours followed by a continuous decline in the degradation rate which reaches 0.00039 mmol/L/h at 228 hours.

The initial net nitrate formation rate is 0.00009 mmol/L/h which increases to a maximum of 0.00065 mmol/L/h at 108 hours. Net nitrate degradation in the system begins at 180 hours and continues until 228 hours. The net degradation rate rapidly increases between 180 hours and 228 hours. The maximum net nitrate degradation rate is seen at 228 hours where the degradation rate is 0.001 mmol/L/h.

The initial net nitrite formation rate is 0.000065 mmol/L/h with a net formation of nitrite from 0 hours to 108 hours. There is net degradation of nitrite in the system from 108 hours to 228 hours with the highest net degradation rate of 0.0001 mmol/L/h occurring at 222 hours.

The graph on the bottom right of Figure 7.10 shows the orthophosphate removal rate for Run C at 0.5 L/min. This decreases from an initial rate of 0.0008 mmol/L/h to 0.000017 mmol/L/h at 108 hours.

Figure F1 in Appendix F shows the temperature profile at five points in the biofilter system: inside the Eco Tank (inlet), 5 cm below surface in the biofilter (1 m along the length of the biofilter), 35 cm below surface in the biofilter (1.25 m along the length of the biofilter), inside the sump (outlet) and the ambient temperature.

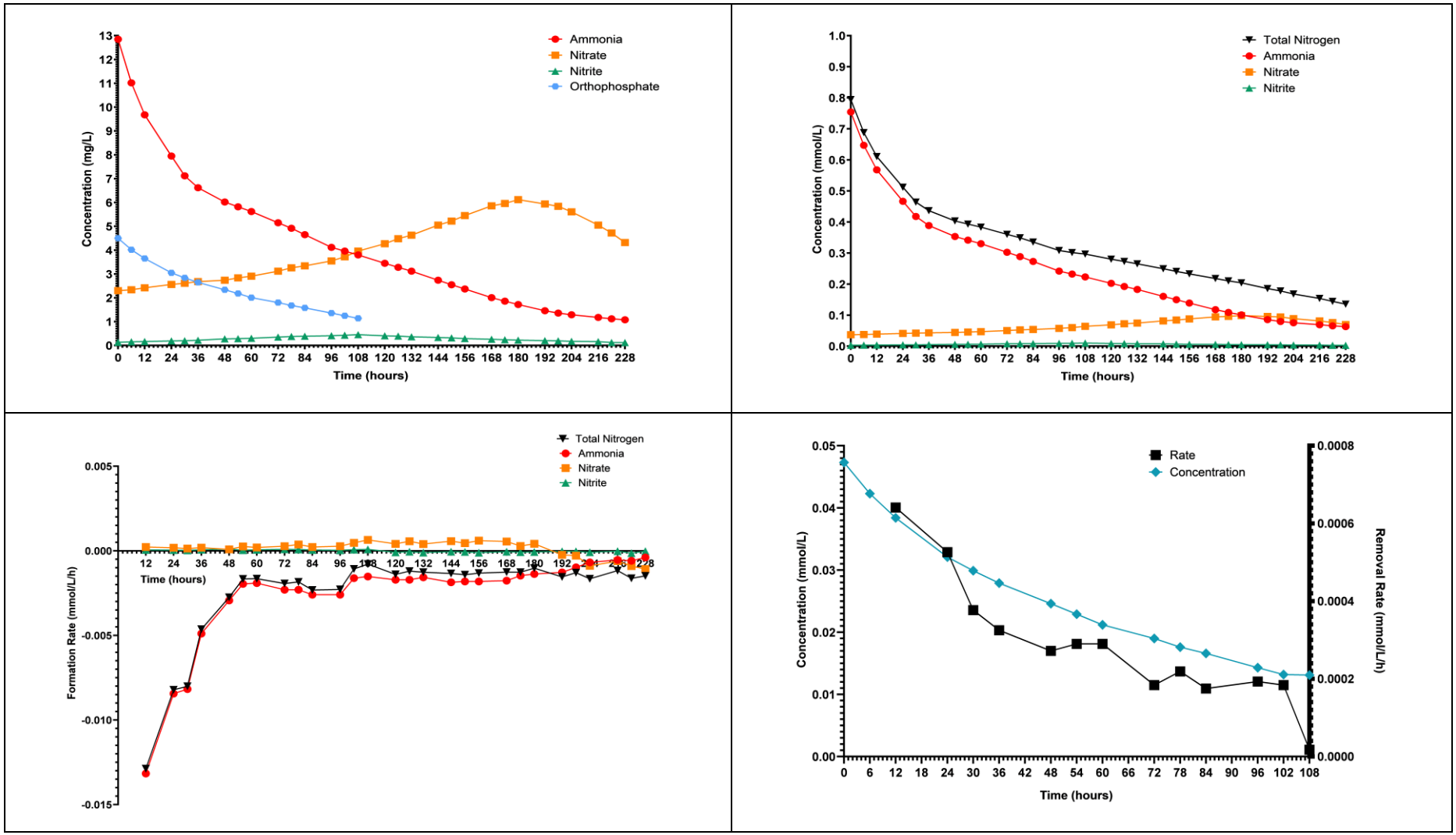

Figure 7.10: Ammonia, nitrate, nitrite and orthophosphate concentration over time in mg/L (top left); ammonia, nitrate, nitrite and total nitrogen concentration over time in mmol/L (top right); ammonia, nitrate, nitrite and total nitrogen formation rates over time (bottom left); orthophosphate concentration and removal rate over time (bottom right) for Run C at 0.5 L/min

It is noted that the ambient temperature within the laboratory is constant at 21.6°C. The outlet temperature is 22.15°C while the inlet temperature varies between 21.1°C and 21.6°C. This minimal temperature variation implies that a fluctuating temperature is not the cause of the 12-hour fluctuation cycles for ammonia and nitrate degradation rates seen in Run B at 0.5 L/min. Further, these fluctuations were not observed in Run C.

7.3.4. Run A at 1.5 L/min

The graph on the top left of Figure 7.11 shows the ammonia, nitrate and nitrite concentrations over the experimental period for Run A at 1.5 L/min, while that on the top right provides molar concentrations. The initial ammonia concentration is 14.5 mg/L. This decreased continually until it reached 1.19 mg/L at 228 hours. The initial nitrate concentration of 1.8 mg/L decreased to 1.6 mg/L at 24 hours, before increasing to 5.42 mg/L at 156 hours. The nitrate concentration then decreased to 4.32 mg/L at 228 hours. The nitrite concentration increased from 0.0.36 mg/L/h at 0 hours to 0.7 mg/L at 228 hours. The orthophosphate concentration decreased from an initial concentration of 1.45 mg/L to a final concentration of 0.17 mg/L at 102 hours.

The molar concentrations of ammonia, nitrate, nitrite and total nitrogen (top right graph of Figure 7.11) were used to determine the extent of nitrification and denitrification in the system for Run A at 1.5 L/min. The extent of nitrification for Run A at 1.5 L/min is 90.2% while the extent of denitrification is 86.7%. The total nitrogen removal for Run A at 1.5 L/min is 82.4%. There was in an orthophosphate removal of 88.2% in the system.

The initial ammonia degradation rate is 0.067 mmol/L/h as seen in the graph on the bottom left of Figure 7.11. The degradation rate steadily increases until it reaches 0.014 mmol/L/h at 36 hours. The ammonia degradation rate then proceeds to rise and fall intermittently until 156 hours. The degradation rate then drops to a minimum at 222 hours.

There is a net nitrate degradation in the system at an initial rate of 0.00017 mmol/L/h followed by a period of net nitrate formation from 6 hours to 120 hours. The maximum rate of net nitrate formation in this period is 0.00071 mmol/L/h at 96 hours. A period of net nitrate degradation occurs from 120 hours to 228 hours. The maximum net degradation rate is 0.000027 mmol/L/h at 144 hours. There is a net formation of nitrite in the system from 0 hours to 168 hours with a maximum net formation rate of 0.00015 mmol/L/h seen at 72 hours. A net degradation of nitrite occurred from 168 hours to 228 hours except for a period between 180 hours and 192 hours where there was a net formation of nitrite. A maximum degradation rate of 0.00015 mmol/L/h was seen at both 180 hours and 204 hours.

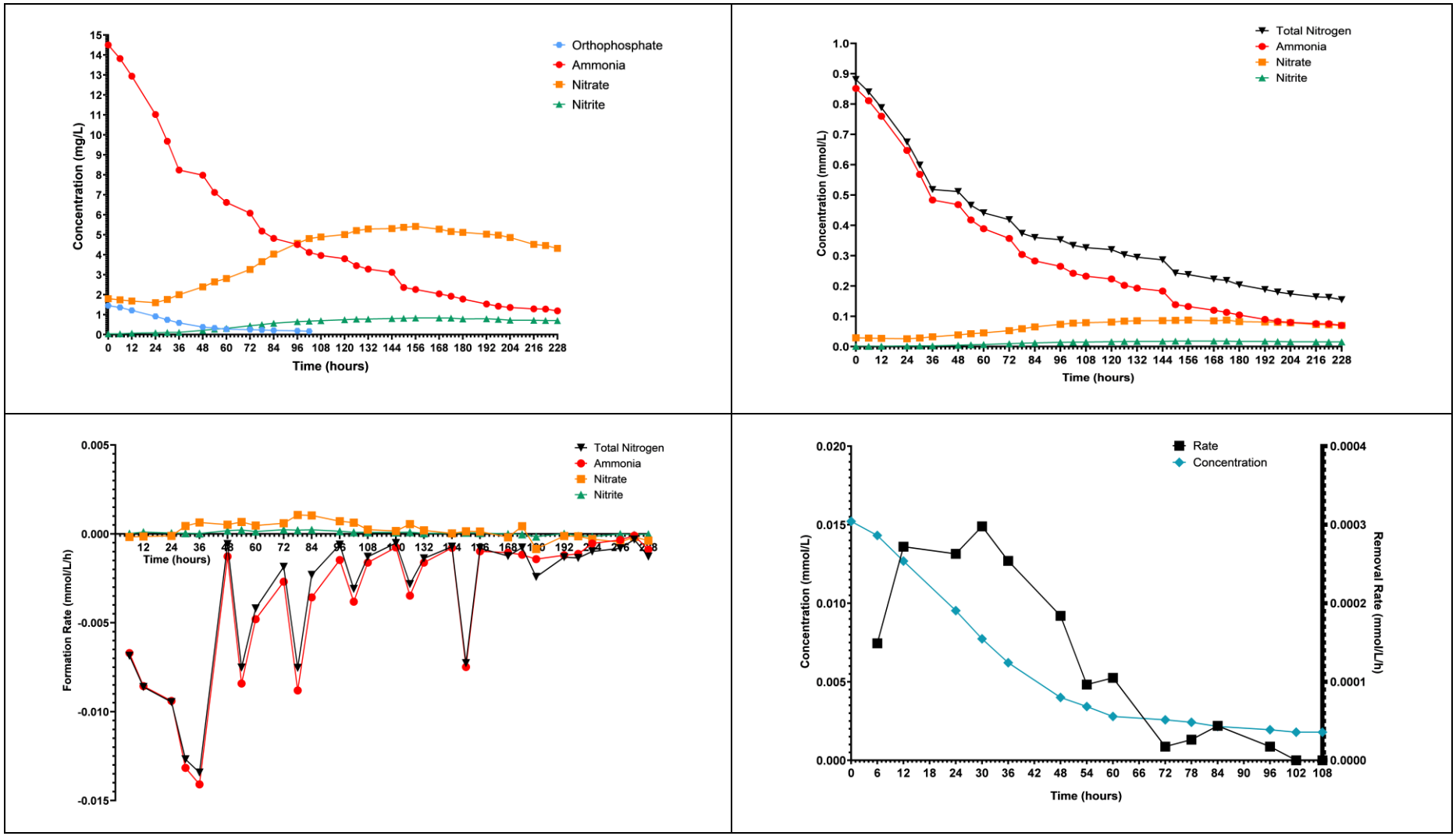

Figure 7.11: Ammonia, nitrate, nitrite and orthophosphate concentration over time in mg/L (top Left); ammonia, nitrate, nitrite and total nitrogen concentration over time in mmol/L (top right); ammonia, nitrate, nitrite and total nitrogen formation rates over time (bottom left); orthophosphate concentration and removal rate over time (bottom right) for Run A at 1.5 L/min

7.3.5. Run B at 1.5 L/min

The graph at the top left of Figure 7.12 shows an initial ammonia concentration of 24.4 mg/L for Run B at 1.5 L/min. The ammonia concentration steadily decreases until it reaches 5.2 mg/L at 228 hours. The initial nitrate concentration is 1.06 mg/L which increases to 8.74 mg/L at 144 hours. The nitrate concentration then decreases to 6.94 mg/L at 228 hours. The nitrite concentration increases from 0.13 mg/L at 0 hours to a final concentration of 0.14 mg/L at 228 hours. The initial orthophosphate concentration is 5.26 mg/L. This orthophosphate concentration decreases to 1.32 mg/L at 228 hours.

The molar concentrations of ammonia, nitrate, nitrite and total nitrogen (top right graph of Figure 7.12) were used to determine the extent of nitrification and denitrification in the system for Run B at 1.5 L/min. The extent of nitrification is 78.5% while the extent of denitrification is 91.5%. The total nitrogen removal was 70.9% while orthophosphate removal was 74.9%.

The initial ammonia degradation rate as seen in the graph at the bottom left of Figure 7.12 is 0.031 mmol/L/h. The ammonia degradation rate rapidly decreases to 0.0044 mmol/L/h at 48 hours. The degradation rate reaches a minimum of 0.00029 mmol/L/h at 192 hours.

There is a net formation of nitrate from 0 hours to 144 hours and net degradation from 144 hours to 228 hours. The initial net nitrate formation rate is 0.00032 mmol/L/h and sharply increases until reaching a maximum of 0.0023 mmol/L/h at 36 hours. The net nitrate formation rate then decreases to 0.00029 mmol/L/h at 96 hours. This is followed by an increase in the net formation rate to 0.0018 mmol/L/h at 126 hours. This is once again followed by a rapid decrease in the net nitrate formation rate until 144 hours. There is net degradation from 150 hours to 228 hours.

The initial orthophosphate removal rate is 0.00091 mmol/L/h as observed in the graph at the bottom right of Figure 7.12. There is an increase in the orthophosphate removal rate from 0.00091 mmol/L/h at 6 hours to 0.0013 mmol/L/h at 12 hours. This is followed by a decrease in the rate of removal until reaching a minimum degradation rate of 0.000096 mmol/L/h at 72 hours. The orthophosphate removal rate then increases until reaching 0.00016 mmol/L/h at 102 hours.

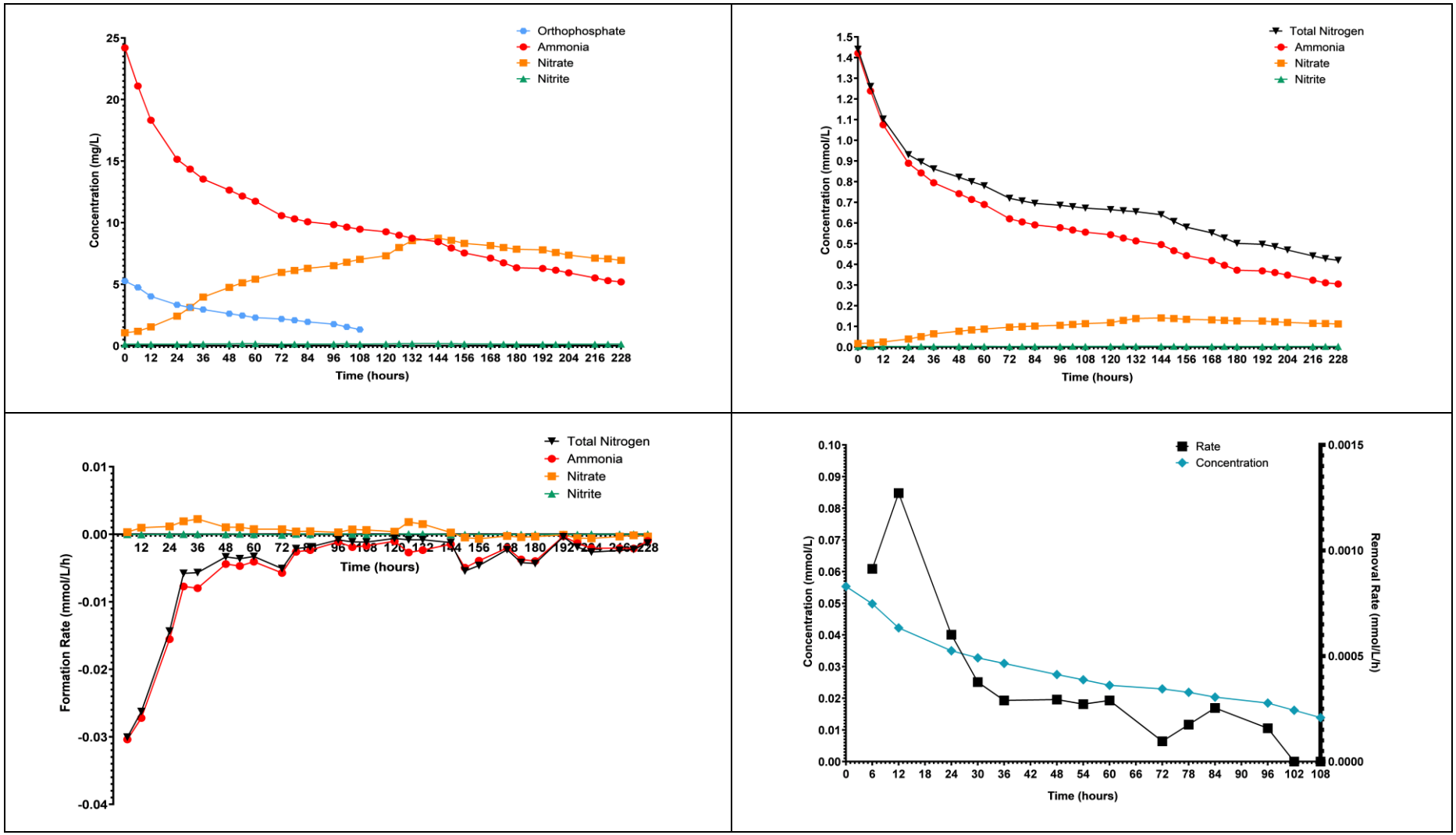

Figure 7.12: Ammonia, nitrate, nitrite and orthophosphate concentration over time in mg/L (top left); ammonia, nitrate, nitrite and total nitrogen concentration over time in mmol/L (top tight); ammonia, nitrate, nitrite and total nitrogen formation rates over time (bottom left); orthophosphate concentration and removal rate over time (bottom right) for Run B at 1.5 L/min

7.3.6. Run C at 1.5 L/min

An initial ammonia concentration of 13.2 mg/L is shown in the graph at the top left of Figure 7.13. The ammonia concentration decreased from 13.2 mg/L at 0 hours to 5.78 mg/L at 228 hours. The initial nitrate concentration of 2.1 mg/L increased to a peak of 4.72 mg/L at 108 hours followed by a decrease in to 1.58 mg/L at 228 hours. The nitrite concentration increased from an initial concentration of 0.011 mg/L to 0.7 mg/L at 228 hours. The orthophosphate concentration declines from an initial concentration of 4.80 mg/L to 2.70 mg/L at 108 hours.

The molar concentrations of ammonia, nitrate, nitrite and total nitrogen (top right graph of Figure 7.13) were used to determine the extent of nitrification and denitrification in the system for Run C at 1.5 L/min. The extent of nitrification (based on amount of ammonia available) was 56.1% while the extent of denitrification (based on the amount of nitrate available for reaction) was 94.4%. The total nitrogen removal was 53.1% and orthophosphate removal was 43.8%.

The ammonia degradation rate sharply decreases from an initial rate of 0.0088 mmol/L/h to 0.0028 mmol/L/ at 36 hours. This is followed by a gentler decrease in the degradation rate until 228 hours with the final degradation rate being 0.0011 mmol/L/h.

An initial net nitrate formation rate of 0.00036 mmol/L/h is seen at the bottom left of Figure 7.13. The net nitrate formation rate reaches a maximum of 0.001 mmol/L/h at 78 hours. This is followed by a decrease in the net nitrate formation rate to 0.0001 mmol/L/h at 108 hours. There is net degradation of nitrate from 108 hours to 228 hours. A maximum net degradation rate of 0.0007 mmol/L/h is seen at 156 hours. The net nitrate degradation rate then proceeds to decrease and reaches a minimum at 216 hours. There is net degradation of nitrite from 0 hours to 30 hours and net formation from 30 hours to 174 hours. This is followed by another period of net degradation until the experiment is completed at 228 hours. A maximum rate of net nitrite formation of 0.00067 mmol/L/h is seen at 54 hours.

The initial orthophosphate removal rate was 0.00046 mmol/L/h as seen in the graph at the bottom right of Figure 7.13. The removal rate decreased to a final rate of 0.00 mmol/L/h at 108 hours.

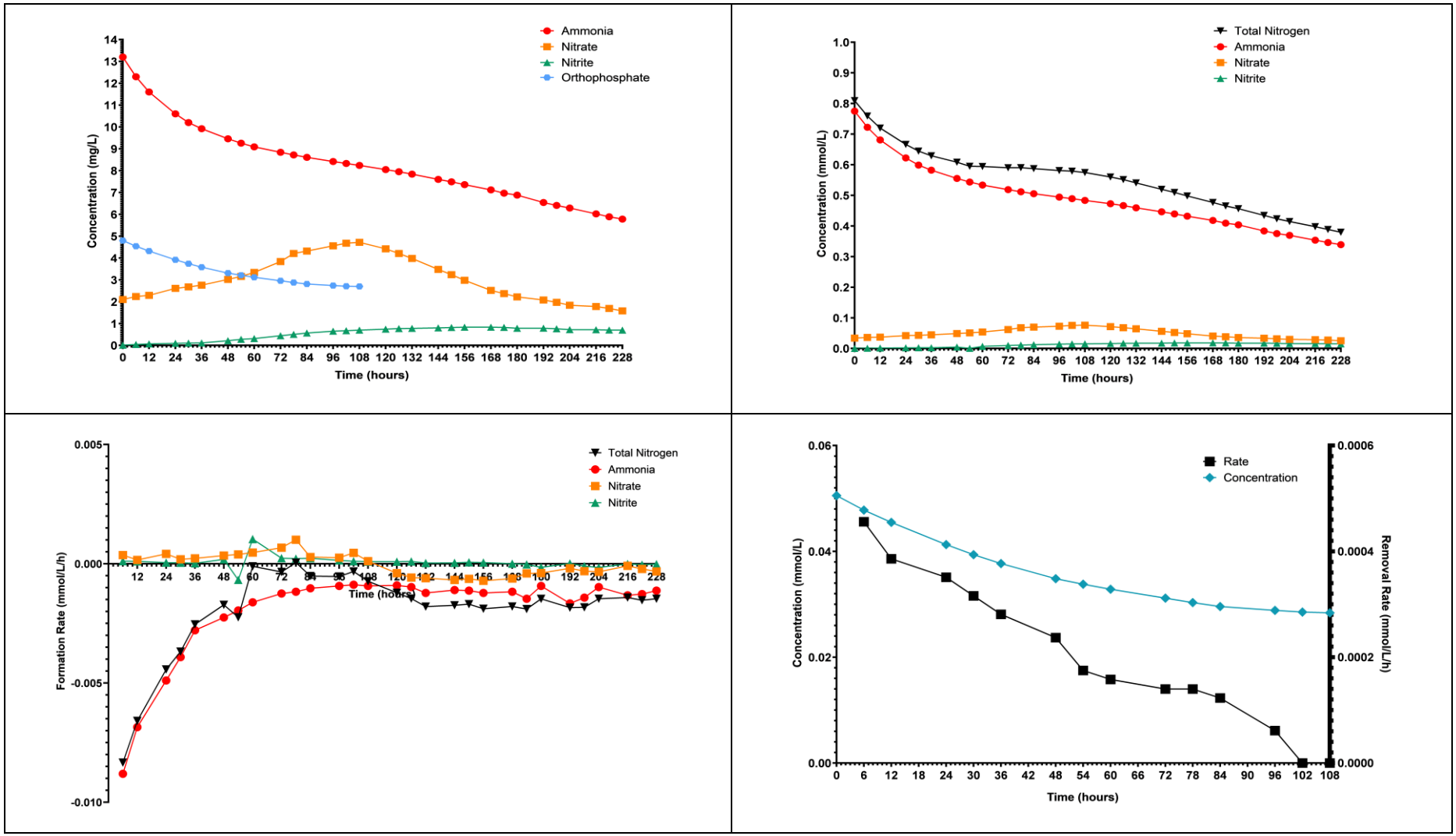

Figure 7.13: Ammonia, nitrate, nitrite and orthophosphate concentration over time in mg/L (top left); ammonia, nitrate, nitrite and total nitrogen concentration over time in mmol/L (top right); ammonia, nitrate, nitrite and total nitrogen degradation/formation rates over time (bottom left); orthophosphate concentration and degradation rate over time (bottom right) for Run C at 1.5 L/min

7.4. System Performance Based on Nutrient Removal and Extent of Nitrification and Denitrification

Figure 7.14 shows total nitrogen concentration over time for the nutrient degradation studies at 0.5 L/min and 1.5 L/min. The greatest amount of total nitrogen removed occurred in Run B at 0.5 L/min where the total nitrogen concentration decreased from 1.44 mmol/L to 0.420 mmol/L, resulting in 1.02 mmol/L of nitrogen being removed from the system. The lowest amount of total nitrogen removed occurred in Run A at 0.5 L/min where the total nitrogen concentration decreased from 0.525 mg/L to 0.157 mg/L, resulting in 0.368 mmol/L of nitrogen being removed from the system. However, the total amount of nitrogen removed is not the most reliable indicator of the pilot biofilter's performance due to the highly variable inlet total nitrogen concentrations which can be seen in Figure 7.14 and the importance of meeting the specifications of fit-for-purpose water for re-use or discharge.

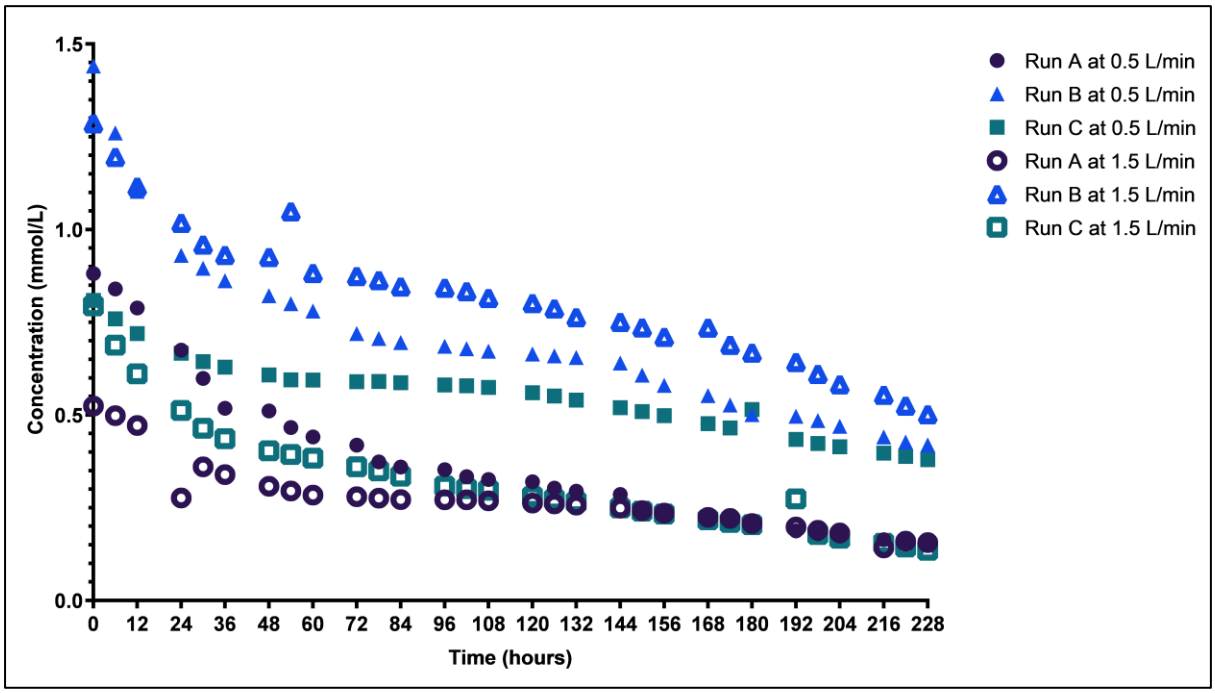

Figure 7.14: Total nitrogen concentrations for Run A, B & C at 0.5 L/min

Figure 7.15 shows the amount of ammonia degraded in the system vs the ammonia introduced to the system for every run except Run C at 1.5 L/min (Run C at 1.5 L/min is an outlier). The grey line is a parity line where y = x. There is a strong positive correlation between the amount of ammonia introduced to the system and the amount of ammonia degraded as suggested by the R^2 value of 0.928 for the linear fit. There is a deviation from the parity line at higher concentrations which points to decreased conversions at higher inlet ammonia concentrations.

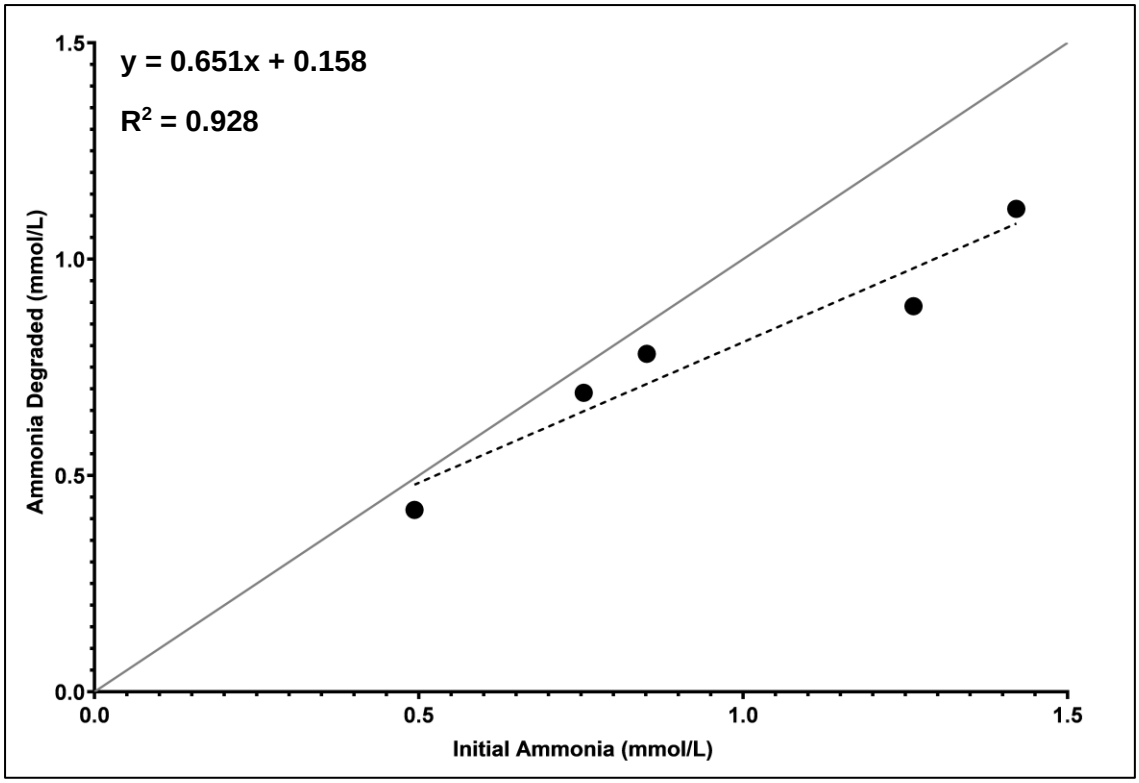

Figure 7.15: Ammonia degraded in system vs ammonia added to system for all runs (excludes Run C at 1.5 L/min)

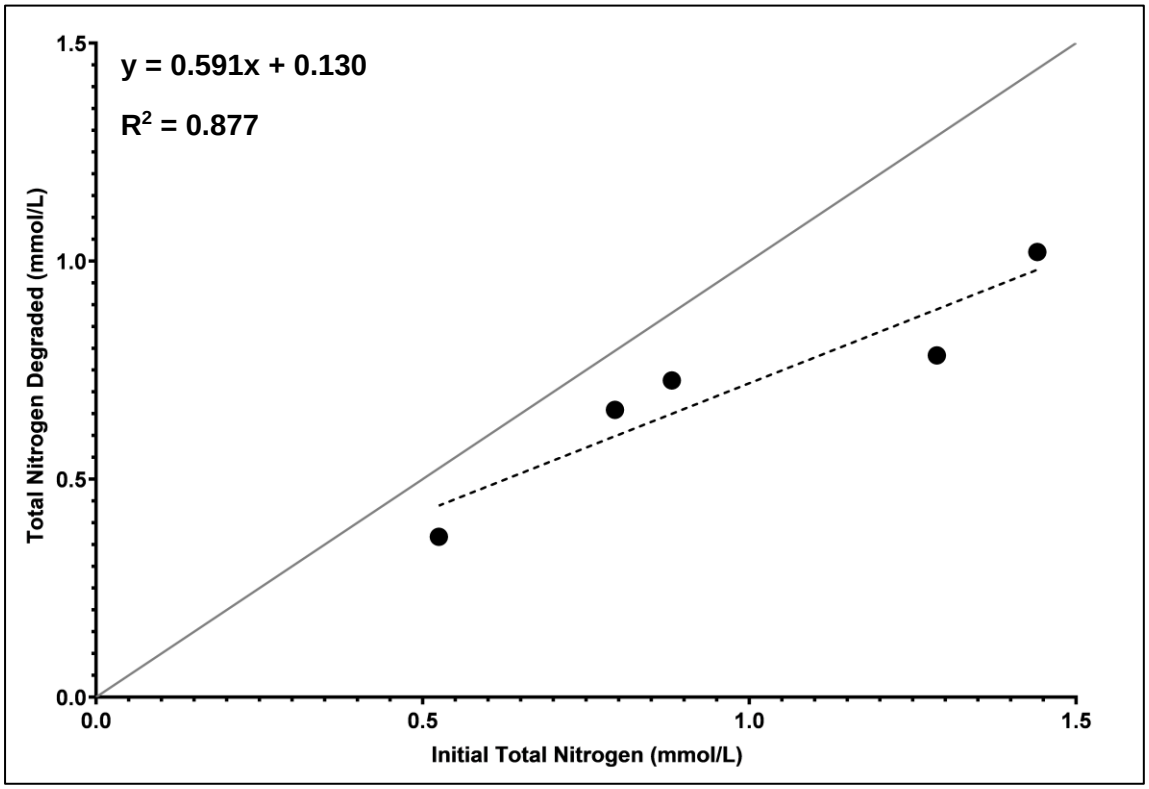

Figure 7.16: Total nitrogen degraded in system vs total nitrogen added to system for all runs (excludes Run C at 1.5 L/min)

Figure 7.16 shows the total nitrogen degraded in the system vs the total nitrogen introduced to the system for every run except Run C at 1.5 L/min (outlier). The grey line is a parity line where y = x. There is a direct correlation between the amount of total nitrogen introduced to the system and the total nitrogen degraded as suggested by the R^2 value of 0.877. This implies that a higher initial total nitrogen concentration results in greater total nitrogen degradation However, the deviation from the parity line at higher concentrations in both Figure 7.15 and Figure 7.16 points to decreased conversions at higher concentrations, possibly due to rate limitation or inhibition.

Table 7.2 summarises the performance of the pilot biofilter for all runs at a recirculation rate of both 0.5 L/min and 1.5 L/min. The first thing to note is the variable nutrient concentration at the system inlet. The ammonia inlet concentration across all runs ranged between 8.41 mg/L and 24.2 mg/L. The nitrate inlet concentration across all runs ranged from 1.22 mg/L to 2.3 mg/L, while the orthophosphate inlet concentration across all runs ranged between 1.6 mg/L and 6.82 mg/L. This emphasises that the three runs at each flow rate cannot be considered replicates of each other due to the highly variable inlet conditions as well as the importance of the system being resilient to fluctuating nutrient concentrations.

Run C at 1.5 L/min can be considered anomalous as the ammonia and orthophosphate reductions in this run are significantly lower than in all the other runs. The poor performance in this run may be attributed to an interruption in the electricity supply during the experiment due to load shedding. This interruption resulted in no aeration or circulation via the sump pump in the system from 96 to 98 hours and 132 to 134 hours.

The total nitrogen and orthophosphate reductions seen are comparable to the performance of horizontally orientated subsurface flow stone constructed wetlands reported by Rasool et al. (2018) where orthophosphate removal of up to 88% and total nitrogen removal of up to 85% are the norm. The highest total nitrogen reduction of 82.4% occurs in Run A at 1.5 L/min. The highest orthophosphate reduction of 88.3% also occurs in Run A at 1.5 L/min. These results show that the pilot biofilter can be relied on to reduce the concentration of total nitrogen and orthophosphate significantly.

The greatest extent of nitrification was seen in Run C at 0.5 L/min and amounted to 91.7%. The extent of denitrification (based on the amount of nitrate available for denitrification, which was the sum of the initial nitrate concentration and the nitrate formed from the nitrification reaction) was also greatest for Run C at 0.5 L/min at 95.6%. There is consistent denitrification in the system for all experimental runs with the lowest extent of denitrification of 86.7% seen in Run A at 1.5 L/min. The pilot biofilter's ability to efficiently metabolise nitrate is also seen in Run C at 1.5 L/min

where the extent of denitrification is 94.4% even though the total nitrogen removal is only 53.1% for this run. The greatest extent of nitrification is seen in Run C at 0.5 L/min with 91.7% nitrification being achieved.

From the results presented in Table 7.2, it can be inferred that the microbial community in the pilot biofilter system are able to metabolise large pulses of nutrients when fresh contaminated water is introduced to the system at varying inlet concentrations. The microbial community is able to survive under nutrient limited conditions and can metabolise lower concentrations of ammonia, nitrate and nitrite as seen in Run A at 0.5 L/min.

Table 7.3 shows the residual nutrient concentrations for all experimental runs at both 0.5 L/min and 1.5 L/min. These residual nutrient concentrations can be compared to the water quality requirements for domestic use in South Africa (Department of Water Affairs and Forestry, 1996) as per Table 2.1. Table 2.1 also shows the limits for discharge into rivers. The instances where the residual nutrient concentrations meet the water quality constraints for domestic use for a particular nutrient are highlighted in blue.

With the exception of Run B at 0.5 L/min, the residual nitrate concentrations for all nutrient degradation studies were below 6 mg/L which is acceptable for domestic use. Residual nitrite concentrations for all nutrient degradation studies were well below 6 mg/L which is acceptable in water intended for domestic use. The residual nitrate concentrations for all runs were below 15 mg/L making it suitable for discharge into rivers according to the South African National Water Quality Act (Department of Water Affairs and Forestry, 1996).

According to the South African Water Quality Guidelines (Department of Water Affairs and Forestry, 1996), ammonia concentrations in water being used for domestic purposes should be less than 2 mg/L. The residual ammonia concentrations in Run A at 0.5 L/min, Run C at 0.5 L/min and Run A at 1.5 L/min were below 2 mg/L. All experimental runs had residual ammonia concentrations less than 6 mg/L making it suitable for discharge (Department of Water Affairs and Forestry, 1996).

The limit for orthophosphate concentrations in water intended for domestic use as per the South African Water Quality Guidelines is 2.5 mg/L. The residual orthophosphate concentrations in Run A, Run B and Run C at 0.5 L/min were below 2.5 mg/L. Residual orthophosphate concentrations in Run A and Run B at 1.5 L/min were also below 2.5 mg/L. The treated water from Run A at 0.5 L/min, Run C at 0.5 L/min and Run A at 1.5 L/min (with regards to nutrient concentrations only) were suitable for domestic use.

The nutrient concentrations in the treated water from all nutrient degradation studies were below the limits for disposal into rivers.

Table 7.2: Summary of performance for all runs at 0.5 L/min & 1.5 L/min

		0.5 L/min			1.5 L/min		
		Run A	**Run B**	**Run C**	**Run A**	**Run B**	**Run C**
Order in which runs were conducted		1	2	6	3	4	5
Inlet Concentration (mg/L)	**NH_3:**	8.41	21.5	12.9	14.5	24.2	13.2
	NO_3-:	1.80	1.22	2.30	1.80	1.06	2.10
	NO_2-:	0.097	0.224	0.135	0.036	0.131	0.011
	PO_4^{3-}:	1.60	6.82	4.50	1.45	5.26	4.80
NH_3 Removal		85.3%	70.6%	91.6%	91.8%	78.6%	56.2%
PO_4^{3-} Removal		83.1%	85.2%	74.7%	88.3%	74.9%	43.5%
Extent of Nitrification		82.8%	70.8%	91.7%	90.2%	78.5%	56.1%
Extent of Denitrification		90.6%	88%	95.6%	86.7%	91.5%	94.4%
Total Nitrogen Removal		70.1%	60.9%	82.3%	82.4%	70.9%	53.1%

Table 7.3: Residual nutrient concentrations for nutrient degradation kinetic studies at 0.5 L/min and 1.5 L/min

		0.5 L/min			1.5 L/min			Water quality requirements for domestic use in SA
		Run A	**Run B**	**Run C**	**Run A**	**Run B**	**Run C**	
Inlet Concentration (mg/L)	**NH_3:**	8.41	21.5	12.9	14.5	24.2	13.2	
	NO_3-:	1.80	1.22	2.30	1.80	1.06	2.10	
	NO_2-:	0.097	0.224	0.135	0.036	0.131	0.011	
	PO_4^{3-}:	1.60	6.82	4.50	1.45	5.26	4.80	
Residual NH_3 Concentration (mg/L)		1.24	6.32	1.08	1.19	5.19	5.78	**2.0**
Residual NO_3- Concentration (mg/L)		4.32	8.04	4.32	4.32	6.94	1.58	**6.0**
Residual NO_2-Concentration (mg/L)		0.649	0.123	0.122	0.702	0.141	0.701	**6.0**
Residual PO_4^{3-} Concentration (mg/L)		0.27	1.01	1.24	0.17	1.31	2.70	**2.50**

7.5. Modelling Ammonia Degradation and Orthophosphate Removal Kinetics for All Nutrient Degradation Studies

7.5.1. Estimating ammonia and orthophosphate concentrations using simple first and second order kinetic models

Simple first order and second order kinetic models were produced for ammonia degradation and orthophosphate removal for Run A, Run B and Run C at 0.5 L/min. Figure G1, Figure G2 and Figure G7 to Figure G28 in Appendix G show the process whereby the rate constants were obtained for ammonia and orthophosphate for all experimental runs. It was found that the order of reaction for nitrate and nitrite cannot be described using first or second order reaction kinetics as per Figure G3 to Figure G6. Table 7.4 shows the R^2 values and rate constants (*k*) for ammonia degradation and orthophosphate removal for all experimental runs at both a first order fit and second order fit. R^2 values were used to as an indicator of the goodness of fit for the first and second order models, with a higher R^2 value signifying a better goodness of fit.

Table 7.4 shows that there is a consistent strong positive correlation for the first order models for ammonia degradation across all runs at 0.5 L/min and 1.5 L/min as per the R^2 values which are greater than 0.952. This is in contrast to the second order R^2 values for ammonia degradation which range from 0.891 to 0.977, indicating a poorer goodness of fit for the second order model across all experimental runs. From Table 7.4, it can be seen that there is a consistent strong positive correlation for the first order models for orthophosphate removal across all runs at 0.5 L/min and 1.5 L/min as per the R^2 values which are greater than 0.951 (with the exception of Run A at 0.5 L/min where the R^2 value is 0.915).

The measured ammonia and orthophosphate concentrations for all experimental runs were plotted against the estimations from the first and second order kinetic models as seen from Figure 7.17 to Figure 7.20. This was done to visualise the accuracy of each model as the R^2 values indicated strong positive correlations for both first and second order kinetic models. Equation 7.4 (simple first order model) and Equation 7.6 (second order model), along with the rate constants shown in Table 7.4 were used to approximate the concentrations at time, t for all Runs at 0.5 L/min and 1.5 L/min.

$$[C] = [C]_0 e^{-kt}$$ Equation 7.4

$$\frac{1}{[C]} = \frac{1}{[C]_0} + kt$$ Equation 7.5

Table 7.4: First and second order kinetic data for ammonia degradation and orthophosphate removal

		0.5 L/min			1.5 L/min		
		Run A	**Run B**	**Run C**	**Run A**	**Run B**	**Run C**
Ammonia	**R^2 First Order**	0.978	0.971	0.991	0.993	0.952	0.961
	***k* First Order (h^{-1})**	0.00769	0.00441	0.0102	0.0111	0.00561	0.00300
	R^2 Second Order	0.945	0.935	0.891	0.920	0.977	0.977
	***k* Second Order ($mmol^{-1}.L.h^{-1}$)**	0.0469	0.00683	0.0596	0.0572	0.010	0.00622
Orthophosphate	**R^2 First Order**	0.915	0.989	0.994	0.951	0.972	0.956
	***k* First Order (h^{-1})**	0.0177	0.0188	0.0120	0.0218	0.0111	0.00539
	R^2 Second Order	0.967	0.8886	0.983	0.978	0.951	0.980
	***k* Second Order ($mmol^{-1}.L.h^{-1}$)**	3.17	0.780	0.518	5.32	0.419	0.149

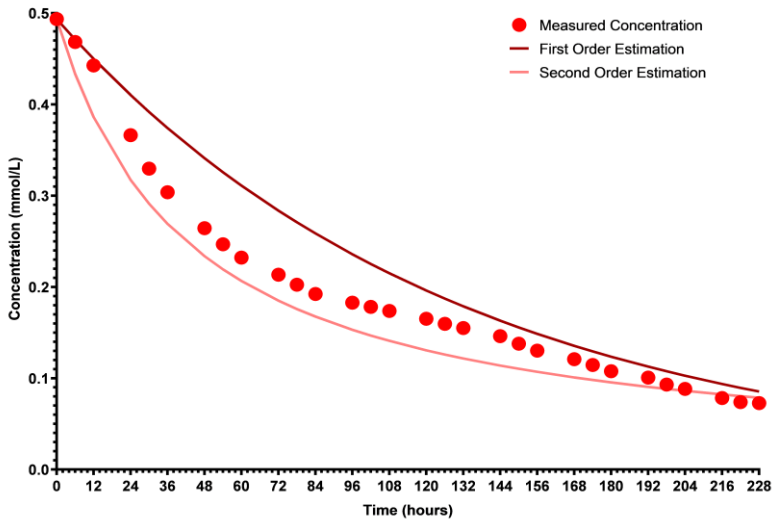

Run A at 0.5 L/min

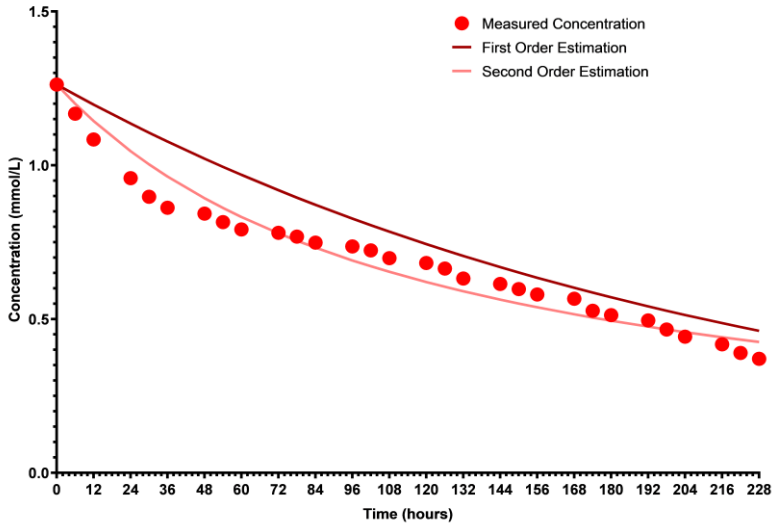

Run B at 0.5 L/min

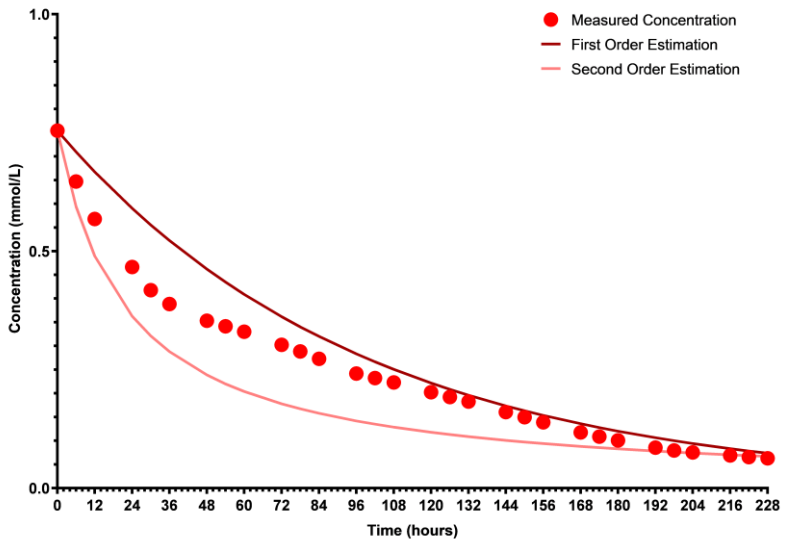

Run C at 0.5 L/min

Figure 7.17: Estimation of ammonia concentration using first and second order kinetic models against measured ammonia concentration for all runs at 0.5 L/min

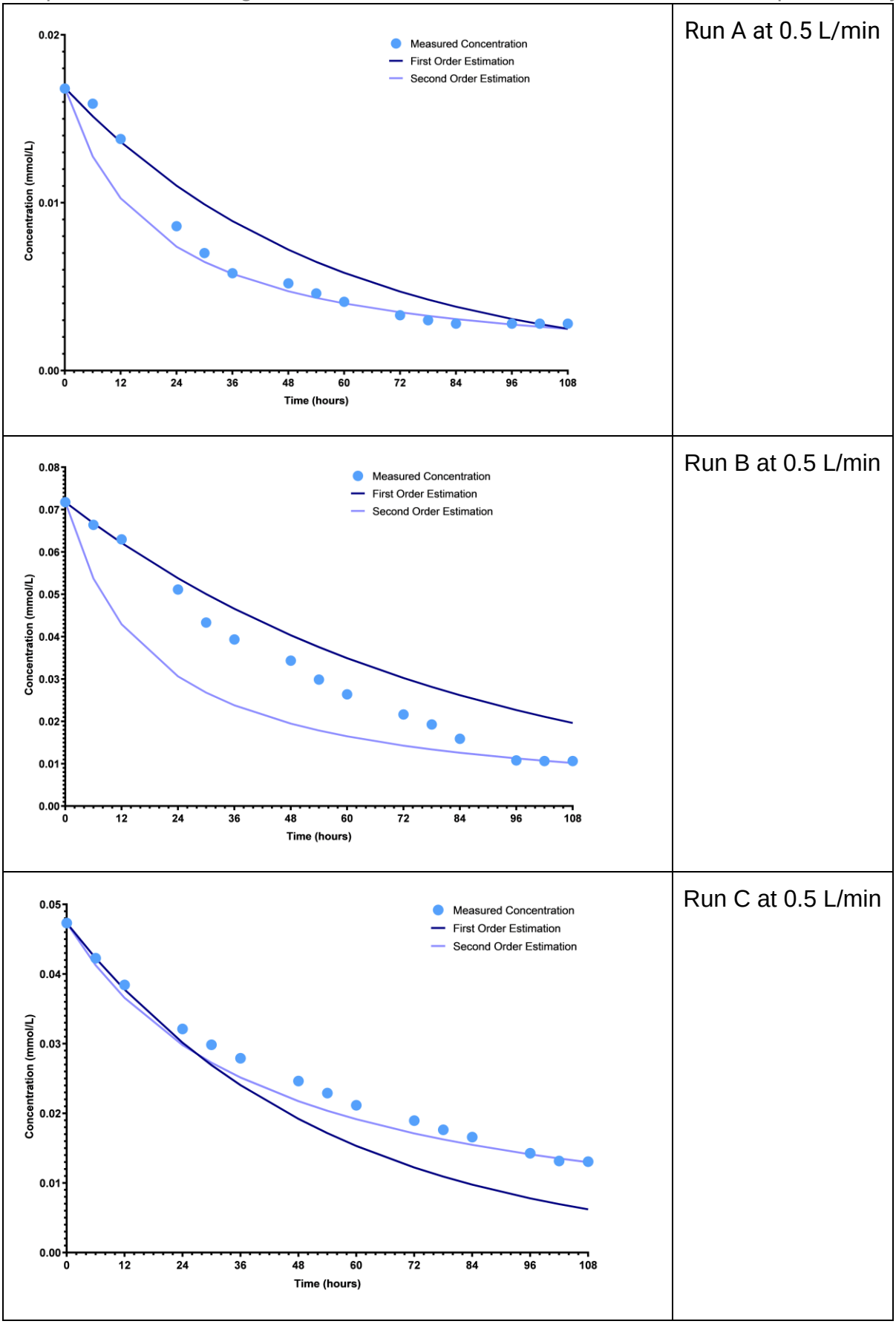

Figure 7.18: Estimation of orthophosphate concentration using first and second order kinetic models against measured orthophosphate concentration for all runs at 0.5 L/min

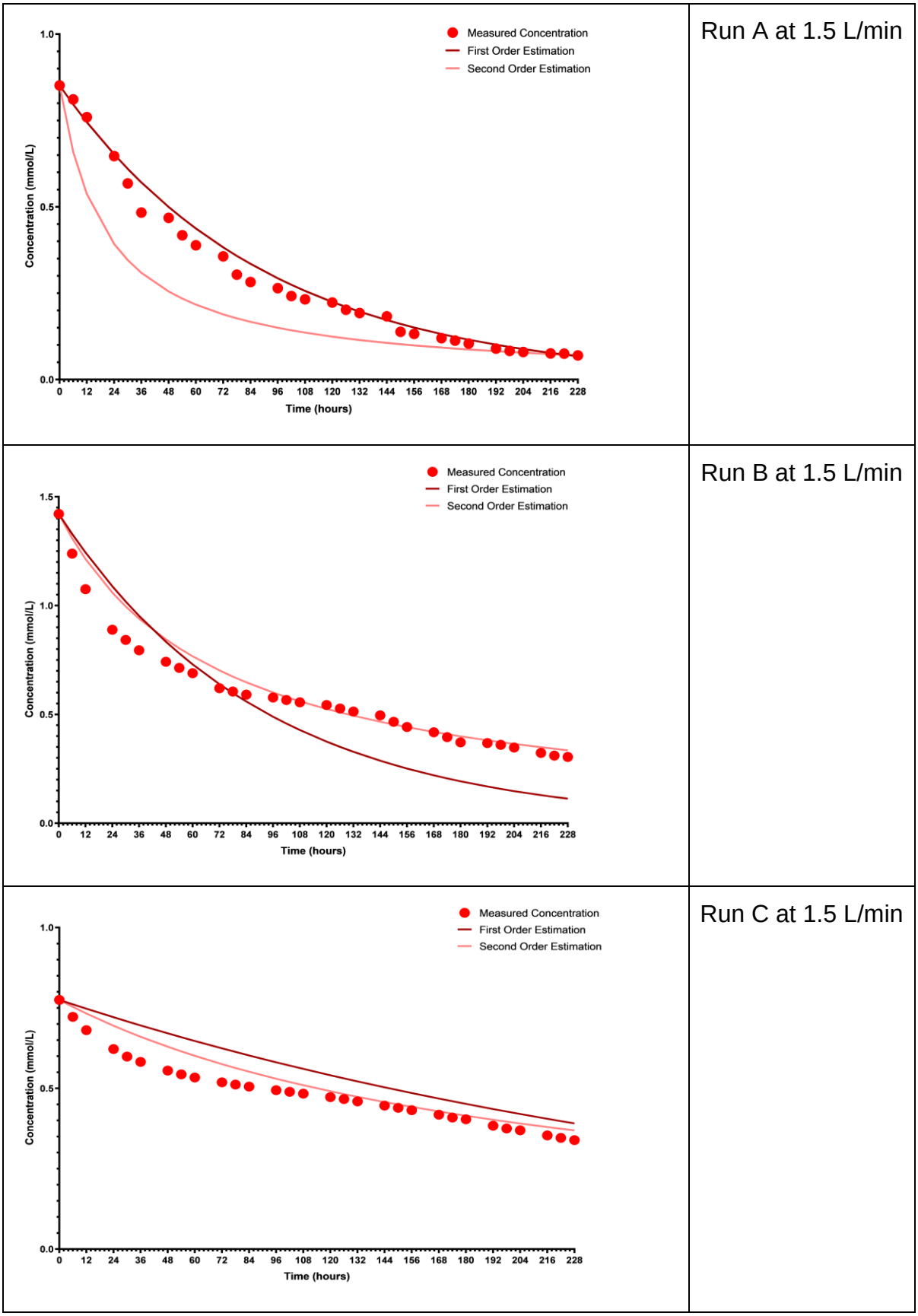

Figure 7.19: Estimation of ammonia concentration using first and second order kinetic models against measured ammonia concentration for all runs at 1.5 L/min

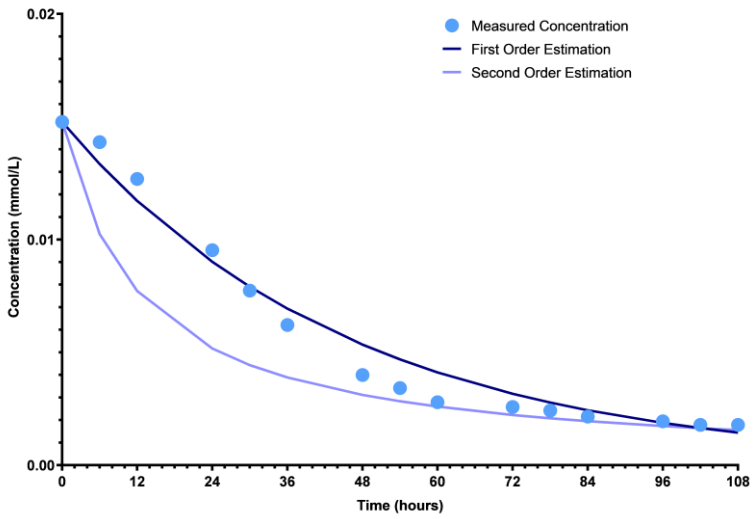

Run A at 1.5 L/min

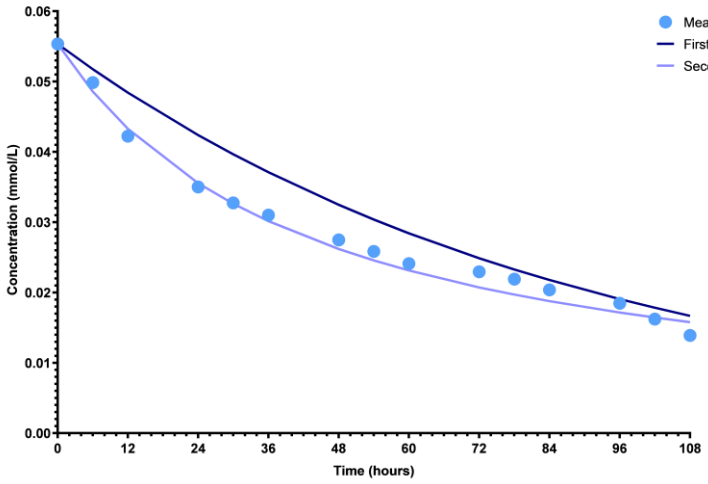

Run B at 1.5 L/min

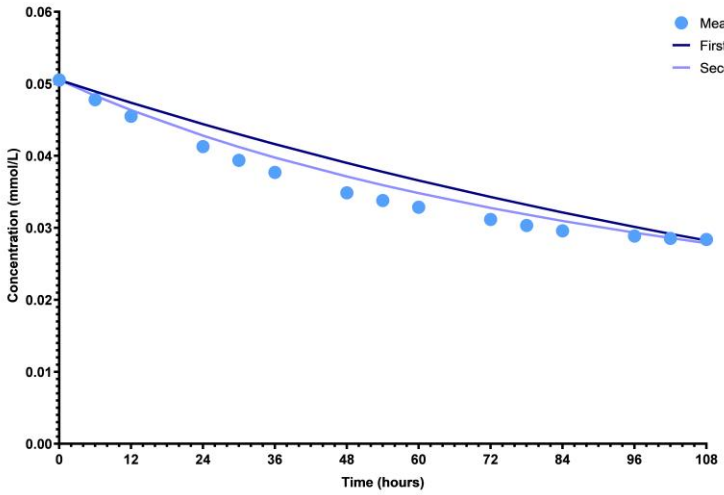

Run C at 1.5 L/min

Figure 7.20: Estimation of orthophosphate concentration using first and second order kinetic models against measured orthophosphate concentration for all runs at 1.5 L/min

Figure 7.17 shows the estimation of ammonia concentration using first and second order kinetic models against measured ammonia concentration for Runs A, B and C at 0.5 L/min. It can be seen that the first order model overestimates the actual ammonia concentration while the second order model underestimates actual ammonia concentrations for Run A and Run C at 0.5 L/min. The second order provides a better approximation of measured ammonia concentration from 72 hours to 228 hours for Run B at 0.5 L/min but overestimates the actual ammonia concentration from 0 hours to 66 hours.

Figure 7.18 shows the estimation of orthophosphate concentration using first and second order kinetic models against measured orthophosphate concentration for Runs A, B and C at 0.5 L/min. The first order model overestimates the actual orthophosphate concentration while the second order model underestimates actual orthophosphate concentrations for Run A and Run B at 0.5 L/min. The first and second order model underestimate orthophosphate concentration for Run C at 0.5 L/min.

Figure 7.19 shows the estimation of ammonia concentration using first and second order kinetic models against measured ammonia concentration for Runs A, B and C at 1.5 L/min. It can be seen that the first order model best represents the ammonia concentrations for Run A at 1.5 L/min but overestimates the concentrations from 36 hours to 108 hours. The second order model underestimates ammonia concentration for Run A at 1.5 L/min. The first and second order model both overestimate ammonia concentration from 0 hours to 66 hours for Run B at 1.5 L/min. The second order model provides the best approximation of ammonia concentration from 96 hours to 228 hours. The first and second order model both overestimate ammonia concentration from 0 hours to 96 hours for Run C at 1.5 L/min with the second order model providing the most accurate estimation of ammonia concentration from 120 hours to 228 hours.

Figure 7.20 shows the estimation of orthophosphate concentration using first and second order kinetic models against measured orthophosphate concentration for Runs A, B and C at 1.5 L/min. Both the first and second order model poorly represent orthophosphate concentration for Run A at 1.5 L/min. The first order model overestimates the orthophosphate concentration for Run B at 1.5 L/min. The second order model provides the most accurate estimation of orthophosphate concentration for Run B at 1.5 L/min from 0 hours to 36 hours, after which the second order model overestimates orthophosphate concentration. Both the first and second order model overestimate orthophosphate concentration for Run C at 0.5 L/min.

Figure 7.17 and Figure 7.19 show that both the simple first order kinetic model and second order kinetic model are poor representations of ammonia concentration for the nutrient degradation studies at both 0.5 L/min and 1.5 L/min. However, stronger R^2

correlations across all runs for the simple first order model indicates that the DOFP model may be able to accurately estimate ammonia concentrations in the system. Figure 7.18 and Figure 7.20 suggest the same for the estimation of orthophosphate concentrations in the system with strong R^2 correlations across all runs for the simple first order model indicating that the DOFP model may be able to accurately estimate orthophosphate concentrations in the system.

7.5.2. Estimating ammonia and orthophosphate concentrations using Double First-Order in Parallel kinetic model for nutrient degradation studies at 0.5 L/min

The DFOP kinetic model was assessed to determine whether it could accurately predict ammonia degradation and orthophosphate removal in the system. Equation 7.3 was used to provide an estimation of ammonia and orthophosphate concentration as per the DFOP model.

$$C_t = C_o g e^{-k_1 t} + C_o(1-g)e^{-k_2 t} \quad \text{Equation 7.3}$$

The Computer Assisted Kinetics Evaluation (CAKE) software was used to determine k_1, k_2 and g for ammonia degradation and orthophosphate removal for all experimental runs at 0.5 L/min. The results from this analysis, seen in Table 7.5, were utilised in Equation 7.3.

Table 7.5: Kinetic data for the DFOP model for ammonia degradation and orthophosphate removal at 0.5 L/min

	Ammonia Degradation			**Orthophosphate Removal**		
	k_1 (h^{-1})	**k_2 (h^{-1})**	**g**	**k_1 (h^{-1})**	**k_2 (h^{-1})**	**g**
Run A	0.0344	0.00583	0.397	0.0355	5.16E-10	0.879
Run B	0.0917	0.00385	0.196	0.0175	0.0174	0.0866
Run C	0.0993	0.00895	0.267	0.0798	0.0107	0.145

Figure 7.21 shows the estimation for ammonia concentration provided by the DFOP kinetic model compared to that of the simple first order and second order kinetic models for the nutrient degradation studies at 0.5 L/min. Figure 7.22 shows the residuals (actual concentration less concentration estimated by kinetic models) for the DFOP, simple first order and second order kinetic models.

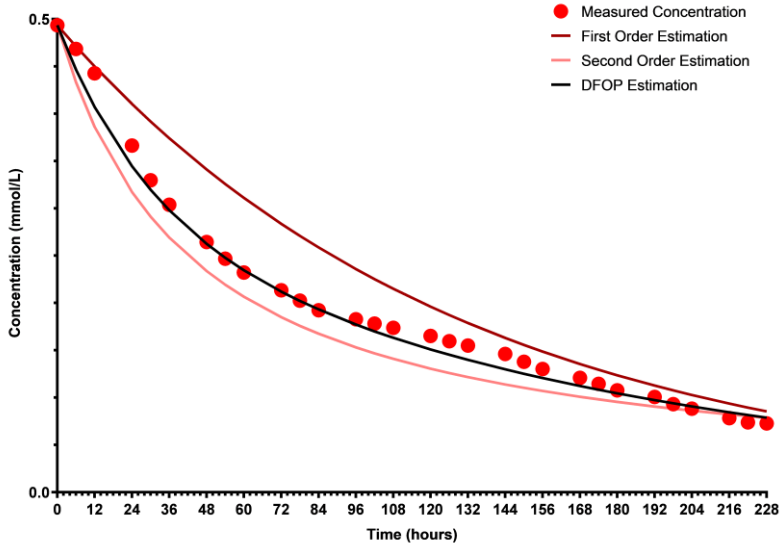

Run A at 0.5 L/min

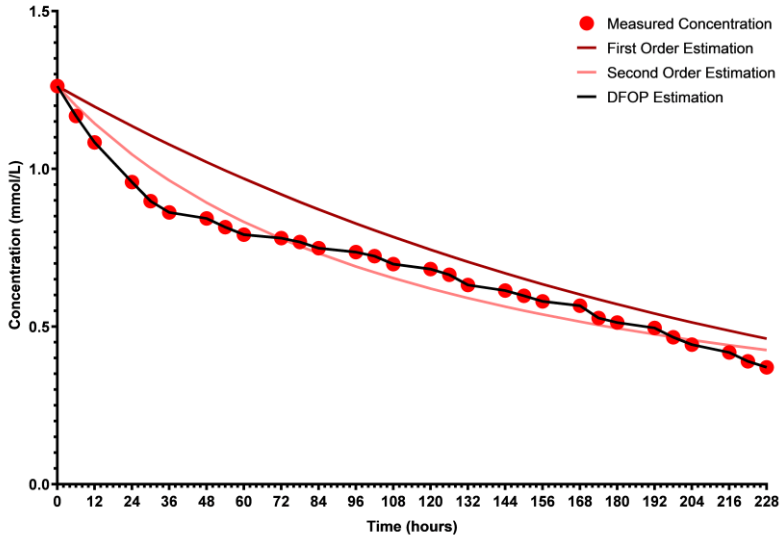

Run B at 0.5 L/min

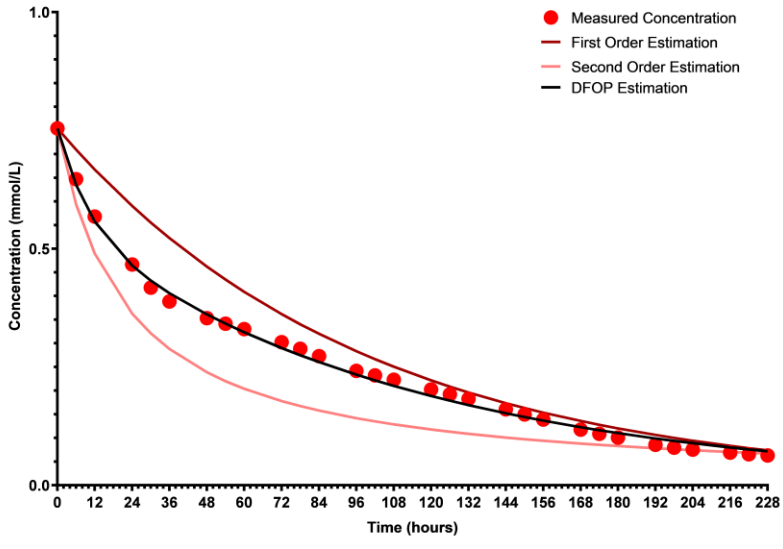

Run C at 0.5 L/min

Figure 7.21: Comparing DFOP kinetic model to simple first order and second order kinetic models for ammonia degradation at 0.5 L/min

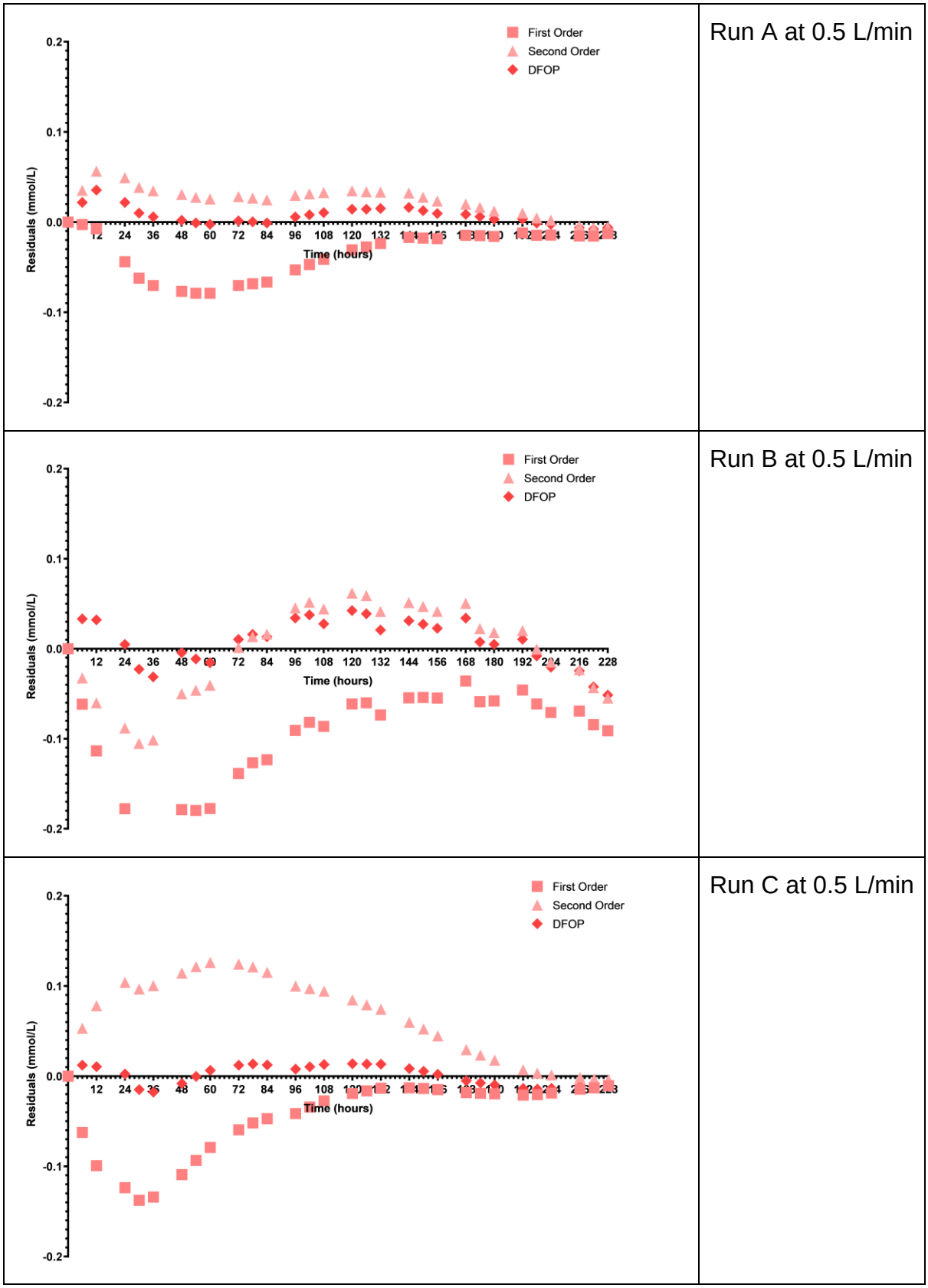

Figure 7.22: Comparing residuals from DFOP kinetic model with residuals from simple first order and second order kinetics models for ammonia degradation at 0.5 L/min

Figure 7.21 shows that the DFOP kinetic model provides the best estimation for the measured ammonia concentration for Runs A, B and C at 0.5 L/min. Figure 7.22 shows that the residuals for all experimental runs at 0.5 L/min are the smallest for the DFOP kinetic model with the simple first order and second order kinetic models having significantly larger residual values. This suggests that the DFOP kinetic model is the most suitable kinetic model for describing ammonia degradation at 0.5 L/min. This does not agree with findings from studies by Wang *et al.* (2017) and Gajewska *et al.* (2020) where ammonia degradation was described as first-order.

Figure 7.23 shows the estimation for orthophosphate concentration provided by the DFOP kinetic model compared to that of the simple first order and second order kinetic models for the nutrient degradation studies at 0.5 L/min. Figure 7.24 shows the residuals for the DFOP kinetic model, simple first order and second order kinetic models for Run A, Run B and Run C at 0.5 L/min.

From Figure 7.23 the DFOP kinetic model provides the most accurate estimation of orthophosphate concentration for all experimental runs at 0.5 L/min as opposed to that of the simple first order kinetic models. This is further affirmed in Figure 7.24 where the residuals for the simple first order kinetic model and second order kinetic model are significantly greater than the residuals for the DFOP kinetic model. This suggests that the DFOP kinetic model is the most suitable kinetic model for describing orthophosphate removal at 0.5 L/min. This is at odds with the adsorption study of orthophosphate onto uncolonized stones presented in Appendix E and suggests that the biological activity in the system influences or inhibits orthophosphate removal. It is possible that orthophosphate removal is hindered by biofilm or aided biologically.

While it is possible to use the DFOP kinetic model to describe both ammonia degradation and orthophosphate removal at 0.5 L/min, it is not possible to describe ammonia degradation or orthophosphate removal in the system with a fixed k_1, k_2 or g value. This is due to the large standard deviation in the fraction of degradation occurring under rate constant k_1 (g) which is 8.32% for ammonia degradation and 36.1% for orthophosphate removal.

Rate constants are dependent on temperature and are also affected by unsteady residence times (differing mixing patterns) in a system (Levenspiel, 1999). Figure F1 and F2 in Appendix F show that the temperature in the pilot biofilter remained consistent over the course of the nutrient degradation studies. The results from the pulse tracer studies (Section 5.4) showed that the system performed at a hydraulic efficiency of 96.3% at a flowrate of 0.5 L/min. The differing k_1 and k_2 values for both ammonia degradation and orthophosphate removal therefore cannot be attributed to differing temperatures or unsteady residence times in the system.

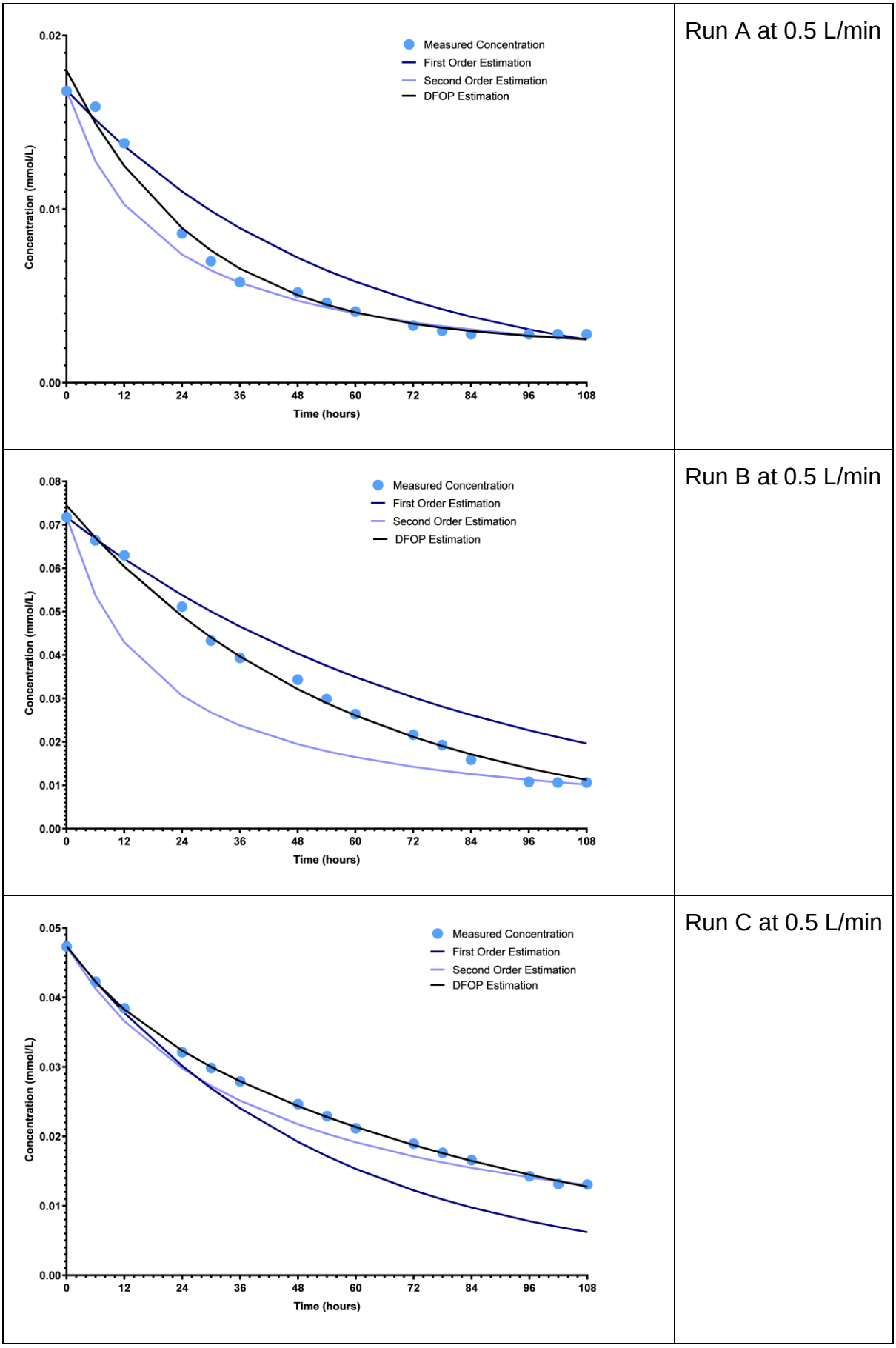

Figure 7.23: Comparing DFOP kinetic model to simple first order and second order kinetics models for orthophosphate removal at 0.5 L/min

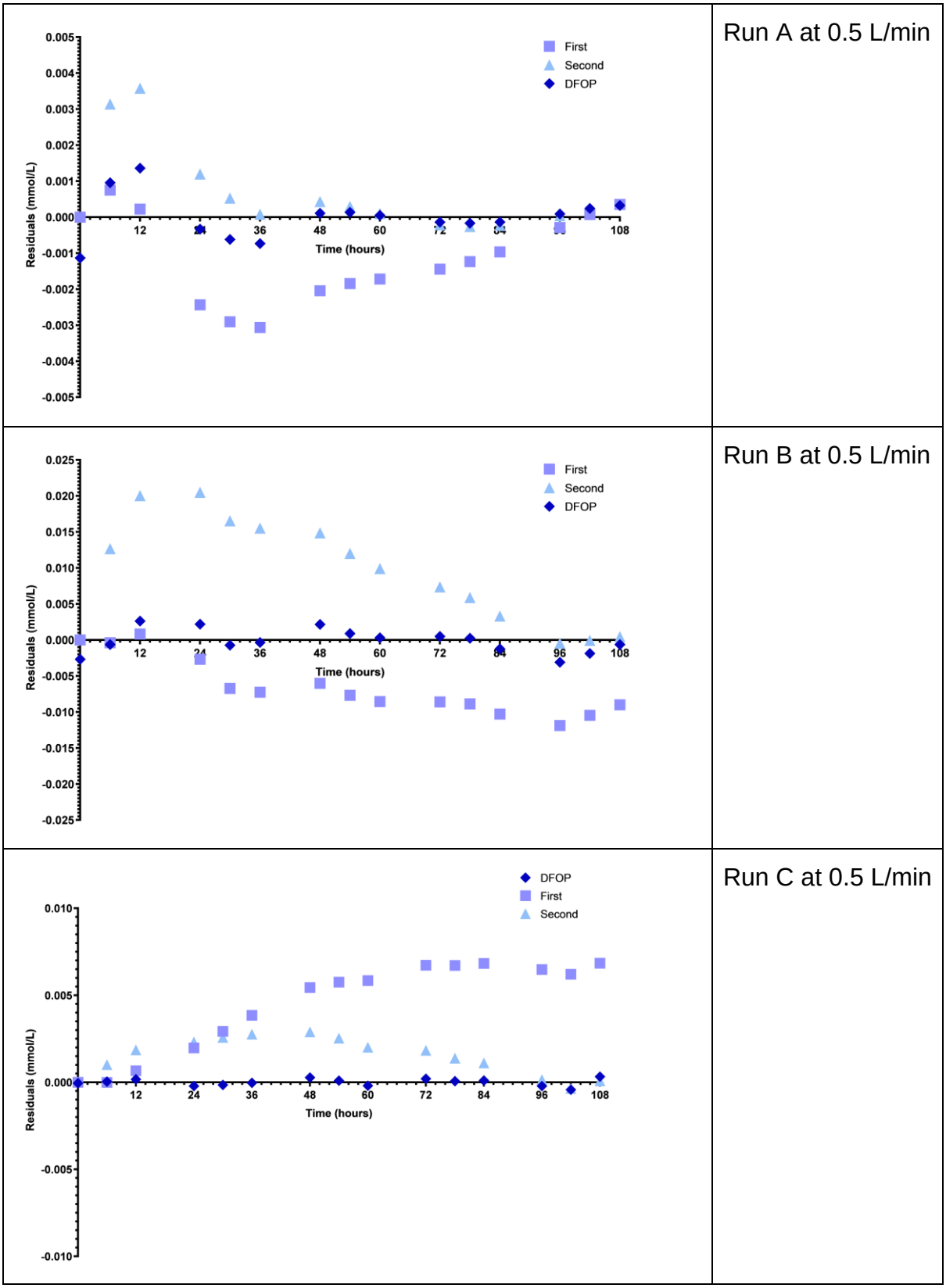

Figure 7.24: Comparing residuals from DFOP kinetic model with residuals from simple first order and second order kinetics models for orthophosphate removal at 0.5 L/min

It is possible that the amount of organic carbon available in the water (no additional organic carbon was added to the system) influenced the point of transition in the rate equation (from k_1 to k_2) for ammonia degradation at 0.5 L/min. The limitation in the amount of carbon available (either due to low concentrations in the influent contaminated water or through depletion throughout the course of the experiment) as an energy source for the microorganisms in the system could affect the rate of reaction, and hence rate constants.

7.5.3. Estimating ammonia and orthophosphate concentrations using Double First-Order in Parallel kinetic model for nutrient degradation studies at 1.5 L/min

The procedure described in Section 7.5.2 was repeated for all nutrient degradation studies at 1.5 L/min. Table 7.6 shows the kinetic data for the DFOP model as determined using the CAKE software. The kinetic data in Table 7.6 was used in Equation 7.3 to provide estimates of the ammonia and orthophosphate concentrations for Run A, Run B and Run C at 1.5 L/min.

Table 7.6: Kinetic data for the DFOP model for ammonia degradation and orthophosphate removal at 1.5 L/min

	Ammonia Degradation			**Orthophosphate Removal**		
	k_1 (h^{-1})	**k_2 (h^{-1})**	**g**	**k_1 (h^{-1})**	**k_2 (h^{-1})**	**g**
Run A	0.0279	0.00970	0.291	0.0273	6.97E-15	0.969
Run B	0.0701	0.00453	0.377	0.0812	0.00892	0.255
Run C	0.0691	0.00253	0.194	0.0199	1.29E-04	0.500

Figure 7.25 shows the estimation for ammonia concentration provided by the DFOP kinetic model compared to that of the simple first order and second order kinetic models for the nutrient degradation studies at 1.5 L/min. Figure 7.26 shows the residuals for the DFOP, simple first order and second order kinetic models.

Figure 7.25 shows that the DFOP kinetic model provides the best estimation for the measured ammonia concentration for Runs A, B and C at 1.5 L/min. Figure 7.26 shows that the residuals for all experimental runs at 1.5 L/min are the smallest for the DFOP kinetic model with the simple first order and second order kinetic models having significantly larger residual values. This suggests that the DFOP kinetic model is the most suitable kinetic model for describing ammonia degradation at 1.5 L/min.

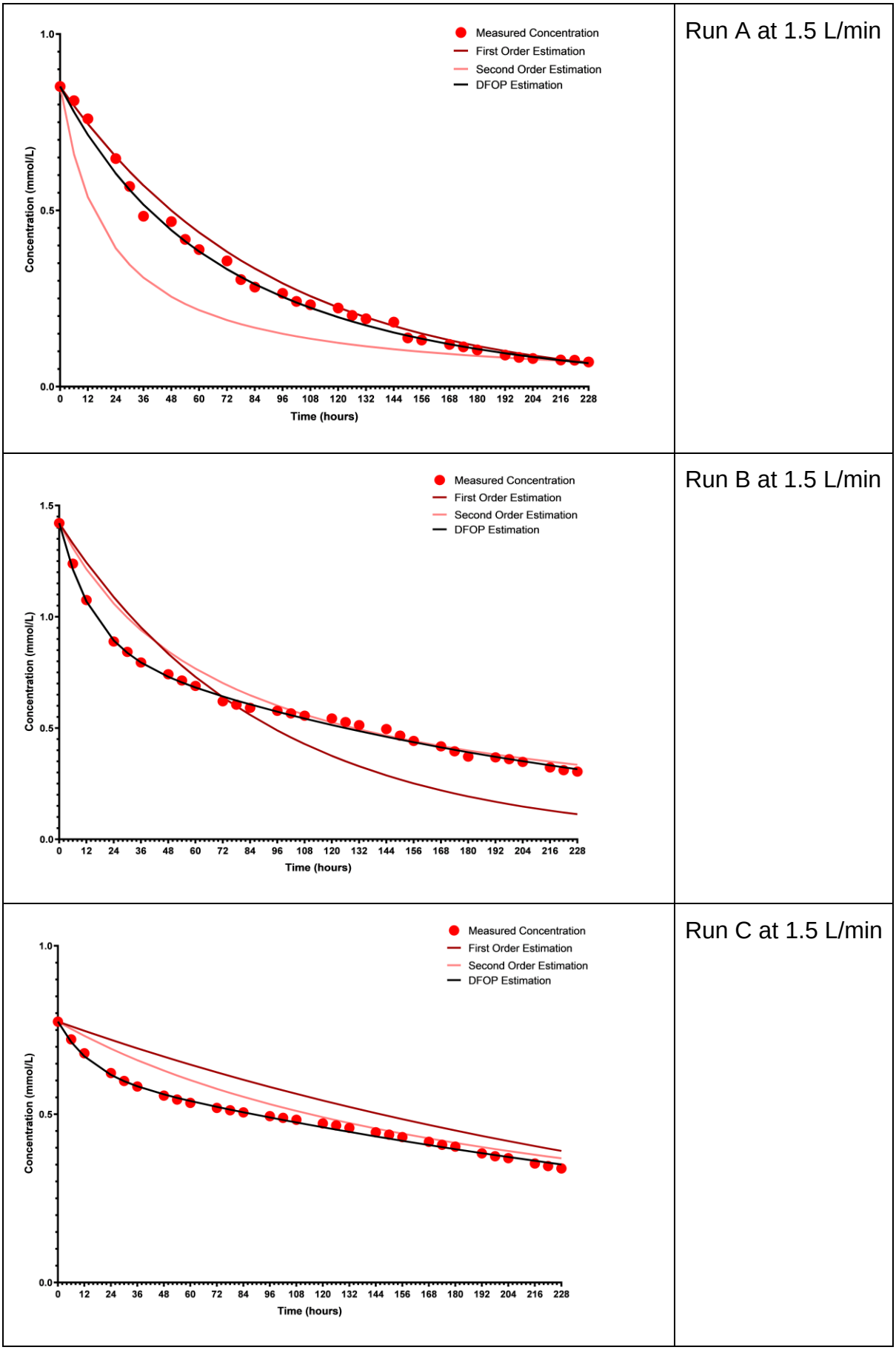

Figure 7.25: Comparing DFOP kinetic model to simple first order and second order kinetics models for ammonia degradation at 1.5 L/min

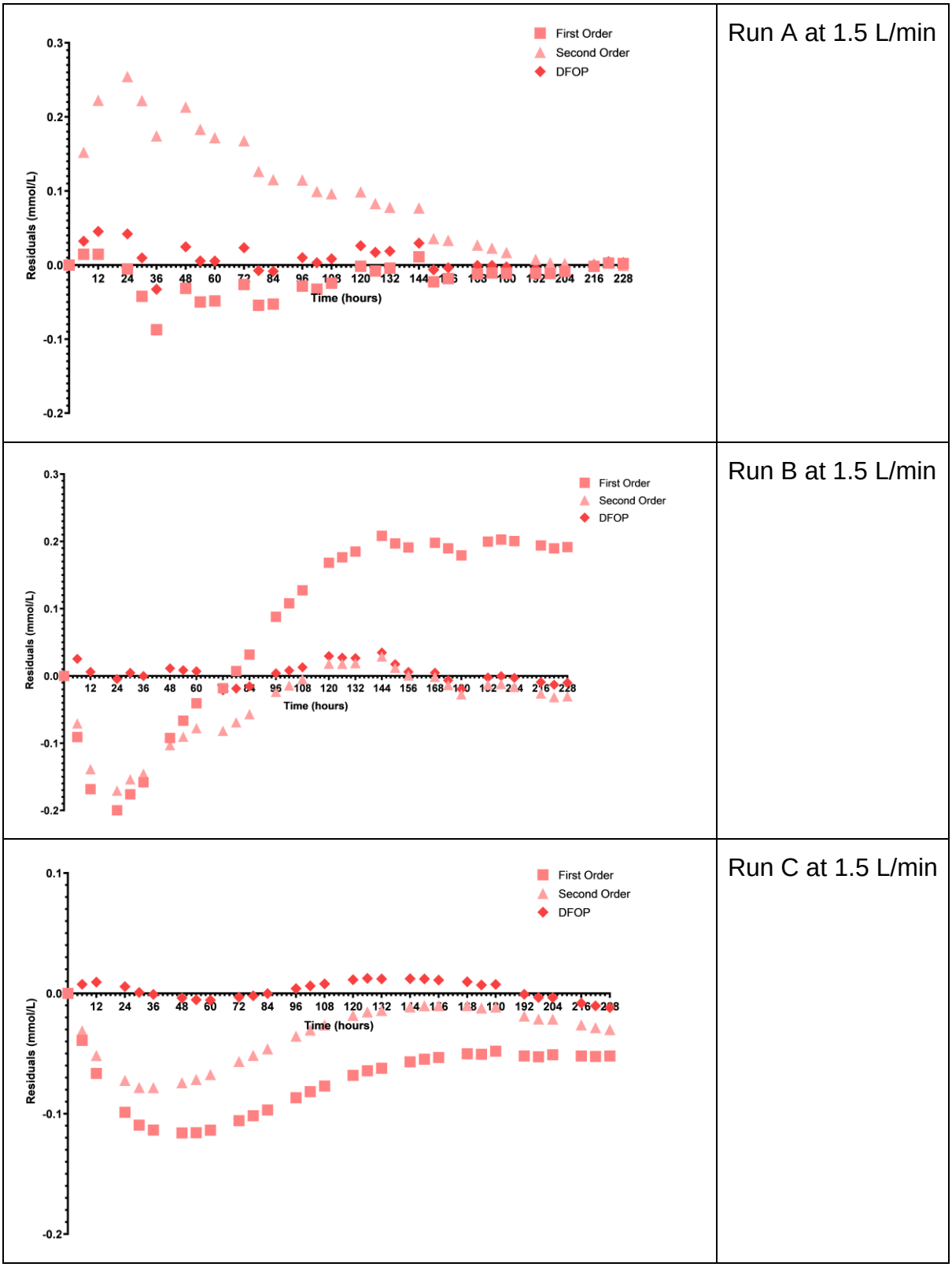

Figure 7.26: Comparing residuals from DFOP kinetic model with residuals from simple first order and second order kinetics models for ammonia degradation at 1.5 L/min

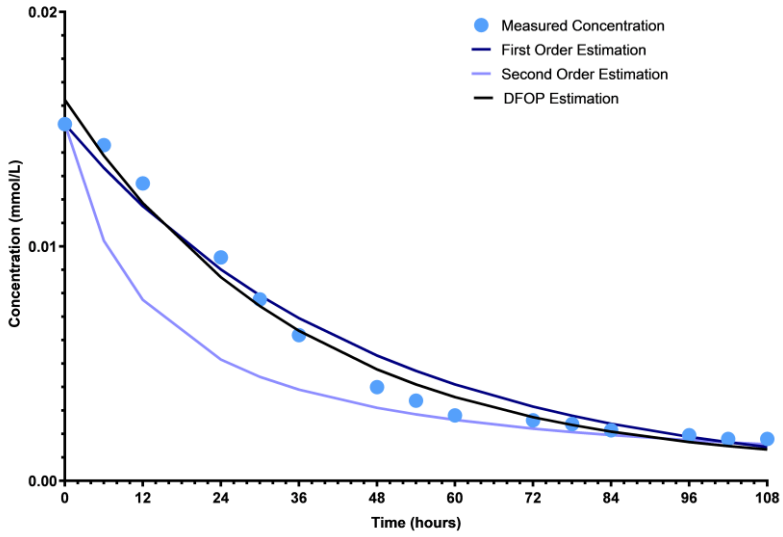

Run A at 1.5 L/min

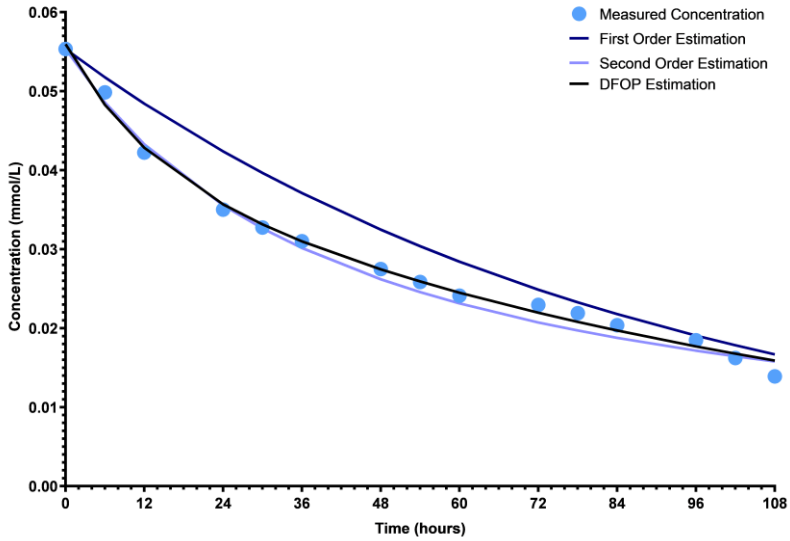

Run B at 1.5 L/min

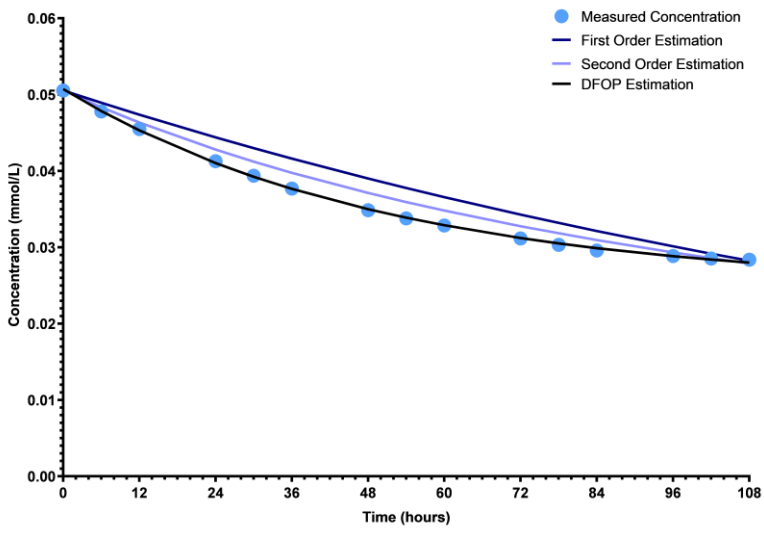

Run C at 1.5 L/min

Figure 7.27: Comparing DFOP kinetic model to simple first order and second order kinetics models for orthophosphate removal at 1.5 L/min

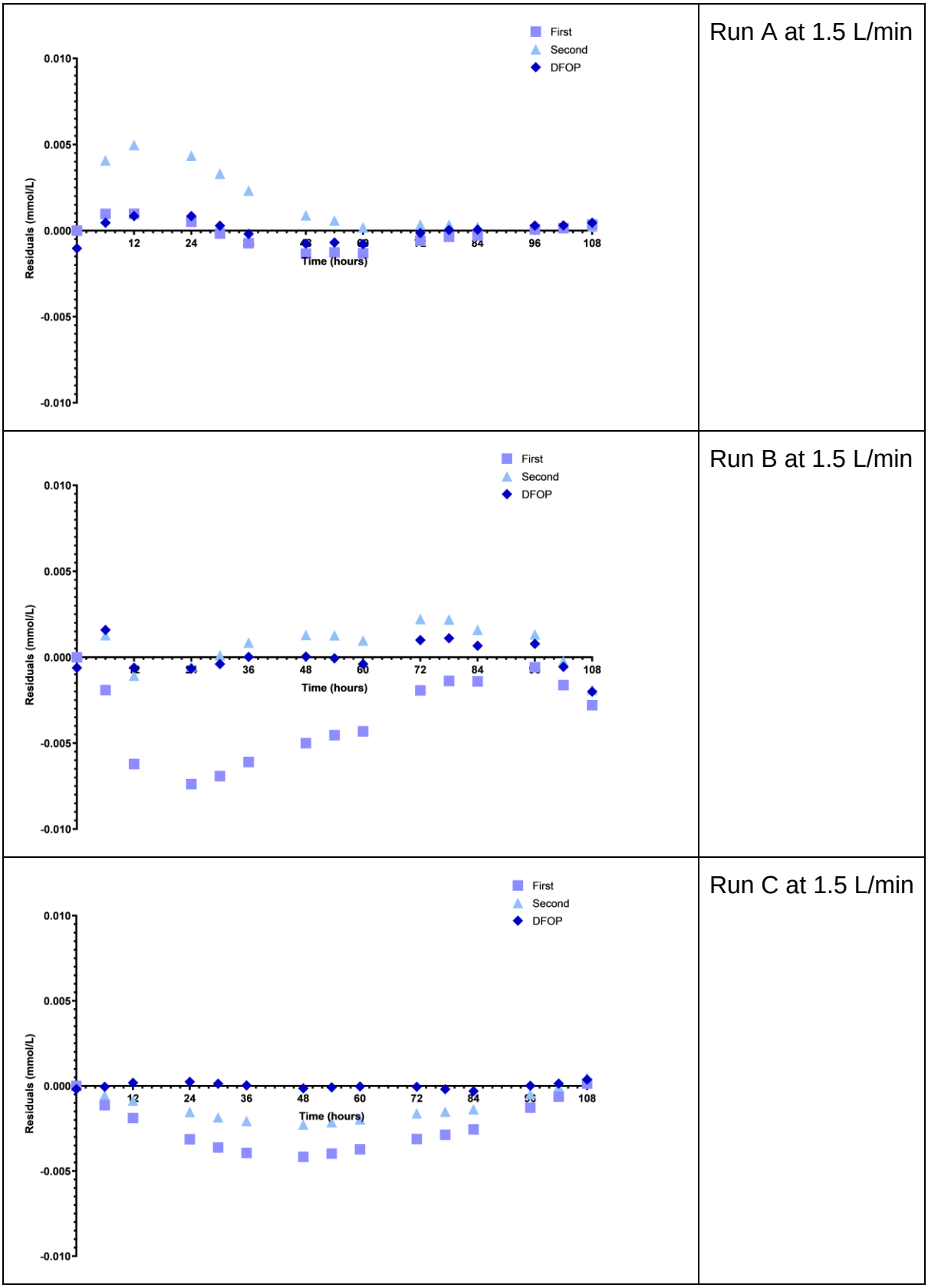

Figure 7.28: Comparing residuals from DFOP kinetic model with residuals from simple first order and second order kinetics models for orthophosphate removal at 1.5 L/min

Figure 7.27 shows the estimation for orthophosphate concentration provided by the DFOP kinetic model compared to that of the simple first order and second order kinetic models for the nutrient degradation studies at 1.5 L/min. Figure 7.28 shows the residuals for the DFOP kinetic model, simple first order and second order kinetic models for Run A, Run B and Run C at 1.5 L/min.

From Figure 7.27 it can be seen that the DFOP kinetic model provides the most accurate estimation of orthophosphate concentration for all experimental runs at 1.5 L/min as opposed to that of the simple first order kinetic models. Figure 7.28 shows that the residuals for the simple first order kinetic model and second order kinetic model are larger than the residuals for the DFOP kinetic model. This suggests that the DFOP kinetic model is the most suitable kinetic model for describing orthophosphate removal at 1.5 L/min. This is again at odds with the adsorption study of orthophosphate onto uncolonized stones presented in Appendix E.

While it is possible to use the DFOP kinetic model to describe both ammonia degradation and orthophosphate removal at 1.5 L/min, it is not possible to describe ammonia degradation or orthophosphate removal in the system with a fixed k_1, k_2 or g value. This is due to the large standard deviation in the fraction of degradation occurring under rate constant k_1 (g) which is 7.48% for ammonia degradation and 29.6% for orthophosphate removal.

The results from the pulse tracer studies (Section 5.4) showed that the system performed at a hydraulic efficiency of 89.8% at a flowrate of 0.5 L/min. The differing k_1 and k_2 values for both ammonia degradation and orthophosphate removal therefore cannot be attributed to unsteady residence times in the system. It is again possible that a limitation in organic carbon affected the rate of ammonia degradation with the rate of degradation being initially higher due to a greater availability of organic carbon at the beginning of the nutrient degradation studies at 1.5 L/min.

7.6. Conclusions

The main challenge associated with the remediation of polluted runoff from informal settlements, such as the runoff from Langrug informal settlement into the Stiebeuel River with the latter used as the contaminated water source in the nutrient degradation studies, are the highly variable nutrient concentrations which may impede consistent nutrient degradation and removal in poorly designed biofiltration systems. The inlet nutrient concentration ranges for the six nutrient degradation studies conducted over a summer season were 8.41- 24.2 mg/L for ammonia, 1.06 - 2.30 mg/L for nitrate, 0.011 - 0.224 mg/L for nitrite, and 1.45 – 6.82 mg/L orthophosphate.

Despite the variable inlet concentrations, the pilot biofilter performed consistently with an ammonia reduction of at least 70.6%, a nitrogen removal of at least 60.9% and an

orthophosphate reduction of at least 74.7% (Run C at 1.5 L/min is not considered as it is an outlier). The greatest total nitrogen reduction of 82.4% was seen at Run A at 1.5 L/min. The total nitrogen reduction achieved is comparable to a study by You *et al.* (2019) where the total nitrogen reduction achieved was 70.1% and higher than a study by Zhang *et al*. (2019) where the total nitrogen reduction achieved was 63.4%. The orthophosphate reduction achieved can be compared to a study done by Merino-Solís *et al.* (2015) where the phosphate reduction achieved was 71.3%.

It was observed that increased initial ammonia concentrations resulted in greater amounts of ammonia degraded in the system. This was also the case for total nitrogen, where there was a strong positive relationship between the total nitrogen added to the system and the total nitrogen degraded in the system.

The biological nitrification and denitrification processes in the system were consistent with an extent of nitrification of at least 70.8% being observed. The denitrification in the system was more efficient with an extent of denitrification of at least 86.7% being observed. Operational flow rate does not have a significant impact on the extent of nitrification and denitrification achieved or on orthophosphate removal achieved. It is noted that, in this batch system, the operational flow rate only influences circulation rate and frequency of re-oxygenation. The operational flow rate also influences the fraction of the bed that is active and the depth of fluid penetration into the bed with lower flow rates favouring greater penetration (as concluded in Section 5.5).

The kinetic model used to describe ammonia degradation at an experimental flow rate of 0.5 L/min and 1.5 L/min is double first-order in parallel with differing rate constants, k_1 and k_2. The double first-order in parallel kinetic model can also be used to describe orthophosphate removal in the pilot biofilter system at experimental flow rates of 0.5 L/min and 1.5 L/min. The large difference in rate constants for ammonia degradation is possibly due to limited organic carbon availability as an energy source for the microorganisms in the system. BOD and COD readings were not taken due to the large number of samples. In future it is recommended that one COD analysis is done every twelve hours to determine the availability of organics.

The treated water from Run A at 0.5 L/min, Run C at 0.5 L/min and Run A 1.5 L/min was classified as suitable for domestic use as per the South African Water Quality Guidelines (Department of Water Affairs and Forestry, 1996). The pilot biofilter's ability to consistently achieve at least 70.8% nitrification and 86.7% denitrification show that the system is able to achieve consistent biological degradation despite highly variable inlet concentrations. The pilot biofilter's performance is even more impressive when considering the fact that this system is a representative $\frac{1}{8}$ "slice" of the stone biofilters at the Water Hub.

8. CONCLUSIONS AND RECOMMENDATIONS

8.1. Conclusions

The aim of this project was to determine the hydraulic characteristics of the pilot-scale biofilter designed for the purpose of remediation of contaminated runoff from an informal settlement, Langrug, and to assess the extent of nutrient degradation that can be achieved by the pilot biofilter, thereby informing the design specifications required for the full-scale filter. As the system was designed to treat polluted runoff from informal settlements, it was also imperative to understand the water quality of the Stiebeuel River which was the source of contaminated water for this project as well as to assess the quality of the water generated i.e., fit-for-purpose for use or at domestic quality or a quality fit for discharge to a river. These aims have been addressed in three sections: Chapter 4 which focused on the water quality of the Stiebeuel River, Chapter 5 which dealt with the design and hydraulic characterisation of the pilot biofilter, and Chapter 7 which focused on the nutrient degradation achieved by the pilot-scale biofilter.

The following key research questions were posed at the end of Chapter 2 and are addressed in this chapter:

a) What nutrient concentrations are observed in the Stiebeuel River over the twelve-month sampling period? Is there a trend observed in the nutrient concentrations over the twelve-month sampling period i.e., season dependent?
b) What mixing pattern best describes the fluid flow behaviour in the pilot biofilter?
c) Does flow rate influence the hydraulic characteristics of the pilot biofilter?
d) What is the extent of non-ideal fluid flow behaviour in the pilot biofilter?
e) What implications do the nutrient concentrations observed in the Stiebeuel River have on the pilot biofilter performance?
f) What biological and physical processes are occurring within the pilot biofilter?
g) Can the nutrient degradation in the pilot biofilter be described by a reaction kinetic model (such as zero order, first order, second order or complex kinetic model)?

The nutrient concentrations in the Stiebeuel River were found to exceed acceptable discharge concentrations into the river system and to be highly variable, however, a general trend was observed over the twelve-month sampling period. Total nitrogen and orthophosphate concentrations are generally higher in periods of low rainfall with lower concentrations observed during periods of high rainfall. Further the higher occupancy of Langrug during the low rainfall summer periods are also aligned with the periods of higher nutrient concentration. The spread of data for the summer (low rainfall) period was found to be smaller than that of the winter (high rainfall) period.

The range of nutrient concentrations in the Stiebeuel River observed throughout the twelve month sampling period were 6.40 - 35.4 mg/L ammonia, 0.415 – 3.42 mg/L nitrate and 0.510 – 5.71 mg/L orthophosphate. The total nitrogen concentration in the Stiebeuel River consists of upwards of 93.8% ammonia with nitrate being the second highest contributor to total nitrogen concentration while nitrite is the lowest contributor to total nitrogen concentration in the Stiebeuel River.

The mean residual nutrient concentrations as measured at the outlet of the large stone biofilters at the Water Hub were 1.47 mg/L ammonia, 0.630 mg/L nitrate and 0.660 mg/L orthophosphate. The mean residual nutrient concentrations as measured at the outlet of the small stone biofilters at the Water Hub were 1.83 mg/L ammonia, 0.410 mg/L nitrate and 0.400 mg/L orthophosphate. The residual nutrient concentrations in the treated water are below the limit for domestic use meaning that the resultant treated water from the non-vegetated stone biofilters at the Water Hub meet the South African water quality requirements for domestic use. The treated effluent also meets the South African discharge standards as the nitrate concentrations are below 15 mg/L and residual ammonia concentrations are below 6 mg/L (Department of Water Affairs and Forestry, 1996). This shows that the stone biofilters at the Water Hub are able to achieve significant ammonia, nitrate and orthophosphate reductions despite the variable inlet nutrient concentrations. Studies on biofilter performance and investigations into the physical and biological processes occurring within the biofilters could not be carried out on the large Water Hub biofilters due to the size of the biofilters making controlled experimentation difficult and insufficient sampling capacity being installed.

To improve our understanding of the biofilter application to contaminated runoff from the Stiebeuel River, a pilot-scale biofilter was constructed based on the design of the biofilters at the Water Hub and used to conduct controlled laboratory studies. These laboratory studies were designed to facilitate in developing an understanding of the hydraulic characteristics and nutrient degradation processes occurring within the horizontal subsurface flow biofilters at the Water Hub. The pilot biofilter was designed to represent a “slice” of the stone biofilters at Water Hub with the width and length of the Water Hub biofilters (3.5 m and 16 m, respectively) being scaled down by a factor of 8 and the depth remaining the same (0.7 m). The pilot biofilter was 2 m long, 0.44 m wide and 0.7 m deep and packed with small river stones 8 – 11 mm in diameter (depth of packing was 0.65 m). The bed voidage was 0.42 and the volume available for liquid in the pilot biofilter was 225 L.

Pulse tracer studies were conducted at flow rates of 3 L/min, 2 L/min, 1.5 L/min, 1 L/min, 0.75 L/min and 0.5 L/min to determine the mixing patterns in the pilot biofilter. The pulse tracer studies at all six flow rates showed that the pilot biofilter system

approximates plug flow behaviour. The extent of plug flow behaviour and degree of mixing in the radial direction increases with a decrease in flow rate with the pulse tracer study at 0.5 L/min exhibiting the greatest extent of plug flow behaviour. This agrees with the literature stating that adequately designed horizontal subsurface flow biofilters should display the characteristics of plug flow dispersion reactors (Narayanan and Narayan, 2019).

The effective volume utilisation and hydraulic efficiency are greatest at a flow rate of 0.5 L/min. The effective volume utilisation at 0.5 L/min is 96.4% while the hydraulic efficiency at 0.5 L/min is 96.3%. The greatest extent of non-ideal fluid flow behaviour occurs at flow rates of 3 L/min and 1.5 L/min with a dead zone of 9.2% and 9.3%, respectively. It was found that the fluid flow rate also influences the fraction of the bed that is active and the depth of fluid penetration into the bed with lower flow rates favouring greater penetration. The greatest depth penetration occurred at a flow rate of 0.5 L/min which aligns with the effective volume utilisation and hydraulic efficiency being greatest at this flow rate.

A biological acclimation period of 35 days as suggested by Nemani et al. (2018) was found to be adequate. The planktonic cell count in the pilot biofilter increased from 0.4 million cells/ml at 5 days after inoculation to 21.7 million cells/ml at 35 days after inoculation. Consistent nutrient (ammonia, nitrate and orthophosphate) removal was achieved in the system during the repeated nutrient replenishment cycles. This confirms that the pilot biofilter was microbially colonised following inoculation.

The highly variable nutrient concentrations in the Stiebeuel River have implications on the potential extent of nutrient degradation achieved in the pilot biofilter. The microbial community in pilot biofilter system must be able to metabolise large pulses of nutrients when fresh contaminated water is introduced to the system at varying inlet concentrations. The microbial community must also be able to survive periods of low nutrient availability such as when the inlet nutrient concentrations are low (for example, during the winter months).

The nutrient degradation studies conducted in batch at recirculation flow rates of 0.5 L/min and 1.5 L/min over 228 hours provided an insight into the ability of the pilot biofilter to reduce nutrient concentrations in contaminated runoff from an informal settlement. Despite the variable inlet nutrient concentrations, the pilot biofilter performed consistently with an ammonia reduction of at least 70.6% and an orthophosphate reduction of at least 74.7% The greatest ammonia and orthophosphate removal of 91.8% and 88.3%, respectively was seen at Run A at 1.5 L/min. Run A at 1.5 L/min also provided the greatest total nitrogen removal of 82.4%.

The main biological processes occurring within the pilot biofilter were nitrification and denitrification. An extent of nitrification of at least 70.8% and extent of denitrification of at least 86.7% was observed. The greatest extent of nitrification was seen in Run C at 0.5 L/min and amounted to 91.7%. The extent of denitrification was also greatest for Run C at 0.5 L/min at 95.6%. The microbial community in the pilot biofilter system were able to metabolise large pulses of nutrients when fresh contaminated water was introduced to the system at varying inlet concentrations. The microbial community was also able to survive under nutrient limited conditions and continue to metabolise nutrients as seen in Run A at 0.5 L/min (inlet nutrient concentrations: 8.41mg/L ammonia, 1.80 mg/L nitrate and 1.60 mg/L orthophosphate) where ammonia and orthophosphate reductions of 85.3% and 83.1% were observed, respectively.

Ammonia degradation and orthophosphate removal could not be accurately described using simple first order and second order kinetic models. It was found that the double first-order in parallel kinetic model best described ammonia degradation and orthophosphate removal for the nutrient degradation studies at flow rates of 0.5 L/min and 1.5 L/min. It is possible that ammonia degradation in the system was limited by the amount of organic carbon available in the system.

It is not clear as to whether the orthophosphate removal can be attributed solely to adsorption onto the surface of the stone filter media. The orthophosphate adsorption study carried out on uncolonised stones showed that orthophosphate degradation is a zero-order reaction. This means that the rate of orthophosphate degradation is not concentration dependent. This is in contrast to the nutrient degradation kinetic studies at 0.5 L/min and 1.5 L/min where the orthophosphate degradation was found to be first order or second order. This could be due to the presence of biofilm which could potentially hinder the adsorption of orthophosphate onto the surface of the filter media or assimilate phosphate or both. A study by Zhao et al. (2018) found that the orthophosphate adsorption onto sediment particles was inhibited due to the presence of a robust biofilm. Bunce et al. (2018) argue that a lack of phosphorus-accumulating organisms in a system can lead to limited phosphorus uptake by a system.

The residual ammonia, nitrate and orthophosphate concentrations from the nutrient degradation studies showed that the treated water from Run A at 0.5 L/min, Run Cat 0.5 L/min and Run A at 1.5 L/min was suitable for domestic use and discharge (based on nutrient concentration limits only). The major contaminant to exceed the water quality limitations for domestic use was ammonia (ammonia concentration exceeded limit for domestic use in Run B at 0.5 L/min, Run B at 1.5 L/ min and Run C at 1.5 L/min).

The lab studies on the pilot biofilter system were valuable due to the opportunity the controlled laboratory environment afforded with regards to determining the hydraulic

characteristics of a stone biofilter, modelling reaction kinetics and determining extent of nitrification and denitrification. The findings from this study can be used to improve the design of the large scale Water Hub biofilters as well as to design new horizontally orientated subsurface flow biofilters that are able to produce treated water that is fit-for-purpose or fit for discharge into rivers.

8.2. Recommendations for Further Research

The findings from this project showed that an engineered horizontally orientated subsurface flow biofilter is suitable for treating contaminated runoff from informal settlements. However, further research is required in order to develop a deeper understanding of the pilot biofilter system. The premise of this study was to assess the performance of a non-vegetated stone biofilter where runoff from an informal settlement is the contaminated water source thus, studying the biofilter's potential to handle highly variable water quality at the inlet. While some valuable findings were made; it was difficult to assess the pilot biofilter's performance due to a lack of baseline data on how the biofilter should be performing.

It would therefore be advantageous to conduct the nutrient degradation studies using artificial wastewater of uniform compositions, followed by the nutrient degradation studies using water from the Stiebeuel River. This would be valuable as it would provide baseline data on how the biofilter performs under uniform inlet conditions. This could then be compared to the nutrient degradation studies using water from the Stiebeuel River with the baseline data being used to assess how well the biofilter performs under variable inlet water quality. In future it is recommended that one COD analysis is done every twelve hours to determine the availability of organic carbon..

Further improvements to the design of the pilot biofilter should be explored, specifically the manner in which the feed is introduced into the biofilter. In future studies, the feed to the pilot biofilter can be introduced at various depths to ensure complete use of the bed depth. An effort should be made in future studies to create distinct aerobic and anaerobic zones within the pilot biofilter system to understand how these conditions affect nitrification and denitrification.

An analysis of the microbial consortia, focusing on both the diversity of species present as well as the function of each species, would provide further context to the pilot biofilter's performance. It would be especially valuable to perform an analysis of the microbial consortia at various depths and lengths along the pilot biofilter to determine whether specific microbial species are located within certain zones of the pilot biofilter i.e., whether zoning occurs naturally in the biofilter to match microbial consortium to function and ideal conditions. This can provide insights into the type of microbial activity occurring within each section of the pilot biofilter.

Biofilm and stone media samples from the pilot biofilter should be analysed to determine whether orthophosphate is predominantly adsorbed onto the surface of the stone media or onto the biofilm itself. Further, studies on orthophosphate uptake on virgin media and biologically active media should be carried out using standard solutions of orthophosphate. This will assist in determining the effect of the biofilm and planktonic species present in the system on orthophosphate removal in the system.

The nutrient degradation studies in this project were batch experiments with a complete recycle and no purge stream. This was due to a limited water transport and storage capacity. The complete recycle with lack of a purge means that the planktonic cells remained in the system and were not washed out, resulting in enhanced nutrient reduction.

In future, nutrient degradation studies should be carried out as open continuous flow studies on a system where multiple pilot-scale biofilters are linked together, forming a treatment train. This will maintain the plug flow fluid behaviour in the system and will also zones to develop with tailored microbial consortia. The results from such nutrient degradation studies will allow for validation and refinement of the batch data and further assist in improving the design of the large scale biofilters.

REFERENCES

Atabaki, M., Siong, Y. K. and Idris, J. (2013) Performance of activated carbon in water filters, *Water Resources*, 40(1), pp. 31–53.

Barnes, J. M. (2003) *The Impact of Water Pollution from Formal and Informal Urban Developments Along the Plankenbrug River on Water Quality and Health Risk (PhD Thesis)*. Division of Community Health, Stellenbosch University.

Benjamin, M. and Lawler, D. (2013) *Water Quality Engineering*, *Water Quality Engineering*. John Wiley & Sons.

Bonner, R., Aylward, L., Kappelmeyer, U. and Sheridan, C. (2017) A comparison of three different residence time distribution modelling methodologies for horizontal subsurface flow constructed wetlands, *Ecological Engineering*, 99, pp. 99–113. doi: http://dx.doi.org/10.1016/j.ecoleng.2016.11.024.

Bonner, R., Aylward, L., Harley, C., Kappelmeyer, U. and Sheridan, C. M. (2017) Heat as a hydraulic tracer for horizontal subsurface flow constructed wetlands, *Journal of Water Process Engineering*, 16, pp. 183–192. doi: http://dx.doi.org/10.1016/j.jwpe.2017.01.007.

Bratieres, K., Fletcher, T. D., Deletic, A. and Zinger, Y. (2008) Nutrient and sediment removal by stormwater biofilters: A large-scale design optimisation study, *Water Research*, 42(14), pp. 3930–3940. doi: 10.1016/j.watres.2008.06.009.

Bunce, J. T., Ndam, E., Ofiteru, I. D., Moore, A. and Graham, D. W. (2018) A review of phosphorus removal technologies and their applicability to small-scale domestic wastewater treatment systems, *Frontiers in Environmental Science*. Frontiers Media S.A. doi: 10.3389/fenvs.2018.00008.

Cheng, Q., Nengzi, L., Bao, L., Huang, Y., Liu, S., Cheng, X., Li, B. and Zhang, J. (2017) Distribution and genetic diversity of microbial populations in the pilot-scale biofilter for simultaneous removal of ammonia, iron and manganese from real groundwater, *Chemosphere*, 182, pp. 450–457. doi: http://dx.doi.org/10.1016/j.chemosphere.2017.05.075.

Cohen, Y. (2001) Biofiltration: the treatment of fluids by microorganisms immobilized into the filter bedding material: a review, *Bioresource Technology*, pp. 257–274.

Community Organisation Resource Centre (2011) *Langrug Settlement Enumeration Report*. Stellenbosch University. Available at: http://sasdialliance.org.za/wp-content/uploads/docs/reports/Enumerations/Langrug_Enumeration_Report.pdf (Accessed: January 2020).

Department of Water Affairs and Forestry (1996) *South African Water Quality Guidelines*. Second. Edited by S. Holmes. CSIR Environmental Services.

di Tommaso, C., Taylor-Edmonds, L., Andrews, S. A. and Andrews, R. C. (2019) The contribution of biofilm to nitrogenous disinfection by-product formation in full-scale cyclically-operated drinking water biofilters, *Water Research*, 155, pp. 403–409. doi: https://doi.org/10.1016/j.watres.2019.02.025.

Dittrich, E., Klincsik, M., Somfai, D., Dolgos-Kovács, A., Kiss, T. and Szekeres, A. (2021) Analysis of conservative tracer measurement results inside a planted horizontal subsurface flow constructed wetland filled with coarse gravel using Frechet distribution, *Environmental Science and Pollution Research*, 28, pp. 5180–5240. doi: 10.1007/s11356-020-10246-9/Published.

Fell, J. (2017) *An analysis of surface water from an informal settlement, Langrug, Franschhoek: down a slippery slope (MSc Dissertation)*. Department of Environmental and Geographical Science, University of Cape Town.

Fishman, M. J., Skougstad, M. W. and Scarbro, G. F. (1964) Diazotization Method for Nitrate and Nitrite, *American Water Works Association*, 56(5), pp. 633–638. doi: 10.1002/j.1551-8833.1964.tb01253.x.

Fogler, H. S. (2011) *Essentials of Chemical Reaction Engineering*. International. Pearson Education.

Fu, J., Lee, W. N., Coleman, C., Meyer, M., Carter, J., Nowack, K. and Huang, C. H. (2017) Pilot investigation of two-stage biofiltration for removal of natural organic matter in drinking water treatment, *Chemosphere*, 166, pp. 311–322. doi: http://dx.doi.org/10.1016/j.chemosphere.2016.09.101.

Gajewska, M., Skrzypiec, K., Jóźwiakowski, K., Mucha, Z., Wójcik, W., Karczmarczyk, A. and Bugajski, P. (2020) Kinetics of pollutants removal in vertical and horizontal flow constructed wetlands in temperate climate, *Science of the Total Environment*, 718, pp. 32–40. doi: 10.1016/j.scitotenv.2020.137371.

Gangoo, A. (2003) *Informal Communities and their Influence on Water Quality: The Case of Umlazi (MA Dissertation)*. University of Kwa-Zulu Natal.

Greenstein, K. E., Lew, J., Dickenson, E. R. V. and Wert, E. C. (2018) Investigation of biotransformation, sorption, and desorption of multiple chemical contaminants in pilot-scale drinking water biofilters, *Chemosphere*, 200, pp. 248–256.

HACH Company (2008) *HACH Water Analysis Handbook*. Seventh Edition.

Hauer, F. and Lamberti, G. (2017) *Methods in Stream Ecology*. Third. Edited by F. R. Hauer and G. A. Lamberti. Academic Press.

Housing Development Agency (2012) *South Africa: Informal Settlements Status*.

Ilyas, H. and Masih, I. (2017) The performance of the intensified constructed wetlands for organic matter and nitrogen removal: A review, *Journal of Environmental Management*, 198, pp. 372–383. doi: http://dx.doi.org/10.1016/j.jenvman.2017.04.098.

Jiang, C., Jia, L., Zhang, B., He, Y. and Kirumba, G. (2014) Comparison of quartz sand, anthracite, shale and biological ceramsite for adsorptive removal of phosphorus from aqueous solution, *Journal of Environmental Sciences (China)*, 26(2), pp. 466–477. doi: 10.1016/S1001-0742(13)60410-6.

Jing, Z., He, R., Hu, Y., Niu, Q., Cao, S. and Li, Y. Y. (2015) Practice of integrated system of biofilter and constructed wetland in highly polluted surface water treatment, *Ecological Engineering*, 75, pp. 462–469. doi: http://dx.doi.org/10.1016/j.ecoleng.2014.12.015.

Jones, M. (1984) Nitrate reduction by shaking with cadmium: Alternative to cadmium columns, *Water Research*, 18(5), pp. 643–646. doi: 10.1016/0043-1354(84)90215-X.

Jones, P. (2017) Formalizing the informal: Understanding the position of informal settlements and slums in sustainable urbanization policies and strategies in Bandung, Indonesia, *Sustainability*, 9, pp. 3–27. doi: 10.3390/su9081436.

LaMorte, W. (2017) *Nonparametric Tests: Wilcoxon Signed Rank Test*, *Boston University School of Public Health*. Available at: https://sphweb.bumc.bu.edu/otlt/mph-modules/bs/bs704_nonparametric/BS704_Nonparametric6.html (Accessed: November 2021).

Lappalainen, H. K., Kerminen, V. M., Petäjä, T. and Kurten, T. (2016) Pan-Eurasian Experiment (PEEX): Towards a holistic understanding of the feedbacks and interactions in the land-Atmosphere-ocean-society continuum in the northern Eurasian region, *Atmospheric Chemistry and Physics*, 16(22), pp. 14421–14461. doi: 10.5194/acp-16-14421-2016.

Lauderdale, C. (2011) *Engineered Biofiltration for Enhanced Hydraulic and Water Treatment Performance (PhD Thesis)*. Department of Environmental Engineering Sciences, University of Florida.

Levenspiel, O. (1999) *Chemical Reaction Engineering*. Third Edition. New York: John Wiley and Sons.

Li, C., Ling, F., Zhang, M., Liu, W. T., Li, Y. and Liu, W. (2017) Characterization of bacterial community dynamics in a full-scale drinking water treatment plant, *Journal of Environmental Sciences (China)*, 51, pp. 21–30. doi: http://dx.doi.org/10.1016/j.jes.2016.05.042.

Li, H., Zhang, Y., Yang, M. and Kamagata, Y. (2013) Effects of hydraulic retention time on nitrification activities and population dynamics of a conventional activated sludge system, *Frontiers of Environmental Science and Engineering in China*, 7(1), pp. 43–48. doi: 10.1007/s11783-012-0397-8.

Li, J., Zheng, B., Chen, X., Li, Z., Xia, Q., Wang, H., Yang, Y., Zhou, Y. and Yang, H. (2021) The use of constructed wetland for mitigating nitrogen and phosphorus from agricultural runoff: A review, *Water,* 13(4), pp. 1–16. doi: https://doi.org/10.3390/w13040476.

Lin, Z., Wang, Y., Huang, W., Wang, J., Chen, L., Zhou, J. and He, Q. (2019) Single-stage denitrifying phosphorus removal biofilter utilizing intracellular carbon source for advanced nutrient removal and phosphorus recovery, *Bioresource Technology*, 277, pp. 27–36. doi: https://doi.org/10.1016/j.biortech.2019.01.025.

Liu, X., Dang, Y., Sun, D. and Holmes, D. E. (2021) Identification of optimal parameters for treatment of high-strength ammonium leachate by mixed communities of heterotrophic nitrifying/aerobic denitrifying bacteria, *Bioresource Technology*, 336. doi: 10.1016/j.biortech.2021.125415.

Lucas, R., Earl, E. R., Babatunde, A. O. and Bockelmann-Evans, B. N. (2015) Constructed wetlands for stormwater management in the UK: a concise review, *Civil Engineering and Environmental Systems*, 32(3), pp. 251–268. doi: https://doi.org/10.1080/10286608.2014.958472.

Manirakiza, B. and Sirotkin, A. C. (2021) Bioaugmentation of nitrifying bacteria in up-flow biological aerated filter's microbial community for wastewater treatment and analysis of its microbial community, *Scientific African*, 14. doi: 10.1016/j.sciaf.2021.e00981.

McKie, M. J., Bertoia, C., Taylor-Edmonds, L., Andrews, S. A. and Andrews, R. C. (2019) Pilot-scale comparison of cyclically and continuously operated drinking water biofilters: Evaluation of biomass, biological activity and treated water quality, *Water Research*, 149, pp. 488–495. doi: https://doi.org/10.1016/j.watres.2018.11.033.

Merino-Solís, M., Villegas, E., de Anda, J. and López-López, A. (2015) The Effect of the Hydraulic Retention Time on the Performance of an Ecological Wastewater Treatment System: An Anaerobic Filter with a Constructed Wetland, *Water*, 7(12), pp. 1149–1163. doi: 10.3390/w7031149.

Moges, M. E., Todt, D., Eregno, F. E. and Heistad, A. (2017) Performance study of biofilter system for on-site greywater treatment at cottages and small households, *Ecological Engineering*, 105, pp. 118–124. doi: http://dx.doi.org/10.1016/j.ecoleng.2017.04.060.

Morgan, G. (2019) *Ideas Towards Water Sensitive Settlements*. Water Research Commission. WRC Report No. 2519/1/19.

Murphy, J. and Riley, J. P. (1962) A modified single solution method for the determination of phosphate in natural waters, *Analytica Chimica Acta*, 27, pp. 31–36. doi: 10.1016/S0003-2670(00)88444-5.

Narayanan, C. M. and Narayan, V. (2019) Biological wastewater treatment and bioreactor design: A review, *Sustainable Environment Research*. BioMed Central Ltd. doi: 10.1186/s42834-019-0036-1.

Nemani, V. A., McKie, M. J., Taylor-Edmonds, L. and Andrews, R. C. (2018) Impact of biofilter operation on microbial community structure and performance, *Journal of Water Process Engineering*, 24, pp. 35–41. doi: https://doi.org/10.1016/j.jwpe.2018.05.009.

Nivala, Jaime., Puigagut, Jaume., von Sperling, Marcos., Dotro, Gabriela., Stein, Otto., Molle, Pascal. and Langergraber, Gunter. (2017) *Treatment Wetlands.* First. IWA Publishing.

Nyenje, P. M., Foppen, J. W., Uhlenbrook, S., Kulabako, R. and Muwanga, A. (2010) Eutrophication and nutrient release in urban areas of sub-Saharan Africa - A review, *Science of the Total Environment*, pp. 447–455. doi: 10.1016/j.scitotenv.2009.10.020.

Oh, S., Hammes, F. and Liu, W. T. (2018) Metagenomic characterization of biofilter microbial communities in a full-scale drinking water treatment plant, *Water Research*, 128, pp. 278–285. doi: https://doi.org/10.1016/j.watres.2017.10.054.

Oral, H. V. *et al.* (2020) A review of nature-based solutions for urban water management in European circular cities: A critical assessment based on case studies and literature, *Blue-Green Systems*. IWA Publishing, pp. 112–136. doi: 10.2166/bgs.2020.932.

Pretorius, E. and de Villiers, G. (2002) The Impact of Informal Living Conditions on Water Quality in the Bloemfontein Municipality, *South African Geographical Journal*, 84(2), pp. 199–207. doi: https://doi.org/10.1080/03736245.2002.9713771.

Ramírez-Agudelo, N. A., Anento, R. P., Villares, M. and Roca, E. (2020) Nature-based solutions for water management in peri-urban areas: Barriers and lessons learned

from implementation experiences, *Sustainability.* MDPI AG, pp. 1–36. doi: 10.3390/su12239799.

Rasool, T., Rehman, A., Naz, I., Ullah, R. and Ahmed, S. (2018) Efficiency of a locally designed pilot-scale trickling biofilter (TBF) system in natural environment for the treatment of domestic wastewater, *Environmental Technology,* 39(10), pp. 1295–1306. doi: https://doi.org/10.1080/09593330.2017.1329346.

Robertson, W. D., Feng, D., Kobylinski, S., Finnigan, D. S., Merkley, C. and Schiff, S. L. (2018) Low cost media can filter particulate phosphorus from turbid stream water under short retention times, *Ecological Engineering*, 123, pp. 95–102. doi: https://doi.org/10.1016/j.ecoleng.2018.08.015.

Ross, P. S., van der Aa, L. T. J., van Dijk, T. and Rietveld, L. C. (2019) Effects of water quality changes on performance of biological activated carbon (BAC) filtration, *Separation and Purification Technology*, 212, pp. 676–683. doi: https://doi.org/10.1016/j.seppur.2018.11.072.

Russo, R. E. (2008) *Wetlands : ecology, conservation and restoration*. Nova Science Publishers.

Sampath, P., Zanetta, C., Kothari, M., Chaudhry, S., Williams, C., Majale, J., Mukungu, P., Ndoye, S., Riunga, W., Agonga-Williams, B., Ray, W., Idukitta, A., Kahwae, E. and Dibo, M. (2010) *State of The World's Cities: Bridging the Urban Divide*. Edited by A. Tibaijuka. Nairobi: United Nations Human Settlements Programme.

Samsó, R., García, J., Molle, P. and Forquet, N. (2016) Modelling bioclogging in variably saturated porous media and the interactions between surface/subsurface flows: Application to Constructed Wetlands, *Journal of Environmental Management*, 165, pp. 271–279. doi: http://dx.doi.org/10.1016/j.jenvman.2015.09.04.

Sbardella, L., Comas, J., Fenu, A., Rodriguez-Roda, I. and Weemaes, M. (2018) Advanced biological activated carbon filter for removing pharmaceutically active compounds from treated wastewater, *Science of the Total Environment*, 636, pp. 519–529. doi: https://doi.org/10.1016/j.scitotenv.2018.04.214.

SERI (2018) *Informal Settlements and Human Rights in South Africa*. Available at: https://www.blacksash.org.za/.

Singh Chaudhary, D., Vigneswaran, S., Ngo, H.-H., Geun Shim, W. and Moon, H. (2003) Biofilter in Water and Wastewater Treatment, *Korean Journal of Chemical Engineering*, 20(6), pp. 1054–1065. doi: 10.1007/BF02706936.

Sletto, B., Tabory, S. and Strickler, K. (2019) Sustainable urban water management and integrated development in informal settlements: The contested politics of co-

production in Santo Domingo, Dominican Republic, *Global Environmental Change*, 54, pp. 195–202. doi: 10.1016/j.gloenvcha.2018.12.004.

Taing, L., Armitage, N., Ashipala, N. and Spiegel, A. (2013) *Sanitation Services in Informal Settlements - Sewering Lessons From Western Cape*. Edited by V. Naidoo and J. Mwale. Water Research Commission. doi: WRC Report No. TT 557/13.

Takaijudin, H., Osman, M., Yusof, K. W., Ghani, A. A. and Weng, G. H. (2021) The effectiveness of cascaded bioretention system in treating urban stormwater runoff, in *Lecture Notes in Civil Engineering*. Springer Science and Business Media Deutschland GmbH, pp. 39–46. doi: 10.1007/978-981-33-6311-3_5.

Tilley, E. A., Zurich, E., Ulrich, L. and Luthi, C. (2014) *Compendium of Sanitation Systems and Technologies*. Second. Edited by C. Zurbrugg, C. Williams, and J. Parkinson. The International Water Association.

United Nations Human Settlement Programme (2003) *The Challenge of Slums: Global Report on Human Settlements*. Earthscan Publications Ltd.

van Niekerk, A. and Rudert, W. (1999) *High rate biological filtration*. Water Research Commission. doi: WRC Report No 569/1/99.

Velten, S., Boller, M., Köster, O., Helbing, J., Weilenmann, H. U. and Hammes, F. (2011) Development of biomass in a drinking water granular active carbon (GAC) filter, *Water Research*, 45(19), pp. 6347–6354. doi: 10.1016/j.watres.2011.09.017.

Verdouw, H., van Echteld, C. J. A. and Dekkers, E. M. J. (1978) Ammonia determination based on indophenol formation with sodium salicylate, *Water Research*, 12(6), pp. 399–402. doi: 10.1016/0043-1354(78)90107-0.

Vymazal, J. and Březinová, T. (2015) The use of constructed wetlands for removal of pesticides from agricultural runoff and drainage: A review, *Environment International*, 75, pp. 11–20. doi: http://dx.doi.org/10.1016/j.envint.2014.10.026.

Wang, H., Tian, C., Zhong, H., An, X. and Quan, B. (2017) Nitrogen Degradation Kinetic Analysis in Different Subsurface Constructed Wetlands, *Nature Environment and Pollution Technology*, 16, pp. 1107–1112. Available at: www.neptjournal.com.

Wang, M., Zhang, D., Dong, J. and Tan, S. K. (2018) Application of constructed wetlands for treating agricultural runoff and agro-industrial wastewater: a review, *Hydrobiologia*, 805(1), pp. 60-76. doi: 10.1007/s10750-017-3315-z.

White, K., Eckel, W. P., Bohaty, R. and Shamim, M. (2021) *Guidance for Evaluating and Calculating Degradation Kinetics in Environmental Media*.

Wu, S., Wallace, S., Brix, H., Kuschk, P., Kirui, W. K., Masi, F. and Dong, R. (2015) Treatment of industrial effluents in constructed wetlands: Challenges, operational strategies and overall performance, *Environmental Pollution*, 201, pp. 107–120. doi: http://dx.doi.org/10.1016/j.envpol.2015.03.006.

Yapsakli, K. and Çeçen, F. (2010) Effect of type of granular activated carbon on DOC biodegradation in biological activated carbon filters, *Process Biochemistry*, 45(3), pp. 355–362. doi: 10.1016/j.procbio.2009.10.005.

Zhang, H., Zhang, K., Jin, H., Gu, L. and Yu, X. (2015) Variations in dissolved organic nitrogen concentration in biofilters with different media during drinking water treatment, *Chemosphere*, 139, pp. 652–658. doi: http://dx.doi.org/10.1016/j.chemosphere.2014.10.092.

Zhang, J., Wu, H., Xu, J., Fan, J., Liu, H. and Liang, S. (2016) *Green Technologies for Sustainable Water Management*. First, *Green Technologies for Sustainable Water Management*. First. Edited by H. Ngo et al. Reston: American Society of Civil Engineers.

Zhang, W., Sang, M., Che, W. and Sun, H. (2019) Nutrient removal from urban stormwater runoff by an up-flow and mixed-flow bioretention system, *Environmental Science and Pollution Research*, 26(17), pp. 17731–17739. doi: 10.1007/s11356-019-05091-4.

Zhao, H., Zhang, Y., Tang, L., Wang, C., Wang, Y. and Liu, D. (2018) Changes in Phosphorus Adsorption Characteristics of Sediment Particles Associated with Biofilm Growth, in *American Geophysical Union, Fall Meeting 2018*.

Zheng, Z. Z., Zheng, L. W., Xu, M. N., Tan, E., Hutchins, D. A., Deng, W., Zhang, Y., Shi, D., Dai, M. and Kao, S. J. (2020) Substrate regulation leads to differential responses of microbial ammonia-oxidizing communities to ocean warming, *Nature Communications*, 11(1). doi: 10.1038/s41467-020-17366-3.

APPENDICES

Raw data and extended SEM images available on the following link: https://figshare.com/s/f64b77047dacf7064b01

Appendix A: Using the HACH Reagent Set to Analyse Nutrient Concentrations

The HACH reagent set, and spectrophotometer was used to analyse ammonia, nitrate, nitrite and orthophosphate concentrations in various samples as per the method described in the HACH Water Analysis Handbook (HACH Company, 2008). The following methods were used to determine NH_3, NO_3^-, NO_2^- and PO_4^{3-} concentrations:

- The Salicylate Method was used to determine NH_3 concentrations (Verdouw, van Echteld and Dekkers, 1978).
- The Diazotization Method was used to determine NO_2^- concentrations (Fishman, Skougstad and Scarbro, 1964).
- The Cadmium Reduction Method was used to determine NO_3^- concentrations (Jones, 1984).
- The Ascorbic Acid Method was used to determine PO_4^{3-} concentrations (Murphy and Riley, 1962).

In each instance a reagent sachet was added to 10 ml of the sample being analysed. The resulting solution was then agitated and set aside for the specified amount of time to allow the reactor to occur. The sample was then poured into a cuvette and analysed using the HACH spectrophotometer. If the concentration of ammonia, nitrate, nitrite or orthophosphate was at a higher concentration than the limit of detection for the relevant method; the sample was first diluted before the addition of the reagent sachet. The method outlined in the HACH methods manual was followed with an explanation of each reaction given below.

Ammonia

Ammonia compounds in the sample combine with chlorine to form monochloramine. Monochloramine reacts with salicylate to form 5-aminosalicylate. The 5-aminosalicylate is oxidized in the presence of a sodium nitroprusside catalyst to form a blue-coloured compound. The blue colour is masked by the yellow colour from the excess reagent to give a final, green-coloured solution. The measurement wavelength is 655 nm for spectrophotometers. The ammonia detection range is 0.100 – 50.0 mg/L for this method. Figure A1 shows the standard curve for the Salicylate Method to determine ammonia concentration while Table A1 shows the mean concentrations and standard deviations of the measured concentrations against the known concentration of the standard solutions. The analysis was done three times to determine the error

associated with the analysis method. There is a maximum error of 2.31% associated with the method of analysis as seen in Table A1.

Nitrite

Nitrite in the sample reacts with sulphanilic acid to form an intermediate diazonium salt. This couples with chromotropic acid to produce a pink coloured complex directly proportional to the amount of nitrite present. The measurement wavelength is 507 nm for spectrophotometers. The nitrite detection range is 0.001 – 6.00 mg/L for this method. Figure A2 shows the standard curve for the Diazotization Method to determine nitrite concentration while Table A2 shows the mean concentrations and standard deviations of the measured concentrations against the known concentration of the standard solutions. The analysis was done three times to determine the error associated with the analysis method. There is a maximum error of 2.31% associated with the method of analysis as seen in Table A2.

Nitrate

Cadmium metal reduces nitrate in the sample to nitrite. The nitrite ion reacts in an acidic medium with sulphanilic acid to form an intermediate diazonium salt. The salt couples with gentisic acid to form an amber coloured solution. The measurement wavelength is 400 nm for spectrophotometers. The nitrate detection range is 0.100 – 30.00 mg/L using the HACH spectrophotometer. Figure A3 shows the standard curve for the Cadmium Reduction Method to determine nitrate concentration while Table A3 shows the mean concentrations and standard deviations of the measured concentrations against the known concentration of the standard solutions. The analysis was done three times to determine the error associated with the analysis method. There is a maximum error of 2.40% associated with the method of analysis as seen in Table A3.

Orthophosphate

Orthophosphate reacts with molybdate in an acid medium to produce a mixed phosphate/molybdate complex. Ascorbic acid then reduces the complex, which gives an intense molybdenum blue colour. The measurement wavelength is 880 nm for spectrophotometers. The orthophosphate detection range is 0.0001- 20.00 mg/L for this method. Figure A4 shows the standard curve for the Ascorbic Acid Method to determine orthophosphate concentration while Table A4 shows the mean concentrations and standard deviations of the measured concentrations against the known concentration of the standard solutions. The analysis was done three times to determine the error associated with the analysis method. There is a maximum error of 2.31% associated with the method of analysis as seen in Table A4.

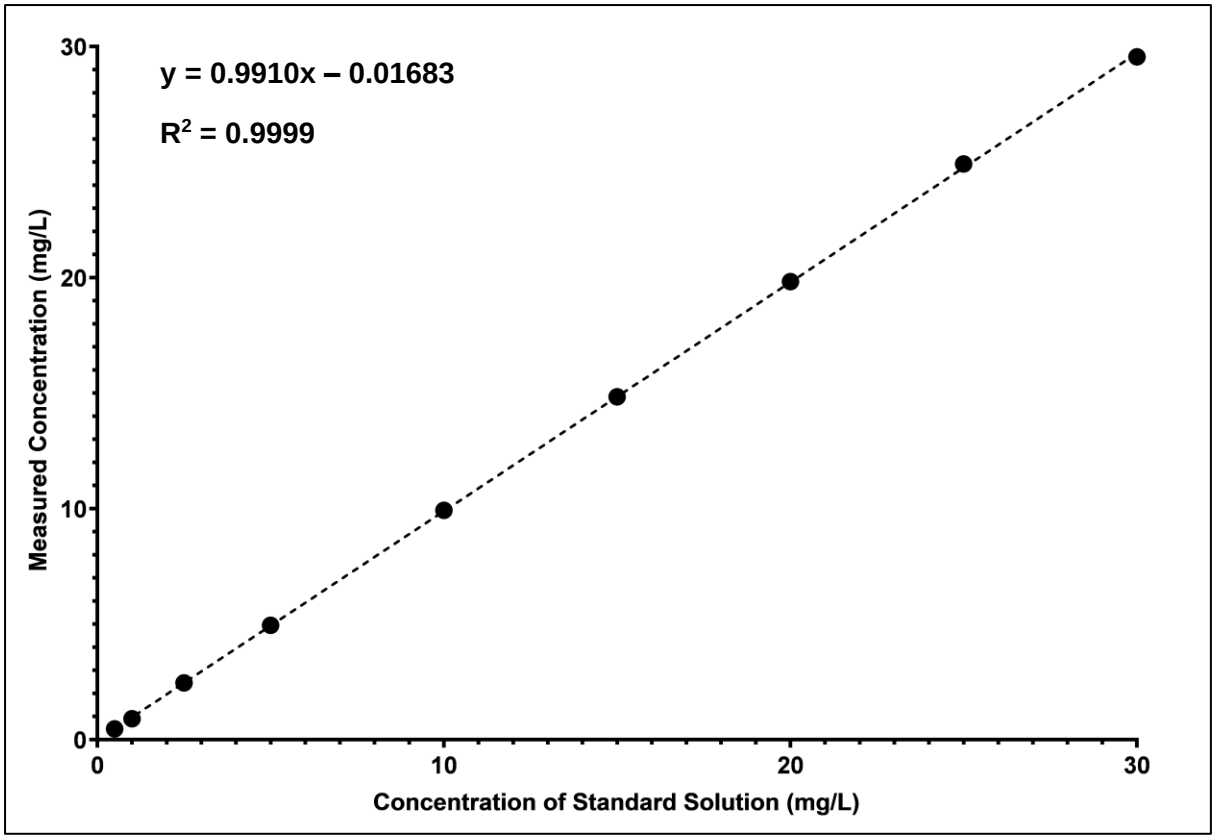

Figure A1: Standard curve for the Salicylate Method to determine ammonia concentration

Table A1: Mean measured concentration and standard deviation for the Salicylate Method to determine ammonia concentration

Concentration of Standard Solution (mg/L)	Mean Measured Concentration (mg/L)	Standard Deviation (mg/L)	% Error
0.500	0.47	0.012	2.31
1.00	0.91	0.006	0.58
2.50	2.46	0.015	0.61
5.00	4.95	0.031	0.61
10.0	9.93	0.079	0.79
15.0	14.84	0.173	1.16
20.0	19.83	0.078	0.39
25.0	24.92	0.040	0.16
30.0	29.53	0.167	0.56

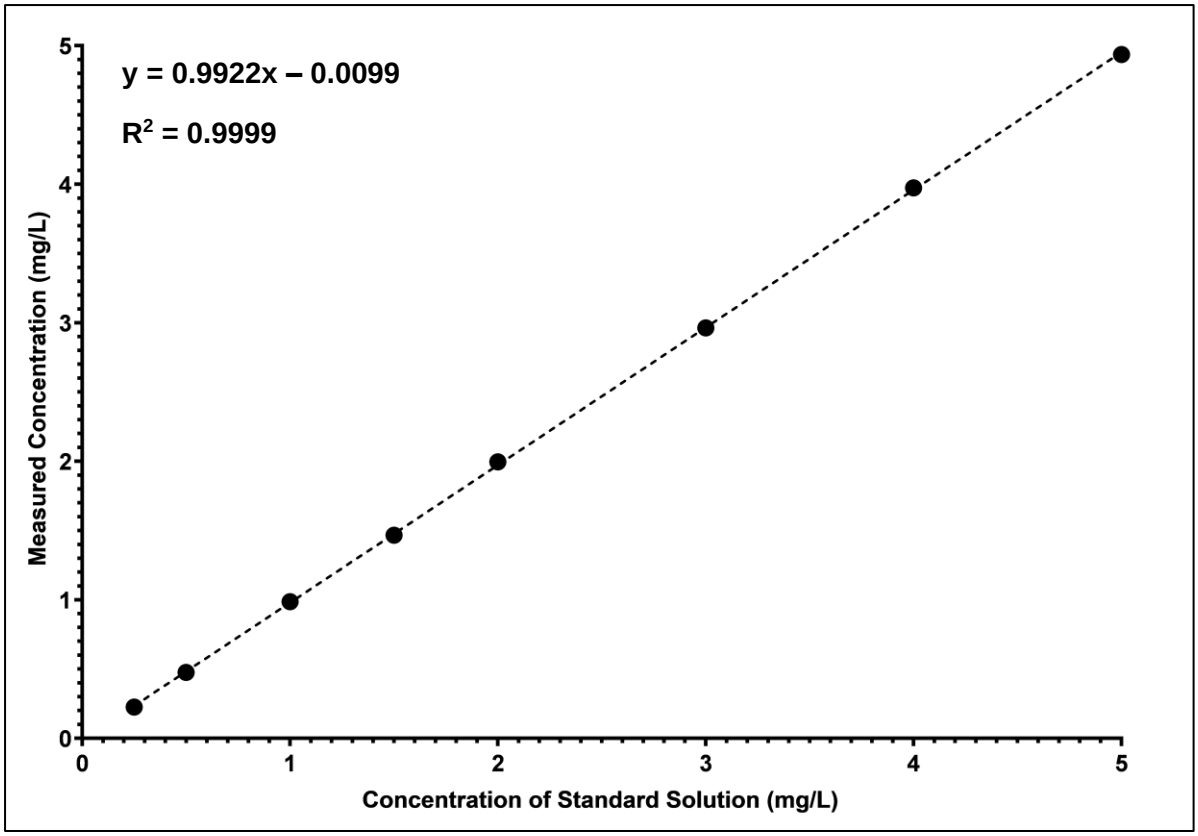

Figure A2: Standard curve for the Diazotization Method to determine nitrite concentration

Table A2: Mean measured concentration and standard deviation for the Diazotization Method to determine nitrite concentration

Concentration of Standard Solution (mg/L)	Mean Measured Concentration (mg/L)	Standard Deviation (mg/L)	% Error
0.250	0.227	0.015	2.31
0.500	0.477	0.006	1.15
1.00	0.987	0.015	1.53
1.50	1.467	0.006	0.38
2.00	1.997	0.006	0.29
3.00	2.963	0.015	0.51
4.00	3.973	0.006	0.14
5.00	4.937	0.015	0.31

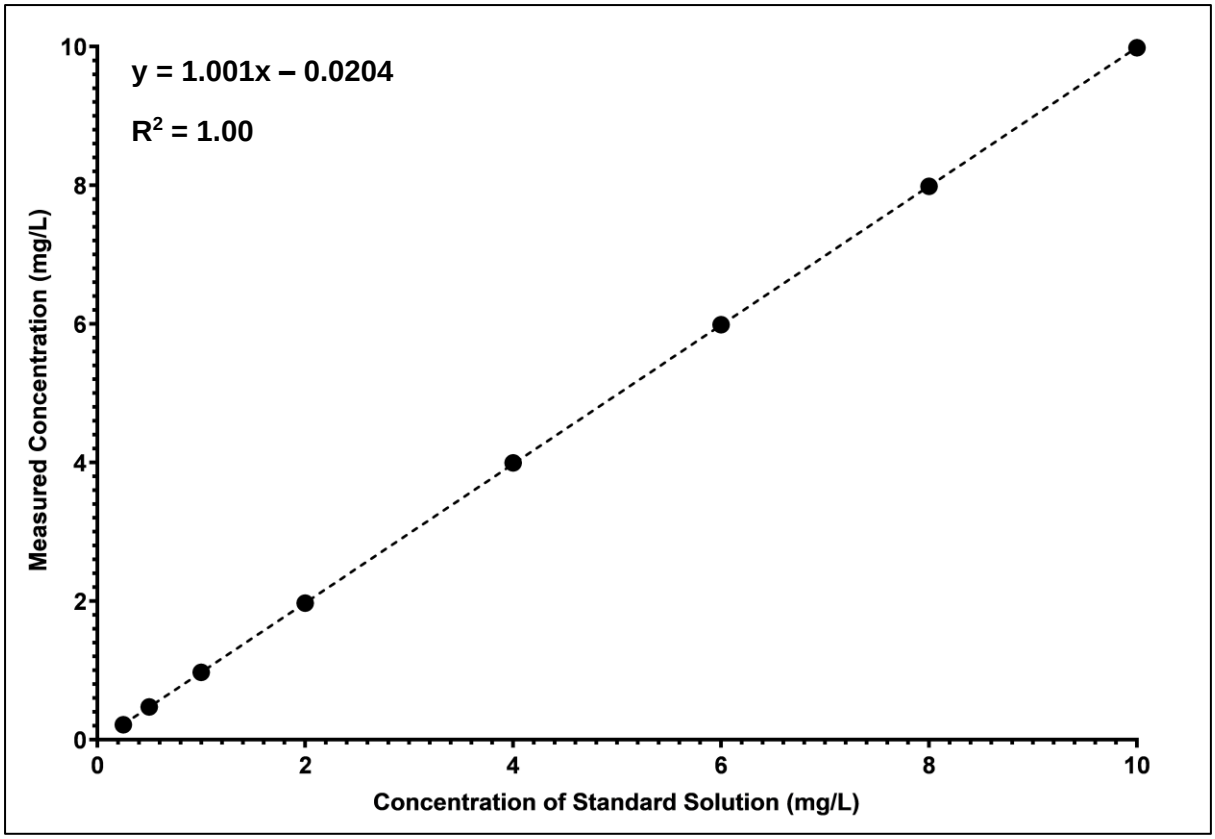

Figure A3: Standard curve for the Cadmium Reduction Method to determine nitrate concentration

Table A3: Mean measured concentration and standard deviation for the Cadmium Reduction Method to determine nitrate concentration

Concentration of Standard Solution (mg/L)	Mean Measured Concentration (mg/L)	Standard Deviation (mg/L)	% Error
0.250	0.243	0.006	2.40
0.500	0.47	0.006	1.15
1.00	0.97	0.021	2.08
2.00	1.97	0.010	0.50
4.00	3.99	0.006	0.14
6.00	5.99	0.015	0.25
8.00	7.98	0.015	0.19
10.0	9.98	0.038	0.38

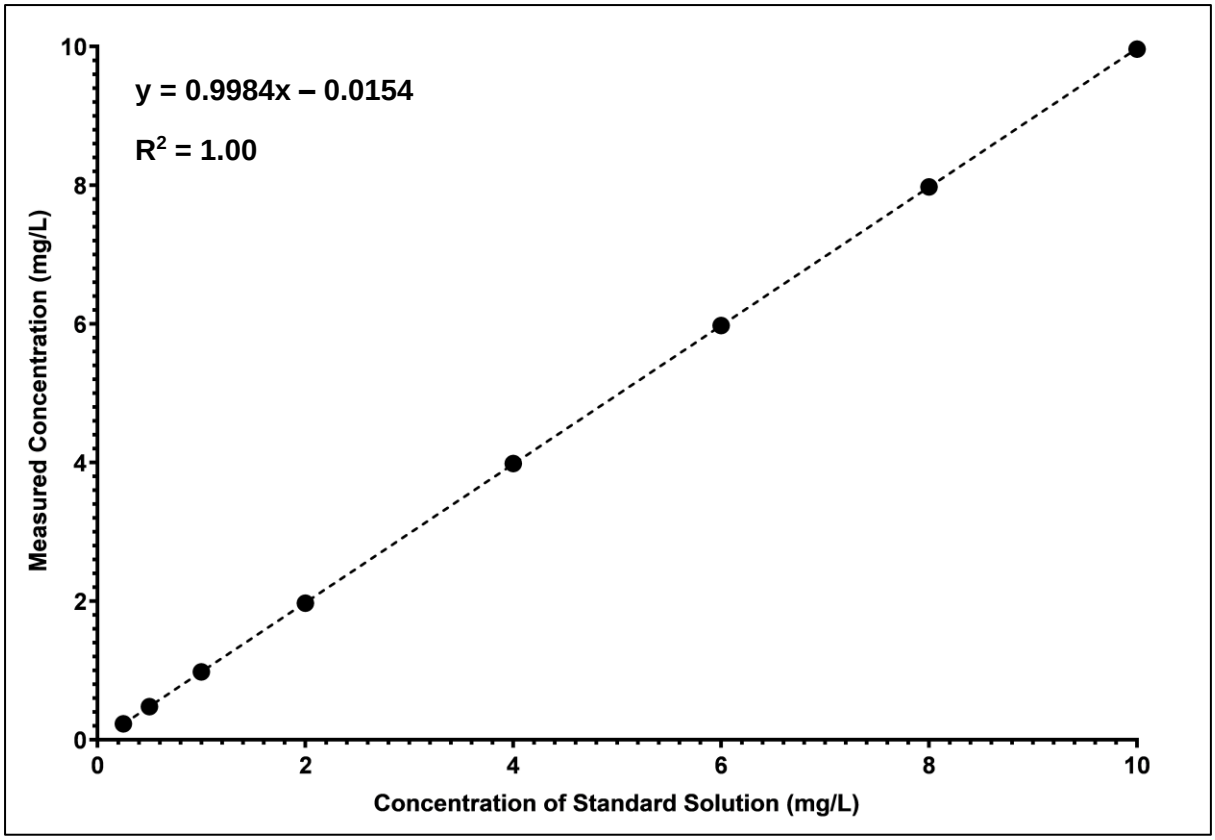

Figure A4: Standard curve for the Ascorbic Acid Method to determine orthophosphate concentration

Table A4: Mean measured concentration and standard deviation for the Ascorbic Acid Method to determine orthophosphate concentration

Concentration of Standard Solution (mg/L)	Mean Measured Concentration (mg/L)	Standard Deviation (mg/L)	% Error
0.250	0.243	0.006	2.31
0.500	0.480	0.010	2.00
1.00	0.980	0.020	2.00
2.00	1.97	0.020	1.00
4.00	3.99	0.010	0.38
6.00	5.98	0.032	0.54
8.00	7.98	0.015	0.19
10.0	9.96	0.021	0.21

Appendix B: Statistical Analysis for LSO and SSO

Wilcoxon Signed-Rank Tests were carried out for the samples that were taken at the LSO (outlet of large stone biofilter) and SSO (outlet off small stone biofilter). The Wilcoxon Signed-Rank test was chosen as it compares the probability of observing higher values from a group of data (group 1) with another (group 2) for datasets that do not have normal distributions (LaMorte, 2017).These statistical tests were carried out to compare the nutrient concentrations at these two sampling points and to determine whether the difference between the concentrations observed at each sampling point is statistically significant.

Wilcoxon Signed-Rank Test for Ammonia Concentrations Observed at LSO and SSO

The ammonia concentrations in the samples taken from the LSO and SSO sampling sites were compared using a two-tailed Wilcoxon Signed-Rank Test. The following data sets were considered:

Sampling Date	NH_3 concentration in LSO (mg/L)	NH_3 concentration in SSO (mg/L)
29 March 2019	0.290	1.50
12 April 2019	0.100	2.60
27 April 2019	3.60	3.75
16 May 2019	0.500	1.45
23 May 2019	3.25	4.25
30 May 2019	1.05	1.05
6 June 2019	0.600	0.200
14 June 2019	2.60	1.70
27 June 2019	2.90	1.65
11 July 2019	0.870	1.30
25 July 2019	1.01	2.64
14 August 2019	1.45	0.890

23 August 2019	1.22	1.24
29 August 2019	2.15	2.69
12 September 2019	1.87	1.51
26 September 2019	1.53	1.48
10 October 2019	1.47	1.31
24 October 2019	0.940	1.08
14 November 2019	0.510	0.85
28 November 2019	0.970	0.82
17 December 2019	0.810	1.13
30 December 2019	1.06	0.96
16 January 2020	1.24	1.53
30 January 2020	2.26	3.42
10 February 2020	1.72	3.37
26 February 2020	2.23	3.12

H_0: $[NH_3]_{LSO} = [NH_3]_{SSO}$ (i.e. $[NH_3]_{LSO} - [NH_3]_{SSO} = 0$)

H_1: $[NH_3]_{LSO} \neq [NH_3]_{SSO}$

Significance Level (α) = 0.05; critical Z-value = 1.96

Expected difference (μ_0) = 0

Sample Z-value = -1.91832

p-value = 0.0551

The sample Z-value is in the 95% region of acceptance.

P-value > α. H_0 is accepted.

∴ the difference between the values of $[NH_3]_{LSO}$ and $[NH_3]_{SSO}$ is not big enough to be statistically significant.

Wilcoxon Signed-Rank Test for Nitrate Concentrations Observed at LSO and SSO

The nitrate concentrations in the samples taken from the LSO and SSO sampling sites were compared using a two-tailed Wilcoxon Signed-Rank Test. The following data sets were considered:

Sampling Date	NO_3^- concentration in LSO (mg/L)	NO_3^- concentration in SSO (mg/L)
29 March 2019	0.840	0.600
12 April 2019	0.740	0.510
27 April 2019	0.310	0.350
16 May 2019	0.365	0.310
23 May 2019	1.00	0.900
30 May 2019	0.400	0.350
6 June 2019	0.550	0.300
14 June 2019	1.10	0.900
27 June 2019	0.320	0.145
11 July 2019	0.210	0.180
25 July 2019	0.420	0.340
14 August 2019	0.260	0.220
23 August 2019	0.510	0.310
29 August 2019	0.860	0.480
12 September 2019	0.410	0.310
26 September 2019	0.620	0.520
10 October 2019	0.460	0.240

24 October 2019	0.380	0.310
14 November 2019	0.730	0.490
28 November 2019	0.760	0.520
17 December 2019	0.860	0.470
30 December 2019	0.630	0.160
16 January 2020	0.750	0.410
30 January 2020	0.840	0.220
10 February 2020	0.910	0.360
26 February 2020	1.02	0.740

H_0: $[NO_3^-]_{LSO} = [NO_3^-]_{SSO}$ (i.e. $[NO_3^-]_{SSO} - [NO_3^-]_{LSO} = 0$)

H_1: $[NO_3^-]_{LSO} \neq [NO_3^-]_{SSO}$

Significance Level (α) = 0.05; critical Z-value = 1.96

Expected difference (μ_0) = 0

Sample Z-value = -4.395

p-value = 0.00001

The sample Z-value is not in the 95% region of acceptance.

P-value < α. fail to accept H_0.

∴ the difference between the values of $[NO_3^-]_{LSO}$ and $[NO_3^-]_{SSO}$ is big enough to be statistically significant.

Wilcoxon Signed-Rank Test for Nitrite Concentrations Observed at LSO and SSO

The nitrite concentrations in the samples taken from the LSO and SSO sampling sites were compared using a two-tailed Wilcoxon Signed-Rank Test. The following data sets were considered:

Sampling Date	NO_2^- concentration in LSO (mg/L)	NO_2^- concentration in SSO (mg/L)
29 March 2019	0.160	0.110
12 April 2019	0.221	0.080
27 April 2019	0.300	0.190
16 May 2019	0.007	0.012
23 May 2019	0.030	0.006
30 May 2019	0.080	0.030
6 June 2019	0.038	0.010
14 June 2019	0.003	0.014
27 June 2019	0.037	0.017
11 July 2019	0.021	0.090
25 July 2019	0.031	0.010
14 August 2019	0.024	0.017
23 August 2019	0.041	0.024
29 August 2019	0.012	0.004
12 September 2019	0.080	0.080
26 September 2019	0.053	0.012
10 October 2019	0.092	0.040

24 October 2019	0.075	0.090
14 November 2019	0.086	0.060
28 November 2019	0.085	0.050
17 December 2019	0.120	0.080
30 December 2019	0.094	0.140
16 January 2020	0.071	0.075
30 January 2020	0.099	0.004
10 February 2020	0.087	0.032
26 February 2020	0.059	0.076

H_0: $[NO_2^-]_{LSO} = [NO_3^-]_{4SSO}$ (i.e. $[NO_2^-]_{SSO} - [NO_2^-]_{LSO} = 0$)

H_1: $[NO_2^-]_{LSO} \neq [NO_2^-]_{SSO}$

Significance Level (α) = 0.05; critical Z-value = 1.96

Expected difference (μ_0) = 0

Sample Z-value = 2.7313

p-value = 0.0063

The sample Z-value is not in the 95% region of acceptance.

P-value < α. fail to accept H_0.

∴ the difference between the values of $[NO_2^-]_{LSO}$ and $[NO_2^-]_{SSO}$ is big enough to be statistically significant.

Wilcoxon Signed-Rank Test for Total Nitrogen Concentrations Observed at LSO and SSO

The total nitrogen (TN) concentrations in the samples taken from the LSO and SSO sampling sites were compared using a two-tailed Wilcoxon Signed-Rank Test. The following data sets were considered:

Sampling Date	TN concentration in LSO (mmol/L)	TN concentration in SSO (mmol/L)
29 March 2019	0.034	0.100
12 April 2019	0.023	0.163
27 April 2019	0.223	0.230
16 May 2019	0.035	0.090
23 May 2019	0.208	0.264
30 May 2019	0.070	0.068
6 June 2019	0.045	0.017
14 June 2019	0.170	0.115
27 June 2019	0.176	0.100
11 July 2019	0.055	0.081
25 July 2019	0.067	0.161
14 August 2019	0.090	0.056
23 August 2019	0.081	0.078
29 August 2019	0.140	0.166
12 September 2019	0.118	0.095
26 September 2019	0.101	0.096
10 October 2019	0.096	0.082

24 October 2019	0.063	0.070
14 November 2019	0.044	0.059
28 November 2019	0.071	0.058
17 December 2019	0.064	0.076
30 December 2019	0.074	0.062
16 January 2020	0.086	0.098
30 January 2020	0.148	0.204
10 February 2020	0.118	0.204
26 February 2020	0.154	0.197

H_0: $[TN]_{LSO} = [TN]_{SSO}$ (i.e. $[TN]_{SSO} - [TN]_{LSO} = 0$)

H_1: $[TN]_{LSO} \neq [TN^-]_{SSO}$

Significance Level (α) = 0.05; critical Z-value = 1.96

Expected difference (μ_0) = 0

Sample Z-value = -1.4859

p-value = 0.1373

The sample Z-value is in the 95% region of acceptance.

P-value > α. accept H_0.

∴ the difference between the values of $[TN]_{LSO}$ and $[TN]_{SSO}$ is not big enough to be statistically significant.

Wilcoxon Signed-Rank Test for Orthophosphate Concentrations Observed at LSO and SSO

The orthophosphate concentrations in the samples taken from the LSO and SSO sampling sites were compared using a two-tailed Wilcoxon Signed-Rank Test. The following data sets were considered:

Sampling Date	PO_4^{3-} concentration in LSO (mg/L)	PO_4^{3-} concentration in SSO (mg/L)
29 March 2019	1.28	0.940
12 April 2019	0.950	0.780
27 April 2019	0.840	0.640
16 May 2019	0.525	0.490
23 May 2019	0.310	0.160
30 May 2019	0.450	0.110
6 June 2019	0.585	0.250
14 June 2019	0.620	0.280
27 June 2019	0.530	0.350
11 July 2019	0.480	0.320
25 July 2019	0.210	0.140
14 August 2019	0.380	0.280
23 August 2019	0.960	0.760
29 August 2019	0.420	0.270
12 September 2019	0.460	0.140
26 September 2019	0.265	0.180
10 October 2019	0.460	0.240

24 October 2019	0.740	0.280
14 November 2019	0.630	0.130
28 November 2019	0.960	0.290
17 December 2019	0.950	0.340
30 December 2019	0.840	0.180
16 January 2020	1.05	0.940
30 January 2020	0.960	0.760
10 February 2020	0.520	0.390
26 February 2020	0.830	0.740

H_0: $[PO_4^{3-}]_{LSO} = [PO_4^{3-}]_{SSO}$ (i.e. $[PO_4^{3-}]_{SSO} - [PO_4^{3-}]_{LSO} = 0$)

H_1: $[TN]_{LSO} \neq [TN^-]_{SSO}$

Significance Level (α) = 0.05; critical Z-value = 1.96

Expected difference (μ_0) = 0

Sample Z-value = 4.4454

p-value = 0.000009

The sample Z-value is not in the 95% region of acceptance.

P-value < α. fail to accept H_0.

∴ the difference between the values of $[PO_4^{3-}]_{LSO}$ and $[PO_4^{3-}]_{SSO}$ is big enough to be statistically significant.

Appendix C: Sampling Regimes for Pulse Tracer Studies

Table C1: Sampling regime for pulse tracer studies at 2 L/min

Time	SP 1	SP 2 & 3	SP 4	SP 5 & 6	SP 7	SP 8 & 9	SP 10
0	X						
5	X						
10	X						
15	X						
20	X	X					
25	X	X					
30	X	X	X				
35		X	X				
40		X	X				
45		X	X				
50		X	X	X			
55			X	X			
60			X	X	X		
65				X	X		
70				X	X		
75				X	X		
80				X	X	X	
85					X	X	
90					X	X	X
95						X	X
100						X	X
105						X	X
110						X	X
115							X
120							X

Table C2: Sampling regime for pulse tracer studies at 1.5 L/min

Time	SP 1	SP 2 & 3	SP 4	SP 5 & 6	SP 7	SP 8 & 9	SP 10
0	X						
10	X						
20	X	X					
30	X	X					
40	X	X	X				
50		X	X				
60		X	X	X			
70			X	X			
80			X	X	X		
90				X	X		
100				X	X	X	
110					X	X	
120					X	X	X
130						X	X
140						X	X
150							X
160							X

Table C3: Sampling Regime for Pulse Tracer Studies at 1 L/min

Time	SP 1	SP 2 & 3	SP 4	SP 5 & 6	SP 7	SP 8 & 9	SP 10
0	X						
10	X						
20	X						
30	X	X					
40	X	X					
50	X	X					
60	X	X	X				
70		X	X				
80		X	X				

90		X	X	X			
100			X	X			
110			X	X			
120			X	X	X		
130				X	X		
140				X	X		
150				X	X	X	
160					X	X	
170					X	X	
180					X	X	X
190						X	X
200						X	X
210						X	X
220							X
230							X
240							X

Table C4: Sampling regime for pulse tracer studies at 0.75 L/min

Time	SP 1	SP 2 & 3	SP 4	SP 5 & 6	SP 7	SP 8 & 9	SP 10
0	X						
10	X						
20	X						
30	X						
40	X	X					
50	X	X					
60	X	X					
70		X					
80		X					
90		X	X				
100		X	X				
110			X				

120			X				
130			X				
140			X	X			
150			X	X			
160				X			
170				X			
180				X			
190				X	X		
200				X	X		
210					X		
220					X		
230					X	X	
240					X	X	
250					X	X	
260						X	
270						X	X
280						X	X
290						X	X
300							X
310							X
320							X
330							X

Table C5: Sampling regime for pulse tracer studies at 0.5 L/min

Time (min)	SP 1	SP 2 & 3	SP 4	SP 5 & 6	SP 7	SP 8 & 9	SP 10
0	X						
20	X						
40	X						

60	X	X					
80	X	X					
100	X	X					
120	X	X	X				
140		X	X				
160		X	X				
180		X	X	X			
200			X	X			
220			X	X			
240			X	X	X		
260				X	X		
280				X	X		
300				X	X	X	
320					X	X	
340					X	X	
360					X	X	X
380						X	X
400						X	X
420						X	X
440							X
460							X
480							X

Appendix D: Standard Curve relating concentration and absorbance for Allura Red AC Dye

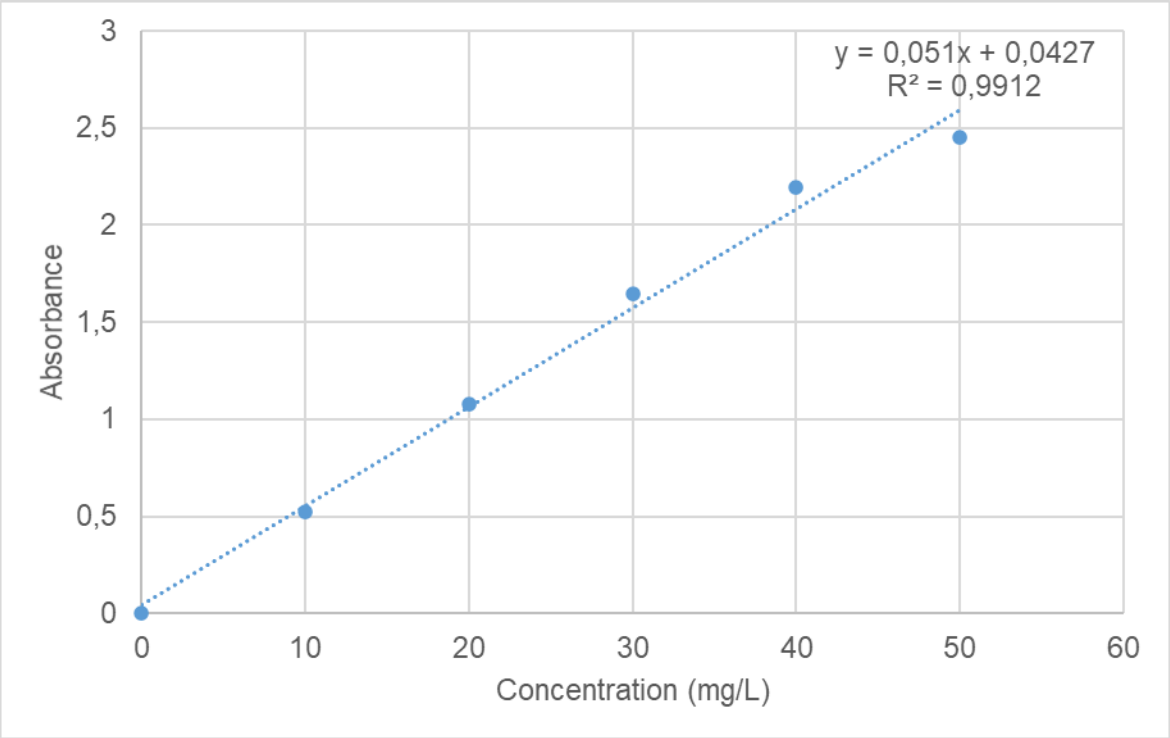

Figure D1: Standard curve for Allura Red AC Dye (absorbance measured at 504 nm)

Appendix E: Orthophosphate Adsorption Control Experiment

An orthophosphate adsorption study was conducted using uncolonised stones. The study was carried out at orthophosphate concentrations of 6.0 mg/L, 4.0 mg/L, 2.0 mg/L, 1.0 mg/L, and 0.5 mg/L.

Uncolonised stones, 8-11 mm in diameter, were placed in a 1 L glass beaker which was filled with an orthophosphate solution at the desired concentration. Samples were drawn from the beaker after every 30 minutes. The orthophosphate concentration in the sample was analysed immediately using the HACH benchtop reagent set (Appendix A). The experiment was conducted over a 6-hour period at each orthophosphate concentration.

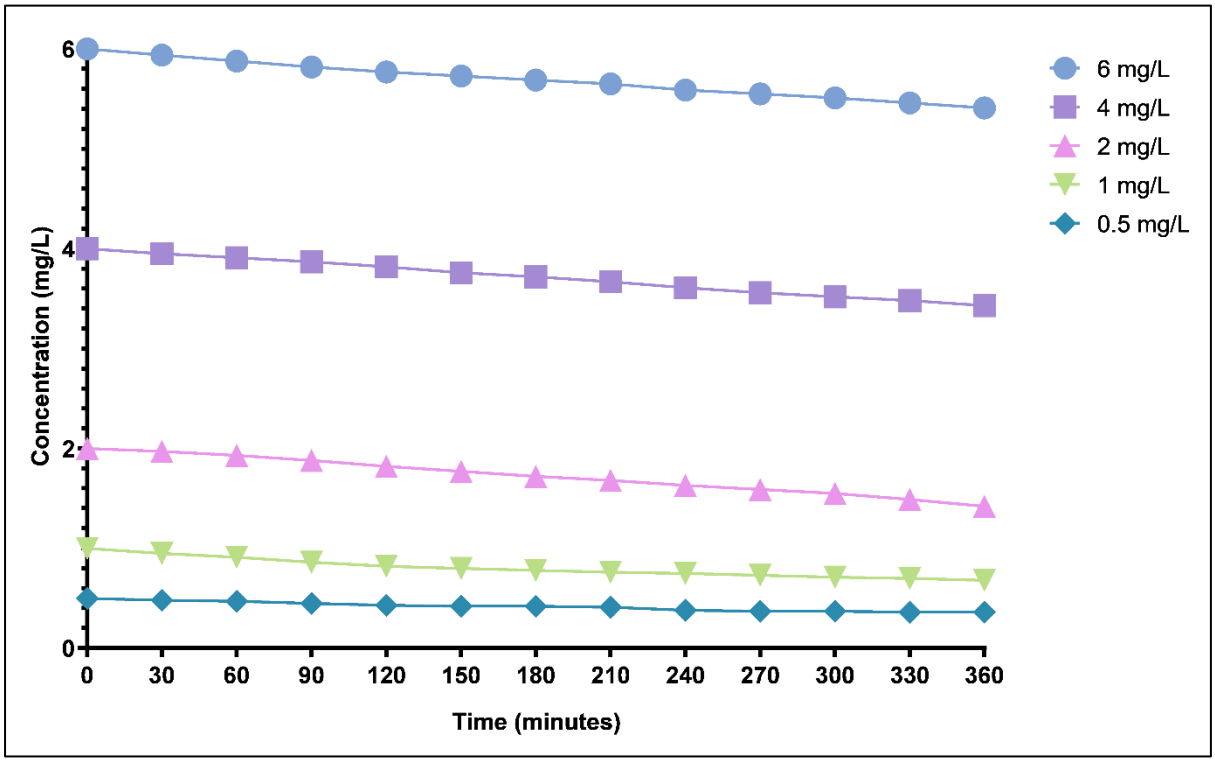

Figure E1: Orthophosphate concentration over time for orthophosphate adsorption control experiment

The straight-line plots suggest that orthophosphate follows a zero-order adsorption rate. The rate constants. *k*. for each orthophosphate concentration. shown in Table E1. suggest that the rate of adsorption is independent of inlet concentration at concentrations equal to and above 1.5 mg/L. The rate constant of 0.0016 mg/L/h at orthophosphate concentrations above 1.5 mg/L decrease in proportion to the decreasing orthophosphate concentration from 0.0016 mg/L/h at a starting concentration 2 mg/L or above to 0.0008 mg/L/h at the initial orthophosphate concentration of 1 mg/Land 0.0004 mg/L/h at an initial concentration of 0.5 mg/L.

Table E1: Rate constant at different initial orthophosphate concentrations

Initial Orthophosphate Concentration (mg/L)	***k (mg/L/h)***
6	0.0016
4	0.0016
2	0.0016
1	0.0008
0.5	0.0004

Appendix F: Temperature Profiles for Nutrient Degradation Kinetic Studies

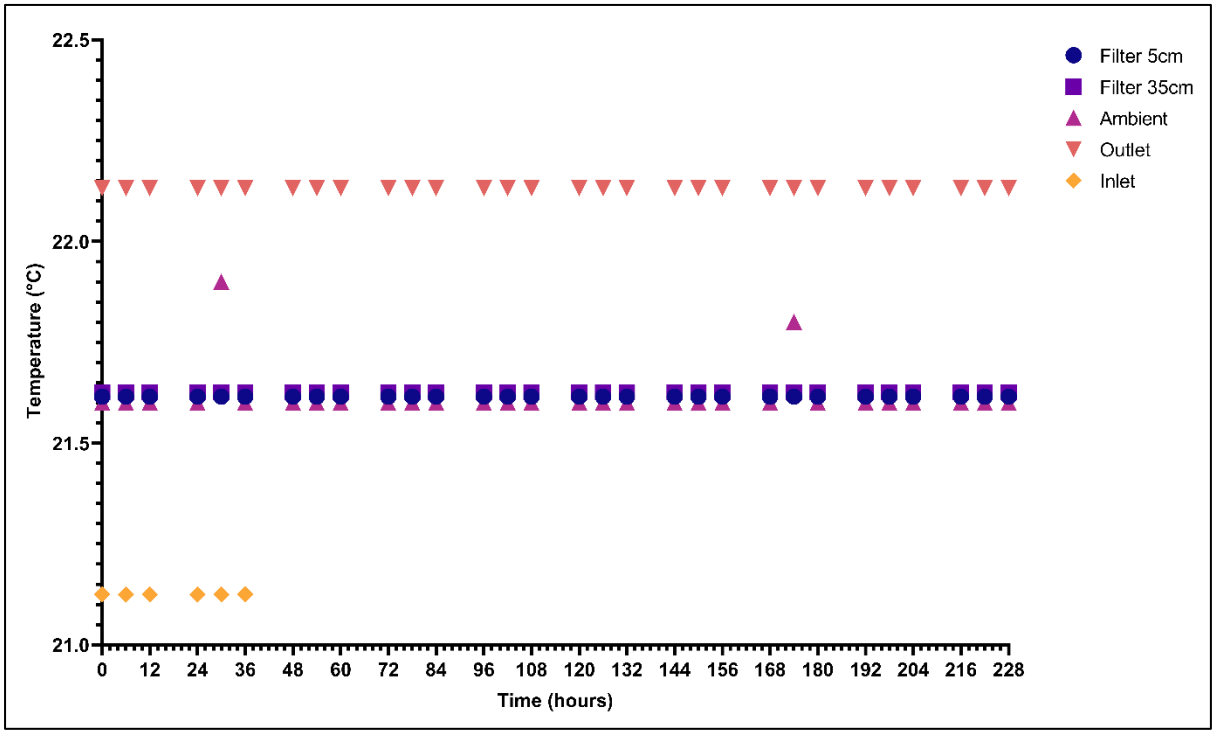

Figure F1: Temperature profile for Run C at 0.5 L/min

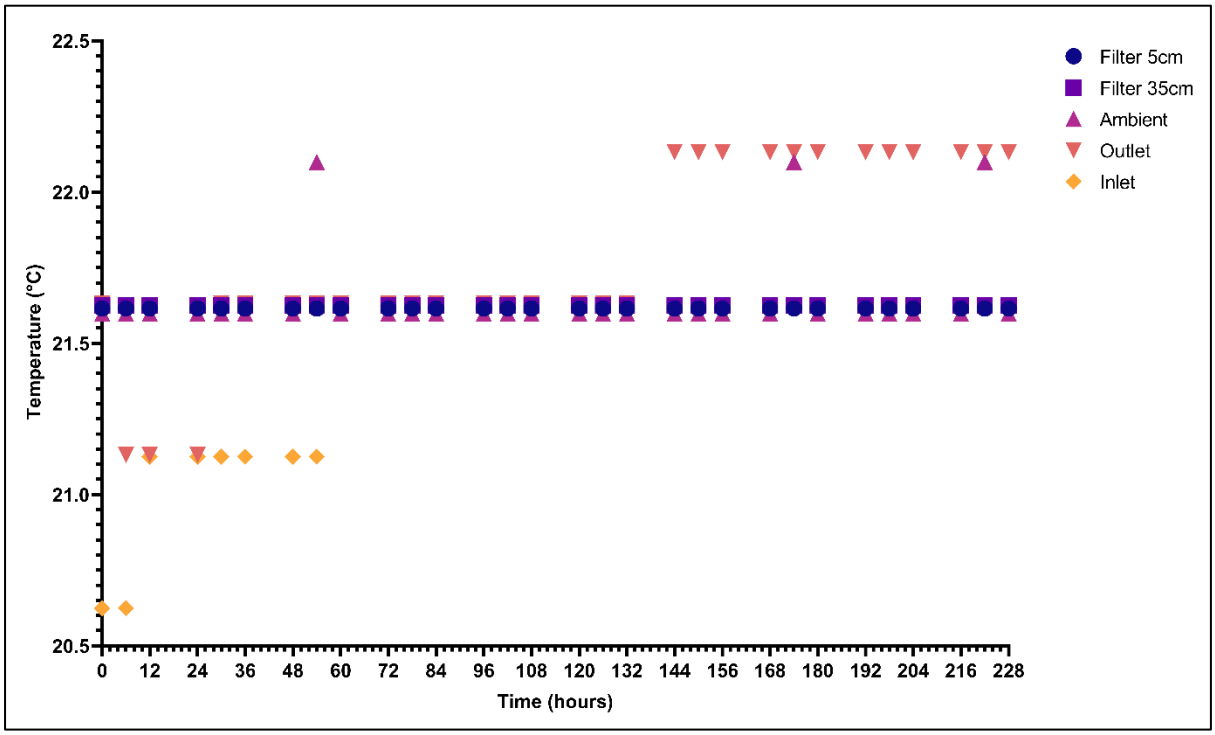

Figure F2: Temperature profile for Run C at 1.5 L/min

Appendix G: Testing First and Second Order Reaction Fits for All Nutrient Degradation Studies

Zero order reaction kinetics are excluded as the graphs of concentration over the experimental time period do not yield straight line plots.

Detailed Example for Run A at 0.5 L/min

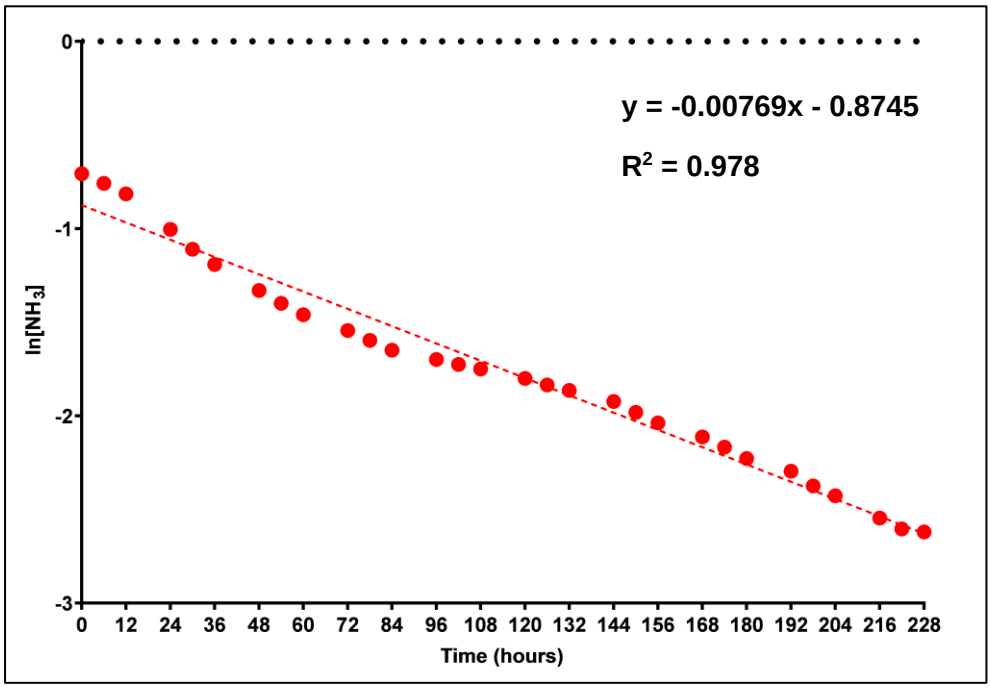

Figure G1: First order fit for ammonia (Run A at 0.5 L/min)

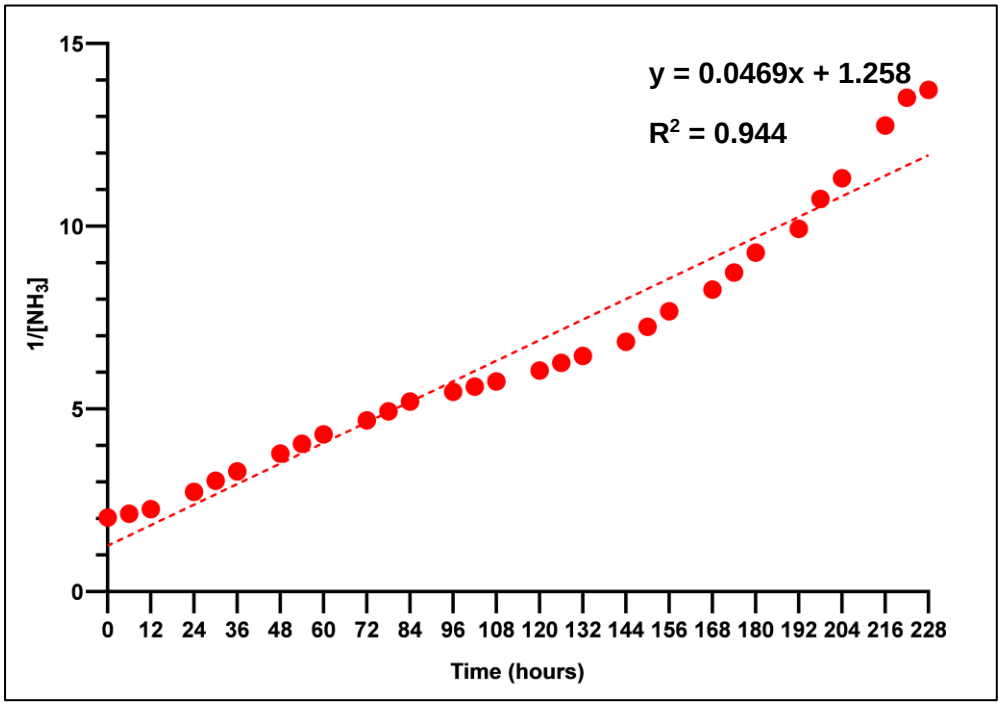

Figure G2: Second order fit for ammonia (Run A at 0.5 L/min)

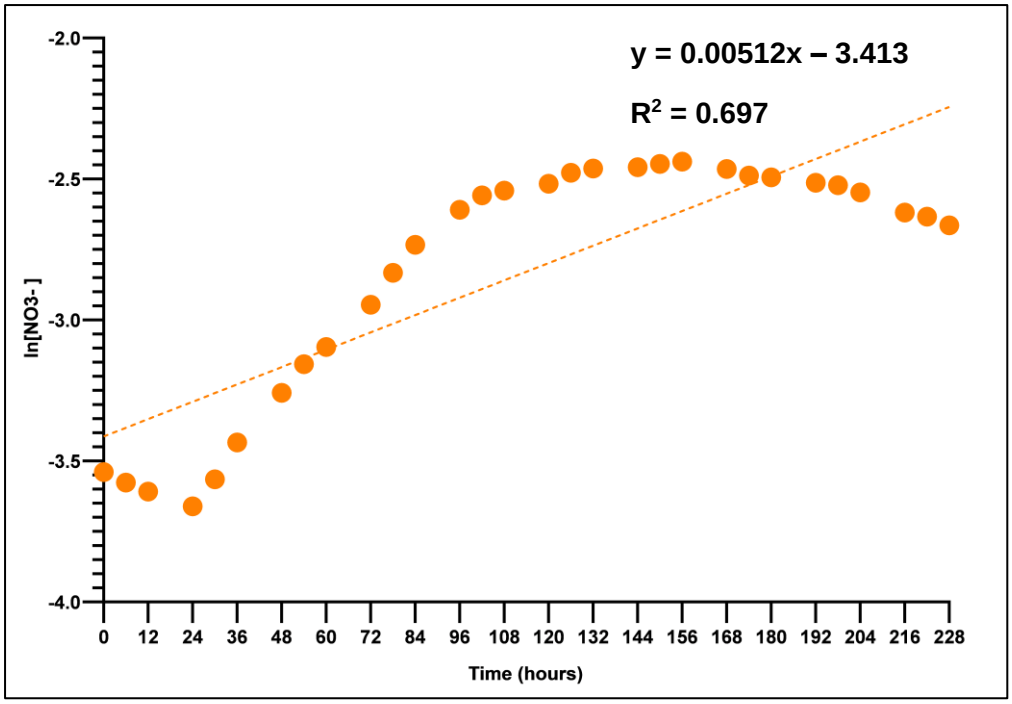

Figure G3: First order fit for nitrate (Run A at 0.5 L/min)

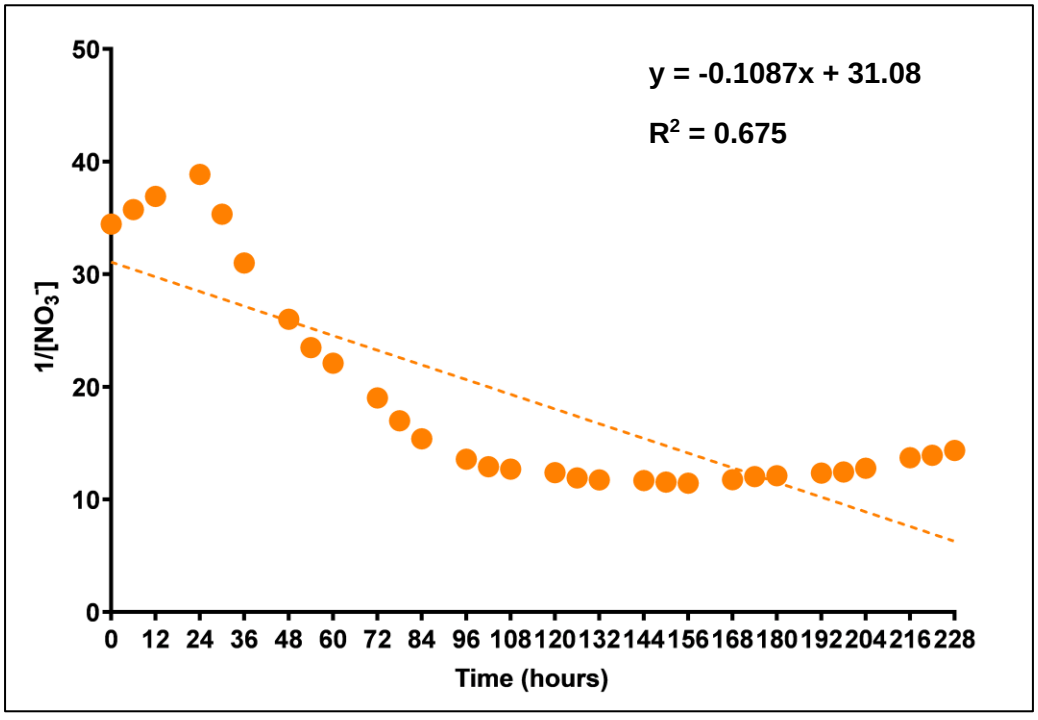

Figure G4: Second order fit for nitrate (Run A at 0.5 L/min)

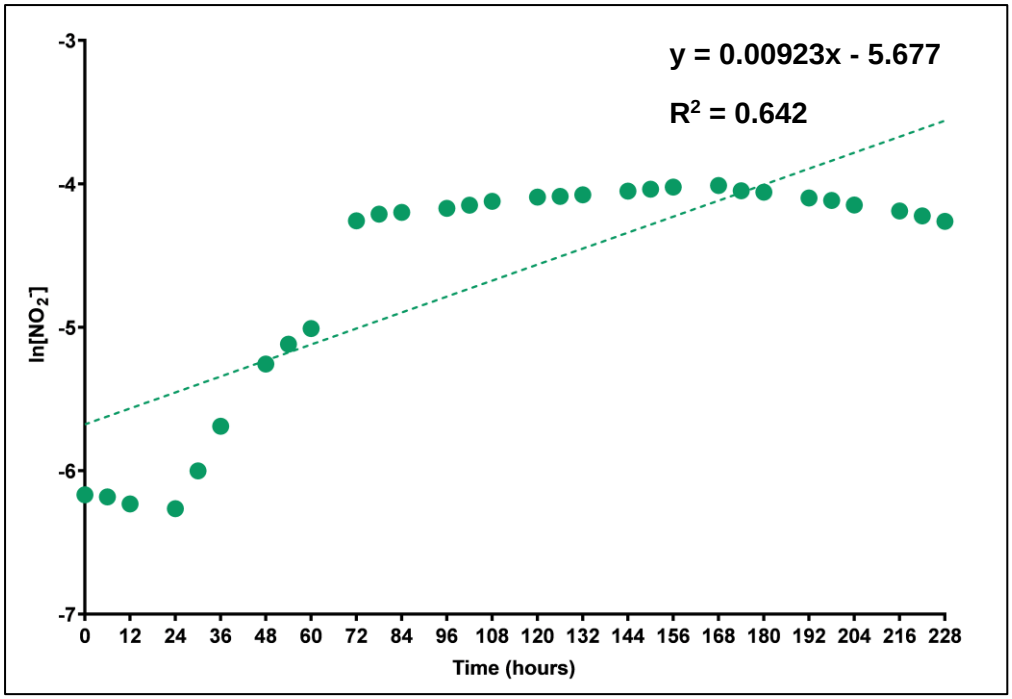

Figure G5: First order fit for nitrite (Run A at 0.5 L/min)

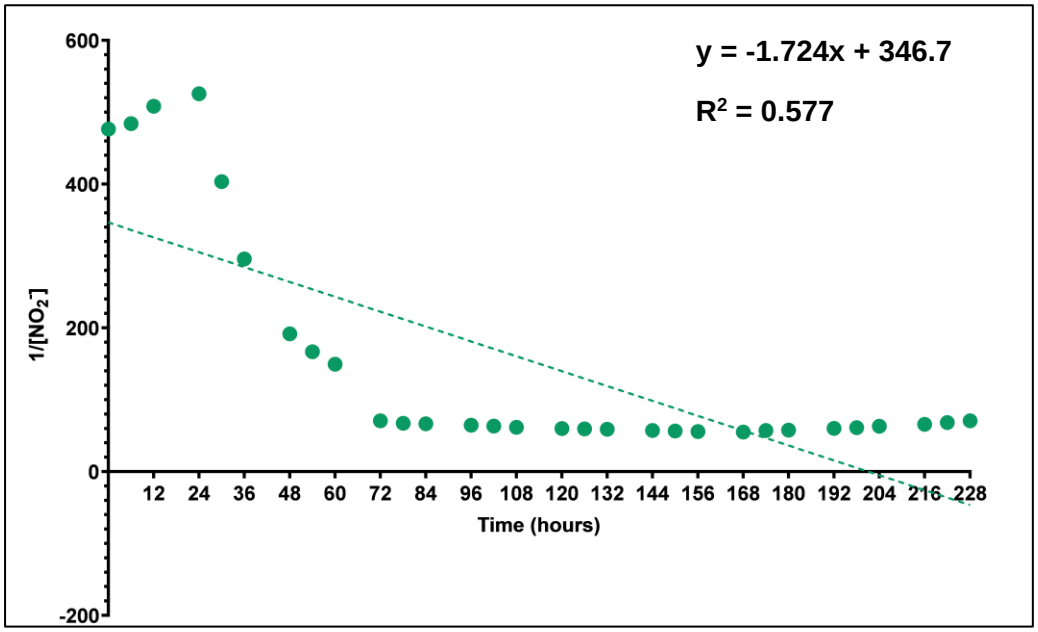

Figure G6: Second order fit for nitrite (Run A at 0.5 L/min)

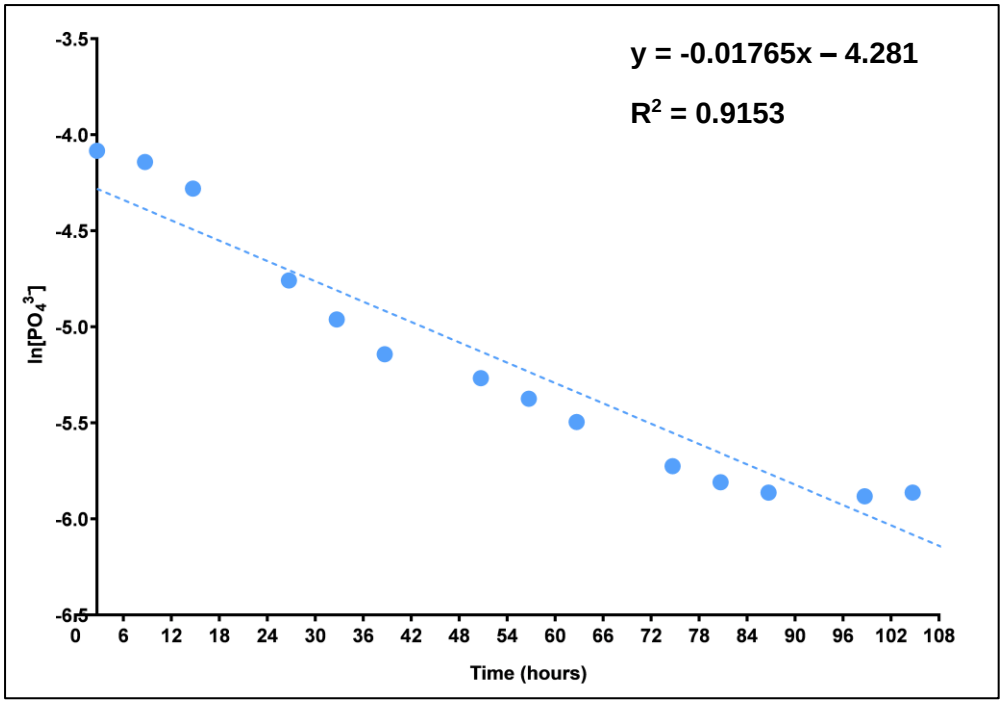

Figure G7: First order fit for orthophosphate (Run A at 0.5 L/min)

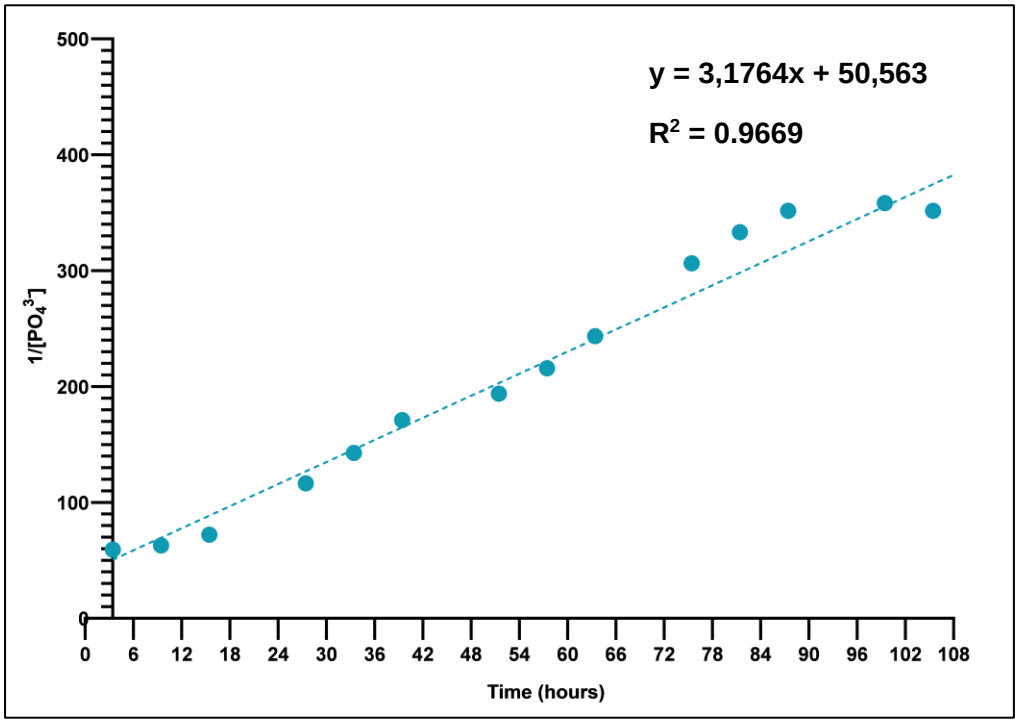

Figure G8: Second order fit for orthophosphate (Run A at 0.5 L/min)

Figure G9 to G28 show the first and second order fit for ammonia degradation and orthophosphate removal. Nitrate and nitrite are not included as Figure G3 to Figure G6 show that the overall order of reaction for nitrate and nitrite has a poor first order and second order fit.

Run B at 0.5 L/min

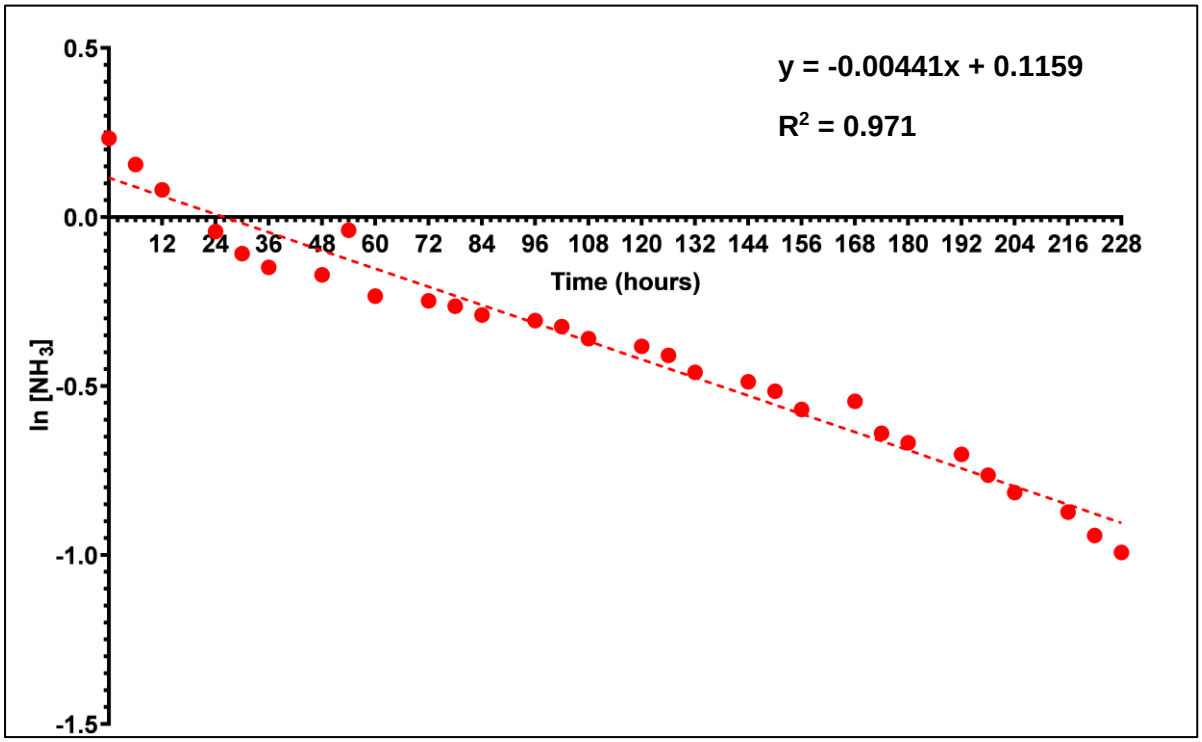

Figure G9: Natural logarithm of ammonia concentration vs. time for Run B at 0.5 L/min

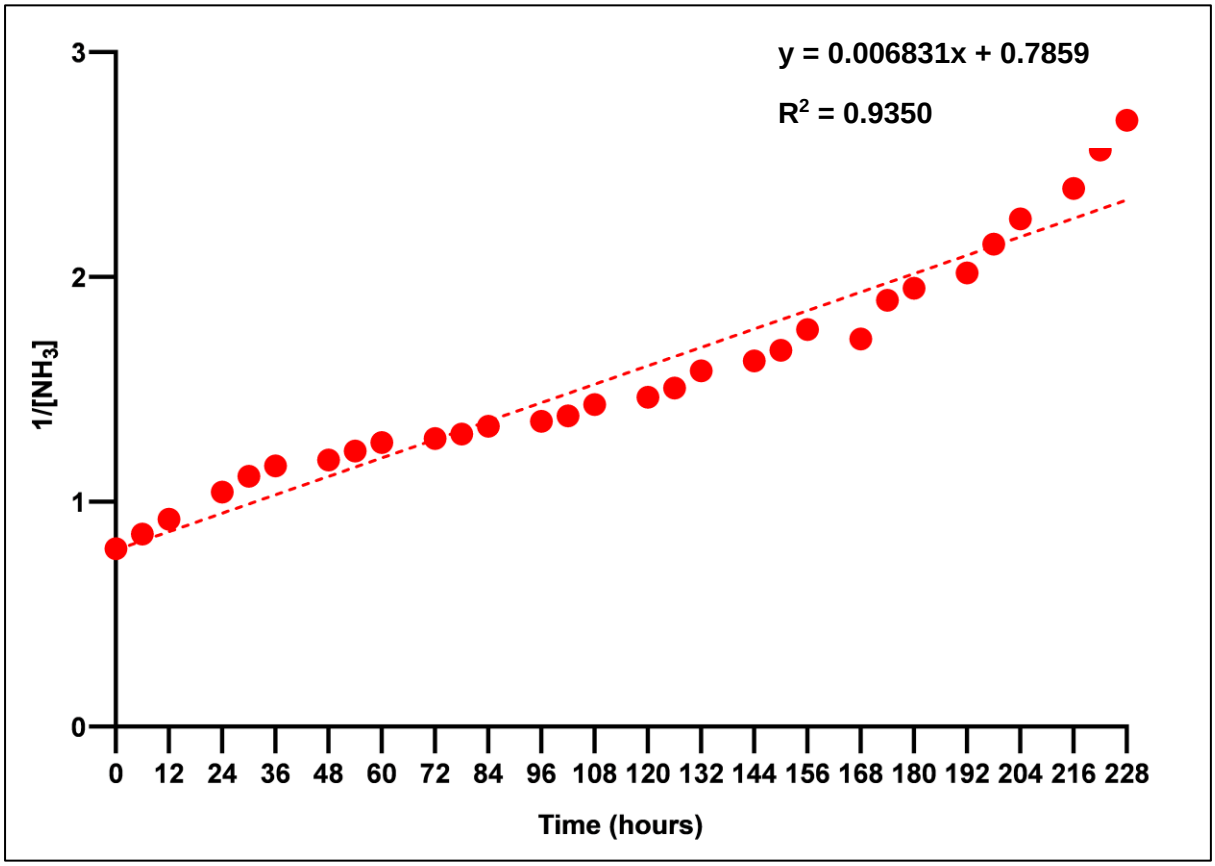

Figure G10: Inverse of Ammonia Concentration vs. Time for Run B at 0.5 L/min

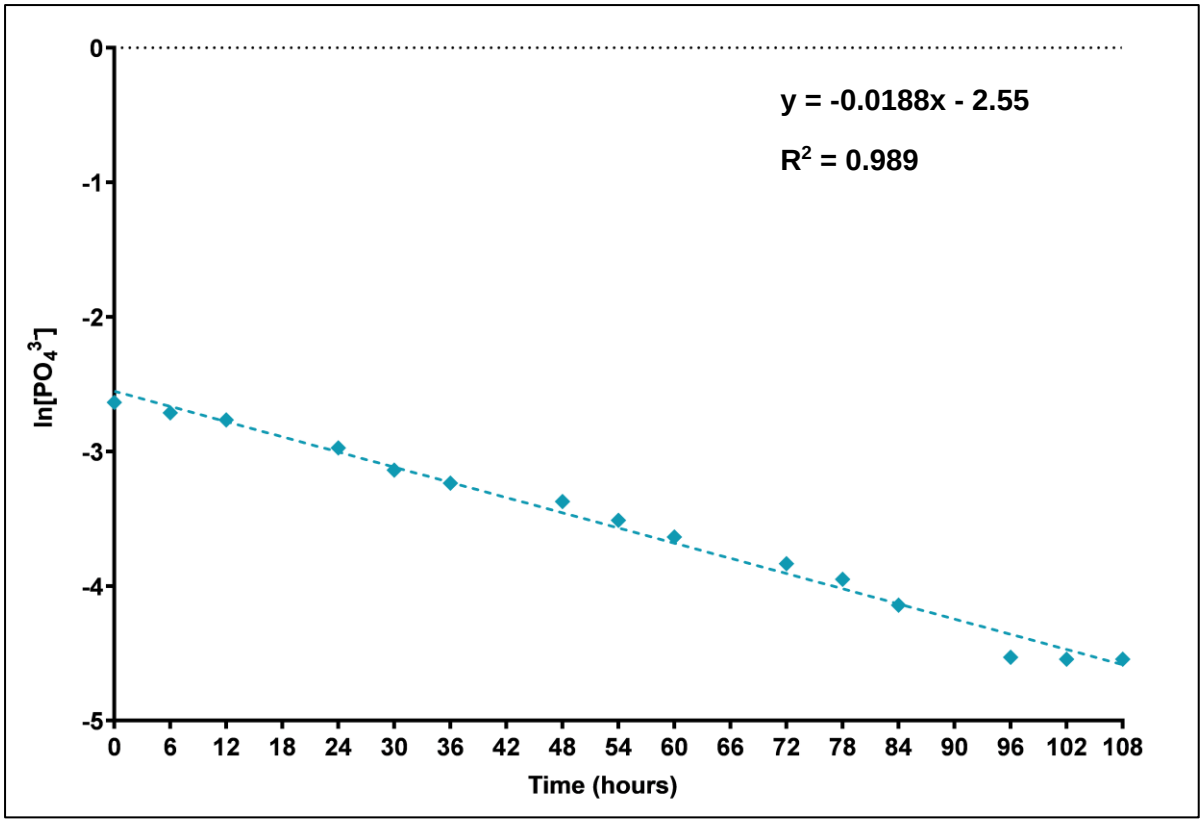

Figure G11: Natural logarithm of orthophosphate concentration vs. time for Run B at 0.5 L/min

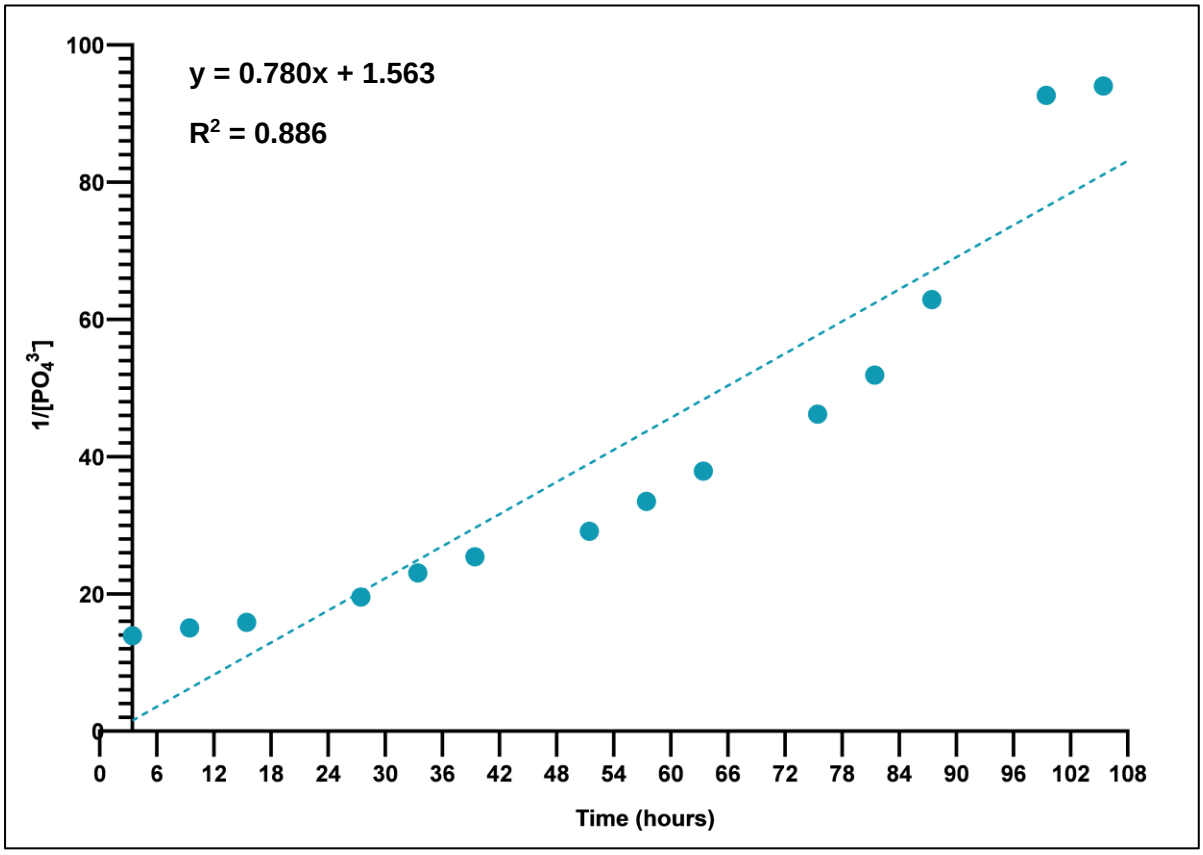

Figure G12: Inverse of orthophosphate concentration vs. time for Run B at 0.5 L/min

Run C at 0.5 L/min

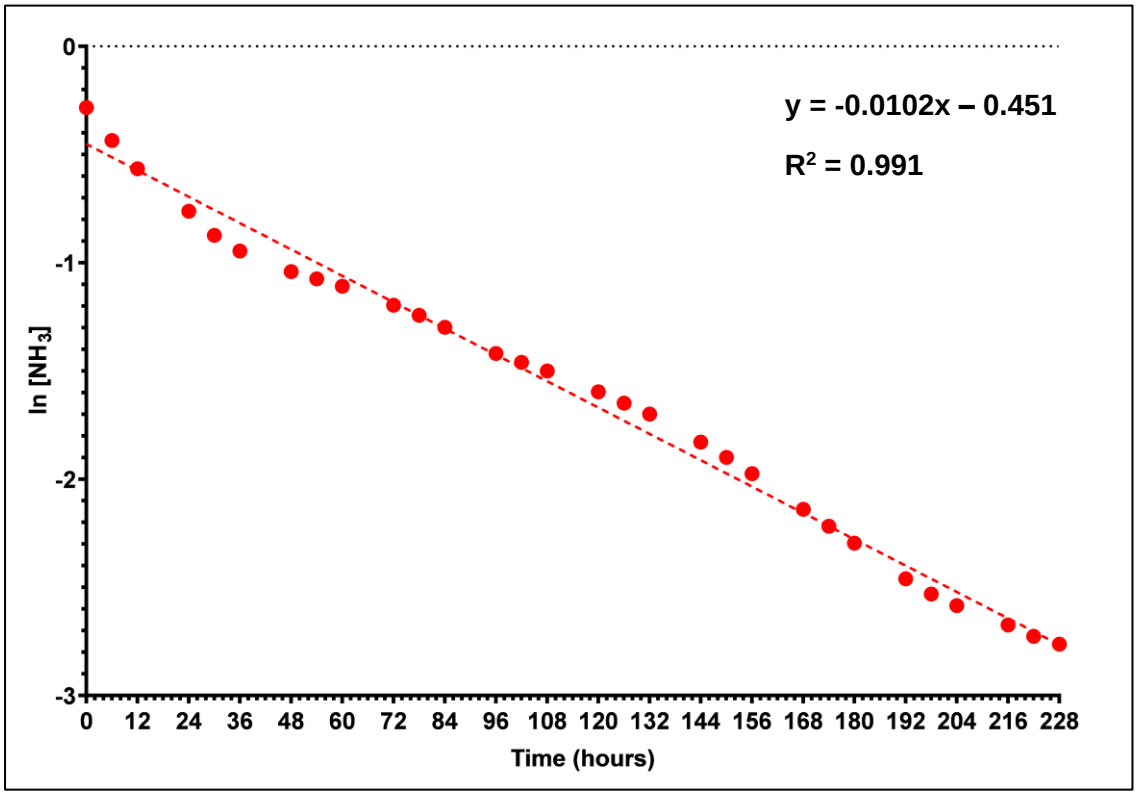

Figure G13: Natural logarithm of ammonia concentration vs. time for Run C at 0.5 L/min

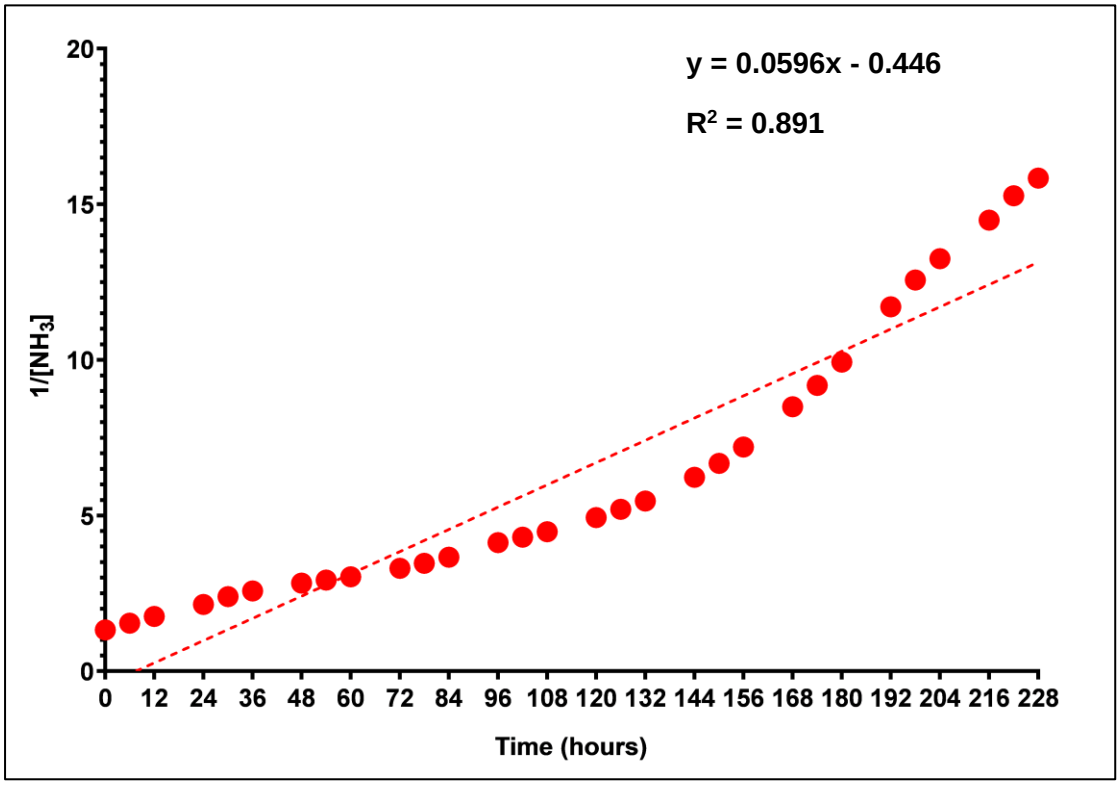

Figure G14: Inverse of ammonia concentration vs. time for Run C at 0.5 L/min

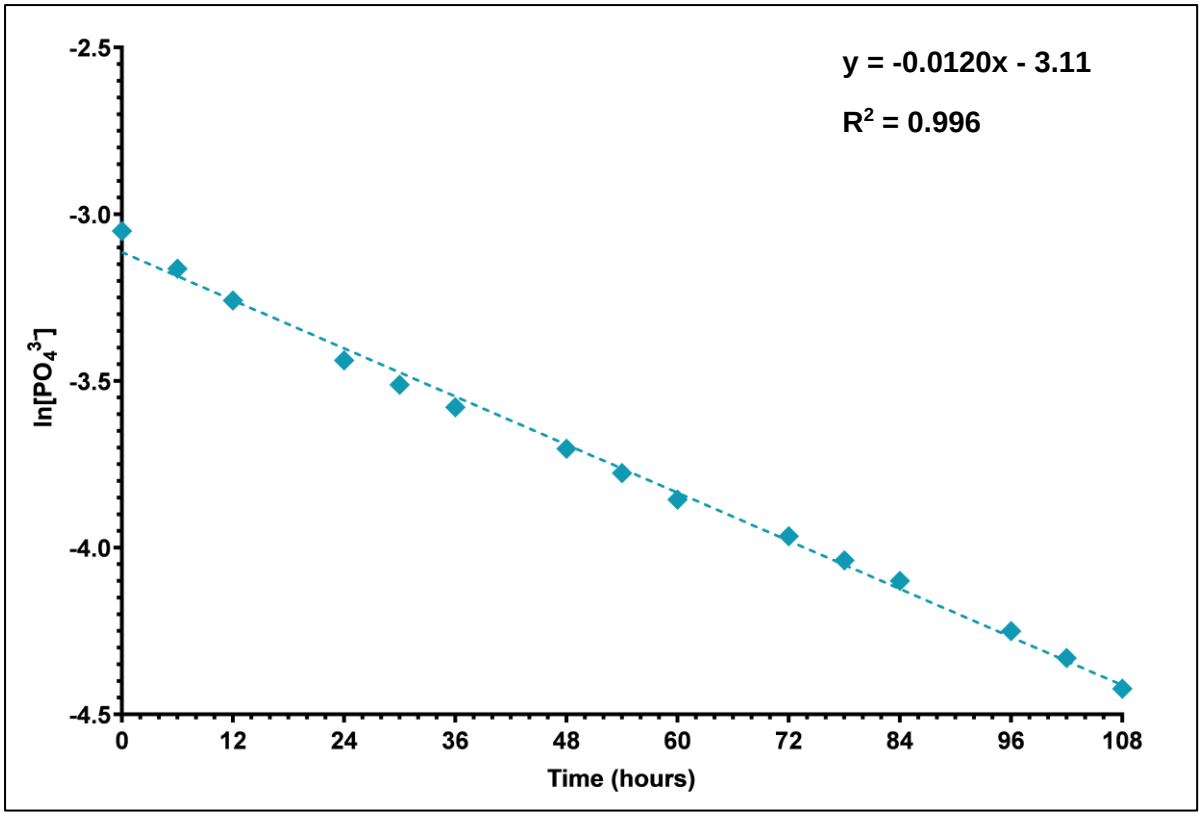

Figure G15: Natural logarithm of orthophosphate concentration vs. time for Run C at 0.5 L/min

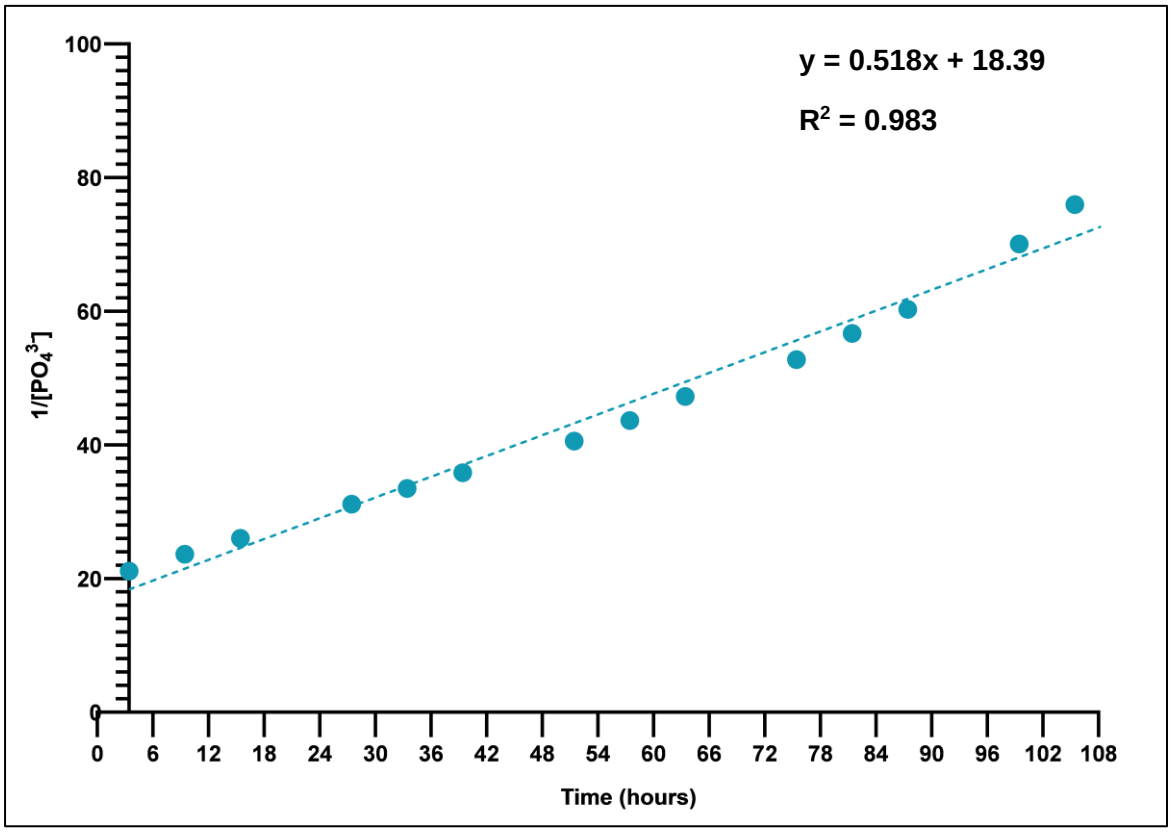

Figure G16: Inverse of orthophosphate concentration vs. time for Run C at 0.5 L/min

Run A at 1.5 L/min

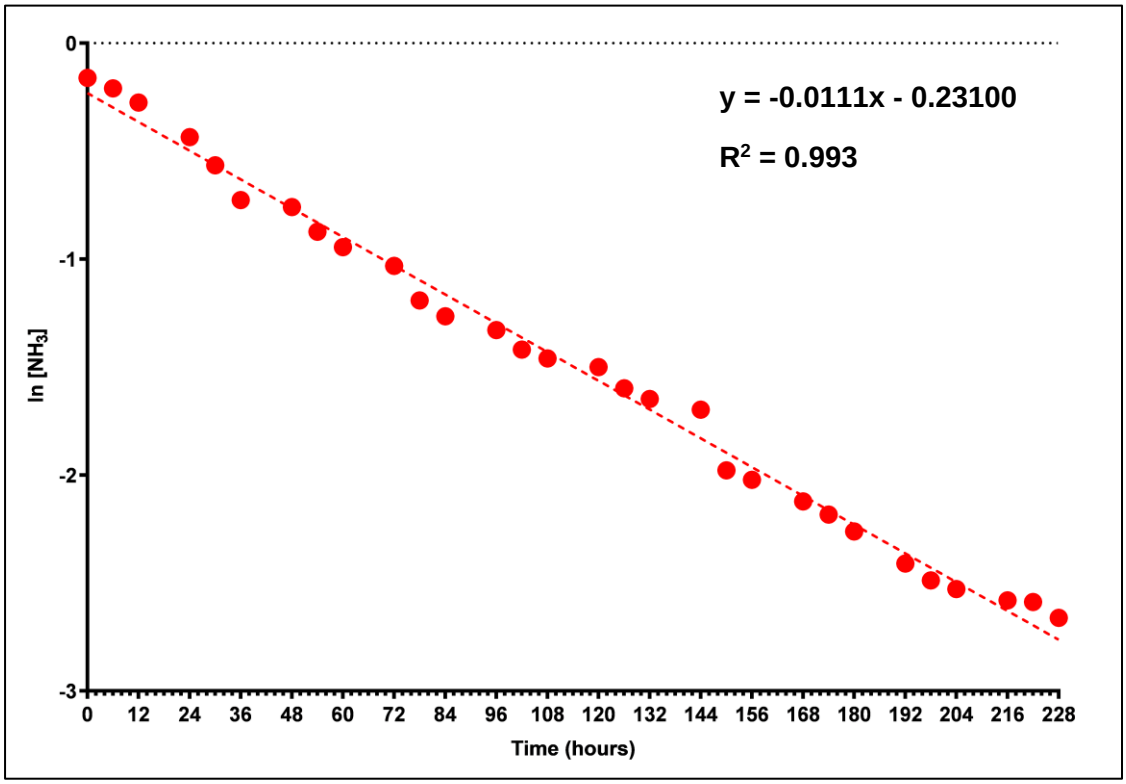

Figure G17: Natural logarithm of ammonia concentration vs. time for Run A at 1.5 L/min

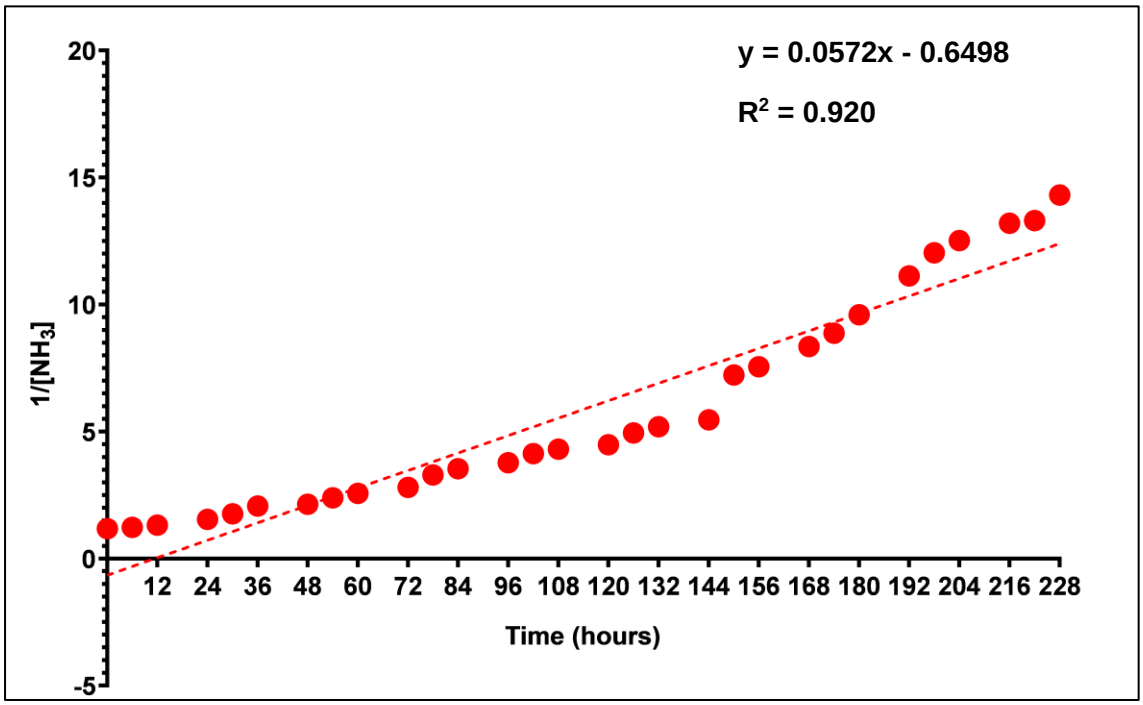

Figure G18: Inverse of ammonia concentration vs. time for Run A at 1.5 L/min

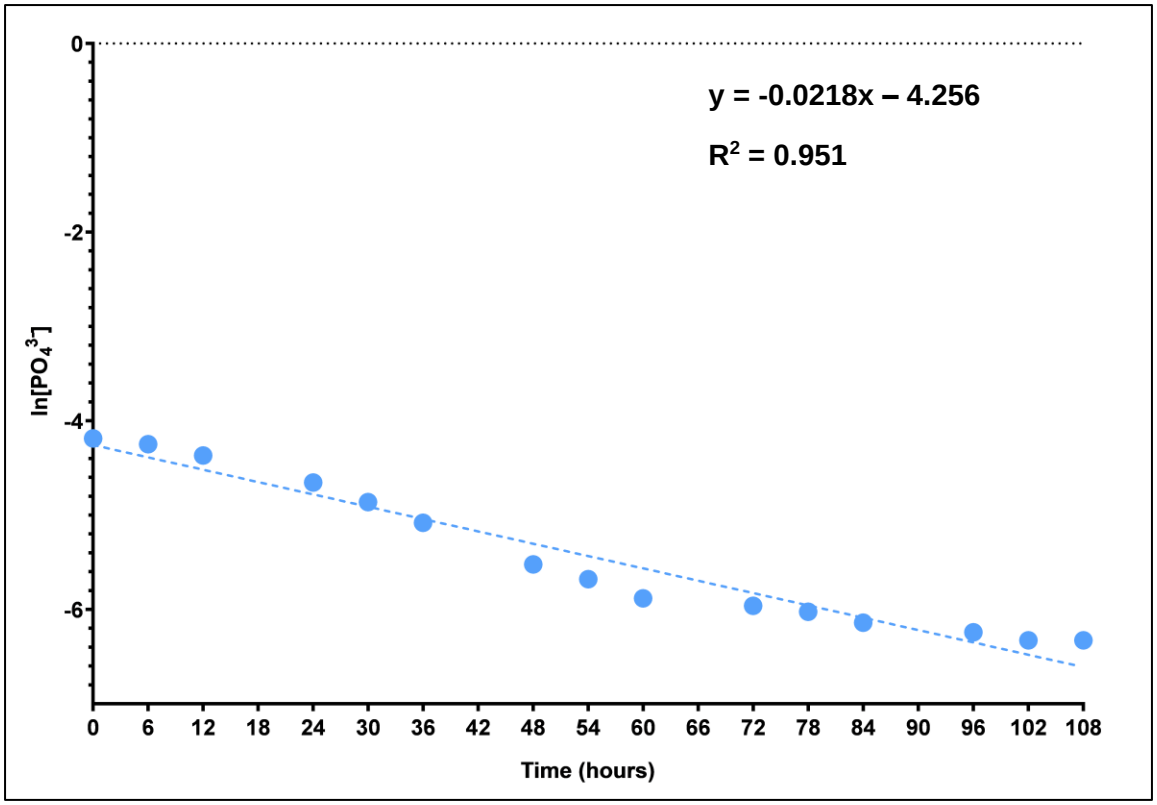

Figure G19: Natural logarithm of orthophosphate concentration vs. time for Run A at 1.5 L/min

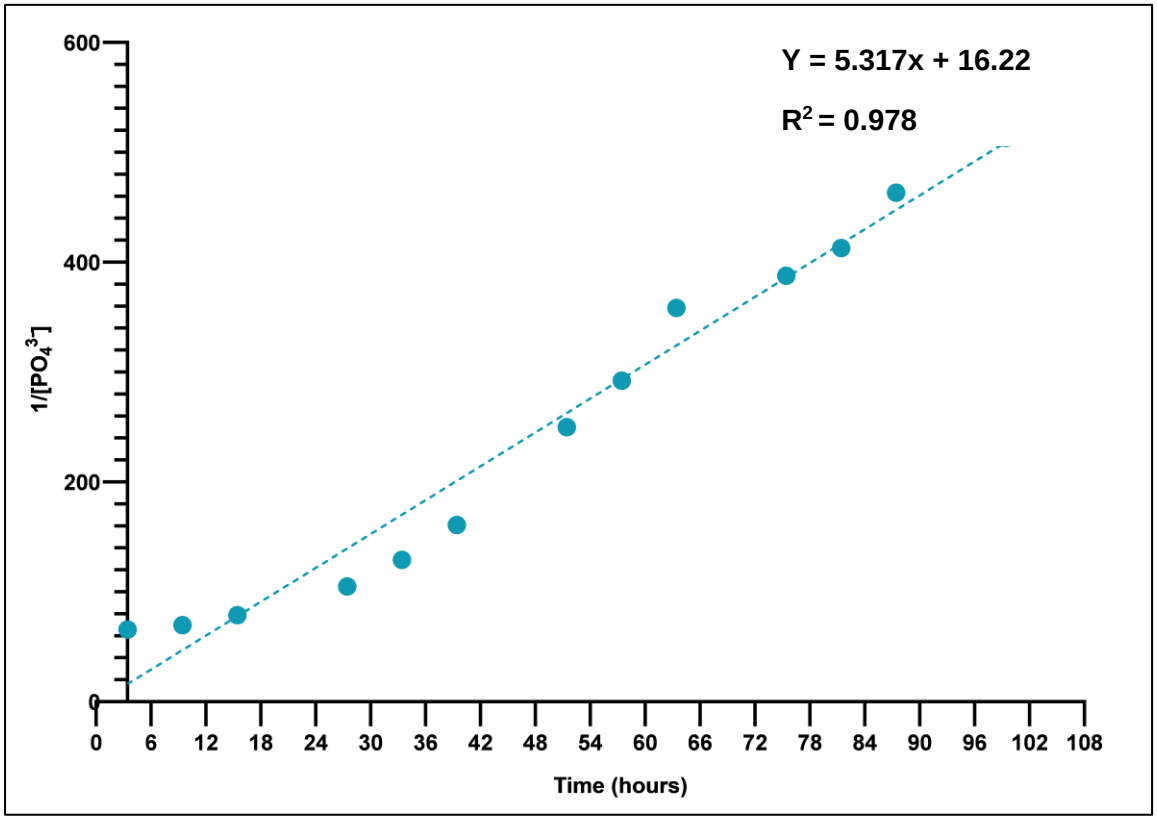

Figure G20: Inverse of orthophosphate concentration vs. time for Run A at 1.5 L/min

Run B at 1.5 L/min

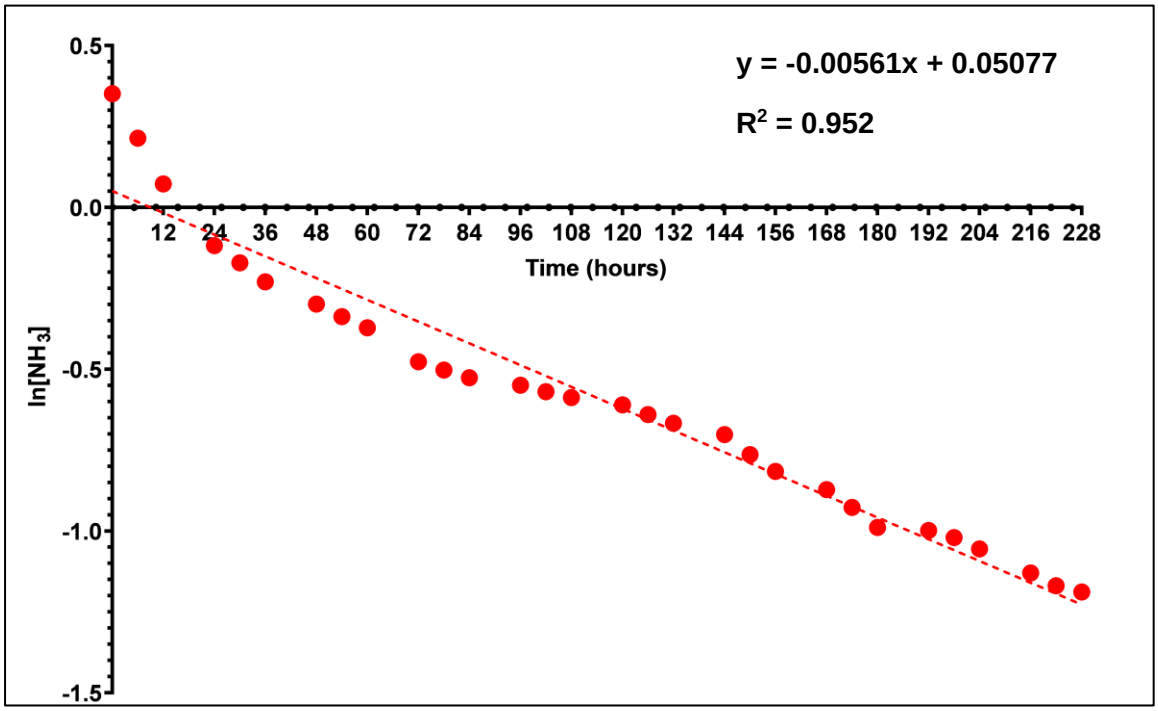

Figure G21: Natural logarithm of ammonia concentration vs. time for Run B at 1.5 L/min

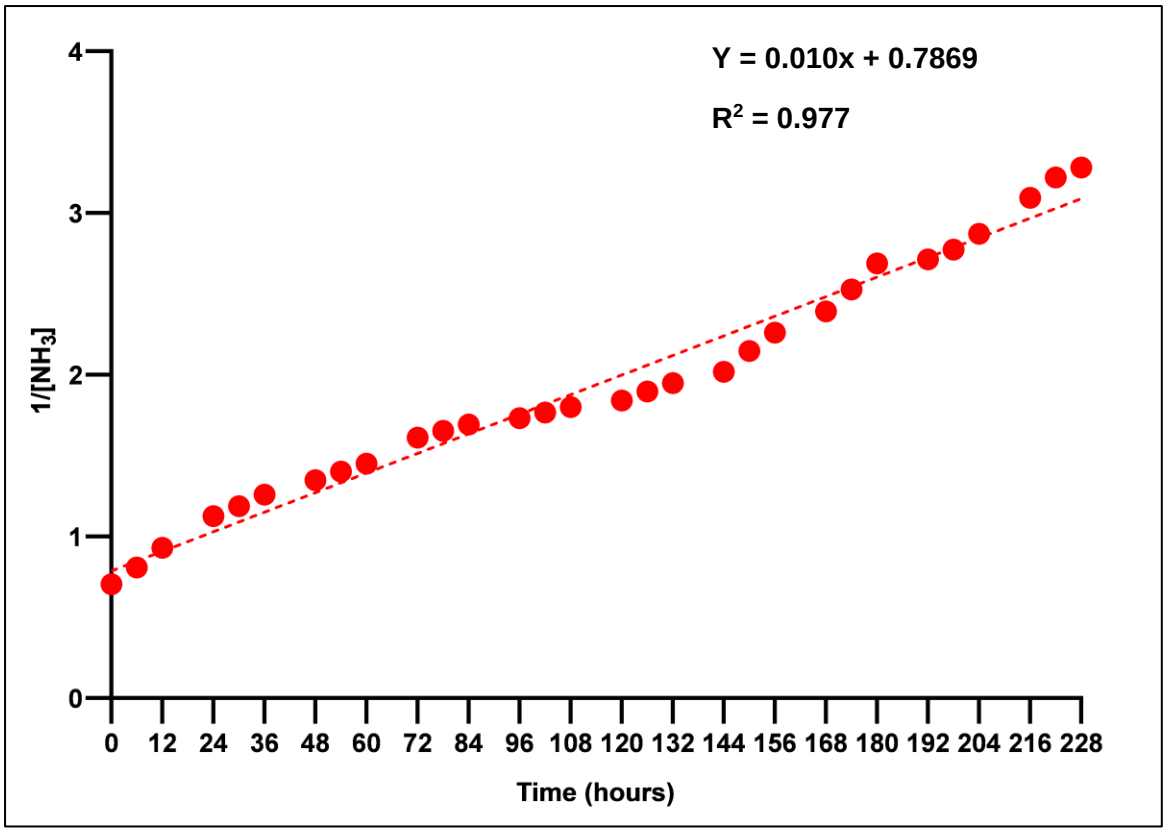

Figure G22: Inverse of ammonia concentration vs. time for Run B at 1.5 L/min

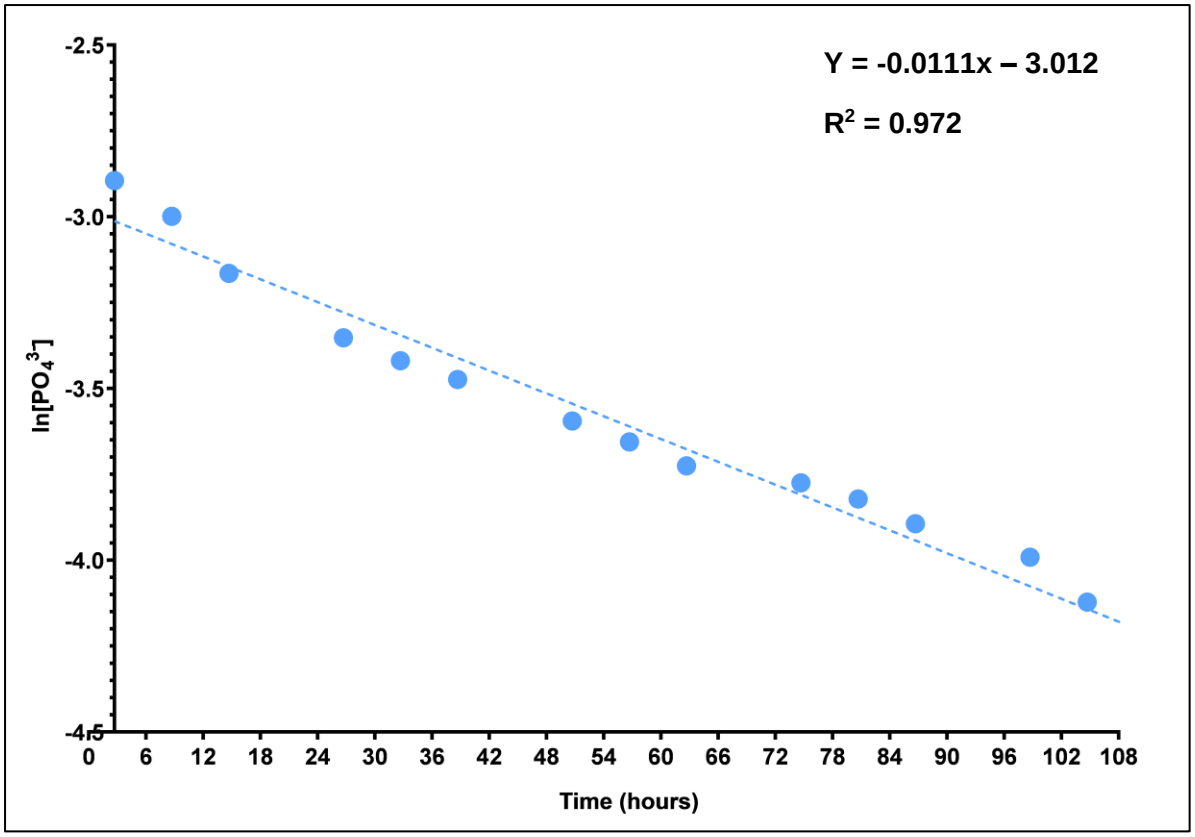

Figure G23: Natural logarithm of orthophosphate concentration vs. time for Run B at 1.5 L/min

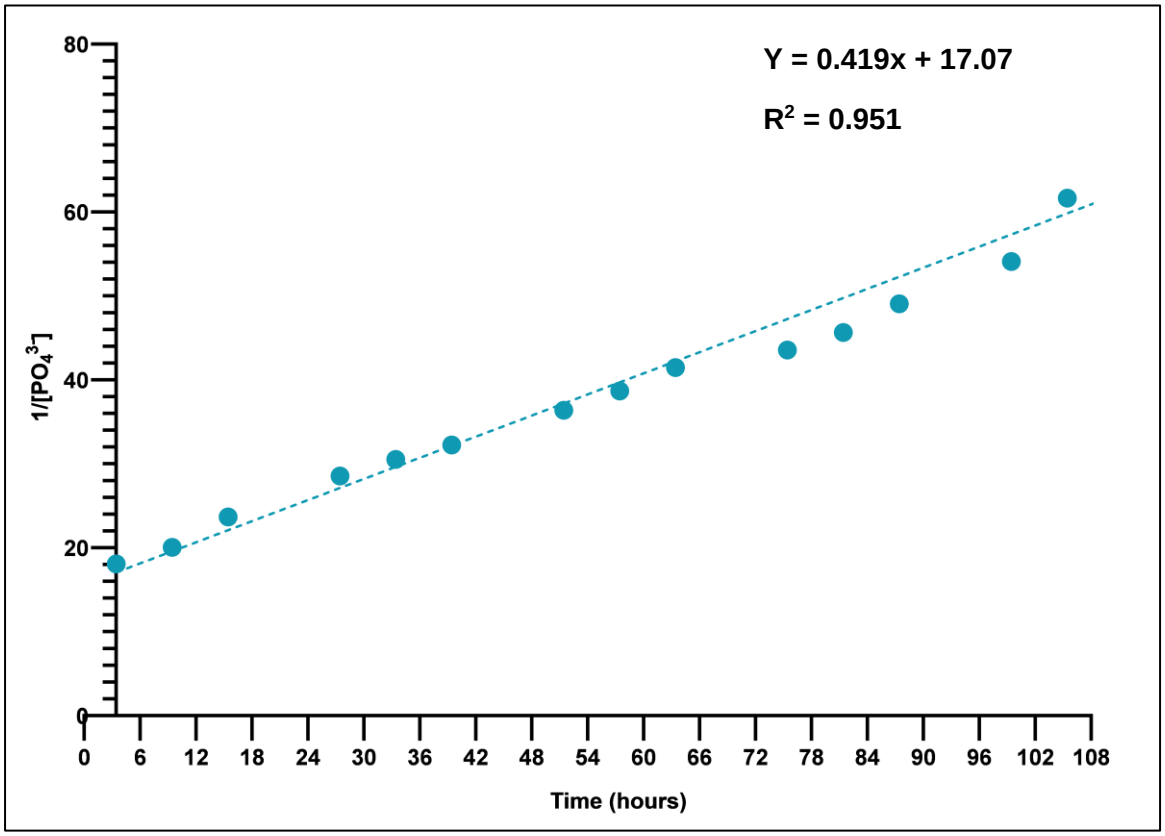

Figure G24: Inverse of orthophosphate concentration vs. time for Run B at 1.5 L/min

Run C at 1.5 L/min

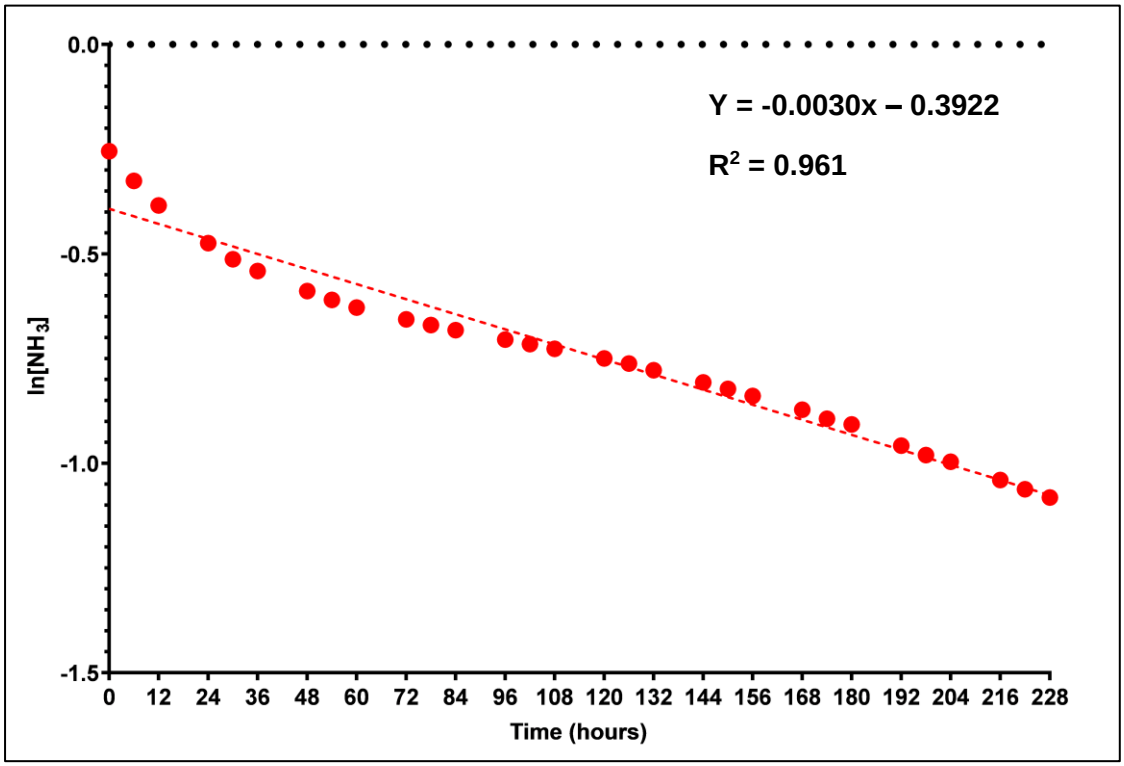

Figure G25: Natural logarithm of ammonia concentration vs. time for Run C at 1.5 L/min

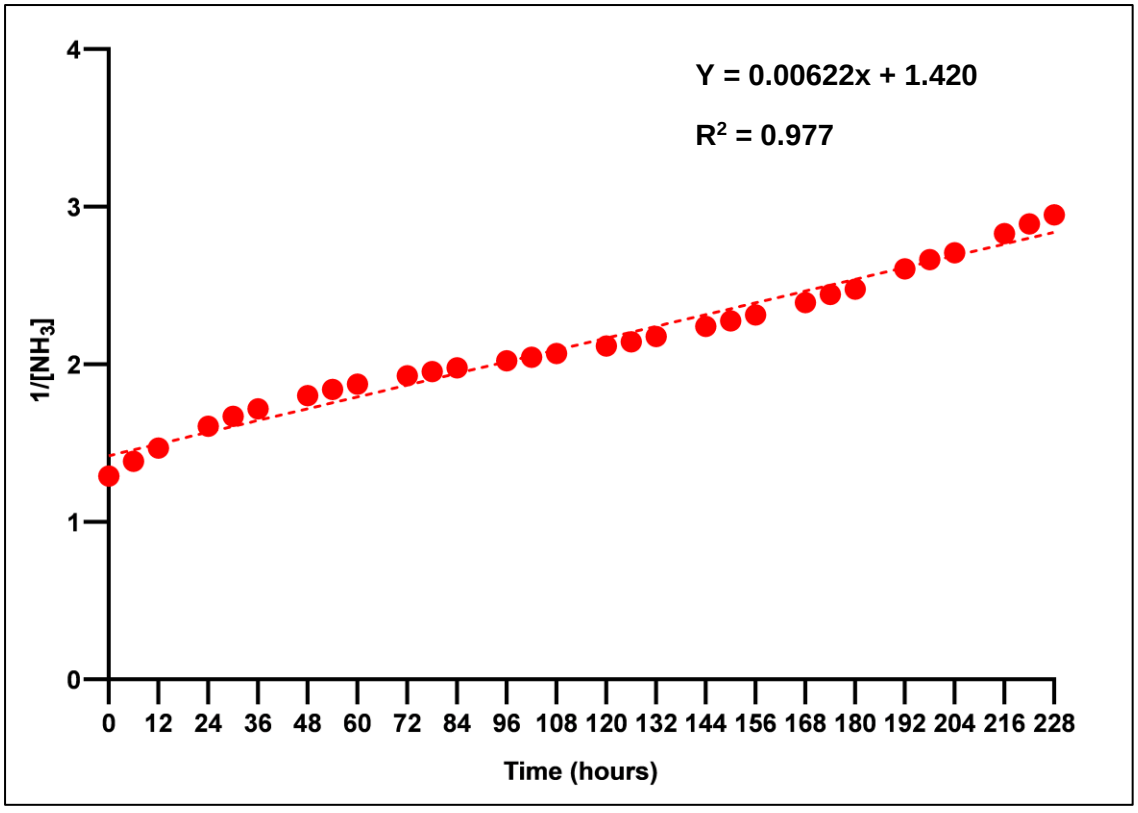

Figure G26: Inverse of ammonia concentration vs. time for Run C at 1.5 L/min

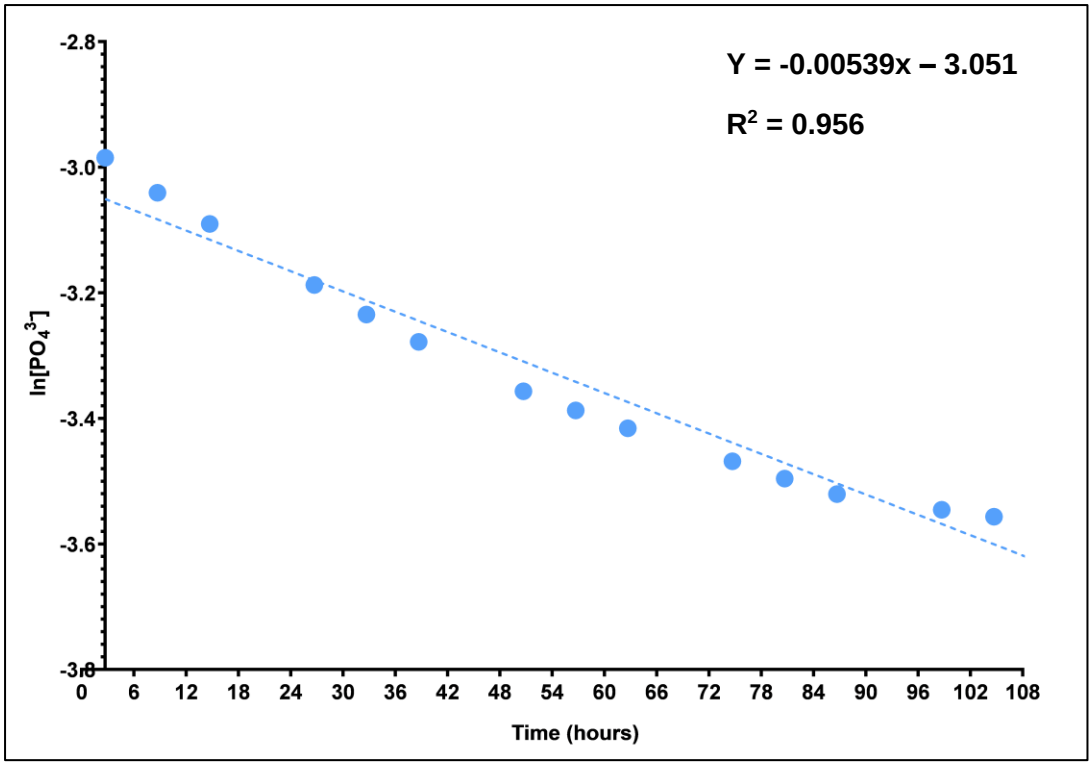

Figure G27: Natural logarithm of orthophosphate concentration vs. time for Run C at 1.5 L/min

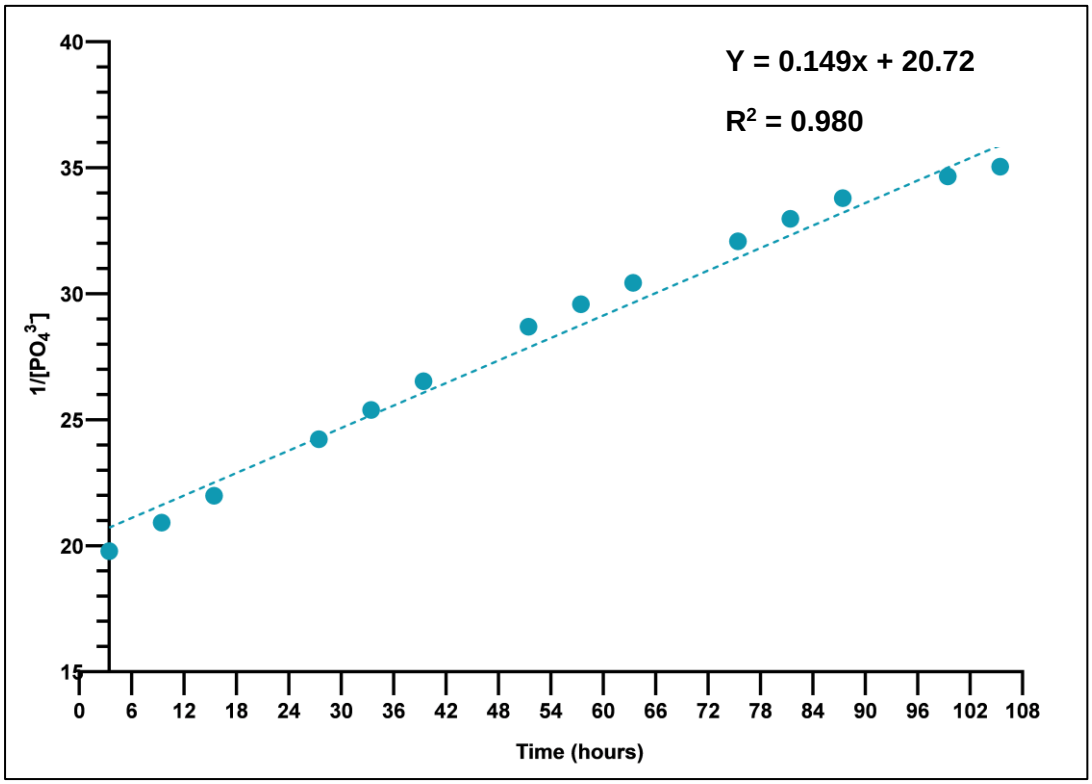

Figure G28: Inverse of orthophosphate concentration vs. time for Run C at 1.5 L/min

Appendix H: Determining Extent of Nitrification and Denitrification

Sample calculations for determining the extent of nitrification and denitrification for Run A at 0.5 L/min can be seen below. The same method of calculation was applied for the rest of the nutrient degradation kinetic studies. Nitrification occurs as per Equation 2.6 and Equation 2.7. Denitrification occurs as per Equation 2.8. It is assumed that the dominant mechanism of nitrogen removal in the system is biological (through nitrification and denitrification) with adsorption of nitrogen onto the stone media being negligible. The extent of nitrification is measured as the conversion of **available ammonia** to nitrite (Equation 2.6) and subsequently, nitrite to nitrate (Equation 2.6). The extent of denitrification is measured as the degradation of **available nitrate**.

$$NH_4^+ + \frac{3}{2}O_2 \rightarrow NO_2^- + H_2O + H^+$$ Equation 2.6

$$NO_2^- + \frac{1}{2}O_2 \rightarrow NO_3^-$$ Equation 2.7

$$4NO_3^- + 5C + 2H_2O \rightarrow 2N_2 + 4HCO_3^- + CO_2$$ Equation 2.8

The table shows the initial and final ammonia, nitrate, nitrite and total nitrogen concentrations for Run A at 0.5 L/min.

Compound	Initial Concentration (mmol/L)	Net Change in Concentration (mmol/L)	Final Concentration (mmol/L)
Ammonia	0.494	-0.421	0.073
Nitrate	0.029	+0.0410	0.070
Nitrite	0.002	+0.012	0.014
Total Nitrogen	0.525	-0.368	0.157

Nitrification:

0.494 mmol/L ammonia initially available.

0.421 mmol/L ammonia degraded should result in the formation of 0.421 mmol/L nitrite as per reaction stoichiometry of Equation 2.6.

Nitrite reacted to form nitrate

= nitrite formed from ammonia degradation – net change in nitrite concentration in system

= 0.421 mmol/L nitrite formed – 0.012 mmol/L

= 0.409 mmol/L

0.409 mmol/L nitrite reacted to form nitrate

→Total nitrate formed in system is 0.409 as per reaction stoichiometry shown in Equation 2.7

Extent of nitrification = $\frac{0.409\frac{mmol}{L}}{0.494\frac{mmol}{L}} = 82.8\%$

Denitrification:

A total of 0.409 mmol/L was formed in the system as calculated above.

Available nitrate for denitrification = initial nitrate in system + nitrate formed in system from nitrification

=0.029 mmol/L + 0.409 mmol/L

= 0.438 mmol/L

→ 0.438 mmol/L nitrate available for denitrification

Nitrate participating in denitrification

= available nitrate – net change in nitrate concentration in system= 0.438 mmol/L – 0.041 mmol/L

= 0.397 mmol/L

Extent of denitrification = $\frac{0.397\frac{mmol}{L}}{0.438\frac{mmol}{L}} = 90.6\%$

“Working hard is important. But there is something that matters even more: believing in yourself.”

- J.K Rowling, Harry Potter & the Order of the Phoenix

-Fin-